VOLUME 38 MARCH 1960 NUMBER 3

Canadian Journal of Physics

Published by THE NATIONAL RESEARCH COUNCIL

OTTAWA CANADA

CANADIAN JOURNAL OF PHYSICS

Under the authority of the Chairman of the Committee of the Privy Council on Scientific and Industrial Research, the National Research Council issues THE CANADIAN JOURNAL OF PHYSICS and five other journals devoted to the publication, in English or French, of the results of original scientific research. Matters of general policy concerning these journals are the responsibility of a joint Editorial Board consisting of: members representing the National Research Council of Canada; the Editors of the Journals; and members representing the Royal Society of Canada and four other scientific societies.

Manuscripts for publication should be submitted to Dr. H. E. Duckworth, Editor, Canadian Journal of Physics, Hamilton College, McMaster University, Hamilton, Ontario.
For instructions on preparation of copy, see **NOTES TO CONTRIBUTORS** (back cover).

Proof, correspondence concerning proof, and orders for reprints should be sent to the Manager, Editorial Office (Research Journals), Division of Administration and Awards, National Research Council, Ottawa 2, Canada.

Subscriptions, renewals, requests for single or back numbers, and all remittances should be sent to Division of Administration and Awards, National Research Council, Ottawa 2, Canada. Remittances should be made payable to the Receiver General of Canada, credit National Research Council.

The journals published, frequency of publication, and subscription prices are:

Canadian Journal of Biochemistry and Physiology	Monthly	$9.00 a year
Canadian Journal of Botany	Bimonthly	$6.00 a year
Canadian Journal of Chemistry	Monthly	$12.00 a year
Canadian Journal of Microbiology	Bimonthly	$6.00 a year
Canadian Journal of Physics	Monthly	$9.00 a year
Canadian Journal of Zoology	Bimonthly	$5.00 a year

The price of regular single numbers of all journals is $2.00.

Canadian Journal of Physics

Issued by THE NATIONAL RESEARCH COUNCIL OF CANADA

VOLUME 38 MARCH 1960 NUMBER 3

CONDENSATION OF SUPERSATURATED He^4 VAPOR IN A CLOUD CHAMBER[1]

M. H. EDWARDS AND W. C. WOODBURY

ABSTRACT

The critical supercooling, ΔT_c, required to produce visible condensation in pressure-limited adiabatic expansions of presumably ion-free saturated He^4 vapor has been measured in a small glass cloud chamber. The transient gas temperatures were measured during expansions by using a carbon resistance thermometer in a Wheatstone bridge. An oscilloscope was used in place of a galvanometer, and its trace was photographed during expansions. Low-amplitude temperature oscillations in the gas, which might not normally have been detected, were frequently observed in the early stages of this work. These oscillations either appeared spontaneously ("Taconis Resonances"), or could be shock-excited by an expansion. These oscillations were subsequently eliminated. Condensation thresholds were then measured using starting temperatures from 4.2 to 1.7° K. ΔT_c dropped from about 50 to 60 mdeg above the λ point to less than 20 mdeg below the λ point. The critical supersaturations required to produce condensation were thus always less than 105%. The supersaturations were calculated without making the usual, but highly implausible, assumption that the expanding gas is ideal. Assuming that the condensation nuclei are embryonic droplets arising accidentally from density fluctuations in the supersaturated vapor, the critical droplet radius is found to be about 10^{-6} cm above 2.5° K, although the theoretical treatment here is not rigorous.

1. INTRODUCTION

The physical processes involved in the initiation of condensation from a supersaturated vapor are by no means clear. Most cloud chamber experiments have involved the use of some condensable vapor mixed with another 'carrier' gas which does not participate in the condensation. Both gases are always assumed to be ideal in attempts at theoretical analyses of the processes.

The authors undertook to examine condensation in a single-component system, using pure He^4 at low temperatures. Furthermore, the measurements of supercooling and consequent calculations of supersaturations were made without using the totally implausible assumption that a vapor on the verge of condensation behaves as an ideal gas.

2. EXPERIMENTS

2.1 Apparatus and Method

The condensation cloud chamber used (Fig. 1) consisted of a glass chamber C of about 110 cm^3 volume, which had an offset lower tip L. The chamber was

[1]Manuscript received October 13, 1959.
Contribution from the Department of Physics, Royal Military College, Kingston, Ontario. Supported in part by the Defence Research Board of Canada under Grant No. 9510-10. Project D44-95-10-10.

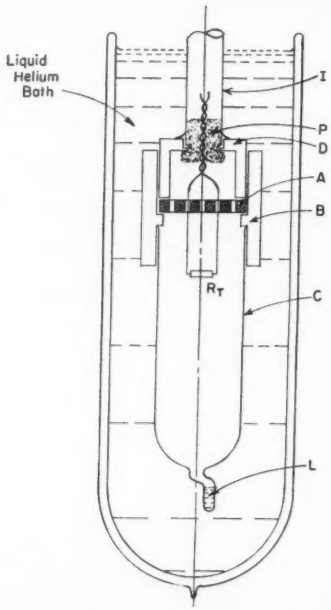

FIG. 1. The apparatus.

immersed in a liquid helium bath and connected to room temperature by a 5/8-in. outside diameter Inconel tube I, about 1 meter long, and then through a fast-acting Veeco solenoid vacuum valve (SV) to a large tank of approximately 24 liters volume. Tube I was soft-soldered into the brass top D of the chamber. The seal between D and C was effected by means of a Teflon bushing B, which was machined to be a press fit at room temperature. A light film of vacuum grease was wiped on the parts before each assembly. Upon cooling, the Teflon contracts so much more than either brass or glass that a seal tight to liquid helium II was regularly, but not invariably, formed. A bakelite spacer A was used to support the 56-ohm 1/2-w Allen Bradley carbon composition resistance thermometer R_T. Holes were drilled through A to permit easy gas flow past it. The leads to R_T were of No. 40 HF copper wire.

The cotton batten plug P was loosely stuffed into the lower end of I to eliminate temperature oscillations in the gas (see *2.2* later).

The chamber was illuminated by a 6-volt microscope illuminator used with three heat-absorbing filters. The chamber was viewed visually through the slits in the silvering of the liquid air and helium Dewars, in a darkened room. The helium clouds formed could best be seen when looking almost directly towards the light source.

A small amount of liquid L was condensed from an external filling system, into the offset tip of the cloud chamber, using He^4 gas which had been purified

by a liquid-air-cooled charcoal trap. The initial saturated vapor pressure, P_{1s}, in the chamber was then read and the SV closed. The large tank was adjusted to some pressure less than P_{1s}. Then the SV was opened so that an expansion to an essentially constant final pressure (the tank pressure) occurred. After a preset time, usually between 0.4 and 1.5 seconds, the SV was closed again. The cloud chamber was watched to determine whether or not a fog or cloud appeared in the supersaturated vapor. The temperature of the vapor was measured during expansions using the suspended carbon resistance thermometer R_T as one arm of a Wheatstone bridge. A medium persistence DuMont Type 403 oscilloscope with a d-c. sensitivity of 100 μv per cm was used in this bridge instead of a galvanometer. The drop in temperature ΔT of the vapor during expansion was recorded by photographing the oscilloscope trace. As the temperature fell the resistance R_T rose, and the bridge unbalanced, producing a deflection of the trace of the oscilloscope. This method of following the cooling during expansions was developed by Stachórska (1954, 1956). The power dissipated in R was kept below 1 μw and our sensitivity was then between 1 and 2×10^{-3} ° K per mm deflection of the oscilloscope trace.

Figure 2 shows a typical photograph of the oscilloscope trace, taken during an expansion from an initial temperature $T_1 = 2.725°$ K. The sweep speed was 250 milliseconds per division. The camera shutter was opened for a total of about 5 seconds showing parts of three sweeps. Starting near the upper right, the bridge was in balance. After about 1 second, the SV was opened (at about 1.8 divisions from left) and the temperature fell about 50 mdeg in about 100 milliseconds, and then remained nearly constant. After about 1.7

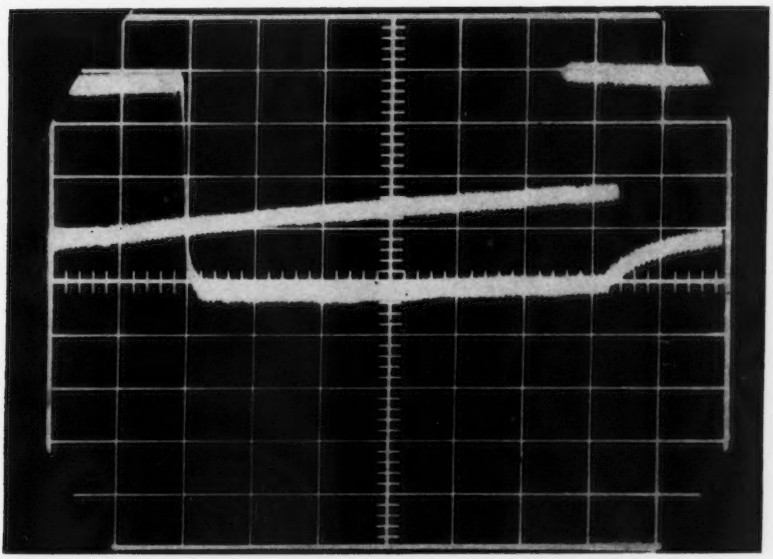

FIG. 2. Temperature record of a typical expansion.

seconds the SV was closed and the temperature began to rise towards the bath temperature. After a further 2.7 seconds, the shutter was closed again.

2.2 Temperature Oscillations in the Gas

(a) Spontaneous Oscillations

When the apparatus was first set up, without the cotton batten plug P (see Fig. 1) in place, low-amplitude temperature oscillations in the gas frequently occurred. Temperature oscillations in a gas column, one end of which is at room temperature, and the other at a low temperature, have been known to exist for many years (Keesom 1942) and are usually referred to as "Taconis resonances". The exact nature of the phenomenon is not clear (Taconis *et al.* 1949; Kramers 1949; ter Haar 1955). Audible resonances often are able to transport an impressive amount of heat (up to several watts) into a cryostat. Such large amplitude oscillations are very easy to detect when they occur because of the sound and/or the increased boil-off rate of the bath liquid.

The low-amplitude temperature oscillations which we observed might very easily have been overlooked without a cathode-ray oscilloscope in the bridge circuit of the resistance thermometer in the gas. Figure 3 shows such a low-amplitude resonance which occurred when the chamber was at a pressure of 21.5 mm Hg at 3.24° K (S.V.P. = 255.5 mm). The temperature amplitude is ±22 mdeg at a frequency of 25 cycles/sec. At the same temperature with P = 49.1 mm Hg the amplitude was reduced to ±12 mdeg, and above P = 85 mm Hg no resonance could be detected.

On some runs temperature oscillations occurred even at the saturated vapor pressure and below the λ point.

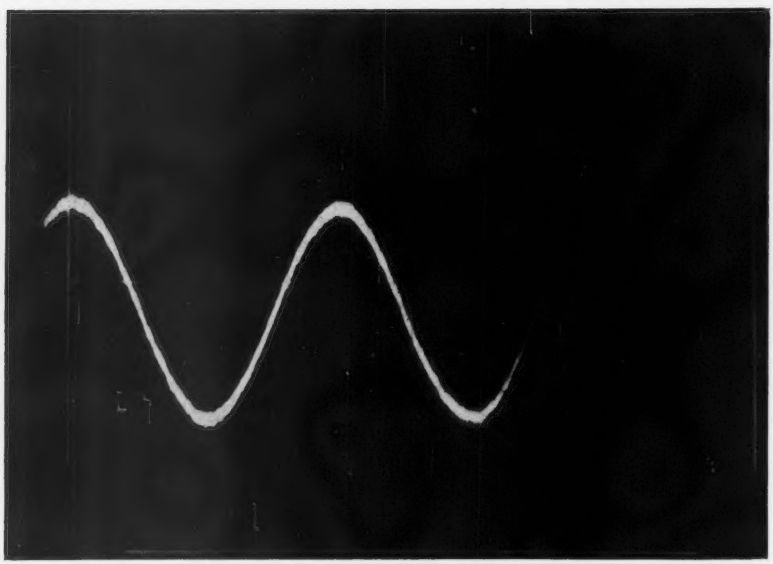

FIG. 3. Spontaneous temperature oscillation or "Taconis resonance".

Such oscillations, if undetected in apparatus of similar geometry in experiments to measure the He II film thickness or flow properties, might have very serious effects upon those measurements, because of the extreme sensitivity of such experiments to small temperature differences. It would be easy to install a carbon thermometer in a circuit such as we have described, in any film experiment. This could then act as a low-amplitude Taconis resonance detector.

(b) Shock-excited Oscillations

Even when we had chosen initial conditions for expansions where no temperature oscillations occurred, we regularly found that the expansion itself could excite a damped oscillation, as shown in Fig. 4, taken at 3.2° K with the SV kept open for 0.3 second. The frequency of this oscillation was about

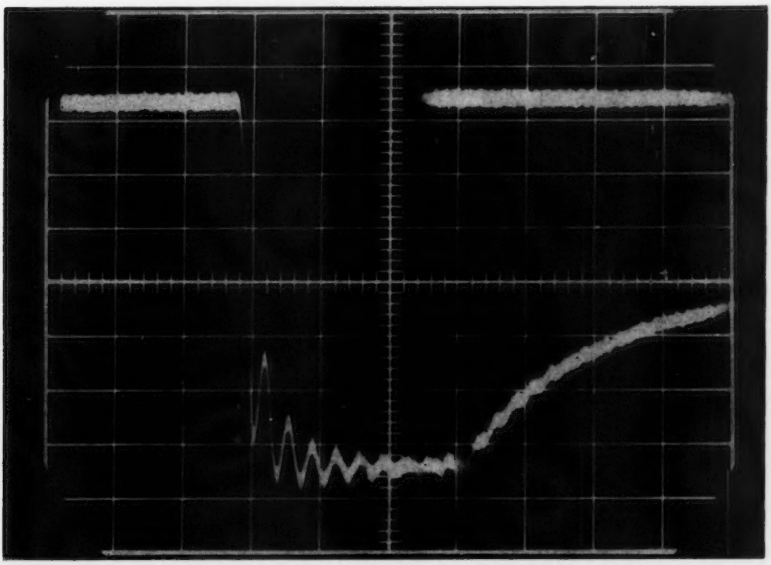

FIG. 4. Temperature oscillation shock-excited by an expansion.

33 cycles/sec. After the cotton batten plug P was stuffed into the lower end of the tube I (see Fig. 1) both the spontaneous and shock-excited temperature oscillations in the gas were damped out and did not reappear in any subsequent run.* All the later expansions were then similar to that shown in Fig. 2.

2.3 Results

At each of seven temperatures, from 1.7 to 4.2° K, from 10 to 25 expansions were performed. In any such run the initial temperature T_1 was kept constant. The cooling ΔT was subsequently measured from enlargements of the photographs of the C.R.O. trace. At any temperature, large expansions produce persistent fogs of helium from the supersaturated vapor, whereas small expansions produce no condensation. Each series of expansions was performed

*We are grateful to Dr. L. C. Jackson for this suggestion.

in such a way as to try to determine the critical supercooling required to produce visible condensation. As this threshold supercooling is more nearly realized, the condensation produced sometimes seemed to be only a few large drops like rain, or else a brief flash of fog. The measurements finally give two numbers for any initial temperature T_i, viz. a maximum temperature drop ΔT_{no} giving no visible condensation, and a minimum temperature drop ΔT_{yes} giving visible condensation. Presumably the true threshold lies between these two numbers. Figure 5 is a graph of these measurements showing ΔT_{no} as circles and ΔT_{yes} as plus signs. At 1.7° K the + point is believed to be rather high because the vapor density is so low (1/50 of its value at 4.2° K) that the first condensation may not have been seen. The accuracy of the other points is probably no better than ±5 mdeg.

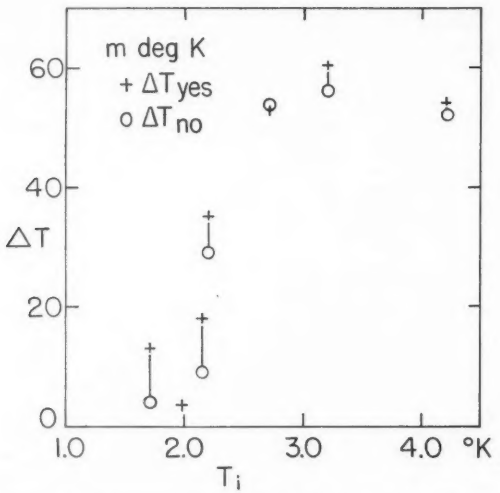

FIG. 5. Maximum temperature drop ΔT_{no} which gives no visible condensation, and minimum temperature drop ΔT_{yes} which gives condensation, as a function of the temperature T_i before expansion of saturated He^4 vapor.

3. ANALYSIS

3.1 Supersaturation of an Imperfect Gas

We follow Wilson (1897) in defining supersaturation, S, as the ratio of the actual density of the vapor ρ_t immediately after expansion to the saturation density ρ_{ts} at the lower final temperature T_t. Only when the vapor is an ideal gas does this definition become equivalent to P/P_∞ where P is the actual pressure and P_∞ is the saturation vapor pressure over a plane surface.

We wish to find a method of calculating S from the measured cooling ΔT, without having to assume that the expanding gas is ideal. The initial conditions before expansion are: $P_i = P_{is}$ the saturated vapor pressure, $V_i = V_{is}$ the saturated molar volume, and T_i. After adiabatic expansion through the critical temperature interval ΔT, we have P_t, V_t, and $T_t = T_i - \Delta T$.

We wish to evaluate the critical supersaturation

$$S \equiv \frac{\rho_t}{\rho_{ts}} = \frac{V_{ts}}{V_t}$$

where V_{ts} is the saturated molar volume at the final temperature. Now

$$V_{ts} = V_{1s} + \int_0^{\Delta T} \left(\frac{dV}{dT}\right)_{SVP} dT = V_{1s} + \left(\overline{\frac{dV}{dT}}\right)_{SVP} \Delta T$$

where $(\overline{dV/dT})_{SVP}$ is the average rate of change of molar volume along the saturated vapor curve. And $V_t = V_{1s} + \Delta V_s$ where ΔV_s is the actual change in molar volume during the adiabatic expansion.

We now calculate ΔV_s for an imperfect gas. First we obtain a relationship between V and T in an adiabatic change. The equation of state of any gas may be written as $f(T,V,S) = 0$ where S is now the entropy.

Then

$$\begin{aligned}\left(\frac{\partial T}{\partial V}\right)_S &= -\left(\frac{\partial T}{\partial S}\right)_V \left(\frac{\partial S}{\partial V}\right)_T \\ &= -\frac{T}{C_V}\left(\frac{\partial S}{\partial V}\right)_T \\ &= -\frac{T}{C_V}\left(\frac{\partial P}{\partial T}\right)_V\end{aligned}$$

by one of Maxwell's relations. Now for any imperfect gas the equation of state may be written as a volume virial expansion

$$PV = RT\left(1 + \frac{B}{V} + \frac{C}{V^2} + \ldots\right).$$

Then

$$\begin{aligned}T\left(\frac{\partial P}{\partial T}\right)_V &= \frac{RT}{V}\left(1 + \frac{B}{V} + \frac{C}{V^2} + \ldots\right) \\ &= P \text{ for an imperfect gas (and for an ideal gas also).}\end{aligned}$$

So

$$\left(\frac{\partial T}{\partial V}\right)_S = -\frac{P}{C_V}.$$

And hence

$$\Delta V_S = -\int_{P_1,T_1}^{P_f,T_f} \frac{C_V}{P}\, dT = -\left(\overline{\frac{C_V}{P}}\right) \Delta T.$$

Thus the supersaturation

$$S = \left[V_{1s} + \left(\overline{\frac{dV}{dT}}\right)_{SVP} \Delta T\right]\left[V_{1s} - \left(\overline{\frac{C_V}{P}}\right) \Delta T\right]^{-1}. \tag{3.1}$$

This is the expression desired.

3.2 Temperature Dependence of the Critical Supersaturation

In order to apply eq. (3.1), we need detailed information of the equation of state of the saturated vapor. $(\overline{C_V/P})$ values were obtained by graphical averaging of the measurements of van Itterbeek and Laet (1958). The values of V_{ls} and $(dV/dT)_{SVP}$ used were calculated from the refractive index data of Edwards (1957) for He^4-saturated vapor. The Lorenz–Lorentz law was used, taking as the polarizability of He^4 vapor, the liquid value (Edwards 1958) of (0.12454 ± 0.00021) cm^3 mole^{-1}. Thus,

$$V_{ls} = (0.521672\pm0.00089)(n^2+2)(n^2-1)^{-1}, \tag{3.2}$$

where n is the refractive index, was used to calculate the saturated molar volumes from Edwards' (1957) data.

Table I shows the resulting critical supersaturations taking the critical supercooling ΔT_c to be the average of the ΔT_{yes} and ΔT_{no} points of Fig. 2. The

TABLE I

Condensation data for He^4, showing final temperatures, critical supercooling, experimental and theoretical critical supersaturations, and critical radii, and number of molecules per droplet calculated by two different methods

T_f, ° K	ΔT_c, mdeg K	S, expt.	S, theory	r_K, Å	g_K	r_F, Å	g_F
4.181	53.0	1.018	1.077	104	8.84×10^4	61.7	1.84×10^4
3.147	58.2	1.033	1.297	137	2.26×10^5	66.3	2.56×10^4
2.671	53.6	1.047	1.549	135	2.21×10^5	73.5	3.58×10^4
2.167	32.2	1.045	2.129	202	7.58×10^5	118.	1.53×10^5
2.139	13.6	1.020	2.206	465	9.22×10^6	280.	2.03×10^6
1.980	3.8	1.007	2.586	1570	3.52×10^8	950.	7.86×10^7
1.705	8.5	1.022	3.593	579	1.77×10^7	392.	5.49×10^6

results show that down to about 2.2° K a lower temperature requires a greater supersaturation to produce condensation. Below about 2.2° K there seems to be a drop in the critical supersaturation required. Because of the rapidly decreasing vapor density and therefore the added difficulty in observing condensation, the critical supercooling ΔT_c seems more likely to have been overestimated than underestimated at these lowest temperatures. Such an error, if present, would then tend to make the critical supersaturations at the lowest temperatures appear too high, rather than too low.

Volmer and Flood (1934) and later Farley (1952) have discussed the kinetics of the condensation process and have predicted that the temperature variation of the critical supersaturation should be given by

$$\frac{P}{P_\infty} = \exp\left[K\left(\frac{\sigma}{T}\right)^{3/2} V_l\right] \tag{3.3}$$

where K is a constant, empirically equal to 0.557 according to Volmer and Flood. σ is the surface tension of the liquid, T is the absolute temperature, and V_l is the molar volume of the liquid.

P/P_∞ is only 0.7% less than $S(= V_{ls}/V_l)$ at 4.18° K, and still closer at lower temperatures; as may be verified using the second and third virial

coefficients for He^4 gas. In Table I the values of (P/P_∞) calculated from eq. (3.3) are shown as S (theory). It is clear that the predicted temperature variation of S is far greater than is observed experimentally.

In these calculations we used the data of Allen and Misener (1938) for σ, and obtained V_l from Edwards (1958) data of liquid He^4 density.

3.3 The Mechanism of Condensation

It has long been recognized that condensation requires nucleation (see, for example, Wilson 1951). Dust particles in water-saturated air are known to be very effective as condensation nuclei. Ions are also known to be effective—this fact leads to the usefulness of cloud chambers in tracking ionizing particles. Even in the absence of foreign particles or ions, however, condensation can take place, by self-nucleation, at what is sometimes referred to as the 'cloud limit'.

The possibility that the condensation in our experiments occurred on foreign nuclei or on ions cannot be entirely ruled out. However, care was taken to avoid vacuum leaks which might produce solid air on the walls of the Inconel tube I (see Fig. 1) which might become dislodged during an expansion and fall into the chamber. The cotton batten plug P and the bakelite spacer A would of course tend to stop any such particles before they could enter the chamber.

No experiments were undertaken to determine the effect of ionization on the condensation thresholds. However, the high energy (46 ev) required to form an ion pair in helium gas at low temperatures (Hanauer *et al.* 1959) and the reasonably high density of the clouds produced in our chamber are taken as evidence that we were studying self-nucleated condensation of ion-free vapor. In this case the condensation nuclei are presumed to be embryonic droplets of neutral molecules arising accidentally from density fluctuations in the vapor. The range of sizes of these embryonic droplets is assumed to be larger for higher supersaturations, until finally some of the embryonic droplets exceed a critical size and then persist. When this size is reached, the vapor is then in unstable equilibrium, since smaller drops will tend to evaporate and larger drops will tend to grow. The critical radius is usually calculated using Kelvin's equation (Thomson 1870)

$$r_K = \frac{2\sigma V_l}{RT \ln (P/P_\infty)} \tag{3.4}$$

where r_K is the critical radius, R is the gas constant per mole, σ is the specific surface energy of the droplet (Frenkel (1946, p. 368) has stated that this is equivalent to the ordinary surface tension corresponding to $r = \infty$), V_l is the liquid molar volume, P is the vapor pressure over a drop of radius r_K, and P_∞ is the saturated vapor pressure over a plane surface ($r = \infty$) at the absolute temperature T. Equation (3.4) has been derived also by Frenkel (1946, p. 368) and Farley (1952).

In its derivation, the density of the vapor is neglected in comparison to the liquid density, and the vapor is treated as an ideal gas. It is hardly likely that the assumption of ideality is justified here, since the condensation process

clearly requires interactions between molecules. Moreover, it should be noted that for substances which condense at small supersaturations, eq. (3.4) suggests very large critical radii, tending to infinity as the supersaturation tends to unity. In order to make some comparison of this theory with our experiments, we show the result in Table I of the critical radii, calculated according to eq. (3.4), but replacing P/P_∞ by our experimental values of the supersaturation S.

Frenkel (1946, p. 373) has also given an expression for the critical droplet radius, which may be written

$$r_F = \frac{2\sigma V_l T}{L\Delta T} \tag{3.5}$$

where L is the latent heat per mole, and ΔT is the undercooling required to produce condensation. Equation (3.5) is derived from eq. (3.4) with the aid of the Clapeyron–Clausius equation (which does not hold exactly here because the Gibb's functions are not exactly equal inside and outside of the drop (Pippard 1957)). Table I shows the critical radii, r_F, calculated using eq. (3.5) and our directly measured critical supercoolings, ΔT_c. It will be noted that these values are between 1.5 and 2.1 times smaller than those given by eq. (3.4). The latent heats, L, used were those of Berman and Mate (1958) for the three highest temperatures, and the smoothed values collected by van Dijk and Durieux (1957) for the lower temperatures.

The number of molecules, g, in a droplet of critical radius is also shown, in Table I, for r_K and for r_F. These numbers are very high compared with other substances, e.g., for water, where g is less than 100. (Das Gupta and Ghosh (1946, p. 238) calculated $g = 10^4$ for water, but their calculation involved a numerical slip.)

Farley (1952, p. 538) has calculated the number of drops per cubic centimeter, N^*, in a supersaturated system which may be expected to reach the critical size r_K. He gives

$$N^* = N_0 \exp(-4\pi\sigma r_K^{2/3} kT) \tag{3.6}$$

where N_0 is the number of vapor molecules per cm^3 and k is Boltzmann's constant. From the data of Table I, N^* is equal to 2.5×10^{-326} drops per cm^3 at 4.181° K and 8.4×10^{-1570} drops per cm^3 at 3.147° K. For lower temperatures the values of N^* are even smaller. This implies that no helium droplets as large as r_K could appear statistically.

We therefore conclude that the present state of the theory of homogeneous nucleation is inconsistent with our data. Whether this is a defect of the underlying assumptions, or, as seems more likely, is due to the "ideal gas" and other approximations made in the theoretical treatment, is not at present clear.

ACKNOWLEDGMENTS

We are grateful to Mr. C. D. Pearse, who assisted in several of the experimental runs.

REFERENCES

ALLEN, J. F. and MISENER, A. D. 1938. Proc. Cambridge Phil. Soc. **34**, 299.
BERMAN, R. and MATE, C. F. 1958. Phil. Mag. **3**, 461.
DAS GUPTA, N. N. and GHOSH, S. K. 1946. Revs. Modern Phys. **18**, 225.
EDWARDS, M. H. 1957. Phys. Rev. **108**, 1243.
——— 1958. Can. J. Phys. **36**, 884.
FARLEY, F. J. M. 1952. Proc. Roy. Soc. (London), A, **212**, 530.
FRENKEL, J. 1946. Kinetic theory of liquids (Clarendon Press, Oxford).
HANAUER, S. H., DABBS, J. W. T., and ROBERTS, L. D. 1959. Bull. Am. Phys. Soc. Ser. II, **4**, 6.
KEESOM, W. H. 1942. Helium (Elsevier Pub. Co., Inc., Amsterdam), p. 174.
KRAMERS, H. A. 1949. Physica, **15**, 971.
PIPPARD, A. B. 1957. Elements of classical thermodynamics (Cambridge University Press, London), p. 110.
STACHÓRSKA, D. 1954. Ann. Univ. Mariae Curie-Sklowdowska, Lublin-Polonia, **7**, 117.
——— 1956. Acta Physica Polon. **15**, 5.
TACONIS, K. W., BEENAKKER, J. J. M., NIER, A. O. C., and ALDRICH, L. T. 1949. Physica, **15**, 733.
TER HAAR, D. 1955. Proc. Conf. de Physique des Basses Températures, Paris, p. 347.
THOMSON, W. (later Lord Kelvin). 1870. Proc. Roy. Soc. Edinburgh, **7**, 63.
VAN DIJK, H. and DURIEUX, M. 1957. Progress in low temperature physics, *edited by* C. J. Gorter (North Holland Publ. Co., Amsterdam), p. 431.
VAN ITTERBEEK, A. and DE LAET, W. 1958. Physica, **24**, 59.
VOLMER, M. and FLOOD, H. 1934. Z. Phys. Chem. **170**, 273.
WILSON, C. T. R. 1897. Proc. Roy. Soc. (London), **61**, 240.
WILSON, J. G. 1951. The principles of cloud chamber technique (Cambridge University Press, London), p. 1.

A CONDENSER MEMORY UNIT FOR IMPROVING SIGNAL-TO-NOISE RATIOS[1]

D. M. HUNTEN

ABSTRACT

The unit contains 30 low-leakage condensers which can store a signal for several hours if necessary. If the signal is repeated over and over, the successive scans can be added in and the signal-to-noise ratio builds up as the square root of the number of repetitions. In principle, the final signal-to-noise ratio is only slightly better than would be obtained from a single scan stretched out to fill the same total time, but in practice the result may be considerably better, especially if the signal fluctuates slowly. It has been used successfully in several investigations of twilight spectra with photoelectric and photoconductive spectrometers. The original version took 1 minute per scan and was rather bulky; a recent modification can scan 32 channels in 10 seconds if required.

1. INTRODUCTION

A problem which arises in many lines of research is the measurement of repetitive signals in the presence of noise. We have in mind especially the photoelectric spectra of aurora and twilight, or similar faint and somewhat variable sources, and will discuss the matter with reference to this particular case; thus, one repetition will be called a scan. If the signal-to-noise (S/N) ratio is inadequate it can be improved by increasing the time of observation, and this is normally done by slowing down the rate of scan and increasing the time constant of the filter. But if the source is an aurora, the total intensity may vary so much during the scan that the results are useless, even if the length is only 1 minute; and this time is often insufficient. Although twilight does not vary nearly so quickly, great difficulty would still be present in interpreting a 10-minute scan. The other possibility is to take a large number of short scans and average them, or what is essentially the same thing, add them together. This has sometimes been done manually from a number of recorder tracings, but an automatic method is obviously much to be preferred. It is not difficult to show that for a constant source this scheme gives the same S/N ratio as a single scan taking the same time, but for a fluctuating source the averaging method is far superior. In addition, the method to be described lends itself naturally to time integration of the signal in each channel, and thus provides a further small factor of improvement over the conventional one. Any device which can add successive scans must be able to store information and recall it when needed; it is convenient to call it a "memory" and our device will therefore be called a "condenser memory", since the information is stored in the form of voltages on a bank of low-leakage condensers. The stored spectrum is divided into a number of channels, one for each condenser; the bank is scanned in synchronism with the scan of the spectrometer. A

[1]Manuscript received November 11, 1959.
Contribution from the Department of Physics, University of Saskatchewan, Saskatoon, Saskatchewan. Supported by the Geophysics Research Directorate of the Cambridge Research Center, Air Research and Development Command, under Contract AF19 (604)-1831.

suitable device adds the new spectrum to the old sum and stores the new sum back in the memory. This adder is the principal novelty of the instrument to be described. The natural field of application of this memory is to scans of several seconds or longer, and to a fairly small number of channels of which 30 is typical.

It is of interest to consider some previous methods which have been used for a similar purpose; the survey does not pretend to be complete, however. A photographic time exposure to the repeating trace on an oscilloscope is described by Bloch and Garber (1949); they were observing nuclear induction signals, but the same technique is fairly common with radar displays. While simple, the method is inefficient because the individual signals are always added even when they should, part of the time, be subtracted. Suryan (1950) used a magnetic recording on a drum rotating in synchronism with the signal; the recording head was moved slowly parallel to the axis so that the signals were impressed along a helical track. The reading head covered the whole drum and added all the signals together. The biggest difficulty with this scheme is its mechanical complexity; but it is not suitable in any case for signals which repeat as slowly as ours, since the drum would rotate so slowly that pickup from it would be too small. Harrington and Rogers (1950) stored radar signals in a storage cathode-ray tube; in a sense, this memory is of the condenser type, but the condensers are so small that the signals leak off in a few seconds at the most; also, the fidelity is not high. A dielectric recording drum described by Anderson (1957) is much better in both respects but was not available when our apparatus was being developed.

A direct ancestor of our system is the memory commutator of Beard and Skomal (1953). Though it rotated much faster, the important difference is that they fed the condensers through a relatively small resistor and allowed each condenser to charge exponentially. Thus if the input signal is constant, the voltage on the condenser will approach it asymptotically. In our system, the voltage continues to rise until the circuit overloads, and can be many times larger than the input; the stored voltage is the true time integral of the input. The device of Beard and Skomal gives the same approximation to this integral that an RC circuit does. The "analogue memory" of Kozak (1958) is rather similar, though used for an entirely different purpose.

The principle of our method is the following. As each condenser is switched into the circuit, the voltage on it is duplicated on a second "transfer" condenser by a special amplifier of unit gain. Then the transfer condenser is switched in series with the incoming signal and the sum voltage duplicated on the memory condenser by the same amplifier. The action is accurate enough so that a stored signal can be read off and back on again a large number of times with little degradation. The condensers used have polystyrene dielectric so that the "absorption" effect is small and a signal can be stored for hours without leaking away. The unit has been found valuable in making accurate measurements on twilight spectra, adding from 10 to 30 one-minute scans for a total "exposure" of as much as $\frac{1}{2}$ hour. Application to aurora has been prevented by the scanning mechanism which could not be

made to go around in 10 seconds; 1-minute scans are too long to be useful with aurora. The new switching scheme described below removes this limitation.

2. OPERATION AND CIRCUITS

The most natural way to add a series of voltages on a condenser is to feed them in succession through a constant-current device, such as a large resistor or a suitable type of feedback amplifier. But for a bank of condensers this has the serious disadvantage that the voltage generated is inversely proportional to the capacitance, so that all the condensers must be closely matched. The method to be described operates on voltages instead of currents and is therefore independent of capacitance. Moreover, it gives a readout of the stored signal which may be observed during operation. It is based on a precision voltage follower shown as the triangle in Fig. 1. This device accepts a signal at a very high-impedance level, drawing essentially no current, and reproduces it at a low impedance with negligible error, estimated to be less than 0.01%.

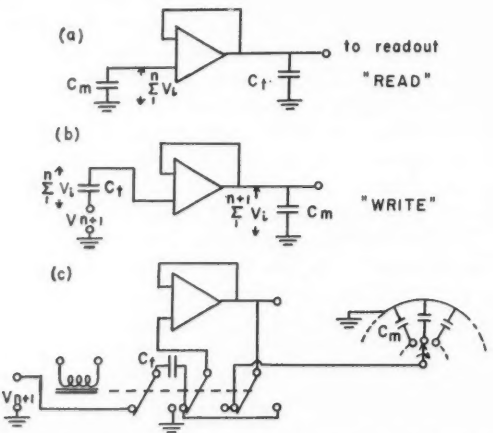

FIG. 1. (*a*) Effective circuit of the memory while reading from one condenser in the bank. The triangle represents a voltage follower with a gain very close to 1.
(*b*) Circuit for adding the input and storing the result back in the bank.
(*c*) Actual circuit shown with the relay in the (*b*) position.

First let the follower be connected as in Fig. 1(*a*). C_M represents one of the condensers in the memory bank and C_T is a "transfer" condenser. Whatever voltage is on C_M will be reproduced on C_T and is also available for monitoring. If the circuit is then switched into the arrangement of Fig. 1(*b*) the voltage on C_T is connected in series with the input from the spectrometer, and the sum will appear on C_M. The next time this action is repeated, a new C_M is in the circuit. The switching is done by the three-pole relay shown in Fig. 1(*c*) which is drawn in the (*b*) position. The input voltage does not come directly from the spectrometer, but passes first into a feedback integrator (Korn and

Korn 1952) which is reset to zero just after the end of part (*b*) of the memory cycle. Thus, the voltage in each condenser of the bank is the integral of the signal for the total time it has been in the circuit.

The follower itself is essentially a high-gain direct-coupled amplifier with 100% negative feedback. The circuit is shown in Fig. 2; it was developed after a brief qualitative description by Bousquet (1956). It can be regarded as a three-stage cathode follower; the output is fed back to the first tube by the

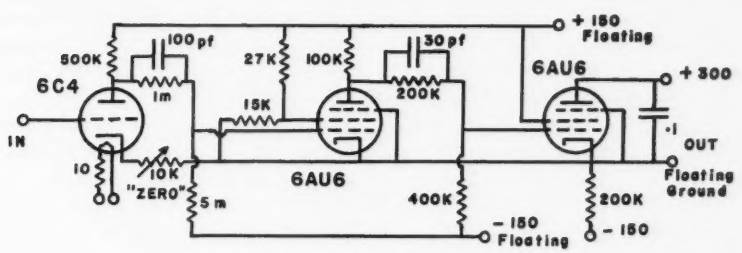

FIG. 2. Circuit of the follower.

common cathode connection. For some purposes it is also useful to regard the circuit in the following way: transfer the ground from the end of the source to the common cathode connection, leaving the source floating between the input and the plate of the third tube. The essentials of this arrangement are shown in Fig. 3. The 220-kΩ resistor now acts as the plate load of the third stage, even though it is on the other side of its power supply. The amplifier

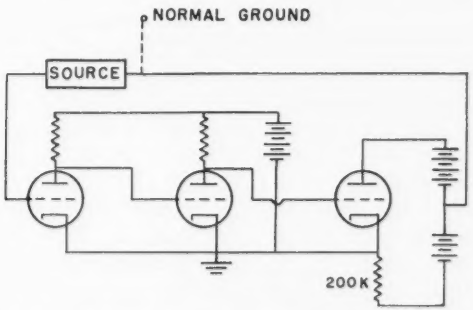

FIG. 3. The circuit of Fig. 2 with a different ground point.

is thus an ordinary three-stage one except that 100% feedback is applied through the floating source. The loop gain will be about 10^5 for the circuit shown; thus the external gain should be 0.99999. This large loop gain means that there is great danger of high-frequency oscillation; the condensers in the plate circuits control the shape of the high-frequency cutoff to prevent this.

The high loop gain is realized only if the plate and bias power supplies can float along with the output as indicated in Fig. 2. We have used a single 350-volt supply feeding two miniature regulator tubes; the complete circuit thus includes five tubes and a rectifier. Normal grounded supplies provide the plate and cathode-return voltages of the last stage; they need not be regulated. The rheostat at the cathode of the 6C4 allows the level of the output to be set equal to that of the input; this must be done rather accurately or the voltages stored in the memory will drift by twice the offset each time the information is cycled. Often a small drift of this sort is not important, since all channels are affected the same, but a large drift might take the circuit out of its range of correct operation. The first stage operates with low heater and plate voltages so that the grid current is less than 10^{-10} ampere.

If the output of the follower is connected to a condenser at a considerably different potential, it may not be able to supply the required current and the output will not be able to follow the input for a moment. During this moment the input may draw a large burst of current. To eliminate this trouble, the series resistors shown in Fig. 1(*c*) are included; they must be small enough to let the condensers charge fully during the time available. More charging current could be made available by replacing the third tube with a power tetrode; this would be useful in a memory with a very short time per channel.

3. SWITCHING

The very low leakage of a polystyrene condenser is realized only if there are no leakage paths in parallel with it. This dictated the design of the commutator in the first version, since no ordinary switches of adequate performance were available. The condensers were arranged in a circle and contact springs attached to and supported by the inside terminal of each; the arrangement was similar to the sketch in Fig. 1(*c*). An arm carrying another contact was rotated in steps to make connection to each in turn. The intermittent motion was obtained from a synchronous motor driving through a six-point Geneva movement and then a 1:5 gear ratio. This operated well at a rate of one step in 2 seconds, but would not quite keep time at three steps per second. Probably a slightly more powerful motor would have been able to run at the fast speed, but this was not pursued.

The shaft which drove the Geneva movement also carried a cam which operated a microswitch and thereby the relay shown in Fig. 1(*c*). It was left in the "read" position while the commutator was switching, and for a short time after, so that the transfer condenser could become fully charged; the "write" part of the cycle occupied the rest of the time, a little less than half. Just after the end of the "write" operation, the integrator at the input was reset to zero by another relay making a brief contact. At first this was operated by a second cam, but later by a transient generated when the transfer relay moved to the "read" position. Not only is this simpler; it also guarantees synchronization between the two relays.

A much more compact and faster arrangement is possible by taking advantage of the properties of the "Glaswitch", or dry-reed switch, as suggested by

Helmer and Hemmendinger (1957). This switch has the high insulation resistance needed, and the commutator may be an ordinary one occupying little space. The high speed of the Glaswitches suggests their use also for resetting the integrator. The commutator available required the use of 32 channels instead of 30.

It is worth while to pay some attention to the method of setting all the condensers to zero initially. The easiest to build is a switch to ground the wiper of the commutator, or the equivalent point if the Glaswitches are used. But it is often inconvenient to have to wait for a complete cycle of the memory, and a separate shorting bar which can connect to all the condensers at once is preferable.

A switch should be provided to lock the transfer relay in the "read" position. Then the contents of the memory remain undisturbed and may if desired be observed one or more times. This switch can also be used to start the memory operating at any suitable time after it has been set to zero.

4. OPERATION

The contents of the memory are easily recorded on a strip-chart potentiometer; the output of the follower is a low-impedance point and can drive a calibrated voltage divider or a helical potentiometer so as to give a suitably low voltage. The recording in memory should be made at as high a voltage level as possible to reduce the importance of drift and other stray voltages; the output may then be attenuated to the magnitude required by the recorder. It is often useful to follow the accumulation of the signal on the recorder; if any large interfering pulses are stored, they can be allowed for. Records of this sort show two steps per channel, corresponding to the old and new contents. A record made at the end of the run with the transfer relay off shows only one. The final recording may be repeated several times if desired until the best settings of gain and time constants are found.

An example of a run on the sodium *D* lines in the twilight is shown in Fig. 4 (Lytle 1958). The way in which the S/N ratio builds up as more and more spectra are included may be observed. The lines appear above a continuum caused by nonresonant scattering in the atmosphere. The width of the lines and their triangular shape arise entirely from the spectrometer; there is no detectable degradation introduced by the memory except for the steps corresponding to the individual channels. The area of a line recorded in this way is a good measure of its intensity; it is easily found by adding up all the steps within the line. The fact that the intensity ratio of the two lines is much less than the normal 2:1 results from self-absorption in the sodium layer in the upper atmosphere (Chamberlain, Hunten, and Mack 1958). The measurements could not have been made with nearly as much accuracy without the memory; a single 12-minute scan would have been hopelessly distorted by variations in intensity and atmospheric transparency.

The memory was also used by Harrison to study the O_2 band discovered by him in the twilight at 1.58 microns (Vallance Jones and Harrison 1958). He was able to use much better resolution than would otherwise have been

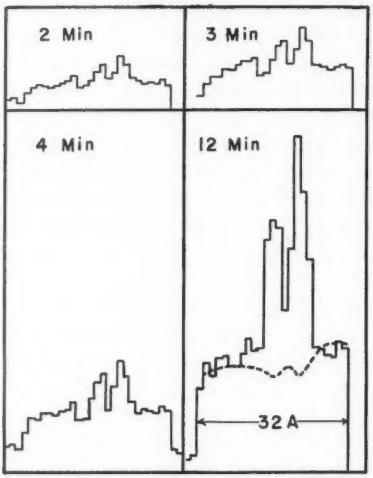

FIG. 4. Part of a run on the *D* lines in twilight.

possible. The intensity decays with a half-life of about 30 minutes, so that single long scans are again not practical. But 30 scans of 1 minute each added up by the memory gave a useful result and allowed the band to be identified.

A search for the potassium resonance line at 7699 Å in twilight has recently been carried out by Lytle (1958). In this case the radiation was not detected, but use of the memory enabled the limit of detection to be set much lower than would otherwise have been possible. It appears that other studies of twilight may also be made possible by this new technique, which offers a considerable increase in available sensitivity and permits photoelectric spectrometers to compete on nearly equal terms with fast spectrographs. It is expected to be just as valuable for studies of the auroral spectrum now that it can be used with a 10-second scan. Until now, only the brighter auroral forms gave a large enough signal for quantitative studies; the fainter forms are not only much more plentiful, but may also give different results.

Many studies would profit from the use of a memory with more channels than the 30 to 32 used here; and a faster repetition rate might also be useful. It is doubtful if the present adding unit would operate well beyond three or four channels per second; and it might be economic to make a condenser memory with 64 channels or even 96. It is likely that the capacitance of the condensers could be reduced to 0.1 microfarad without impairing the operation; but there is no point in reducing their cost much below the cost of the switching system. With this in mind, the best size is probably about 0.2 microfarad.

A great increase in both speed and number of channels is possible by adopting digital-computer techniques, as has been done widely in recent years for multichannel pulse-height analyzers (Hutchinson and Scarrott 1951; Schultz, Pieper, and Rosler 1956). The memory requirements for the two

purposes are almost identical, except that fast random access to any channel is important in most cases in nuclear physics, but is of no importance whatever here. The ultrasonic delay-line memory is then just as good as the more expensive magnetic-core type. It has also the advantages that the stored spectrum is continuously displayed on a cathode-ray tube, and that information may be read in and out at arbitrary rates, simultaneously if desired.

If a speed of five channels per second is sufficient, another possibility is to record the individual spectra in digital form on punched paper tape, similar to teletype tape. This may later be read into a general-purpose digital computer and the averaging done by a suitable program. This requires much less equipment, as long as the computer is available, but has the disadvantages that the averaged spectrum is not immediately visible; if anything has gone wrong, it will not be known until the next day. If the observations are of an experiment that can be repeated, this is of little importance; but it may be very important for observations of uncontrolled natural phenomena.

It is a pleasure to acknowledge the help of several colleagues with the construction and testing of the instrument: A. W. Harrison, G. F. Lyon, E. A. Lytle, and J. F. Noxon.

REFERENCES

ANDERSON, V. C. 1957. Rev. Sci. Instr. **28**, 504.
BEARD, C. I. and SKOMAL, E. N. 1953. Rev. Sci. Instr. **24**, 276.
BLOCH, F. and GARBER, D. H. 1949. Phys. Rev. **76**, 585.
BOUSQUET, A. G. 1956. General Radio Exp. **30** (10).
CHAMBERLAIN, J. W., HUNTEN, D. M., and MACK, J. E. 1958. J. Atmospheric and Terrest. Phys. **12**, 153.
HARRINGTON, J. V. and ROGERS, T. F. 1950. Proc. I.R.E. **38**, 1197.
HELMER, R. J. and HEMMENDINGER, A. 1957. Rev. Sci. Instr. **28**, 649.
HUTCHINSON, G. W. and SCARROTT, G. C. 1951. Phil. Mag. **42**, 792.
KORN, G. A. and KORN, T. M. 1952. Electronic analog computers (McGraw-Hill Book Co., Inc.).
KOZAK, W. S. 1958. Can. Electronics. Eng. **2** (2), 38.
LYTLE, E. A. 1958. M.Sc. Thesis, University of Saskatchewan, Saskatoon, Saskatchewan.
SCHULTZ, H. L., PIEPER, G. F., and ROSLER, L. 1956. Rev. Sci. Instr. **27**, 437.
SURYAN, G. 1950. Phys. Rev. **80**, 119.
VALLANCE JONES, A. and HARRISON, A. W. 1958. J. Atmospheric and Terrest. Phys. **13**, 45.

IMPURITY CONCENTRATION PROFILES IN ICE BY AN ANTHRONE METHOD[1]

M. Smith and E. R. Pounder

ABSTRACT

Solutions of sodium carboxymethyl cellulose (CMC), sodium chloride, ethylene glycol, and ethyl alcohol in water were prepared and frozen under controlled conditions. The ice in each case was divided into horizontal sections, melted, and the amount of each impurity measured. The organic liquid and salt concentrations were found from refractive index values using a dipping refractometer, and the CMC content, after treatment with an anthrone solution, was measured with a spectrophotometer. Developments in the anthrone method are described. Qualitative tests were also made by freezing solutions of soluble dyes.

In the freezing of aqueous solutions of CMC and the dyes, rejection of the impurity is almost complete. When solutions of salt or alcohol or glycol in water, or of CMC and alcohol or glycol in water, are frozen a surface concentration peak and a second peak about 7 mm below the surface, corresponding to a previously observed discontinuity in the crystal structure of impure ice, are found. The ability of alcohol or glycol to carry CMC or a dye to places in the ice structure not available to them in the absence of the organic liquid is noted.

INTRODUCTION

It has been shown by Perey and Pounder (1958) that when water containing added foreign material is frozen, a transition layer indicating a radical change in crystal structure is clearly visible at a distance of the order of 1 cm below the surface. It was assumed that such change is associated with changes in concentration of the added foreign material. The present work was undertaken to verify the assumption by quantitative measurement of the distribution of the foreign material in the ice.

It seems probable that impurity distribution is a major factor in determining the mechanical properties of any form of impure ice (see Pounder 1958). This is particularly true in the extremely important case of sea ice.

According to a theory suggested by Anderson (1958) and elaborated by Assur (1958) the properties of sea ice are very largely dependent on the distribution of salts and brine within the ice. In the present work additive materials other than those found in sea water have been studied but one example is included where pure sodium chloride was the additive and it is hoped to extend the work in this direction soon.

METHODS OF MEASUREMENT

The impure melts studied by Perey and Pounder (1958) contained various alcohols and other organic solvents, and a variety of carbohydrates, particularly sodium carboxymethyl cellulose (grade D435 as supplied by Chemical

[1]Manuscript received June 29, 1959.
Contribution from the Ice Research Project, Department of Physics, McGill University, Montreal, Que.

Developments of Canada, said to contain a minimum of 66% sodium carboxymethyl cellulose, the other salts present being principally sodium chloride and sodium glycolate).

It was decided to confine the present quantitative analyses largely to D435, ethyl alcohol (Reliance Chemicals 650P = 82½% by volume), and ethylene glycol (Purified Fisher Laboratory Chemical). Since the behavior on freezing of CMC and sodium chloride is quite different as far as rejection is concerned, it is unfortunate that grade D435 contains some sodium chloride. No grade of CMC free of sodium chloride was available, however, and in any event the concentrations of D435 used in freezing tests were so low (about 0.15‰ by weight) that the small amount of sodium chloride contained in it introduced negligible errors in the tests for CMC and alcohol or glycol. All of the tests were made with D435 samples from a single batch so that the composition of the D435 was assumed to be uniform.

Ethylene glycol was chosen to provide, with the alcohol, examples of both relatively non-volatile and volatile solvents; they serve also as examples of both heavier than water and lighter than water solvents.

The method which was found to be the most suitable for D435 estimation was a spectrophotometric technique which will be referred to as the anthrone method. This method consists essentially of adding anthrone in solution to the test samples. When a carbohydrate (CMC in these tests) is present, a green color develops through chemical reaction between the anthrone and the carbohydrate. The optical density of the solution, as measured with the spectrophotometer, can be used to calculate the concentration of CMC and hence of D435 in the test sample. It was found convenient to use the concentration of D435 in calibrating the method as well as in citing results.

The anthrone method was suggested by Dreywood (1946) of the Eastman Kodak Laboratories as a qualitative general test for carbohydrates. It has been carefully developed for quantitative use by Black (1951) at the DuPont Laboratories and is frequently quoted in research literature.

Its use, however, presents several difficulties; the results vary for example with the temperature at which the reaction takes place, with the age of the reagent and of the solution, with the acid concentration, and with the degree of substitution of the sodium carboxymethyl cellulose. The presence of various other carbohydrates or their derivatives interferes with the reaction. Black states that calibration curves should be made every 2 or 3 weeks and that the reagent used should be between 4 and 24 hours old. Under these conditions Black achieved a relative accuracy of 2%, if the degree of substitution was known. The anthrone is dissolved in sulphuric acid and the quantities used are large (50 ml of 60% acid for each test), so that in 1 day of testing it might be necessary to use, and dispose of, about 1500 ml of 60% sulphuric acid.

A modification of the method has been suggested by Loewus (1952). Loewus used ethyl acetate as solvent for the anthrone and states that this prevents the gradual darkening of the reagent which occurs when the solvent is sulphuric acid, a darkening which varies with any slight changes in the purity of the sulphuric acid. The expected accuracy is not stated in his paper.

As used in tests in this laboratory Loewus' modification was very disappointing in accuracy, in consistency, and with regard to the aging of the reagent. Further the results were affected by the alcoholic content of the samples tested, making its use impossible for this investigation.

In two recent papers, Scott and Melvin (1953) and Mokrasch (1954) returned to dissolving anthrone in sulphuric acid but stored it in a cool dark place and emphasized the importance of controlling the temperature of samples and reagent before mixing. Scott and Melvin used 90° C for the development of color; Mokrasch used 80° C.

Scott and Melvin gave a detailed account of sources of errors and felt that standardization is necessary for each set of samples. As they could not compare one day's absorbance with another as an indication of precision, they measured the standard deviation of 97 sets of duplicate blanks and 345 sets of duplicate sample determinations as 0.48% of absorbance at 0.600 absorbance. They found their most important source of error was variation of readings obtained in blank tests. Mokrasch found his reagent to be stable for 2 months when stored at 4° in the dark. He gave no estimate of accuracy.

Roe (1955) has suggested adding thiourea to the reagent as a means of increasing its stability and found that in this way it could be used for 2 weeks when stored in a refrigerator. He states that when the heat of mixing is used as a means of developing color, the accuracy to be expected is only ±5%. In Roe's (1954) careful experiments with dextran the coefficient of variation, using duplicates, was ±0.36%.

The following procedure has been found most satisfactory in this laboratory and was used in the experiments reported.

Preparation of the Reagent

A 200-ml volume of concentrated sulphuric acid (Fisher Reagent 95–98%) is diluted with 60 ml of distilled water. Both volumes are measured into beakers at room temperature, and the beakers are then cooled in crushed ice before mixing and again after mixing. With the beaker of diluted acid remaining in the ice, 0.200 g of anthrone (Fisher Reagent grade) and 2.000 g of thiourea (Fisher Certified Reagent) are added and stirred until the solution is clear and dissolving seems complete, which takes about half an hour. The resulting reagent is stored in the dark at from 1° to 5° C and, in general, is used within 1 week of preparation.

Test Procedure

Samples of 1 ml each of the solutions to be tested for carbohydrate content are pipetted into screw-top pyrex test tubes. A quantity of 6 ml of the reagent is measured into each of several additional test tubes, using a burette. All test tubes are then cooled for 15 minutes in crushed ice, after which the test solution and reagent samples are mixed in pairs (by pouring backwards and forwards twice) and returned to the crushed ice. The test tubes, with their tops on loosely, are arranged in a rack and plunged into boiling water for 10 minutes, returned to the ice bath again for 5 minutes, and then allowed to stand (covered to exclude light) at room temperature for 20 minutes. After this time, the absorbance of each sample is measured at 620 mμ using a Beck-

man Model B spectrophotometer. This procedure, developed after many trials, insures a precisely controlled and reproducible temperature regime for the color-producing reaction, and gives quite reproducible results for the carbohydrate content.

In each experiment one blank is included by using distilled water instead of a test solution. The optical density of the blank, compared with the reading given by distilled water (without any reagent), serves as a check on the experimental conditions and on the condition of the reagent. A great improvement in consistency is obtained by using the optical density of the blank as zero, rather than that of pure distilled water.

The use of thiourea as one of the components of the reagent not only increases the length of time for which the reagent can be kept without deterioration, but also decreases the variation between successive tests of the same solution.

The measured optical density for D435 solutions was not affected by the presence of ethyl alcohol in the concentrations tested, up to 5% of alcohol.

The method is very sensitive. Up to a concentration of about 200 μg/ml it is possible to distinguish differences in optical density corresponding to differences in concentration of 1 μg/ml, i.e. one part in a million, but the reproducibility is not as high. There are the uncertainties introduced by the measurement of the volumes of test samples and reagent and by slight variation in the heat treatment, etc. Several authors mention the erratic behavior of reagent aging, and of color stability, and of unaccountable variation in blanks. For single tests the possible error is estimated by us as 2%.

The calibration curve is given in Fig. 1. All D435 solutions were filtered through Whatman's No. 1 filter paper, as this was found necessary to obtain reproducible results, probably because D435 does not form a completely clear aqueous solution. However, the concentration figures plotted on the graph are the original values before filtration. The curve was checked over a period of 5 months, using a number of preparations both of reagent and of standardizing D435 solutions. Each value plotted is thus the average of 6 to 10 measurements. The deviation of individual readings from average values was from 1 to 1.5%.

Tests were made with four different commercial grades of sodium carboxymethyl cellulose (D235, D435, L245, T253 made by Chemical Developments of Canada), in various concentrations and using solutions both filtered and unfiltered.

Using filtered solutions, and plotting optical density against the actual amount of sodium carboxymethyl cellulose in each preparation, according to the manufacturer's specifications, it was found that the values for all four preparations lay along one straight line. This shows that the anthrone test for sodium carboxymethyl cellulose is not affected by the presence of varying amounts of other salts such as are found in these preparations.

Figure 2 illustrates the effect of filtering, using D435. Points marked by crosses were obtained using unfiltered solutions; points marked by circles represent filtered solutions. The concentration values plotted are the values before filtering, in each case.

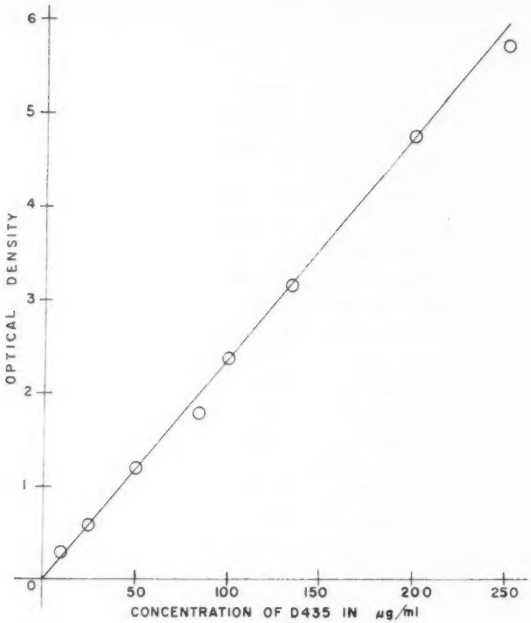
OPTICAL DENSITY
0
1
2
3
4
5
6
50
100
150
200
250
CONCENTRATION OF D435 IN μg/ml

FIG. 1.

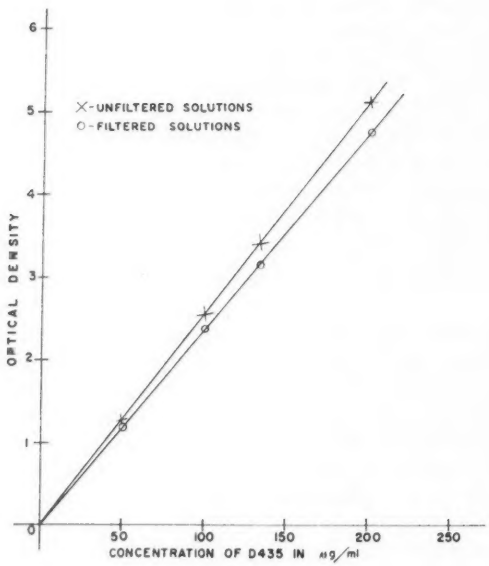
X-UNFILTERED SOLUTIONS
O-FILTERED SOLUTIONS
OPTICAL DENSITY
0
1
2
3
4
5
6
50
100
150
200
250
CONCENTRATION OF D435 IN μg/ml

FIG. 2.

At the beginning of this investigation alcohol concentrations were measured by means of distillation and specific gravity measurements, a method both lengthy and uncertain. For most of the work here reported a Bausch and Lomb dipping refractometer was used (with prism A of range 1.32–1.36 refractive index, and occasionally No. 3 auxiliary prism). In it, rays of light (from an incandescent lamp) pass through a beaker containing the sample, and enter the prism. The position of the grazing or critical ray forming the boundary between the light and dark parts of the field of view may be measured.

A calibration curve for alcohol concentration was prepared using solutions containing both D435 and ethyl alcohol in the proportions used in ice preparation, since the D435, or probably the small amount of sodium chloride in it, does raise the values a trifle over those found when using the alcohol alone. This effect is very slight, being undetectable for D435 concentrations of less than 75 μg per ml.

Using a water bath and measuring temperatures to 1/10 Centigrade degree when equilibrium was established, measurements could be made to 1/100 of a scale division. By using an average of 10 determinations these were usually reproducible to ± 0.01 of a scale division. When the auxiliary prism was used (in cases when only small amounts of liquid were available) the uncertainty became at least ± 0.02 of a scale division. Similar calibration curves were prepared for aqueous solutions of ethylene glycol and of sodium chloride, as it was found that the refractive index of these solutions changed appreciably with concentration. This method is much more sensitive, more reliable, and far quicker than the specific gravity method which had previously been used for sodium chloride determinations. A variation of ± 0.02 refractometer scale divisions corresponds, at 25° C, to $\pm 0.016\%$ ethyl alcohol, $\pm 0.008\%$ ethylene glycol, $\pm 0.004\%$ sodium chloride. In these three cases the refractive index varies linearly with concentration in the ranges tested. All concentrations were converted to a standard temperature of 25° C.

PREPARATION OF ICE

For each ice study 1.000 g of D435 was dissolved in 975 ml of distilled water. This was filtered through Whatman's No. 1 filter paper and the volume made up to 975 ml. To this was added 25 ml ethyl alcohol and 5100 ml distilled water, or 25 ml ethylene glycol and 5100 ml water, or 5125 ml distilled water.

About 100 ml was retained for testing, and the other 6 liters of solution were placed in a rectangular plastic vessel about 10 cm deep, surrounded by sufficient insulating material to ensure essentially one-dimensional cooling.

The solution was frozen at a constant ambient temperature, usually $-28°$ C, until solid. The ice was then taken to a cold room kept at $-15°$ C and the sides of the ice block were trimmed off with a band saw, to eliminate edge effects.

In some cases the ice was then divided into horizontal sections with the band saw, the sections were placed in screw-top bottles and then melted at room temperature and analyzed. The minimum thickness of sections obtainable with the band saw is 3 mm (the usual section cut in this way was 9 mm)

and about 1.5 mm of ice is lost between sections in the saw cuts. If the ice is soft the uncertainties of thickness increase.

Where the concentration of impurities in the ice changed rapidly with depth, thinner sections were prepared by either planing the surface of the ice or by melting. Planing is a very tedious, slow process, but very fine sections may be obtained in this way. For melting, the block of ice was held vertically on a horizontal pyrex tray which was gently warmed from below, the melt being poured off in small batches. The thickness of the layers so melted was determined from a knowledge of the dimensions of the block and the weights of the samples. Great care is needed to keep the block vertical as melting proceeds.

The advantages of melting and planing are that they enable very thin layers to be separated, and that no material is lost between sections as it is with saw cuts. It might be expected that the volatile ethyl alcohol would be partially lost by these methods, but the values obtained were consistent with samples prepared by sawing.

RESULTS

Concentration profiles are given for four blocks of ice containing water, D435, and ethyl alcohol; for two blocks of ice containing distilled water and D435 only; and for one block containing pure sodium chloride and water. In all these cases the blocks were frozen at an ambient temperature of $-28°$ C.

In addition profiles are shown for three blocks of ice containing D435 and ethylene glycol, which were frozen at ambient temperatures of $-28°$ C, $-19°$ C, and $-5°$ C respectively.

Some samples of alcohol and water and of glycol and water were frozen in insulated vessels (cylinders about 8 cm in diameter and 7.5 cm deep) and the additive (alcohol or glycol) concentration in the ice measured as freezing proceeded.

As a visual indication of distribution, water-soluble dyes (methylene blue, methyl violet, and eosin) were dissolved in pure water and in water containing a trace of ethyl alcohol, and the solutions frozen.

The concentration profiles for ices I, II, III, and IV, each containing D435 and ethyl alcohol, are shown in Fig. 3, where crosses indicate that the samples were prepared by planing, circles by sawing, and squares by melting. The results for ice I and ice II which were made up from the same stock solution have been combined. This was done because the alcohol values were few and unreliable, some of them having been measured by distillation and specific gravity measurements before the dipping refractometer was available.

It will be seen that there is no inconsistency between values for samples prepared by the different methods. Values for ice I and ice II fit well into the same curve.

The graphs show that the profiles are similar for both D435 and alcohol. At approximately the position of the visually observed transition layer there is a marked peak in the concentration of both D435 and alcohol. It will also be seen that there is a high concentration of both added substances in the

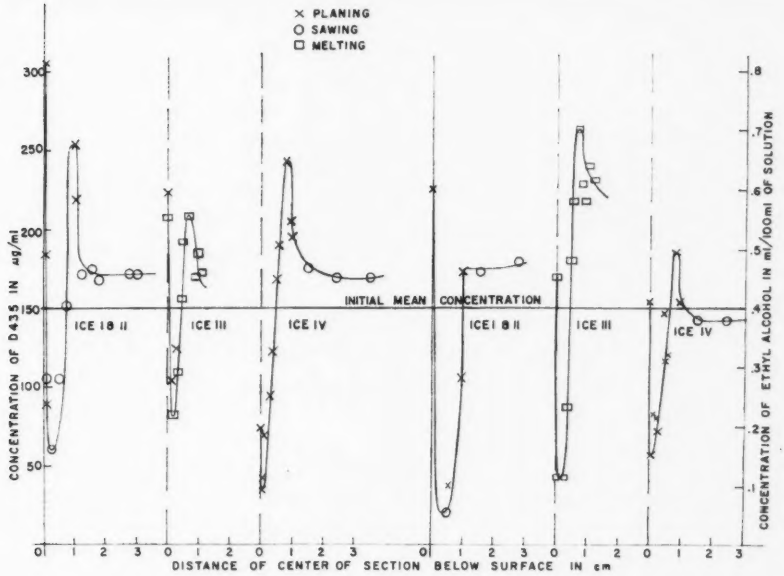

FIG. 3.

surface layer. There is considerable variation in the values obtained at the surface and this appears to result from variations in the thickness of the surface layer examined. It seems probable that the high concentration is confined to a very thin layer, perhaps even a monomolecular layer, and that the concentration drops sharply below this.

Below the transition layer the concentration decreases rapidly to a value which remains fairly constant throughout most of the depth of the block.

To ensure that the variation of the concentration with depths is a consequence only of the freezing process, solutions containing D435 and ethyl alcohol, and D435 and ethylene glycol, both of the same dilution as used in the freezing tests, were left undisturbed at room temperature for some time. The vessels were covered and insulated to guard against evaporation and sudden changes in temperature. After periods of up to 2 weeks, samples carefully pipetted from various levels showed no surface concentration nor any variation in concentration with depth.

Two tests (V and VI) were made with ice containing D435 alone. The results were almost identical and are illustrated for ice V in Fig. 4. A slight concentration was observed in the surface layer but below this the D435 was almost totally rejected from the ice until near the bottom of the vessel where the concentration rose rapidly. Visual inspection foretold this result before the block of ice was sectioned. In both tests, most of the ice was clear and glassy and there was a bottom layer which was white and opaque.

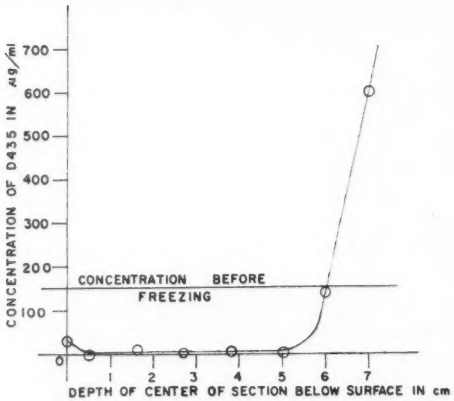

FIG. 4.

Figure 5 shows the concentration profile for ice VII. This is an example of the results obtained by freezing pure sodium chloride brine of concentration 35‰ (parts per thousand). In this case the freezing was done in a much deeper vessel so that the brine was initially 21.6 cm deep and the very high

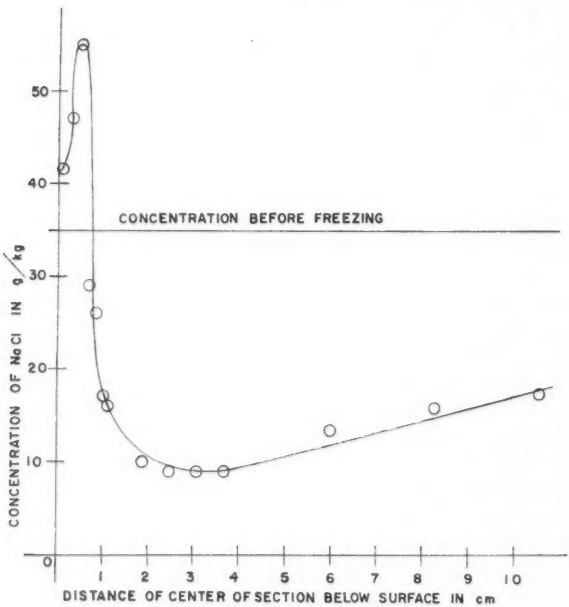

FIG. 5.

concentrations of salt found towards the bottom of the vessel after freezing do not appear over the depths here plotted. In this case also there was a transition layer clearly visible above the 1-cm level and the graph shows a corresponding concentration in the sodium chloride. There is, however, no evidence of a surface layer concentration.

Tests on ice frozen from melts containing D435 and ethylene glycol were undertaken to avoid the uncertainty of losses by evaporation, which are involved in the study of ice containing alcohol. Three concentration profile pairs are shown: for ice VIII (Fig. 6) the ambient freezing temperature was

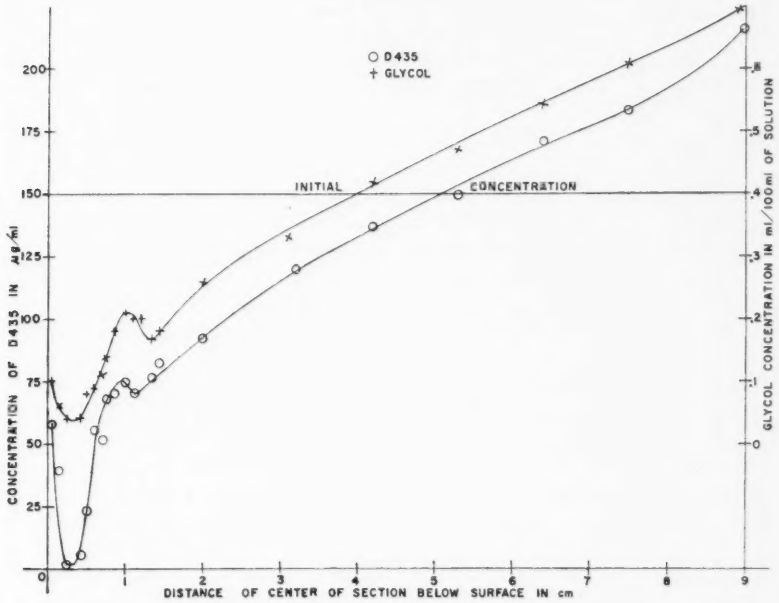

FIG. 6.

−28° C, for ice IX (Fig. 7) it was −19° C, and for ice X (Fig. 8) −5° C. As with the alcohol samples discussed previously, the D435 concentration follows closely that of the organic solvent, although the shape of these profiles differs considerably from those obtained in the alcohol tests. With alcohol the concentration throughout the bulk of the ice was uniform, whereas with glycol it rose more or less uniformly with depth. This indicates some rejection of glycol (and D435) by the ice, a rejection which is more pronounced when freezing takes place more slowly. In each of the three tests some glycol was expelled completely from the ice, remaining as a liquid film at the bottom of the vessel. The profiles all show evidence of a surface concentration and also of a transition layer, if not in the form of a concentration peak at least as a

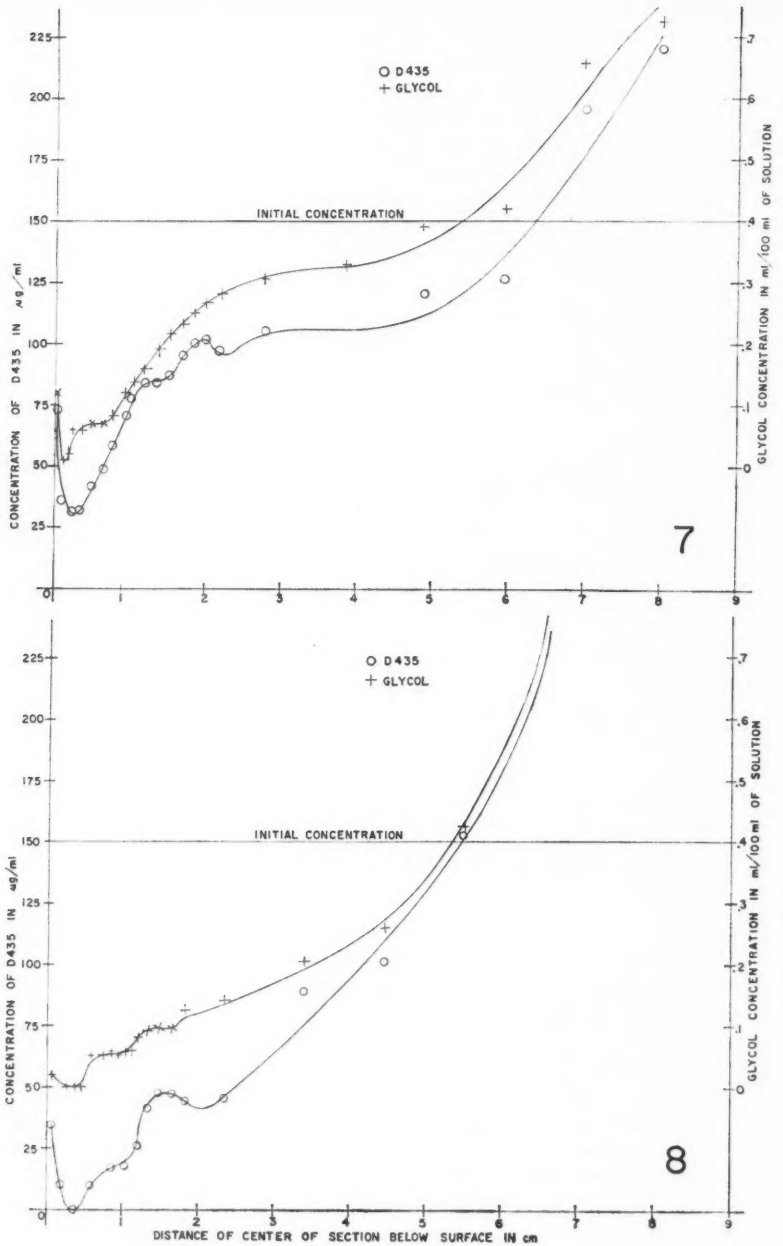
O D435
+ GLYCOL
INITIAL CONCENTRATION
CONCENTRATION OF D435 IN µg/ml
GLYCOL CONCENTRATION IN ml/100 ml OF SOLUTION
7
O D435
+ GLYCOL
INITIAL CONCENTRATION
CONCENTRATION OF D435 IN µg/ml
GLYCOL CONCENTRATION IN ml/100 ml OF SOLUTION
8
DISTANCE OF CENTER OF SECTION BELOW SURFACE IN cm

FIGS. 7 AND 8.

change of slope in the curve. In ice IX and ice X the transition layer was observable visually in vertical sections through the blocks and was seen to be quite jagged. In the analysis of thin horizontal sections covering a fairly broad area this irregularity would have the effect of flattening the transition peak.

Visual examination of ice IX and ice X also showed patches of clear crystal growth surrounded by regions containing numerous air bubbles. It appears probable that thin sections may give erratic values in such non-uniform ice. This may account for points lying off smooth curves. Note that in Fig. 7 the same irregularities occur in both glycol and D435 concentrations.

To study possible evaporation losses, concentration measurements were made for a large number of samples of alcohol and water and of glycol and water, frozen in small cylindrical vessels (8 cm in diameter by 7.5 cm deep). Freezing was done with both covered and uncovered vessels, and in a number of the tests the surface layer of ice was removed repeatedly for analysis while freezing was proceeding.

These experiments showed that the first ice that forms on the surface of alcohol–water solutions is in the form of a fairly compact layer consisting of horizontal thin "sheets" which are well bonded together when the alcohol content of the solution is low (up to about 0.7%), but are weak and easily separated when the alcohol content of the solution is high (about 4% or more).

The alcohol content of this surface ice layer, and of successive ice layers that form after each in turn is removed, is lower than the average solution concentration and is surprisingly constant (about 0.4% with an initial concentration of 0.7%).

For closed vessels, analysis of the ice and of the unfrozen melt confirmed that no alcohol had been lost by evaporation. For open vessels the alcohol concentration of the surface ice does decrease slowly with time. (For example, two similar samples of ice were stored, with and without covers, in a cold room at −15° C for 1 week. The concentration of alcohol in the top 1-cm layer was then 3.23% and 2.90% respectively. Below about 1.5 cm the concentration remained alike in the two vessels.)

After the ice layer reaches a thickness of the order of 1 cm, the ice begins to grow in long pendent vertical plates. In these experiments, the plates were 1 to 1.5 cm in width, very thin (probably about 0.1 mm thick), and crystal clear. They were observed up to 3 or 4 cm in vertical length and were spaced about 0.5 cm apart, in groups at least roughly parallel. The alcohol concentration of these plates, strained from the solution (so that inevitably a little liquid adhered), did not differ from the value found for the surface ice layers.

When the solution is allowed to freeze completely, alcohol is extruded from the block and remains as a liquid film on the inside of the vessel.

The concentrations of alcohol found throughout the ice, when the sample was allowed to freeze completely, were somewhat higher than the concentrations found in ice formed on similar solutions, when only part of the melt was allowed to freeze. This is probably owing to the fact that horizontal layers cut from a solid block of ice contain both ice crystals and some concentrated alcohol solution trapped between them. The sections analyzed were

relatively thick, so that the fine detail of Fig. 3 was not obtained but the concentrations were consistent with the profiles of Fig. 3.

Melts containing glycol and water were frozen and analyzed in a similar fashion. The freezing pattern found was very much like that for alcohol–water mixtures; the horizontal layer and its pendent vertical plates contained equal concentrations of glycol, and this concentration was surprisingly similar, quantitatively, to that in the alcohol case. When glycol melts are frozen solid, however, the concentration profile below the 2-cm level is markedly different; comparing ice IV (Fig. 3) with ice VIII (Fig. 6) it is evident that below the transition layer the alcohol values remain constant throughout most of the ice, whereas the glycol values increase steadily with depth.

As the ice crystals form, both alcohol and glycol are rejected. But the alcohol, free to move between the pendent ice crystals, will tend to rise, since it is lighter than water, whereas the glycol being heavier than water will tend to sink. In the case of alcohol then, the rejection and gravity effects are in opposition, and throughout the bulk of the volume, measurements of the alcohol content of a horizontal layer give an almost constant value.

In the case of glycol, where the effects of rejection and gravity move the glycol in the same direction, the trapped solution in the lower layers will have a higher concentration than in those above.

Solutions containing water-soluble dyes (methylene blue, methyl violet, and eosin) were next investigated, with most striking results. When the solutions contained only a dye and water the dye was so strongly rejected as freezing proceeded that the ice was quite clear and colorless except at the bottom where the dye was concentrated in a sharply defined region. But when these solutions contained both dye and ethyl alcohol, the ice appeared to be uniformly colored throughout.

Examination of this ice was attempted under the microscope in the cold room. When sufficiently thin sections could be set up at the right angle, it was possible to see that the ice consisted of clear platelets of colorless ice separated by thin highly colored films.

DISCUSSION

The concentration profiles shown in this paper give strong evidence for a peak in concentration values at the position below the surface found by Perey and Pounder (1958) to be the position of a transition layer in the crystal structure. At this transition layer a rapid change occurs in both crystal sizes and orientations. In most of the ice samples tested a concentration peak was also found in the surface layer. The absolute size of this concentration is uncertain, because the value found in each case must be a function of the thickness of the layer of ice in which it was measured. The thinner the layer the higher was the measured concentration, suggesting that the concentration is a maximum in a very thin, possibly even monomolecular, surface film. The same argument applies to the value found for the transition layer peak, with an added complication. Visual examination of a vertical section usually showed the transition layer to be very thin but not in a horizontal plane. Sometimes

it was quite jagged, occasionally varying in depth by as much as half a centimeter. If the transition layer itself could be isolated, one would expect to find very much higher concentrations than any here recorded.

It has been shown that when pure aqueous solutions of sodium carboxymethyl cellulose (CMC), various water-soluble dyes, sodium chloride, ethylene glycol, and ethyl alcohol are frozen, the amount of solute trapped in the ice varies widely. For the concentrations and freezing rates used, the CMC and dyes are virtually completely rejected by the ice. Some salt is trapped; in Fig. 5 the region from about 2 to 6 cm in depth might be considered normal and shows that about 30% of the salt was retained in the ice. The concentrations of alcohol and glycol vary too much with depth to speak of a normal concentration but a reasonable guess is that 90% of the alcohol and possibly 50 to 60% of the glycol are trapped in the ice. These results suggest the possibility that the solubility in water of the additive is a factor— the CMC and the dyes are only slightly soluble in water compared to salt and the two organic liquids are infinitely soluble in water.

The freezing of solutions containing both alcohol (or glycol) and CMC (or a dye) is interesting, since the presence of the CMC does not appear to alter the distribution of the alcohol or glycol in the ice but the distribution of the CMC now conforms closely to that of the organic liquid. Apparently the CMC is carried by the alcohol or glycol to positions in the ice not available to pure CMC. By some physical or chemical process the small alcohol molecule (or possibly several of them) takes the huge CMC molecule "under its wing" and persuades the growing ice lattice to treat them approximately as equals. It is perhaps important to note that the number of alcohol molecules is greater by several orders of magnitude than that of CMC molecules, so that even if some of the alcohol enters into a chemical reaction there is plenty of it left to alter the refractive index of the solution. A possible chemical reaction is esterification of the CMC. Although esterification ordinarily reduces the solubility in water, this is not necessarily the case. Noller (1951, p. 303) points out that cellulose is insoluble in water because of strong van der Waals forces and proton bonding between chains. Etherification to CMC separates the chains because of the size of the carboxymethyl group and reduces these forces greatly. Possibly esterification of the CMC carries this process a step farther. A possible physical mechanism for retaining the CMC in the ice is through lattice defects. There is no evidence that alcohol can fit permanently into an ice lattice, but alcohol affects the properties of ice so markedly that it is tempting to suppose that alcohol can attach temporarily to a growing ice crystal, giving rise to imperfections in the lattice. If these imperfections are large the CMC molecules may be trapped in them, although not of course forming part of the lattice. The present experiments do not suggest which of these speculations is the more likely, or, indeed, if either of them is the correct explanation.

The results illustrated in Figs. 6, 7, and 8 show that the amount of solute trapped in the ice increases with the decrease in ambient temperature and hence increase in freezing rate. This result is well known in field studies of sea ice.

This work was supported by the Defence Research Board under D.D.P. Contracts C.69-700102 and GC.69-800103. Professor C. B. Purves offered valuable advice on the measurement of low concentrations of alcohol.

REFERENCES

ANDERSON, D. L. 1958. A model for determining sea ice properties. Arctic Sea Ice, Washington, NAS–NRC Pub. No. 598.
ASSUR, A. 1958. Composition of sea ice and its tensile strength. Arctic Sea Ice, Washington, NAS–NRC Pub. No. 598.
BLACK, H. J., Jr. 1951. Anal. Chem. **23**, 1792.
DREYWOOD, R. 1946. Ind. Eng. Chem. Anal. Ed. **18**, 499.
LOEWUS, F. A. 1952. Anal. Chem. **24**, 219.
MOKRASCH, L. C. 1954. J. Biol. Chem. **208**, 55.
NOLLER, C. R. 1951. Textbook of organic chemistry (W. B. Saunders, Philadelphia).
PEREY, F. G. J. and POUNDER, E. R. 1958. Can. J. Phys. **36**, 494.
POUNDER, E. R. 1958. Can. J. Phys. **36**, 363.
ROE, J. H. 1954. J. Biol. Chem. **208**, 889.
——— 1955. J. Biol. Chem. **212**, 335.
SCOTT, T. A. and MELVIN, E. H. 1953. Anal. Chem. **25**, 1656.

NEGATIVE RESISTANCE IN SEMICONDUCTOR DEVICES[1]

RONALD E. BURGESS

ABSTRACT

Negative resistance can appear in the static and high-frequency characteristics of devices in which the current is determined by both voltage and temperature. The properties of the a-c. impedance arising from the interaction of thermal and non-thermal effects are discussed and criteria for the appearance of negative resistance over certain ranges of frequency are derived. The application of this analysis to devices which do and which do not exhibit isothermal negative resistance is considered. In an Appendix, a current–temperature relation depending on two activation energies is shown to provide a quantitative model for interpreting the observed turnover behavior of germanium diodes.

The appearance of "thermal turnover", i.e. a voltage maximum followed by a negative resistance region in the characteristics of semiconductor devices, has been discussed previously (Burgess 1955*a*, *b*, *c*). In the present paper the combination of thermal and voltage-controlled processes is considered generally and the results are applied to a discussion of the attainment of negative resistance. We exclude the effects obtained by transit time phenomena and also the spurious negative resistance which seemingly occurs in junction diodes under avalanche breakdown conditions and in fact arises from the voltage-controlled statistics of the breakdown process (Burgess 1959).

The voltage-controlled effects most commonly involved are: impact ionization leading to avalanche multiplication, carrier injection and extraction, space-charge-limited flow, internal field emission (or Zener effect), and non-linear carrier mobility in strong electric fields. Except in the simple case of an ohmic device at low electric fields, one or more of these effects will be present.

In general the current may be written $I = I(V,T)$ and the differential resistance r which is the small-amplitude a-c. resistance at zero frequency is given by

$$r = \frac{dV}{dI} = R\frac{1-y}{y+x} \tag{1}$$

where $R = V/I$ is the d-c. resistance, $x = R\,(\partial I/\partial V)_T$, $y = (V/K)\,(\partial I/\partial T)_V$, K = thermal conductance between device and ambient $= \partial(IV)/\partial T$.

The dimensionless quantities x and y are respectively the representative parameters of the isothermal characteristic at the operating temperature and the temperature coefficient of the current at the operating voltage.

The four alternating sectors of positive and negative differential resistance in the x–y plane are separated by the lines $y = 1$ and $x+y = 0$. The line $x = 1$ corresponds to devices which are linear in the isothermal condition (e.g. thermistors). Usually semiconductor devices will have positive values of y

[1]Manuscript received December 9, 1959.
Contribution from the Department of Physics, University of British Columbia, Vancouver, British Columbia. The research for this paper was supported by Defence Research Board of Canada under Grant No. 9512-22.

although in some exceptional cases such as those involving high electric fields it may be possible for y to be negative.

If x is positive then as the current through the device increases attainment of the condition $y = 1$ corresponds to voltage turnover ($r = 0$) after which negative resistance of the current-controlled type is obtained. When x and y are of the same sign the differential resistance must lie between $-R$ and $(\partial V/\partial I)_T$ and this indicates the limits of magnitude of the attainable negative resistance at any operating point beyond turnover.

It may also be inferred from equation (1) that in a diode whose isothermal reverse current does not saturate ($x > 0$) the differential resistance is smaller in magnitude (whether positive or negative) than in an otherwise identical diode exhibiting saturation. Thus avalanche multiplication sharpens the breakdown process compared with that due to thermal effects alone but conversely it reduces the attainable negative resistance beyond turnover.

In a diode displaying isothermal negative resistance ($x < 0$), as in the forward characteristic of narrow germanium junctions (Esaki 1958), the differential resistance is modified by thermal effects once y is no longer small compared with both 1 and $-x$. If thermal effects are sufficient for y to exceed $-x$ and $-x < 1$ then they will dominate over the Zener effect and produce thermal turnover of the voltage maximum type. Circumstances can arise in such a device in which the characteristic on proceeding from the origin could exhibit a current maximum followed by a current minimum followed in turn by a voltage maximum.

The above remarks about the characteristics apply to frequencies sufficiently low for the temperature always to be in a steady state with the applied power. At higher frequencies thermal inertia causes a lag in the temperature variation and the differential resistance derived from the static characteristic must be replaced by the complex impedance. If τ is the thermal time constant this impedance is derived by replacing the thermal conductance K by the complex thermal admittance $K(1+i\omega\tau)$ whence

$$Z(\omega) = R[1-y/(1+i\omega\tau)]/[x+y/(1+i\omega\tau)]. \tag{2}$$

This function has a semicircular locus in the Z plane with the ends of the diameter on the resistance axis occurring at $Z(0) = r$ and $Z(\infty) = (\partial V/\partial I)_T$.

It is immediately seen that the criterion for thermal effects to be absent is not that $\omega\tau$ shall be large compared with unity but large compared with y and y/x.

The condition for negative resistance to appear is

$$x\omega^2\tau^2 < (y-1)(y+x). \tag{3}$$

From this inequality may be derived

(i) the upper frequency limit at which a device without isothermal negative resistance may display negative resistance due to thermal effects, or

(ii) the frequency below which isothermal negative resistance may be suppressed by thermal effects.

In a linear device ($x = 1$) the upper limit for a purely thermally derived negative resistance is simply

$$\omega\tau < (y^2-1)^{\frac{1}{2}}. \tag{4}$$

The presence of thermal effects introduces a reactive component into the impedance which is inductive if $y(1+x)$ is positive and capacitive if $y(1+x)$ is negative. This may be useful or embarrassing depending upon the manner in which the device is being used. An example of benefit occurs in very low-frequency oscillators using thermistors where the inductive reactance produced by the thermal inertia permits frequency control simply by shunting the thermistor with a pure capacitance (Burgess 1955*c*). Similar inductive behavior and oscillations in point-contact or junction germanium diodes are possible but here x is greater than unity due to avalanche multiplication so reducing the upper frequency limit for negative resistance to appear (equation (3)).

In any given circumstances the effective time constant differs from τ to an extent which depends on x and y and also on the external circuit so that the dynamic behavior can only be evaluated by considering the complete system.

One type of dynamic behavior of practical importance is the switching time of a bistable negative resistance device between two stable points. The transition involved is essentially of large amplitude embracing the whole of the negative resistance region and is thus outside the scope of the present small-amplitude theory. However, there is still validity in the observation that the switching time is not simply related to τ even when it is determined by thermal inertia, since x and y and the external circuit determine the fashion in which the variations of current, voltage, and temperature are interrelated.

Thermally produced negative resistance is commonly associated with relatively long relaxation times of the order of milliseconds. If, however, the current-controlling region is of small dimensions and material has a high thermal diffusivity (especially true at low temperatures) the thermal time constant can easily be less than a microsecond. Conditions of this type obtain for instance in the contact region of a point-contact diode.

Furthermore it must be stressed that the upper frequency limit for negative resistance to occur may be appreciably greater than the plausible value $1/2\pi\tau$. In conditions where the temperature control of the current is sharp, y can be much greater than unity; if for instance $y = 100$ and $x = 5$ then it is found from equation (3) that $f_{\max} = 7/\tau$. In this type of situation it is seen by reference to equation (2) that the heat capacity τK and not the thermal conductance K is important.

It is possible, though not yet conclusive, that the negative resistance (McWhorter and Rediker 1959) and oscillations (Koenig and Brown 1959) observed in germanium filaments at low temperatures have thermal origin. The latter authors have suggested that the negative temperature coefficient of the breakdown field associated with impact ionization leads to a local thermal instability of some small region of the filament. The former pair of authors point out that a switching time of 2×10^{-9} second is possible in the negative resistance region. As was remarked above the thermal time constant

will not be as small as this switching time when the parameter y is large compared with unity and, indeed, it is in this phenomenon.

Even in devices with long thermal time constants or those used at frequencies high enough for thermal effects to be unimportant the behavior of the low-frequency differential resistance given by equation (1) is still of importance as it determines the d-c. and low-frequency stability of the device in conjunction with the associated d-c. bias circuit and it must be heeded to obtain monostable operation free from low-frequency oscillations.

In the discussion above, the only inertial process considered was thermal and the isothermal admittance was assumed to be real and frequency independent and equal to the slope of the isothermal characteristic at the operating point.

The treatment can be generalized by replacing $(\partial I/\partial V)_T$ by $Y(\omega,T)$ which is the small-amplitude admittance at ω and at fixed temperature T. The impedance of the device including thermal effects then becomes

$$Z(\omega) = \frac{(1-y)+i\omega\tau}{(1+i\omega\tau)Y+(y/R)} \tag{5}$$

which behaves as $1/Y$ for frequencies sufficiently high for $\omega\tau \gg |1-y|$ and $|y/RY|$.

The condition for negative resistance to occur becomes

$$G\omega^2\tau^2+(1-y)(G+y/R)+B\omega\tau y < 0 \tag{6}$$

where $Y = G+iB$.

At high frequencies where the isothermal admittance may become complex as considered above it is also necessary to examine the parameter y which is determined by $(\partial I/\partial T)_V$. Here I denotes the total current through the device and y is real only if the current variation at constant voltage is cophasal with the temperature variation producing it. This would not be the case, for instance, when the capacitive component of current is temperature modulated by variation of the permittivity of the material or the geometry of a space-charge region. Hence when Y becomes complex at high frequency account must be taken of y also becoming complex though with a phase angle which will in general differ in magnitude and even in sign from that of y.

An important example of a class of semiconducting material in which y is complex and furthermore the temperature coefficient of conductivity is negative occurs in ferroelectric crystals near the Curie point. For instance, barium titanate can be made semiconducting by adding cation impurities of suitable valency (Saburi 1959), and the resulting material can have room temperature resistivity in the range 10–10^4 ohm cm. At the Curie point an increase of 5° in temperature may produce a 100-fold increase of resistivity corresponding to a temperature coefficient of conductivity of -1 deg^{-1}. Thermistors constructed from such materials would have very large negative values of y; for example, if the applied power causes a 10° rise of temperature above the ambient $y = -10$.

In such a ferroelectric material near the Curie point the temperature coefficient of the permittivity would be large and thus y would be significantly complex. For we have

$$\left(\frac{\partial I}{\partial T}\right)_V \propto \left[\frac{\partial(\sigma+i\omega\epsilon)}{\partial T}\right]_E$$

with both $\partial\sigma/\partial T$ and $\partial\epsilon/\partial T$ negative. The comparison of $(\partial\epsilon/\partial T)/(\partial\sigma/\partial T)$ with the thermal time constant τ determines the importance of the ferroelectric behavior in modifying the dispersive properties of the impedance.

APPENDIX

Thermal Turnover in the Two-Activation-Energy Model

In a germanium diode the consistently observed decrease of turnover power with increasing ambient temperature proves to be exacting in the construction of a satisfactory phenomenological model for the characteristics. The suggestion (Cutler 1957) that a current–temperature dependence based on a process involving two activation energies is here shown to yield the correct behavior but with an interpretation of the experimentally derived parameters which differs from that commonly used.

Consider a current I of the form

$$I = F(V)\,[A\exp(-a/T)+B\exp(-b/T)]$$

where $a > b$ and correspondingly $A > B$. The dependence of current on temperature T at constant voltage when plotted logarithmically against $1/T$ will display two asymptotic linear regions with a slope $-b$ at low temperature and $-a$ at high temperature and intersecting at a temperature T_0 where the two components of current are equal:

$$T_0 = (a-b)/\ln(A/B).$$

Now under steady-state operation and for linear thermal conduction the device temperature T and ambient temperature T_a are related by

$$K\,(T - T_a) = IV$$

where K is the thermal conductance between the current-controlling region of the device and the ambient.

The turnover condition ($dV/dI = 0$) is independent of $F(V)$ and given by $y = 1$ or

$$I_1V_1/K = T_1 - T_a = T_1^2/S(T_1)$$

where suffix 1 denotes the values at turnover and S is the slope function given by

$$S(T) = \frac{Aae^{-a/T}+Bbe^{-b/T}}{Ae^{-a/T}+Be^{-b/T}} = -\frac{d(\ln I)}{d(1/T)}.$$

For turnover to occur $S > 4T_a$ is necessary.

The function S has the value b at low temperatures, and a at high temperatures, and $\frac{1}{2}(a+b)$ at T_0 where to a close approximation dS/dT reaches its maximum value.

The dependence of the turnover power ($P_1 = I_1V_1$) on the ambient temperature is found from

$$\frac{dP_1}{dT_a} = K\left[\frac{dT_1}{dT_a} - 1\right] = K\left[\left(1 - \frac{2T_1}{S_1} + \frac{T_1^2}{S_1^2}\frac{dS_1}{dT_1}\right)^{-1} - 1\right].$$

In germanium diodes this quantity is found experimentally to be negative over an extensive range of temperature.

For this to be possible

$$\frac{dS_1}{dT_1} > \frac{2S_1}{T_1}.$$

The most favorable temperature for this to be realized is close to $T_1 = T_0$ for which the inequality becomes

$$\ln\frac{A}{B} > 4\frac{a+b}{a-b}.$$

This condition does not depend on the thermal conductance K and is determined only by the two ratios A/B and a/b.

Introducing the parameter

$$C = [(a-b)^2/2(a+b)T_0] - 2 = \tfrac{1}{2}\frac{a-b}{a+b}\ln\frac{A}{B} - 2$$

which must be greater than zero for the above inequality to hold, we have the following results in the condition $T_1 = T_0$:

$$\begin{aligned} dT_1/dT_a &= [1 + 2T_0C/(a+b)]^{-1}, \\ P_1 &= K(T_0 - T_{a0}) = KT_0^2/S_0 = 2KT_0^2/(a+b), \\ T_{a0} &= T_0 - T_0^2/S_0 = T_0 - 2T_0^2/(a+b), \\ \frac{dP_1}{dT_a} &= -\frac{KC}{C + (a+b)/2T_0}. \end{aligned}$$

Thus the intercept of the tangent at T_{a0} to the (P_1, T_a) plot on the T_a axis is

$$\begin{aligned} T_1 &= T_{a0} - P_1/(dP_1/dT_a) \\ &= T_0(1 + 1/C). \end{aligned}$$

It is this intercept temperature which in the literature (Benzer 1949; Yamaguchi and Hamakawa 1959*a*, *b*) has been identified erroneously with the contact temperature or with the temperature at which the onset of intrinsic conduction occurs. In fact the intercept is larger than the contact temperature by the fraction $1/C$ (which may typically lie between 0.1 and 0.3) and has no relation to intrinsic conductivity. Similarly the slope dP_1/dT_a is usually much less than K whereas it is often assumed to provide a direct measurement of the thermal conductance.

Typical values for a germanium diode are:

$$A/B = e^{20}, \quad a = 8000°, \quad b = 2000°, \quad \text{giving}$$

$$T_0 = 300°, \quad T_{a0} = 282°, \quad T_1 = 375°, \quad C = 4,$$

and

$$(dP_1/dT_a)_{T_1 = T_0} = -0.19K.$$

It will be noted that the thermal conductance K in no way affects the temperature relations as it only appears in expressions involving the power. Furthermore the value of b is not of great influence on the results and it could be zero (corresponding to a current component independent of temperature) and yield the same qualitative features as for a non-zero value.

REFERENCES

BENZER, S. 1949. J. Appl. Phys. **20**, 804.
BURGESS, R. E. 1955*a*. Proc. Phys. Soc. B, **68**, 766.
——— 1955*b*. Proc. Phys. Soc. B, **68**, 908.
——— 1955*c*. J. Electronics, **3**, 297.
——— 1959. Can. J. Phys. **37**, 730.
CUTLER, M. 1957. IRE Trans. on Electron Devices, **ED-4**, 201.
ESAKI, L. 1958. Phys. Rev. **109**, 603.
KOENIG, S. H. and BROWN, R. D. 1959. J. Phys. Chem. Solids, **10**, 201.
MCWHORTER, A. L. and REDIKER, R. H. 1959. Proc. IRE **47**, 1207.
SABURI, O. 1959. J. Phys. Soc. Japan, **14**, 1159.
YAMAGUCHI, J. and HAMAKAWA, Y. 1959*a*. J. Phys. Soc. Japan, **14**, 15.
——— 1959*b*. J. Phys. Soc. Japan, **14**, 232.

THE ELECTRICAL RESISTANCE OF DILUTE MAGNESIUM AND ALUMINUM ALLOYS AT LOW TEMPERATURES[1]

F. T. Hedgcock, W. B. Muir, and E. Wallingford

ABSTRACT

Experimental data on the influence of type and concentration of impurity on the low-temperature resistance of the metals, magnesium and aluminum, is presented. In particular, comparison is made of the electrical behavior of alloys formed using transition element impurities in the divalent metal magnesium, and in the trivalent metal aluminum with the behavior of similar impurities in some of the noble metals.

1. INTRODUCTION

The electrical resistance minimum in metals was discovered 25 years ago in gold by de Haas and van den Berg (1934), and since that discovery a considerable number of pure metals and alloys have been investigated for similar low-temperature anomalies. Most of these experimental studies have involved the noble metals and their alloys. At present some order is beginning to emerge from systematic investigations of the influence of type and concentration of impurity on the temperature of occurrence and relative size of the resistive anomaly.*

Electrical resistance minima in magnesium were first reported by Meissner and Voigt (1930) and later work by MacDonald and Mendelssohn (1950), Garfunkel, Dunnington, and Serin (1950), Thomas and Mendoza (1952), and Spohr and Webber (1957) confirmed these observations. Reports of an electrical resistance minimum occurring in aluminum (Keesom 1933) were not confirmed in later measurements made by Boorse and Niewodniczanski (1936), Garfunkel, Dunnington, and Serin (1950), and later by Thomas and Mendoza (1952). Although low-temperature resistive anomalies have been reported in magnesium and aluminum, no detailed study of the influence of type and concentration of impurity on the minimum has been carried out. Interest in this laboratory in the magnetic properties of magnesium and aluminum prompted an investigation of the electrical properties of a number of dilute alloys of magnesium and aluminum at low temperatures and we wish to report briefly on these measurements.

[1]Manuscript received November 2, 1959.

Contribution from the Department of Physics, University of Ottawa, Ottawa, Ontario. Some of this research will be included in theses by W. B. Muir and E. Wallingford to be submitted in partial fulfillment for the Ph.D. and M.Sc. degrees, respectively, at the University of Ottawa. A preliminary report on the magnesium alloys was presented at the June meeting of the Canadian Association of Physicists held at McMaster University, Hamilton, Ontario, 1958.

*For a comprehensive review article and list of references, see "Electrical conductivity of metals and alloys at low temperatures" by D. K. C. MacDonald, Handbüch der Physik, Vol. XIV, Springer-Verlag, Berlin (1956).

2. EXPERIMENTAL METHOD AND SPECIMEN PREPARATION

2.1 Apparatus

The low-temperature cryostat is similar to the helium desorption unit described by Rose-Innes and Broom (1956) and will not be described here. With freshly activated charcoal in the desorption unit, a temperature run from 4.2 to 30° K could be made very slowly, the run usually taking from 4 to 5 hours. This meant that a number of resistance specimens could be run at one time. All temperatures above 4.2° K were measured with a Simon-type gas thermometer. Relative temperatures could be measured with an accuracy of better than 0.3% whereas the absolute temperature in the higher temperature regions should be within 1%. Between 2 and 4.2° K the temperature was determined using the known vapor-pressure scale. Temperature agreement between the gas thermometer and vapor-pressure measurements was better than 0.2%.

A current-potential method was used to measure the resistance of the samples. Pressed contacts were used and were either of screw- or knife-edge design. The voltages were measured with a galvanometer amplifier as described by MacDonald (1956). Scatter in the experimental points (due to electrical noise and stray thermal voltages) permitted the resistance ratios of the aluminum alloys to be determined with an accuracy of at least 0.5% whereas the magnesium alloys which exhibited large anomalies were not measured to better than 1%.

2.2 Magnesium Specimen Preparation

The alloys were made by Dow Chemical Company metallurgical laboratories and supplied as either chill-cast ingots or 0.25-in. rods. The resistance specimens were made by hot-rolling* the ingots at 400° C into strips approximately 0.005-in. thick and cutting these strips into wires of rectangular cross section. After fabrication, the samples were annealed at 450° C for 48 hours in an atmosphere of helium gas. Table I lists the alloys investigated and their resistance ratios $R_{4.2}/(R_{300}-R_{4.2})$. All of the alloys show a resistance ratio higher than the pure stock so that, if not all, at least some of the impurity is in solution. That alloys had been made in the case of magnesium–manganese and magnesium–iron systems can be seen in Table I where the resistance ratios show an approximate linear increase with nominal impurity content. Hot-rolling of sample 732 produced extremely large impurity gradients in the samples so that values for this specimen given in Table I are to be thought of as averages. The room-temperature resistivity of alloys 702, 730, 731 are 4.62×10^{-6} ohm-cm, 4.67×10^{-6} ohm-cm, and 4.82×10^{-6} ohm-cm, respectively, and are in good agreement with the published values of Salkovitz, Schindler, and Kammer (1957) for these concentrations and type of solute. Micrographic examination of the alloys showed a one-phase system with a minimum of oxide present.

*We are indebted to the Department of Mines, Ottawa, for carrying out the hot-rolling.

TABLE I

Spectrographic analyses and electrical properties of magnesium alloys

Alloy No.	Al	Ca	Cu	Fe	Mn	Ni	Pb	Si	Sn	Zn	Sb	Major impurity	T_{min}, °K	$R_{4.2}/(R_{300}-R_{4.2})$
728	<.001	<.01	<.001	<.001	<.001	<.0005	<.001	<.001	<.01	<.001	—	Pure	—	3.6×10^{-3}
87812	<.002	<.01	<.001	<.001	.005	<.0005	<.001	<.007	<.01	<.004	—	Mn	7.0	18.2×10^{-3}
87813	<.003	<.01	<.001	<.001	.019	<.0005	<.001	<.009	<.01	<.006	—	Mn	10.0	24.1×10^{-3}
87814	<.003	<.01	<.001	<.001	.038	<.0005	<.001	<.010	<.01	<.003	—	Mn	10.8	26.7×10^{-3}
729	<.001	<.01	<.001	<.001	.041	<.0005	<.001	<.001	<.01	<.001	—	Mn	12	36.1×10^{-3}
732A	<.001	<.01	<.001	<.001	.042	<.0005	<.001	<.001	<.01	<.001	—	Mn	13	53.7×10^{-3}
732B	<.001	<.01	<.001	<.001	.042	<.0005	<.001	<.001	<.01	<.001	—	Mn	13.7	87.0×10^{-3}
702	<.0005	<.01	<.001	<.0009	<.0005	<.0005	<.001	<.001	<.001	.02	—	Zn	—	8.54×10^{-3}
730	<.001	<.01	<.001	<.001	<.001	<.0005	<.001	<.001	.035	<.001	—	Sn	—	10.2×10^{-3}
731	<.001	<.01	<.001	<.001	<.001	<.0005	<.001	<.001	<.01	<.001	.07	Sb	—	19.4×10^{-3}
757-3	<.001	<.01	<.001	.013	<.001	<.0011	<.001	<.001	<.01	.039	—	Fe + Zn	6.0	14.2×10^{-3}

2.3 Aluminum Alloy Preparation

The aluminum alloys were prepared by the Aluminum Company of Canada and a spectrographic analysis of these alloys is shown in Table II. The aluminum samples were cold-rolled to the same size as the magnesium alloys and usually given a strain-relieving anneal for 24 hours at 300° C in an atmosphere of helium prior to making measurements. Table II also shows the resistance ratios for the aluminum alloys as a function of nominal impurity content. It should be pointed out that some difficulty was experienced in keeping the iron in solution. The maximum solubility of iron in aluminum at 620° C is 0.035 wt.%.* In order to put as much iron in solution as possible, the samples were quenched from 620° C after having received an homogenizing anneal at this temperature for approximately 24 hours. The purpose of this anneal was to try and remove the large impurity gradients that existed in the original ingots. An estimate of the gradient that existed in the original ingot may be seen in Table II where measurements of the resistance ratio

TABLE II

Spectrographic analyses and electrical properties of aluminum alloys

Alloy No.	Cu	Fe	Mg	Mn	Si	Major impurity	$R_{4.2}/(R_{300}-R_{4.2})$
GKP	<.002	<.002	<.002	<.001	<.001	Pure	3.0×10^{-3}
GKM	<.002	<.003	<.002	.011	<.001	Mn	18.5×10^{-3}
GKN	<.002	<.004	<.002	.053	<.001	Mn	68.2×10^{-3}
GKO	<.002	<.003	<.002	.092	<.001	Mn	111.5×10^{-3}
GKK	<.002	.05	<.002	<.001	<.001	Fe	25.0×10^{-3}
GKL	<.002	.11	<.002	<.001	<.001	Fe	24.7×10^{-3} 16.4×10^{-3}

are given for each end of the GKL ingot which contains a nominal impurity content of 0.11% iron.

3. EXPERIMENTAL RESULTS

3.1 Electrical Resistance of Magnesium Alloys

A series of temperature-resistance runs on magnesium are shown in Fig. 1. Sample 728 is the pure material and exhibited no resistance minimum. Sample 727-1 is an iron alloy which presumably has too small a minimum to be detected with the present method of measurement. Alloy 757-3 has both iron and zinc present and the minimum is presumably due to the presence of iron. None of the alloys listed in Table I containing major impurities of zinc, tin, or antimony exhibited a resistance minimum. The rest of the alloys in Fig. 1 are magnesium–manganese alloys. The depth of the minimum is extremely large in sample 732 and much is larger than any reported for magnesium by previous authors (see above). Both the depth of the minima and the temperature at which the minima occur (T_{min}) increase with increasing impurity content. Using the resistance ratio as defined in Table I as a measure

*We are indebted to Mr. G. Marchand of the Aluminum Laboratories for making the phase diagram of aluminum–iron available to us.

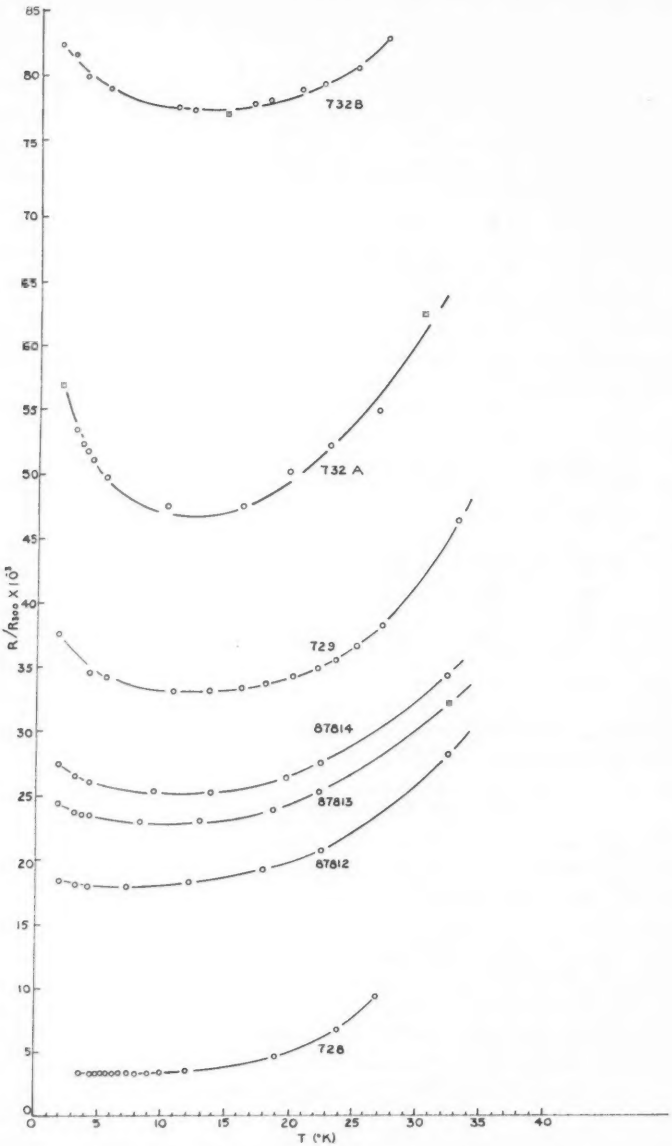

FIG. 1. Temperature dependence of the relative resistance of a number of magnesium alloys described in Table I.

of the impurity concentration, Fig. 2 shows a graph of T_{min} and the normalized depth of the minima as a function of impurity content. The behavior of both of these parameters is similar to that described for certain copper alloys by MacDonald and Pearson (1955).

3.2 Electrical Resistance of Aluminum Alloys

Figure 3 shows the temperature dependence of relative resistance of some of the aluminum–manganese and aluminum–iron alloys described in Table II. None of these alloys exhibit a low-temperature resistive anomaly.

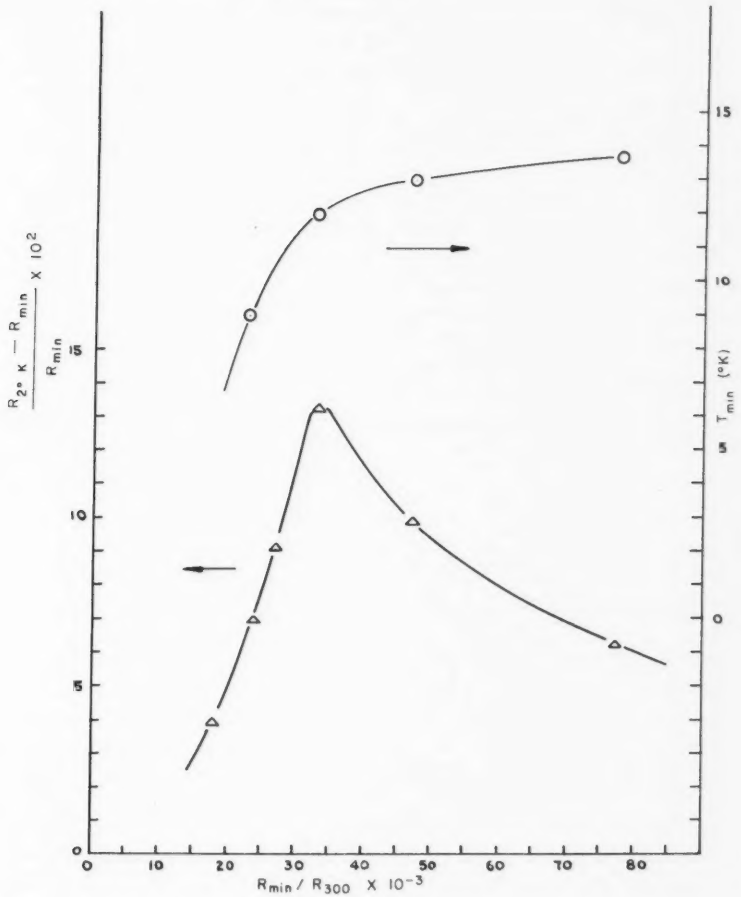

FIG. 2. Temperature of occurrence and the normalized depth of the resistance minimum occurring in magnesium as a function of impurity content.

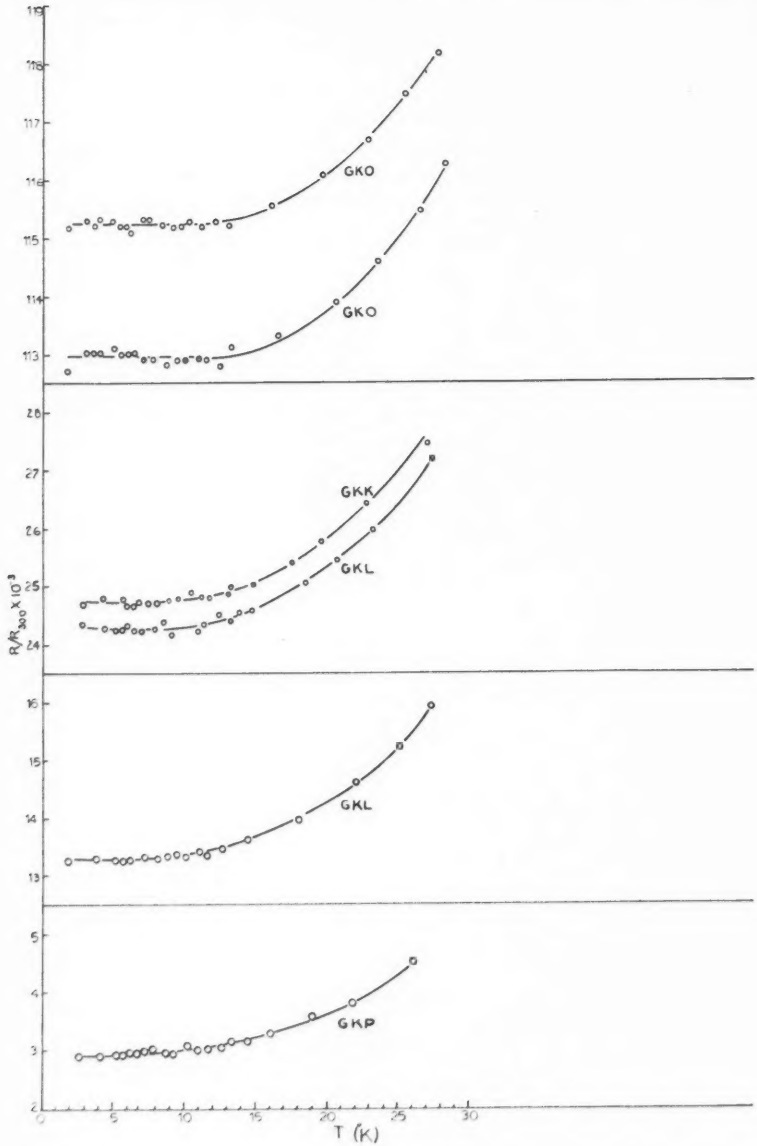

FIG. 3. Temperature dependence of the relative resistance of a number of aluminum alloys described in Table II.

3.3 Room Temperature Resistivity and Residual Resistance of the Magnesium and Aluminum Alloys

Mathiessen's rule states that if the total resistivity of an alloy is considered to consist of a thermal component which is the same as in the pure solvent (ρ_m) and a temperature independent contribution due to scattering from impurity ions (ρ_0), then the total resistivity can be written

$$\rho = \rho_m(T) + \rho_0.$$

Although the statement is of limited value, it is suggested that since all of the resistance temperature curves approach parallelism above the region where impurity scattering dominates the present alloy, systems may be said to obey the Mathiessen rule approximately.

Nordheim (1931), assuming the Mathiessen rule, and using a first-order perturbation calculation, has shown that if the electron concentration and structural properties of the base metal are not modified on alloying, then for low concentrations of solute ($<1\%$) ρ_0 (and hence ρ) should increase linearly with concentration. Using the data in Tables I and II it may be seen that the Nordheim rule is not obeyed well for these very dilute alloys. As has been discussed previously by MacDonald and Pearson (1955), the nominal composition of dilute alloys often bears very little relation to the amount of impurity in solution and for this reason the resistance ratio is a more reliable indication of the actual amount of impurity dissolved.

Values of the room-temperature resistivity for pure magnesium (alloy 728) and pure aluminum (alloy GKP) are 4.66×10^{-6} ohm-cm, and 2.77×10^{-6} ohm-cm respectively. Both the values of room-temperature resistivity and resistance ratio for the pure metals aluminum and magnesium are in good agreement with the most recent values reported by Thomas and Mendoza (1952) and Salkovitz *et al.* (1957).

4. CONCLUSION

Five general conclusions may be drawn from the alloy systems of magnesium and aluminum studied so far:

(i) No sample of nominally pure magnesium showed a resistance minimum within the accuracy of the present measurements.

(ii) Only the transition elements, manganese and iron, appear to induce a minimum in magnesium, manganese being the more effective of the two. Solutes such as antimony, zinc, and tin do not cause a minimum.

(iii) The resistance maximum that manganese induces in copper, gold, and silver (see MacDonald's article, 1956) at temperatures lower than the minimum is not induced in magnesium above a temperature of 2° K.

(iv) The concentration and temperature dependence of the minimum in the magnesium–manganese system exhibits behavior similar to that of the copper alloys with B group solutes gallium, indium, germanium, and tin studied by MacDonald and Pearson (1955). It seems reasonable to conclude therefore that the general behavior of the resistance minimum in a divalent

metal such as magnesium is similar to the behavior of the minimum in a monovalent metal such as copper containing a B group solute.

(v) The present results made on a more complete set of alloys than those previously studied are in agreement with the conclusion of Thomas and Mendoza (1952) that the transition elements iron and manganese do not induce a minimum in aluminum.

ACKNOWLEDGMENTS

The authors would like to thank Dr. W. Pearson for reading the manuscript and wish to acknowledge the support of this research by the National Research Council of Canada.

REFERENCES

BOORSE, H. A. and NIEWODNICZANSKI, H. 1936. Proc. Roy. Soc. A, **153**, 463.
GARFUNKEL, M. P., DUNNINGTON, F. G., and SERIN, B. 1950. Phys. Rev. **79**, 211.
DE HAAS, W. J. and VAN DEN BERG, G. J. 1934. Physica, **1**, 1115.
KEESOM, W. H. 1933. Commun. Kamerlingh Onnes Lab. Univ. Leiden, No. **224**, C.
——— 1934. J. Phys. Radium, **5**, 373.
MACDONALD, D. K. C. and MENDELSSOHN, K. 1950. Proc. Roy. Soc. A, **202**, 523.
MACDONALD, D. K. C. and PEARSON, W. B. 1955. Acta Metallurgica, **3**, 392, 403.
MEISSNER, W. and VOIGT, B. 1930. Ann. Physik (Leipzig), **7**, 761.
NORDHEIM, V. L. 1931. Ann. Physik, **9**, 641.
ROSE-INNES, A. C. and BROOM, R. F. 1956. J. Sci. Instr. **33**, 31.
SALKOVITZ, E. J., SCHINDLER, A. I., and KAMMER, E. W. 1957. Phys. Rev. **105**, 887.
SPOHR, D. A. and WEBBER, R. T. 1957. Phys. Rev. **105**, 1427.
THOMAS, J. G. and MENDOZA, E. 1952. Phil. Mag. **43**, 900.

THE ASSOCIATION OF VISIBLE AURORAL FORMS WITH RADAR ECHOES[1]

G. F. Lyon

ABSTRACT

A peak in 48.2-Mc/sec echo occurrence is observed at Saskatoon corresponding in time to the period of breakup of quiet arcs into active rayed structures. This is also the time of most frequent occurrence of characteristic "curl" forms in the aurora. If, as Gartlein suggests, the "curl" forms are formed by instabilities in a sheet beam then the primary particles are positively charged.

INTRODUCTION

Many observers have noted a close statistical correlation between the occurrence of very high frequency radar echoes and visible aurora. Little, Rayton, and Roof (1956) have summarized much of the previous work and concluded that the radio wave scatterers are closely associated in space and in time with visual aurora, but that because of aspect sensitivity, only aurora occurring at low elevation angles toward the north as seen from the radar station may be expected to give echoes. In general, auroral forms at elevation angles below about 15° will appear to consist of quiet arcs or diffuse forms, whereas the same aurora when viewed near the zenith may exhibit more structure and motion. Thus because the radio-observing site must be some 500 km from the scattering region, zenith observations of the visible form corresponding to a given radar echo are rarely obtained and few workers have attempted to correlate radio echoes with specific visible forms. Currie, Forsyth, and Vawter (1953) at Saskatoon, using simultaneous camera and radar observations from the same site, noted that echoes were usually observed from moderately bright aurora showing some structure and that structure was apparently a more important criterion for echo occurrence than luminosity.

During a recent radar investigation of auroral motions (Lyon and Kavadas 1958) carried out at Saskatoon (latitude 52.1° N., longitude 106.6° W.), an excellent statistical correlation was obtained between echo occurrence and the occurrence of visible aurora as recorded on an I.G.Y. all-sky camera situated at Flin Flon (latitude 54.8° N., longitude 101.8° W.), approximately under the scattering region. This paper concerns an attempt to detect a more detailed correlation between echo occurrence and specific visible auroral forms as observed on the Flin Flon camera.

OPERATIONAL DETAILS

The radar frequency was 48.2 Mc/sec and the radar was in operation during the period January 18 to April 28, 1958. The equipment has been described in a previous paper (Lyon and Kavadas 1958).

[1]Manuscript received November 17, 1959.
Contribution from the Institute of Upper Atmospheric Physics, University of Saskatchewan, Saskatoon, Saskatchewan.

A detailed study was possible only when certain conditions were all fulfilled, namely that (1) the radar was operating, (2) the camera was not obscured by cloud or snow, (3) visible aurora occurred, and (4) the picture quality was such as to permit identification of the auroral form. These conditions were all fulfilled on 33 nights during the period under investigation. For analysis each night was divided into 10-minute periods. In all there were 910 periods in which visible aurora was present. This was considered to be a sufficient number to allow statistical treatment.

The useful field of view of the camera at Flin Flon covered the ranges between 350 km and 650 km from the radar at Saskatoon. Few echoes were received from ranges less than 350 km. Some echoes were received from ranges greater than 650 km and in these cases the form of the visible aurora beyond the camera was taken to be the same as that within the camera field of view. Most of the echoes were received from ranges within the camera field. No attempt was made to correlate the visible aurora and the echoes exactly in range as usually the form present at the exact echo range was also present at lesser and greater ranges at the same time.

RESULTS

1. Echo-Visible Form Correlation

In general, the pattern of the visible aurora for any one night followed that described by Heppner (1954). The form before local midnight was usually a quiet arc and the form after midnight was usually an active form, often exhibiting a rayed structure. During the period around midnight in which the breakup of arcs into rayed structures occurred, the intermediate form which most often developed was that of an arc with a "curl" or spiral discontinuity. A typical camera record of an arc with a "curl" is shown in Fig. 1.

For the purpose of analysis the visible aurora was divided into three main groups, namely:

(*a*) quiet arcs,
(*b*) arcs with a "curl" or spiral discontinuity,
(*c*) active rayed structures.

On this basis the form present in any one 10-minute period was recorded. The radar records were then analyzed using the same 10-minute periods as had been used for the camera records. An echo occurring in any one period was associated with the visible form in the same period as displayed in Table I.

TABLE I

Echo–form correlation

	No. of 10-minute periods			Percentage of visible form giving echoes
	Visible aurora	Echoes	No echoes	
Quiet arcs	365	18	347	5
Curls	174	54	120	31
Rayed structures	371	52	319	14
No aurora	—	4	—	—
Total	910	124	786	14

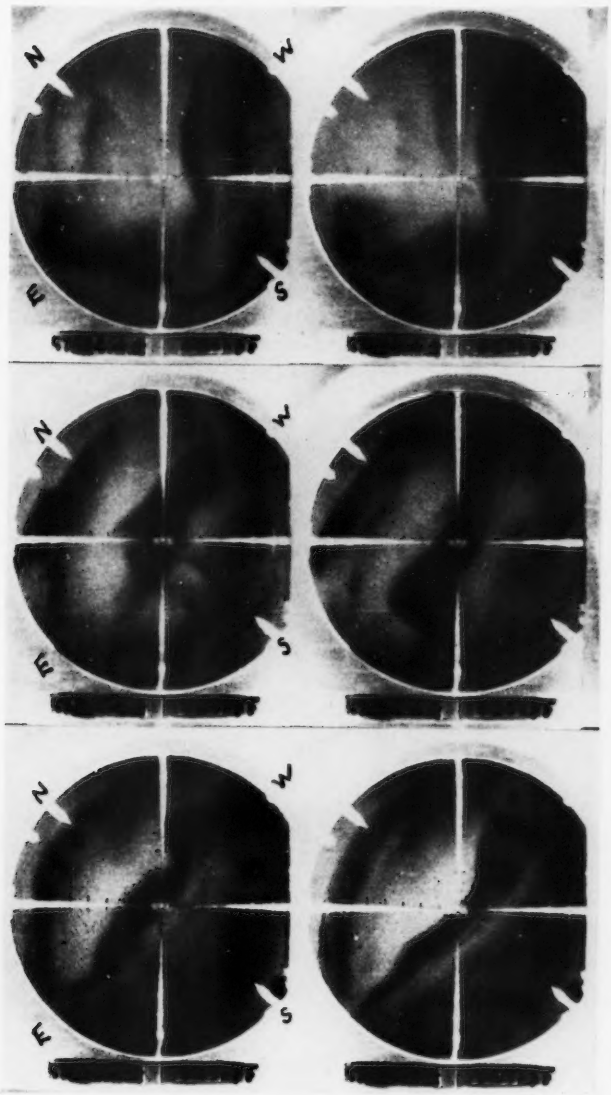

FIG. 1. Some Flin Flon all-sky camera records, showing arcs with "curl" structures, for the night of March 18/19, 1958.
Note that prints are taken from positive film so that the auroral form appears dark.

Thus it is seen that while 14% of all visible aurora could be associated with an echo, only 5% of the quiet arcs could be associated with echoes, the figures for "curls" and active rayed structures being 31% and 14% respectively. Further, it may be noted that

(*a*) quiet arcs occurred 40% of the time but accounted for 14% of the echoes;

(*b*) "curls" occurred 19% of the time but accounted for 42% of the echoes;

(*c*) rayed structures occurred 41% of the time and accounted for 41% of the echoes.

2. Echo and Form Diurnal Variation

Using the same 10-minute periods, the total number of periods in which visible aurora and/or an echo occurred in any one hour throughout the night was computed and plotted against local time as shown in Fig. 2. This diurnal

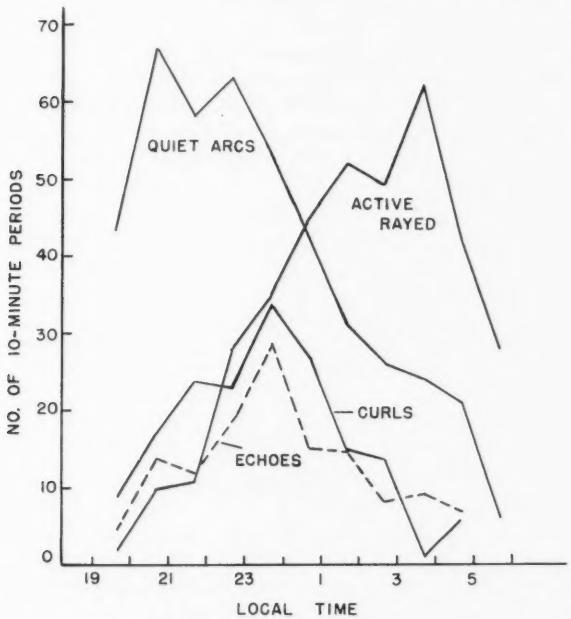

FIG. 2. Diurnal variation of occurrence of visible auroral forms and of echoes.

variation illustrates clearly the general pattern of visible aurora: quiet arcs followed by "curls" and then by active rayed structures. The similarity between the "curl" occurrence curve and the echo occurrence curve is striking.

3. The Direction of the "Curls"

The appearance of an arc developing a "curl" or spiral structure bears a marked resemblance to the characteristic instability profile of a sheet beam of charged particles under the influence of a longitudinal magnetic field.

This fact has also been noted by Gartlein (1959), who has examined qualitatively the expected appearance of an auroral arc assuming the causative agent to be a beam of protons moving downward along the lines of force of the earth's magnetic field. He states that if the beam is not quite uniform, the more intense parts will curve into an S shape figure and if the intensity is raised these curves will go into spirals which, when viewed from the ground looking upward, spiral inward in a clockwise direction. These spirals finally break up into narrow rays. Further, this pattern is not solely an intensity effect but will also occur in a weak beam after more extended travel. Gartlein notes that in the southern hemisphere the spirals observed spiral inward in an anticlockwise direction as would be expected. He concludes that aurora, from the time of arc formation until well after the time of ray formation, is the expected effect of a sheet of protons moving along a magnetic field.

All the spiral forms examined in this investigation spiraled inward in a clockwise direction when viewed from the ground, thus indicating that the primary causative agents for such forms are positively charged particles. Examination of the records of some of the visual observations of aurora made at Chesterfield, N.W.T., during the 1932–33 I.G.Y. (made available by Dr. B. W. Currie, Institute of Upper Atmospheric Physics, University of Saskatchewan) again reveal that when such forms were observed they spiraled in the same direction. Further, Hector (1959), who has examined many all-sky camera records taken from Canadian stations during the 1957–58 I.G.Y. reports over 100 cases of such forms all without exception spiraling in the same direction.

SUMMARY AND DISCUSSION

While the results reported here have been obtained for one station and one frequency (48.2 Mc/sec) only, it would appear that

(*a*) the probability of an echo from a quiet arc is small;

(*b*) the most probable form which will give an echo is a "curl";

(*c*) as active rayed forms occur more frequently than "curls" there is an equal probability of any one echo coming from either a "curl" or an active rayed form.

There is a remarkable similarity between the diurnal variation of echoes and that of "curls" (Fig. 2). The "curl" or spiral form is the one most often seen during the period of breakup of quiet arcs and the formation of rayed structures and is evidently an intermediate form. Thus, there would seem to be a very real case for associating echoes with the period of breakup of quiet arcs into active rayed structures. In this experiment the receiving antenna was fixed in azimuth in a direction 45° east of geomagnetic north. Forsyth (1959) has suggested that a "curl" or spiral form presents a greater volume of ionization to a pulse of electromagnetic radiation than does a quiet arc. Thus, we might expect to receive more echoes from "curl" forms, but by the same token had the radar antenna been directed along the geomagnetic meridian a greater number of echoes might have been obtained from quiet arcs than was obtained with the antenna directed at 45° to the meridian.

All the available evidence from the direction of the "curls" and spirals points to positively charged incoming particles.

Gartlein (1959) has suggested that as particles entering the northern portion of the auroral zone (in the northern hemisphere) traverse longer paths than those entering the southern portion of the zone, then auroras observed in the northern part should more frequently be composed of rayed structures. Possibly more "curls" should be seen also, though in the longer path travelled by the particles the "curl" structure may have developed before the excitation of the visible aurora takes place. It is interesting to note that Collins and Forsyth (1959), in a bistatic radio investigation of auroral ionization over different paths, report that for type A events (signal enhancements related to auroral ionization) occurrence increases with increasing latitude, at least up to the auroral zone. This is just what might be expected if echoes are predominantly associated with "curls" or rayed structures and the occurrence of such structures increases with increasing latitude also.

Forsyth and Green (1959) report that the peak in the diurnal variation of occurrence of type A events occurs progressively earlier with increasing latitude. It is possible that the average time of breakup of quiet arcs into rayed structures also occurs progressively earlier with increasing latitude. It is hoped to report further on this point in a later paper.

ACKNOWLEDGMENTS

The author is indebted to Dr. P. A. Forsyth for his advice and constructive criticism.

REFERENCES

Collins, C. and Forsyth, P. A. 1959. J. Atmospheric and Terrest. Phys. **13**, 315.
Currie, B. W., Forsyth, P. A., and Vawter, F. E. 1953. J. Geophys. Research, **58**, 179.
Forsyth, P. A. 1959. Unpublished.
Forsyth, P. A. and Green, F. 1959. Unpublished.
Gartlein, C. W. 1959. Ann. géophys. **15**, 1, 31.
Hector, F. 1959. Private communication.
Heppner, J. P. 1954. Ph.D. Thesis, California Institute of Technology, Pasadena, California.
Little, C. G., Rayton, W. M., and Roof, R. B. 1956. Proc. IRE, **44**, 992.
Lyon, G. F. and Kavadas, A. 1959. Can. J. Phys. **36**, 1661.

INFRARED TEMPERATURE AND LINE STRENGTH MEASUREMENTS ON CARBON MONOXIDE EXCITED IN A RADIO-FREQUENCY DISCHARGE[1]

D. R. EATON[2]

ABSTRACT

Relative line intensities in the $2 \rightarrow 0$ sequence of bands of carbon monoxide observed in emission from a radio-frequency discharge have been measured. An enhancement of the R branch lines and a diminution of the P branch lines due to vibration–rotation interaction has been observed in agreement with theoretical predictions. Vibrational and rotational temperatures have been calculated and when allowance is made for the vibration–rotation interaction these prove to be equal within experimental error indicating the existence of thermal equilibrium in the discharge.

A. INTRODUCTION

The problem of the relative strengths of individual lines in a vibration–rotation band has been the subject of a number of recent papers. The theory of the effect of the interaction of vibration and rotation on the line strengths has been developed by Herman and Wallis (1955) and extended by other authors. The predicted effect has been observed by means of absorption experiments on the fundamental bands of HCl, DCl (Benedict, Herman, Moore, and Silverman 1956, 1957), HF (Kuipers 1958), and DCN (Eaton 1959). In the case of CO the effect on the fundamental is predicted to be too small for observation and this also is in agreement with experiment (Herman, Silverman, and Wallis 1954; Eaton and Thompson 1959).

The results referred to above have all been obtained from absorption spectra but there are some advantages to be gained by carrying out measurements in emission rather than in absorption. In particular the effect of the finite slit width is such that the relative line strengths can be obtained more easily and directly from the actual measurements and the elevated temperature of the gas allows the extension of the measurements to higher J values and to vibrationally excited states. In most molecules the discrepancy between R and P line strengths becomes pronounced only at high J values. This type of measurement also provides a method of probing the closely related problem of the existence or otherwise of thermal equilibrium among the various rotational and vibrational energy levels of a gas in a flame or discharge.

The present measurements have been carried out on the $2 \rightarrow 0$ sequence of bands of carbon monoxide. This molecule has a very small dipole moment (μ) so that the parameter $\theta = \mu/(d\mu/dr)$ is also small and the nature of the vibration–rotation interaction is rather different from that in molecules such as HCl and HF for which $\theta \sim 1$. The theoretical treatment of Herman and

[1]Manuscript received December 17, 1959.
Contribution from the Division of Pure Physics, National Research Council, Ottawa, Canada.
Issued as N.R.C. No. 5544.
[2]National Research Council Postdoctorate Fellow.

Wallis (1955) and of Herman, Rothery, and Rubin (1958) predicts that the interaction effect in the $2 \rightarrow 0$ band will become appreciable at high J values and that it will be in the opposite sense to that observed in more polar diatomic molecules. This prediction has now been experimentally verified. The intensity distribution in these bands is also of some astrophysical interest since they have been observed in the sun and used to determine solar temperatures (Goldberg and Müller 1953).

B. EXPERIMENTAL

The $2 \rightarrow 0$ sequence of carbon monoxide has been previously observed in emission from flames by Plyler, Benedict, and Silverman (1952) and under lower resolution from an R.F. discharge by Wilkinson, Ford, and Price (1955). The discharge tube used for the present work was of pyrex, 1 meter long and around 10 cm in diameter. It was equipped with a system of multireflection mirrors of the type first suggested by White (1942) for use in absorption work and later adapted for emission experiments by Welsh, Cumming, and Stansburg (1951). It was found that the optimum signal was obtained with a path length of about 40 meters. Power was provided by a 5-kw oscillator operating at 11 Mc/sec. The output from this oscillator could be controlled by adjusting the position of a coupling coil. Power was transferred to the discharge tube either by placing the latter inside a tuned coil or by means of aluminum foil electrodes. The tube was air-cooled but still tended to overheat and crack when the foil electrodes were in use. For this reason the coil method of coupling was used in spite of the rather greater efficiency of the electrodes. Cylinder carbon monoxide was streamed through the tube at a constant pressure of 3 to 4 mm of mercury. Under these conditions a stable discharge giving reproducible line intensities could be maintained for periods of up to 1 hour. The vacuum infrared spectrometer has been described previously (Douglas and Sharma 1953). The detector was a lead sulphide cell cooled to dry ice – acetone temperature and the slit widths employed corresponded to a resolution of about 0.2 cm^{-1}. The amplifier time constant was 0.3 second and the scanning speed was sufficiently slow to allow a maximum throw on the strongest lines. Readjustment of the fore-prism was made every 20 to 30 cm^{-1}.

The variation in the sensitivity of the instrument over the frequency range 3850 cm^{-1} to 4400 cm^{-1} was obtained by calibration with a tungsten filament bulb using the tungsten emissivity curves of De Vos (1954) and the blackbody radiation tables of Lowan and Blanch (1940). The temperature of the filament was measured with an optical pyrometer and it was verified by calculation that the *relative* corrections applied are insensitive to possible errors in this temperature.

C. RESULTS

The observed spectrum consisted of the sequence containing the $2 \rightarrow 0$, $3 \rightarrow 1$, $4 \rightarrow 2$, $5 \rightarrow 3$, $6 \rightarrow 4$, and $7 \rightarrow 5$ bands of CO. In addition some lines of the $8 \rightarrow 6$ and $9 \rightarrow 7$ bands were also observed but not in sufficient number

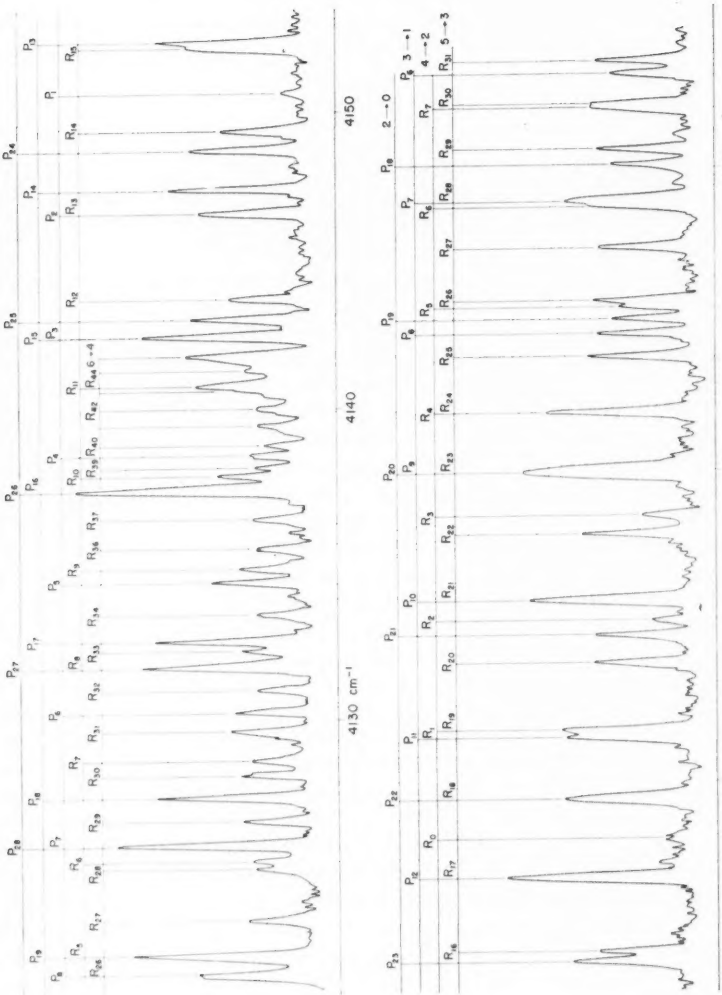

FIG. 1. Radio-frequency discharge spectrum of CO from 4120 cm^{-1} to 4180 cm^{-1}.

TABLE I

Measured line intensities (peak heights)

Line	2→0	3→1	4→2	5→3	6→4	7→5
P_1		19.3	11.6			
P_2		21.0				
P_3						
P_4			28.6			
P_5						
P_6		43.1	41.3		12.0	
P_7				25.7		
P_8		50.5				
P_9	25.7				15.7	
P_{10}	28.3		47.3	28.7	20.1	
P_{11}	32.6	66.6		34.2		
P_{12}	35.2		53.7	31.7	25.5	
P_{13}	36.8	78.3	50.8	37.1		
P_{14}		72.7		40.1	23.2	
P_{15}		85.5	54.5	42.5	22.3	
P_{16}	45.1	81.6				10.3
P_{17}		80.3	57.2			
P_{18}	43.0		61.9		20.5	10.2
P_{19}	43.0			39.7	21.6	10.1
P_{20}				41.0	24.9	
P_{21}	50.7		61.6		28.9	
P_{22}		78.1		37.9		12.2
P_{23}	62.7	78.9	63.9	40.7	25.6	
P_{24}	61.4	74.3		41.5		
P_{25}	60.9	76.9			23.0	12.0
P_{26}						
P_{27}			63.3			
P_{28}		77.2	61.9			10.3
P_{29}		74.9	57.3	38.2		13.5
P_{30}		72.7	56.7	39.1		
P_{31}		71.9	55.5	39.9		
P_{32}	62.0	73.1	54.2			
P_{33}	59.8	67.4	51.7	27.7		
P_{34}				31.0		
P_{35}				27.4		
P_{36}	55.5	69.8				
P_{37}		65.0	40.8	25.9	17.3	
P_{38}	48.5	57.0		26.3	16 2	
P_{39}		57.1	34.7	22.8		
P_{40}		51.9	35.7		13.4	
P_{41}	46.0	51.2		19.3	10.1	
P_{42}	45.5	45.5	36.2			
P_{43}			33.1	14.7		
P_{44}						
P_{45}	36.4	37.2		16.8		
P_{46}	34.6	37.4	34.7	16.1		
P_{47}	35.5	33.5				
P_{48}	30.6	25.6		15.5		
P_{49}	27.6		27.5			
P_{50}	24.8	23.0		9.5		
P_{51}		29.6	18.5			
P_{52}	22.3		12.4			
P_{53}	19.0	21.9	8.1			
P_{54}		15.0				
P_{55}	16.9	16.6				
P_{56}		13.2				
P_{57}						
P_{58}		15.2				
P_{59}		14.1				

Line	2→0	3→1	4→2	5→3	6→4	7→5
R_0		13.2				
R_1		24.7				
R_2		35.4	21.2			
R_3			25.5	17.4		
R_4	13.7	46.1		23.9		
R_5	15.4	54.2				
R_6		59.6		29.7	18.3	
R_7		63.1		30.7	18.4	
R_8		72.9			17.8	
R_9	26.5		58.0	35.8		
R_{10}						
R_{11}						10.2
R_{12}			61.9	41.2		
R_{13}	39.0	90.1			25.9	17.2
R_{14}	38.9	97.3	74.4	44.0	26.8	18.7
R_{15}	40.6	94.6	78.1		28.5	18.8
R_{16}	41.4	101.7	81.7	50.1	27.8	18.9
R_{17}	41.3	104.4	90.7		31.0	19.0
R_{18}	44.6	108.8	89.0			
R_{19}	53.9	112.4	91.8		33.6	
R_{20}	54.6	110.6	92.8	51.5	33.7	
R_{21}	55.5	112.4	92.9			
R_{22}	56.3	112.3		57.9		18.6
R_{23}	61.3	116.8	97.3		33.3	
R_{24}	64.6	118.5	95.7			
R_{25}	67.9	111.3	95.0	55.6		18.8
R_{26}	66.9	118.3	92.4			
R_{27}	71.1	130.8	96.9	49.8	34.4	
R_{28}	75.8	122.7	89.8			
R_{29}		112.0	88.0	50.8	36.2	
R_{30}	76.6	117.3	90.1		36.3	17.6
R_{31}	87.5	116.4	82.7	51.8	40.5	16.9
R_{32}	74.8	114.7			28.3	18.5
R_{33}	74.8	109.3		45.0		17.8
R_{34}	71.4	103.0			27.6	
R_{35}	74.6	101.2	80.1	49.4		15.6
R_{36}	73.8		77.4	46.9	26.9	
R_{37}	70.4	94.1		45.1	27.8	17.2
R_{38}	72.8	99.4	72.1			14.9
R_{39}	71.1		65.9	36.5	26.2	
R_{40}	65.3	89.5		36.5	23.7	
R_{41}	64.5	86.8	65.0	34.8	24.6	
R_{42}	63.6	83.2			24.6	

or with sufficient intensity for the present type of measurement. A portion of the spectrum is shown in Fig. 1 to indicate the degree of resolution. About 50 to 60% of the total number of lines was sufficiently free from overlap to allow reliable measurement. The measured relative intensities of these lines, corrected for changes in instrumental sensitivity, are given in Table I. The absolute values are arbitrary.

The amount of light emerging from the exit slit of the spectrometer when it is set on the center of an emission line is given by an expression of the type

$$T_{\nu'} = \text{constant } I_m \int_0^\infty f_1(\gamma, \nu-\nu')\, f_2(a, \nu-\nu')\, d\nu \ldots . \tag{1}$$

I_m is the integrated intensity of the mth line and f_1 and f_2 are functions describing the line shape and spectrometer slit function respectively. They involve γ, the line width parameter (f_1), and a, the spectral slit width (f_2). Equation (1) is much simpler than the corresponding expression for absorption in that $T_{\nu'}$ is directly proportional to I_m. Under the present experimental conditions the line width arising from Doppler broadening will be around 0.01 cm^{-1} and that from pressure broadening <0.001 cm^{-1} (Eaton and Thompson 1959). Natural line width is negligible in the infrared. Since the slit width a is ~ 0.2 cm^{-1} the slit function f_2 will therefore be approximately constant over the range of frequencies for which f_1 is appreciably large and can therefore be removed from the integral in equation (1). Variation of slit width with frequency is therefore absorbed into the instrumental sensitivity correction. Further, when f_2 has been removed the remaining integral $\int f_1 d\nu$ must by the definition of integrated line intensity be a constant independent of the line width γ. The values given in Table I will therefore be used as a direct measure of the line intensities.

There is a source of error in emission intensity measurements which should also be considered, namely that arising from self-absorption. Errors from this source will be greatest in lines arising from transitions to heavily populated lower states, i.e. to the lower-lying vibrational energy levels and J values. Fortunately it is the high J values which are most significant in the present case. Preliminary experiments showed that self-absorption from gas in the cooler parts of the tube was appreciable for the $2 \rightarrow 0$ band and revealed itself as a distinct curvature in the temperature plot. The measurements from this band have not therefore been used in any of the subsequent calculations. There is, however, no indication of a significant effect in the higher bands and the results from these latter are thought to be reliable.

D. DISCUSSION

The intensity of an emission line in a vibration–rotation band is given by an expression of the type

$$I_m = \text{constant } \nu^4 F(m)\, (J'+J''+1) \exp\left(-\frac{hc}{kT} E_J'\right). \tag{2}$$

The function $F(m)$ (where $m = -J$ for the P branch and $m = J+1$ for the R branch) is introduced to allow for the vibration–rotation interaction. The

other symbols have their usual significance. $F(m)$ is unity at the band origin but becomes increasingly different from unity at higher J values. If $F(m)$ were unity at all J values, i.e. no vibration–rotation interaction, the rotational temperature could be found by plotting $\log\{I/[\nu^4(J'+J''+1)]\}$ against E'_J and obtaining the slope. If, however, the F values for the corresponding lines in the P and R branches are not equal the points for the two branches will fall on separate curves. The separation of the curves will give the ratio of the F factors at a given value of m but the method of temperature determination will fail. Figure 2 shows this plot for the $3 \rightarrow 1$ band. The results for the other bands are very similar. The frequencies and energy levels were calcu-

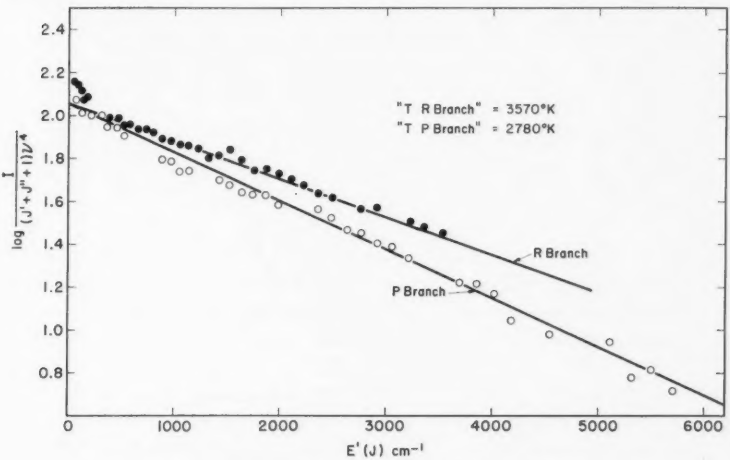

FIG. 2. "Rotational temperature" plot for the $3 \rightarrow 1$ band.

lated from the molecular constants given by Plyler, Benedict, and Silverman (1952). It is apparent that the F factors are appreciably different in the two branches, being largest in the R branch which is in accord with the theoretical treatment of Herman, Rothery, and Rubin (1958). Straight lines drawn through the points for the two branches gave approximate apparent temperatures of 3570° K and 2780° K and since the theory predicts that $F(m)$ will be greater than unity and $F(-m)$ less than unity by roughly equal amounts the true temperature will be between these values and may be estimated as around 3175° K. It is not possible, however, to obtain either the temperature or the F factors independently from these plots.

A vibrational temperature may be obtained from the relative intensities of corresponding lines in the different bands of the sequence. As many pairs as possible from both P and R branches were chosen and from the average ratios the intensities of the other bands relative to the $3 \rightarrow 1$ band were calculated. It is also necessary to know the vibrational transition probabilities (M^2) and the values given by Herman (1952) were taken. These are stated to be uncertain to the extent of 10%. Figure 3 shows the plot of $\log(I/M^2\nu^4)$

against E' (vib.). This leads to a vibrational temperature of 3120° K. Bearing in mind the approximations involved in both cases this value is probably sufficiently close to the estimated rotational temperature of 3175° K to indicate the existence of thermal equilibrium between the vibrational and rotational energies. It is interesting to note that from the flame spectrum of

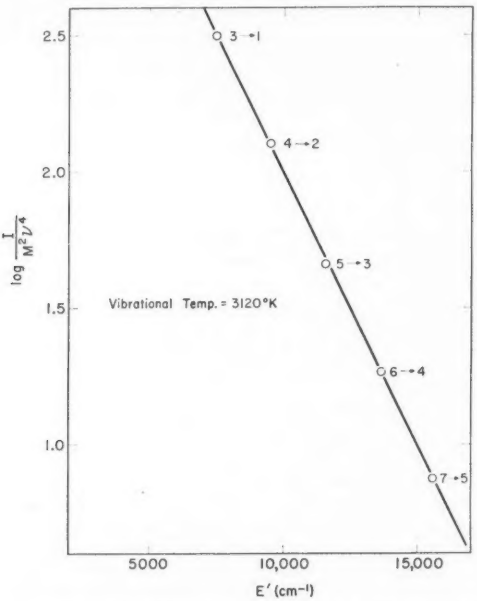

FIG. 3. Vibrational temperature plot for the $2 \rightarrow 0$ sequence of bands.

CO Plyler, Benedict, and Silverman obtained a vibrational temperature of 2360° K and a rotational temperature of 2800° K. This latter temperature, though, was obtained only from R branch lines and the apparent discrepancy is very similar to the corresponding quantity obtained from the present discharge spectrum (3570° K rotational, 3120° K vibrational). A correct allowance for the vibration–rotation interaction could well produce agreement between the two temperatures. It would seem from this that the conditions of energy transfer in carbon monoxide flames and discharges are quite similar and that in both cases there is a sufficiently close approximation to thermal equilibrium to give a physical meaning to the temperature values obtained.

In order to further substantiate this conclusion the vibrational value of 3120° K was taken as a rotational temperature and used to obtain the F values from equation (2). The results are illustrated in Fig. 4, points from the $3 \rightarrow 1$ and $4 \rightarrow 2$ bands being included. The solid curves are obtained from the theory of Herman, Rothery, and Rubin. The theoretically calculated

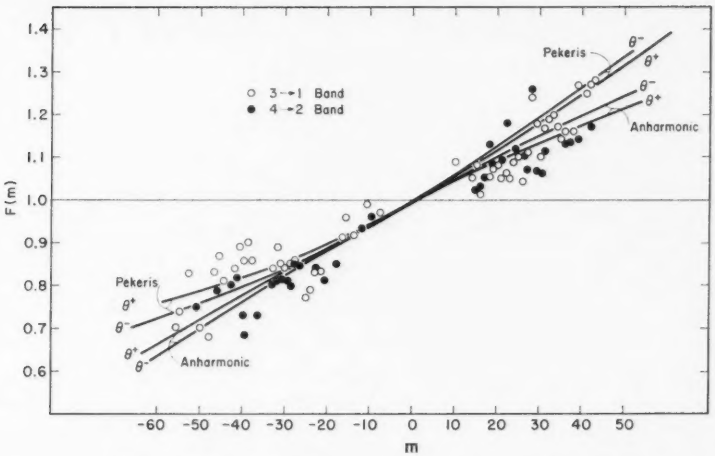

FIG. 4. Comparison of experimental and theoretical F values.

values depend on the form of the potential field assumed and curves for both an anharmonic oscillator and for a Pekeris oscillator are included. The F values also depend on whether the signs of the dipole moment μ and its derivative $d\mu/dr$ for CO are the same or opposite and the curves labelled θ^+ and θ^- represent these alternatives. As can be seen from Fig. 4 the experimental F factors agree well with the theoretical values within the experimental error but this error is too large to enable a choice to be made between the different types of oscillator or between the alternative signs of θ. The F factors for the higher bands show no systematic deviation from those for the lower bands. This also would seem to be in agreement with theoretical expectations.

It may be concluded that the Herman and Wallis theory gives a satisfactory account of the effects of vibration–rotation interaction for the present case where θ is small and the anharmonic effects are predominant as well as for cases previously studied where θ is large. An allowance for this effect must be made if meaningful temperatures are to be obtained from intensity measurements and in the present case the results show that thermal equilibrium between the vibrational and rotational energies has been attained. The results obtained also indicate that in some cases infrared intensities can with profit be studied in emission rather than in absorption. This may prove to be particularly true in the case of unstable radicals such as OH.

ACKNOWLEDGMENTS

The author would like to thank Drs. G. Herzberg and D. A. Ramsay, who read the manuscript and made helpful suggestions.

REFERENCES

BENEDICT, W. S., HERMAN, R., MOORE, G. E., and SILVERMAN, S. 1956. Can. J. Phys. **34**, 830.
BENEDICT, W. S., HERMAN, R., MOORE, G. E., and SILVERMAN, S. 1957. J. Chem. Phys. **26**, 1671.
DE VOS, J. C. 1954. Physica, **20**, 690.
DOUGLAS, A. E. and SHARMA, D. 1953. J. Chem. Phys. **21**, 448.
EATON, D. R. 1959. Proc. Roy. Soc. A, **251**, 486.
EATON, D. R. and THOMPSON, H. W. 1959. Proc. Roy. Soc. A, **251**, 458.
GOLDBERG, L. and MÜLLER, E. A. 1953. Astrophys. J. **118**, 397.
HERMAN, R. 1952. *Quoted in* Plyler, Benedict, and Silverman (1952).
HERMAN, R. and WALLIS, R. F. 1955. J. Chem. Phys. **23**, 637.
HERMAN, R., SILVERMAN, S., and WALLIS, R. F. 1954. Phys. Rev. **94**, 752.
HERMAN, R., ROTHERY, R. W., and RUBIN, R. J. 1958. J. Molecular Spectroscopy, **2**, 369.
KUIPERS, G. A. 1958. J. Molecular Spectroscopy, **2**, 75.
LOWAN, A. N. and BLANCH, G. 1940. J. Opt. Soc. Am. **30**, 70.
PLYLER, E. K., BENEDICT, W. S., and SILVERMAN, S. 1952. J. Chem. Phys. **20**, 175.
WILKINSON, G. R., FORD, M. A., and PRICE, W. C. 1955. Molecular Spectroscopy, Institute of Petroleum.
WELSH, H. L., CUMMING, C., and STANSBURG, E. J. 1951. J. Opt. Soc. Am. **41**, 712.
WHITE, J. U. 1942. J. Opt. Soc. Am. **32**, 285.

TABLES OF THE MODIFIED BESSEL FUNCTIONS OF THE SECOND KIND FOR PARTICULAR TYPES OF ARGUMENT[1]

E. DEMPSEY[2] AND G. C. BENSON

ABSTRACT

Tables of the modified Bessel functions of the second kind $K_n(z)$ for arguments z of the form $(\pi/2)\sqrt{q}$ and $(\pi/3)\sqrt{q}$ where q is an integer and for all integral and half-integral orders n in the range 0–10.5 are presented. For all but a small range of the argument the tables can be relied upon to the 10 figures given; in the omitted range an error of unity in the 10th place may occur. The tables should be useful for the computation of many lattice sums arising in the theoretical calculation of crystal properties.

1. INTRODUCTION

For the theoretical calculation of the properties of ionic crystals it is important to be able to evaluate, reasonably accurately, various summations over the lattice sites, where the quantities summed are usually potential functions involving inverse powers of the distances from the ions to the point at which the potential is required. Since these functions may represent the relatively long-range attractive interactions arising from the electrostatic and dispersive forces within the crystal, it is not surprising that often their sums do not converge very rapidly. Occasionally for inverse powers greater than about three or four, summations of this type have been carried out by direct addition of terms for a large number of lattice points, the summation being completed by an integration over the remainder of the lattice (Lennard-Jones and Dent 1928; Shuttleworth 1949). Alternatively the summation may be effected by transforming the sum to a more rapidly converging form and summing the resulting series directly (see, for instance, Madelung 1918; and van der Hoff and Benson 1953). The latter approach has been used fairly recently in papers dealing with the Coulomb and van der Waals potentials associated with the problem of the adsorption of polarizable atoms or ions onto the surface of an infinite hemicrystal (Hove and Krumhansl 1953; Hartman 1956; Durham and Soderberg 1958) and for the calculation of edge energies (Schreiber and Benson 1955) and surface energies (van Zeggeren and Benson 1957; Benson, Balk, and White 1959; Benson, Dempsey, and Balk, unpublished). All of these applications have the common ground that the series resulting from the various transformations involve the modified Bessel functions of the second kind, $K_n(z)$, although frequently other transcendental functions also arise. For the definition of $K_n(z)$ used here see Watson (1948).

In the work originating from this laboratory (references above to Benson and co-workers) it has been found that the arguments of the Bessel functions

[1]Manuscript received November 11, 1959.
Contribution from the Division of Pure Chemistry, National Research Council, Ottawa, Canada.
Issued as N.R.C. No. 5566.
[2]National Research Council of Canada Postdoctorate Fellow 1958–59. Present address: Atomic Weapons Research Establishment, Aldermaston, Berkshire, England.

which have occurred so far have integral and half-integral orders n in the range 0–8 and that the arguments may all be expressed in one or other of the general forms:

$$(1) \qquad \begin{cases} z = \frac{\pi}{2}\sqrt{q} \\ z = \frac{\pi}{3}\sqrt{q} \end{cases}$$

where q is an integer.

In problems involving distortion of the lattice surface, the potential energies required usually have to be evaluated at points off the regular lattice array. Since the displacements from the regular sites are, in general, small, the summations required may, in these cases, be expanded in Taylor series about a zero displacement. This allows the original summation to be expressed as a linear combination of a number of summations involving functions of the form (1), but with orders which, in general, are higher than those of the original summation. For problems concerned with the interaction of ions situated at an arbitrary distance z above an infinite hemicrystal (as in the references to adsorption problems given above) the argument of the Bessel functions will usually include z. In many of these cases it should also be possible to remove the variable z from the argument by a suitable series expansion.

In order to facilitate the evaluation of lattice summations in our own work, tables of the modified Bessel functions for arguments of the forms (1) have been computed for a fairly wide range of orders and arguments. The purpose of this paper is to present these in the hope that they may be of use to other workers.

2. CALCULATION OF THE TABLES

The computation of the tables was carried out entirely on a Bendix G 15D digital computer operating in a double-precision floating point mode. Although this gave 12 figures in the final results, the entries in the tables were eventually rounded off to 10 figures. To simplify the presentation, the tables have been left in the floating point notation, in which the two figures to the left of the point indicate, on an excess 50 basis, the power of 10 by which the remaining decimal part must be multiplied. This notation should be evident from the following examples:

$$46.123 \equiv 0.123\times10^{-4}$$
$$50.123 \equiv 0.123$$
$$55.123 \equiv 0.123\times10^{5}$$

The basis for most of the computation was the asymptotic expansion for $K_n(z)$:

$$(2) \qquad K_n(z) = \left(\frac{\pi}{2z}\right)^{\frac{1}{2}} e^{-z}\left[1+\frac{4n^2-1^2}{(8z)1!}+\frac{(4n^2-1^2)(4n^2-3^2)}{(8z)^2 2!}+\ldots\right].$$

$K_n\left(\frac{\pi}{2}\sqrt{q}\right)$

q \ n	0	1	2	3	4	5	6	7	8	9	10
1	50.1951287277	50.2507523596	50.5143965479	51.1560652413	51.6475649650	52.3454086526	53.2263696274	54.1763877434	55.1594723913	56.1642011214	57.1897553488
2	49.8698701881	50.1049750604	50.1814977785	50.4317858830	51.1347729405	51.5285316976	52.2514001495	53.1410891109	53.9143138149	54.6726462276	55.5541780745
3	49.4807526926	49.5629569853	49.8945852965	50.1878185581	50.5036577223	51.1668784189	51.6637317345	52.3094354291	53.1658646311	54.1006367158	54.6823936151
4	49.2950868364	49.3391350309	49.5109869626	49.9897437621	50.2401258248	50.7104497680	51.2501557673	51.9026569622	52.4824897403	53.2559957031	54.1514996310
5	49.1932495256	49.2191979399	49.3180630321	49.5814145042	50.1311252791	50.3567976494	51.1146946089	51.4275293323	52.1818771053	52.8712541238	53.4646784673
6	49.1323767817	49.1486731718	49.2096567794	49.3666314655	49.7813795411	50.1991269142	50.5956666810	51.2056884537	51.8079816054	52.3565585377	53.1748843469
7	48.9376518734	49.1044883147	49.1440493128	49.2413131995	49.4950650748	50.1196112307	50.5373146401	51.1093585626	51.4021249411	52.1657505208	52.7581034956
8	48.6817432868	48.7548828252	49.1021559949	49.1674609915	49.3283077894	49.7586227105	50.2035808800	50.6257283747	51.2175303702	51.8459569498	52.3644860171
9	48.5062562983	48.5575847636	48.7429026218	49.1188180094	49.2255740504	49.5017644111	50.1290351201	50.3787616762	51.1254295257	51.4637477200	52.1896815333
10	48.3825817761	48.4194556641	48.5514687608	48.8635354759	49.1594534204	49.3431588281	49.8502899581	50.2397291163	50.7606901383	51.2689964977	52.1050832502
11	48.2934358244	48.3204494137	48.4164551261	48.6402004670	49.1153776664	49.2411906834	49.5783375588	50.1573320116	50.4806278494	51.1633421525	51.6124206214
12	48.2279487581	48.2480716979	48.3191281549	48.4826644621	48.8513418844	49.1734161144	49.4038603898	50.1064071225	50.3141575384	51.1030162475	51.3721907576
13	48.1790552156	48.1942629658	48.2476559014	48.3691739645	48.6387585550	49.1271441152	49.2883698412	49.7381417529	50.2113005905	50.6707520570	51.2340383446
14	48.1420336593	48.1536727807	48.1943265983	48.2859266372	48.4862184502	48.9477430401	49.2098744387	49.5232802957	50.1456334944	50.4487861870	51.1520080792
15	48.1136534369	48.1226612944	48.1539782193	48.2239016769	48.3748006012	48.7167630235	49.1552976369	49.3779999937	50.1025167574	50.3074182814	51.1012087933
16	47.9165843609	47.9869960577	48.1230754964	48.1770519003	48.2921476070	48.5490257864	49.1165949285	49.2775824892	49.7350956822	50.2149488273	50.6892925989
17	47.7444475482	47.7999806853	47.9914863428	48.1412334447	48.2299898179	48.4253233405	48.8867001624	49.2068232050	49.5357476687	50.1530359742	50.4789005399
18	47.6085406482	47.6526950062	47.8044179693	48.1135515421	48.1826714030	48.3328375095	48.6821058371	49.1561059538	49.3961483041	50.1107196039	50.3386628280
19	47.5003802590	47.5357468241	47.6568725409	47.9194933187	48.1462627804	48.2628434575	48.5301472068	49.1191983220	49.2967405180	49.8126243766	50.2433057405
20	47.4136747415	47.4421937948	47.5395695847	47.7494303108	48.1179669294	48.2092861378	48.4158909968	48.9197235686	49.2248840578	49.6041773206	50.1772994894
21	47.3437047607	47.3668452206	47.4456303747	47.6144763578	47.9578154319	48.1678968090	48.3290268520	48.7164049325	49.1722366767	49.4544794248	50.1308704665
22	47.2868937484	47.3057775064	47.3698987596	47.5065996733	47.7824566887	48.1356208620	48.2623208697	48.5628716497	49.1331883432	49.3455249199	49.9773403605
23	47.2405056202	47.2559975318	47.3084700972	47.4197882422	47.6428173242	48.1102431436	48.2106233306	48.4457519525	49.1039018380	49.2652533876	49.7376980644
24	47.2024291738	47.2152012173	47.2583597407	47.3494960596	47.5308607004	47.9013765796	48.1702194760	48.3555768199	48.8171177305	49.2054521035	49.5622828168
25	47.1710224182	47.1816005963	47.2172666303	47.2922535825	47.4405319213	47.7409757129	48.1383971501	48.2855528405	48.6474051862	49.1604435856	49.4324501307
26	47.1449989096	47.1537977995	47.1834026536	47.2453901186	47.3672264664	47.6121800536	48.1131541891	48.2307475251	48.5164823409	49.1262484295	49.3353695324
27	47.1233438981	47.1306923493	47.1553681064	47.2068336173	47.3074125727	47.5081410558	47.9299744549	48.1875399160	48.4146744335	49.1000418129	49.2620912121
28	47.1052518762	47.1114122958	47.1320598646	47.1749646943	47.2583596986	47.4236303824	47.7680286847	48.1532447173	48.3349187075	48.7979489129	49.2062938449
29	46.9007965368	46.9526260036	47.1126030331	47.1485091173	47.2179411356	47.3546244599	47.6371686820	48.1258516978	48.2720067811	48.6403463177	49.1634607286
30	46.7731081063	46.8168612369	46.9629962194	47.1264578736	47.1844890692	47.2980036866	47.5308597573	48.1038427786	48.2220615113	48.5168073260	49.1303297922
31	46.6652856192	46.7023390960	46.8258969261	47.1080072261	47.1566871556	47.2513324602	47.4440614106	47.8606217671	48.1821713762	48.4193346143	49.1045214495
32	46.5739489532	46.6054238541	46.7102171967	46.9251339192	47.1334902068	47.2126968032	47.3728582097	47.7162322979	48.1501320552	48.3419559075	48.8428361417
33	46.4963442498	46.5231574947	46.6122982138	46.7945801762	47.1140636556	47.1805834581	47.3141885511	47.5984087782	48.1242618507	48.2801745908	48.6831493611
34	46.4302181587	46.4531227865	46.5291614977	46.6842169051	46.9773758046	47.1537891260	47.2656436105	47.5018228150	48.1032685536	48.2305790448	48.5564091849
35	46.3737193153	46.3933361940	46.4583718580	46.5906348097	46.8397153949	47.1313518129	47.2253170998	47.4223039151	47.8615252732	48.1905621364	48.4552620239
36	46.3253207222	46.3421636472	46.3973031033	46.5110504284	46.7232749107	47.1124985240	47.1916921324	47.3565685274	47.7213554734	48.1581179613	48.3741186090
37	46.2837582768	46.2982539362	46.3461885795	46.4431818328	46.6244881016	46.9660514613	47.1635554140	47.3020169666	47.6060812569	48.1316932962	48.3087016531
38	46.2479818444	46.2604857764	46.3017843294	46.3851509082	46.5404393094	46.8316547932	47.1399317193	47.2565801122	47.5109021965	48.1100781533	48.2557167618
39	46.2171161316	46.2279255365	46.2635859313	46.3354061254	46.4687352408	46.7176718970	47.1200335347	47.2186028906	47.4320171278	47.9232452828	48.2126110806
40	46.1904292565	46.1997933277	46.2305101096	46.2926612004	46.4074039111	46.6207302861	47.1032221236	47.1867551442	47.3664008230	47.7768564158	48.1773949391
41	46.1673079344	46.1754568626	46.2021921851	46.2558461436	46.3548145997	46.5380608641	46.8897724924	47.1599630324	47.3116339957	47.6557019400	48.1485090964
42	46.1472342411	46.1543034526	46.1775494885	46.2240680182	46.3096141435	46.4673815464	46.7687350181	47.1373559284	47.2657730513	47.5550770189	48.1247252545
43	46.1297743136	46.1359338568	46.1561682113	46.1965793486	46.2706760025	46.4068049658	46.6656169292	47.1182250859	47.2272497387	47.4712206684	48.1050710162
44	46.1145593219	46.1199358481	46.1375807780	46.1727525815	46.2370593589	46.3547649400	46.5775416105	47.1019912972	47.1947933993	47.4011130546	47.8877293384
45	46.1012770068	46.1059781408	46.1213920124	46.1520593608	46.2079761383	46.3099576277	46.5021311109	46.8817946142	47.1673704082	47.3423191679	47.7521303161
46	45.8966196737	45.9377938191	46.1072670703	46.1340536464	46.1824673128	46.2712942413	46.4374131997	46.7639849107	47.1441367684	47.2928676205	47.6392542913
47	45.7948809841	45.8310005607	45.9492153018	46.1183579134	46.1608662070	46.2378628932	46.3817469686	46.6632536385	47.1244008221	47.2511561996	47.5442058174
48	45.7056233611	45.7373579734	45.8411322801	46.1046518327	46.1418108074	46.2088976938	46.3337630320	46.5769241013	47.1075937863	47.2158779124	47.4846529792
49	45.6271947053	45.6551184661	45.7463550963	45.9266295564	46.1251992838	46.1837936296	46.2921152750	46.5027713733	46.9324636695	47.1859628080	47.5376716253
50	45.5581783010	45.5827844501	45.6631163708	45.8215902454	46.1106931033	46.1618860701	46.2564417735	46.4389405255	46.8097012173	47.1605320073	47.3411233755

$K_n(\frac{\pi}{2}\sqrt{q})$

q \ n	0	1	2	3	4	5	6	7	8	9	10
51	45.4973568201	45.5190699482	45.5899013847	45.7294160373	45.9800423849	46.1428339919	46.2253330276	46.3838806601	46.7044254518	47.1388612249	47.2932596526
52	45.4436822163	45.4628685117	45.5254093154	45.6484079386	45.8688707858	46.1262062029	46.1983060517	46.3362915028	46.6139508797	47.1203517044	47.2526458618
53	45.3962504813	45.4132263418	45.4685208353	45.5771082788	45.7713172601	46.1116699934	46.1747831721	46.2950800105	46.5360349673	47.1045069698	47.2181012417
54	45.3542804269	45.3693197139	45.4182709602	45.5142639493	45.6855842643	45.9894176008	46.1542746196	46.2593249966	46.4687999735	46.9091416006	47.1886509569
55	45.3170958073	45.3304359702	45.3738262394	45.4587956282	45.6101292743	45.8777923532	46.1363641966	46.2282482003	46.4106694819	46.7922898721	47.1634877974
56	45.2841102216	45.2959574810	45.3344655494	45.4097719540	45.5436260105	45.7797503153	46.1206974384	46.2011905499	46.3603166985	46.6916357422	47.1419414443
57	45.2548143365	45.2653480791	45.2995638830	45.3663878000	45.4849319621	45.6935126163	46.1069718089	46.1775926318	46.3166221986	46.6047658711	47.1234537215
58	45.2287650486	45.2381415622	45.2685786368	45.3279459554	45.4330611207	45.6175504573	45.9492855749	46.1569785706	46.2786392914	46.5296520309	47.1075585985
59	45.2055762736	45.2139319273	45.2410379871	45.2938416458	45.3871610326	45.5505474827	45.8434593826	46.1389426896	46.2455655439	46.4645855264	46.9386597972
60	45.1849111016	45.1923650592	45.2165310156	45.2635494220	45.3464934436	45.4913681937	45.7503354946	46.1231384407	46.2167193027	46.4081234888	46.8204852201
61	45.1664751041	45.1731316429	45.1946993048	45.2366120346	45.3104179355	45.4390313719	45.6682759600	46.1092691944	46.1915202827	46.3590447664	46.7183088138
62	45.1500106115	45.1559611087	45.1752297698	45.2126309713	45.2783780643	45.3926876670	45.5958691529	45.9708055819	46.1694734755	46.3163135934	46.6298091570
63	45.1352918124	45.1406164486	45.1578485335	45.1912583952	45.2498895923	45.3516006564	45.5318963565	45.8635395314	46.1501557756	46.2790495862	46.5530246695
64	45.1221205494	45.1268897726	45.1423156840	45.1721902618	45.2245304779	45.3151308036	45.4753036035	45.7690123113	46.1332048378	46.2465028982	46.4862942304
65	45.1103227050	45.1145984909	45.1284207782	45.1551604323	45.2019323444	45.2827218446	45.4251778942	45.6856015283	46.1183097702	46.2180335958	46.4282081937
66	44.9974509082	45.1035820294	45.1159789796	45.1399356298	45.1817731950	45.2538892123	45.3807270705	45.6119058079	46.1052033437	46.1930944944	46.3775678754
67	44.9025276531	44.9369899884	45.1048277352	45.1263111102	45.1637711815	45.2282101732	45.3412627480	45.5467126774	45.9365545501	46.1712168410	46.3333519628
68	44.8172671702	44.8482475182	44.9482391100	45.1141069396	45.1476792636	45.2053154099	45.3061858135	45.4889714118	45.8346762962	46.1519983434	46.2946885966
69	44.7406186082	44.7684926995	44.8584131913	45.1031647897	45.1332806249	45.1848818218	45.2749740797	45.4377700309	45.7446839002	46.1350931388	46.2608321119
70	44.6716530212	44.6967533510	44.7776858053	44.9334517205	45.1203847307	45.1666263591	45.2471717546	45.3923157734	45.6650934415	46.1202033693	46.2311436168
71	44.6095483107	44.6321694349	44.7050727370	44.8452505016	45.1088239329	45.1503007311	45.2223804442	45.3519184924	45.5946187585	46.1070720923	46.2050747396
72	44.5535761439	44.5739792861	44.6397032967	44.7659577246	44.9845054151	45.1356868584	45.2002514519	45.3159765078	45.5321433917	45.9547730120	46.1821539973
73	44.5030905742	44.5215076378	44.5808063813	44.6946128177	44.8913429403	45.1225929570	45.1804791748	45.2839645311	45.4766967524	45.8522687352	46.1619753403
74	44.4575181272	44.4741551959	44.5276983549	44.6303656140	44.8076016610	45.1108501625	45.1627954333	45.2554233403	45.4274338434	45.7615429350	46.1441885047
75	44.4163491549	44.4313895486	44.4797724944	44.5724628496	44.7322647429	45.1003096142	45.1469645927	45.2299509367	45.3836179718	45.6811502384	46.1284908712
76	44.3791302833	44.3927372305	44.4364897884	44.5202364147	44.6644322979	44.9083993373	45.1327793604	45.2071949591	45.3446059859	45.6098342258	46.1146205835
77	44.3454578092	44.3577767866	44.3973709034	44.4730931175	44.6033070778	44.8232504036	45.1200571592	45.1868461639	45.3098356471	45.5465011832	46.1023507177
78	44.3149719186	44.3261327018	44.3619891622	44.4305057533	44.5481820260	44.7466225703	45.1086369934	45.1686328150	45.2788148099	45.4901977188	45.9148433628
79	44.2873516187	44.2974700815	44.3299643984	44.3920053045	44.4984294315	44.6776066461	44.9837673623	45.1523158476	45.2511121355	45.4400916419	45.8185028224
80	44.2623102908	44.2714899863	44.3009575714	44.3571741169	44.4534914661	44.6153967083	44.8915077925	45.1376846933	45.2263491097	45.3954556022	45.7329959831
81	44.2395917829	44.2479253333	44.2746660427	44.3256399260	44.4128719198	44.5592776394	44.8084799236	45.1245536713	45.2041931721	45.3556530682	45.6570247227
82	44.2189669729	44.2265372940	44.2508194272	44.2970706194	44.3761289710	44.5086142578	44.7336995084	45.1127588634	45.1843517912	45.3201262914	45.5894562705
83	44.2002307428	44.2071121229	44.2291759453	44.2711696398	44.3428688576	44.4628418294	44.6662939257	45.1021554058	45.1665673493	45.2883859593	45.5293008722
84	44.1831993114	44.1894583632	44.2095192127	44.2476719454	44.3127403276	44.4214577719	44.6054887388	44.9261513705	45.1506127200	45.2600022868	45.4756926465
85	44.1677078811	44.1734043821	44.1916554110	44.2263404571	44.2854297689	44.3840143945	44.5505959683	44.8402455434	45.1362874385	45.2345973354	45.4278731511
86	44.1536085593	44.1587961954	44.1754107927	44.2069629295	44.2606569304	44.3501125367	44.5010038495	44.7628303428	45.1234143811	45.2118383802	45.3851772546
87	44.1407685206	44.1454955437	44.1606294782	44.1893491928	44.2381711580	44.3193959873	44.4561678745	44.6930128244	45.1118368831	45.1914321759	45.3470209724
88	44.1290683805	44.1333781912	44.1471715078	44.1733287186	44.2177480804	44.2915465829	44.4156029495	44.6299998058	45.1014162326	45.1731199907	45.3128909786
89	44.1184007550	44.1223324188	44.1349111201	44.1587484707	44.1991866877	44.2662798995	44.3788765202	44.5730860472	44.9202948942	45.1566733022	45.2823355512
90	44.1086689830	44.1122576890	44.1237352257	44.1454710033	44.1823067536	44.2433414594	44.3456025392	44.5216439155	44.8356758482	45.1418900598	45.2549567428
91	43.9978599275	44.1030634609	44.1135420554	44.1333727793	44.1669465585	44.2225033904	44.3154361662	44.4751143325	44.7593366253	45.1285914365	45.2304036032
92	43.9167329535	43.9466813794	44.1042399604	44.1223426797	44.1529608768	44.2035614782	44.2880691071	44.4329988408	44.6904163027	45.1166190017	45.2083663037
93	43.8426008915	43.8699813324	43.9574634744	44.1122806821	44.1402191954	44.1863325651	44.2632255113	44.3948526402	44.6281489265	45.1058322584	45.1885710381
94	43.7748246347	43.7998703751	43.8798673172	44.1030966878	44.1286041354	44.1706522507	44.2406583554	44.3602784702	44.5718524175	44.9610649356	45.1707755907
95	43.7128268927	43.7357487873	43.8089389494	43.9470947998	44.1180100536	44.1563728584	44.2201462535	44.3289212301	44.5209188477	44.8733090179	45.1547654801
96	43.6560858693	43.6770746229	43.7440713555	43.8704579748	44.1083418005	44.1433616343	44.2014906402	44.3004632420	44.4748059070	44.7940694379	45.1403506008
97	43.6041296230	43.6233578257	43.6847160068	43.8003951054	43.9951361753	44.1314991521	44.1845132814	44.2746200771	44.4330294081	44.7224690988	45.1273622927
98	43.5565310334	43.5741549785	43.6303769041	43.7363088677	43.9144815701	44.1206778970	44.1690540710	44.2511368728	44.3951566952	44.6577266101	45.1156507836
99	43.5129033027	43.5290646126	43.5806052616	43.6776593690	43.8407560960	44.1108010093	44.1549690809	44.2297850816	44.3608008424	44.5991452429	45.1050829529
100	43.4728959346	43.4877230155	43.5349947576	43.6239583118	43.7733292766	44.1017811678	44.1421288316	44.2103595971	44.3296155419	44.5461032311	44.9554037483

$K_n(\frac{\pi}{2}\sqrt{q})$

q \ n	0	1	2	3	4	5	6	7	8	9	10
101	43.4361911362	43.4496004801	43.4931772900	43.5747637835	43.7116313303	43.9353952685	44.1304167587	44.1926762115	44.3012905952	44.4980452447	44.8691760418
102	43.4025005956	43.4159979476	43.4598191797	43.5296756014	43.6551469954	43.8600518197	44.1197278513	44.1766693645	44.2755479327	44.4544748868	44.7912067312
103	43.3715625951	43.3850439997	43.4296177708	43.4883111508	43.6034100189	43.7911366287	44.1039674409	44.1618901477	44.2521380963	44.4149480845	44.7206577135
104	43.3431394213	43.3536921619	43.3872983862	43.4504616606	43.5559982324	43.7280703122	44.1010501255	44.1485045347	44.2308371287	44.3790672614	44.6567808649
105	43.3170150428	43.3267184843	43.3576115972	43.4155888688	43.5125291509	43.6703270432	43.9289881146	44.1362918096	44.2114438186	44.3464761952	44.5989078387
106	43.2929930227	43.3019139698	43.3303307743	43.3836220338	43.4726560338	43.6174316579	43.8544385921	44.1251431708	44.1937772610	44.3168554745	44.5464410835
107	43.2709946448	43.2791096231	43.3052498890	43.3542552549	43.4360643589	43.5689536573	43.7862232253	44.1149604886	44.1776746924	44.2899184819	44.4988459269
108	43.2505572272	43.2581206960	43.2821815379	43.3272650673	43.4024686633	43.5245029372	43.7237726911	44.1056552002	44.1629895699	44.2654078393	44.4556435917
109	43.2318326055	43.2387991101	43.2609551672	43.3024482833	43.3716097100	43.4837257880	43.6665717408	43.9714732496	44.1495898648	44.2430922596	44.4164050295
110	43.2145857674	43.2210050363	43.2414154754	43.2796200509	43.3432519465	43.4463013114	43.6141537793	43.8936458660	44.1373565449	44.2227637546	44.3807454712
111	43.1986936218	43.2046110147	43.2234209754	43.2586121100	43.3171812221	43.4119382099	43.5660960171	43.8224162981	44.1261822498	44.2042351593	44.3483196057
112	43.1840438900	43.1895008025	43.2068426990	43.2392712217	43.2932027379	43.3803719060	43.5220151316	43.7571932114	44.1159969629	44.1873379318	44.3188173127
113	43.1705341047	43.1755683329	43.1915630302	43.2214577553	43.2711392025	43.3513619582	43.4815633809	43.6974412411	44.1066321905	44.1719201989	44.2919598800
114	43.1580707072	43.1627167777	43.1774746519	43.2050444144	43.2508291738	43.3246897389	43.4444251210	43.6426754043	43.9808975565	44.1578450176	44.2674966498
115	43.1465682314	43.1508576987	43.1644795961	43.1899150893	43.2321255656	43.3001563484	43.4103136817	43.5924561007	43.9027107000	44.1449888275	44.2452020420
116	43.1359485670	43.1399108233	43.1524883863	43.1759638212	43.2148943024	43.2775807386	43.3789685629	43.5463846348	43.8311134684	44.1332400716	44.2248729091
117	43.1261402928	43.1298006512	43.1414192621	43.1630936773	43.1990131072	43.2567980247	43.3501529168	43.5040992035	43.7655191987	44.1224979677	44.2063261857
118	43.1170780738	43.1204612292	43.1311974792	43.1512168573	43.1843704074	43.2376579646	43.3236512844	43.4652712986	43.7053963375	44.1126714112	44.1893967963
119	43.1087021155	43.1118301840	43.1217546749	43.1402520298	43.1708643486	43.2200235897	43.2992675607	43.4296024779	43.6502629856	44.1036779963	44.1739357931
120	43.1009576694	43.1038509097	43.1130289356	43.1301255434	43.1584019027	43.2037699693	43.2768231633	43.3968214660	43.5996820114	43.9544314024	44.1598086960
121	42.9373458496	42.9641756213	43.1049610766	43.1207698518	43.1468980633	43.1887830966	43.2561553833	43.3666815495	43.5532566691	43.8789930182	44.1468940127
122	42.8716690363	42.8964463623	42.9750057205	43.1121231401	43.1362751170	43.1749588636	43.2371158934	43.3389582346	43.5106266695	43.8096528063	44.1350819177
123	42.8103249020	42.8332659327	42.9059872837	43.1041288121	43.1264619856	43.1622022519	43.2195694387	43.3134471400	43.4714646517	43.7464559043	44.1242730729
124	42.7535269840	42.7747749423	42.8421149728	42.9673502768	43.1173936296	43.1504263127	43.2033925680	43.2899620997	43.4354730149	43.6882989739	44.1143775732
125	42.7009206719	42.7206070480	42.7829846487	42.8989428199	43.1090105066	43.1395516240	43.1884726037	43.2683334542	43.4023810697	43.6349251644	44.1053140038
126	42.6521804480	42.6704259925	42.7282632434	42.8356302434	43.1012580923	43.1295055195	43.1747066258	43.2484065100	43.3719424773	43.5859195932	43.9700859621
127	42.6070073789	42.6239230251	42.6774992878	42.7770131216	42.9408641708	43.1202215005	43.1620005885	43.2300401506	43.3439239436	43.5409052894	43.8939447296
128	42.5651268342	42.5808145361	42.6304914347	42.7227249676	42.8744968398	43.1116356654	43.1502685152	43.2131055825	43.3179485033	43.4995395475	43.8241096999
129	42.5262864107	42.5408399069	42.5869159115	42.6724293784	42.8130589368	43.1037013107	43.1394317700	43.1974852033	43.2942618527	43.4615106519	43.7600302966
130	42.4902540426	42.5037595515	42.5465091212	42.6258174400	42.7561651517	42.9635827882	43.1294183988	43.1830715790	43.2725245261	43.4263349284	43.7012065566
131	42.4566162905	42.4693531339	42.5090287450	42.5826539670	42.7034618477	42.8956274741	43.1201625323	43.1697665193	43.2523604320	43.3943540913	43.6471842384
132	42.4251776234	42.4374179436	42.4742519388	42.5429233553	42.6546243252	42.8327175718	43.1116038452	43.1574803415	43.2337689762	43.3647328545	43.5975504249
133	42.3956945685	42.4077674158	42.4419736894	42.5053586276	42.6093543344	42.7744589352	43.1036870654	43.1461306134	43.2166207624	43.3374567778	43.5519295712
134	42.3701834077	42.3802297807	42.4120053163	42.4708636529	42.5673778120	42.7204897916	42.9636152944	43.1356426484	43.2007978214	43.3123303252	43.5097799497
135	42.3453096381	42.3546468319	42.3841731062	42.4388445244	42.5284828209	42.6704779489	42.8958077875	43.1259469844	43.1861923283	43.2891751139	43.4713904488
136	42.3221925754	42.3308726032	42.3583170663	42.4091144808	42.4923176750	42.6241182550	42.8330219275	43.1169811212	43.1727056851	43.2678283323	43.4358776911
137	42.3007013627	42.3087733410	42.3342897871	42.3815015578	42.4587892232	42.5811302861	42.7748665599	43.1086871101	43.1602476916	43.2481413120	43.4031834355
138	42.2807160840	42.2882245678	42.3119554040	42.3558473577	42.4276613228	42.5412562425	42.7209825532	43.1010119911	43.1487357938	43.2299782370	43.3730722346
139	42.2621259362	42.2691122245	42.2911886486	42.3320059260	42.3987533581	42.5042590326	42.6710400460	42.9390719198	43.1380944029	43.2132149768	43.3453293218
140	42.2448286717	42.2513308875	42.2718739619	42.3098427260	42.3718990050	42.4692905266	42.6247359423	42.8732814696	43.1282542783	43.1977380298	43.3197587031
141	42.2287299058	42.2347832522	42.2539048013	42.2892337019	42.3469450180	42.4360996646	42.5817916314	42.8123394953	43.1191519676	43.1834435682	43.2961814343
142	42.2137424824	42.2193794770	42.2371827164	42.2700644221	42.3237501566	42.4048325054	42.5419509117	42.7558703707	43.1107292986	43.1702365716	43.2744340635
143	42.1997859937	42.2050365835	42.2216168850	42.2522929262	42.3021841985	42.3809279020	42.5049780993	42.7035290390	43.1029329181	43.1580300433	43.2543672230
144	42.1867857487	42.1916779069	42.2071234063	42.2356308588	42.2821270382	42.3553692927	42.4706563034	42.6549984014	42.9571387254	43.1467442985	43.2358443554
145	42.1746732862	42.1792325922	42.1936247650	42.2201791140	42.2637618625	42.3316120971	42.4387858542	42.6099869407	42.8902722771	43.1363063196	43.2187405606
146	42.1633849280	42.1676351329	42.1810493216	42.2057909351	42.2469139372	42.3095230077	42.4091828686	42.5682265551	42.8283172205	43.1266491706	43.2029415515
147	42.1526618696	42.1568249483	42.1693086459	42.1923895153	42.2299422168	42.2889790683	42.3816779411	42.5294705857	42.7708945186	43.1177114659	43.1883427076
148	42.1430497051	42.1467459949	42.1584080890	42.1799038639	42.2148941130	42.2698668310	42.3561149478	42.4934920170	42.7176558460	43.1094366871	43.1748482172
149	42.1339980820	42.1373464107	42.1482243905	42.1682683450	42.2008795172	42.2520815654	42.3323495553	42.4600818366	42.6682809785	43.1017737441	43.1623702997
150	42.1253603851	42.1285781884	42.1387273187	42.1574222541	42.1878239699	42.2355266534	42.3102502221	42.4290475379	42.6224754154	42.9467457676	43.1508284991

$K_n\ (\frac{\pi}{2}\sqrt{q})$

q \ n	0	1	2	3	4	5	6	7	8	9	10
151	42.1173934462	42.1203968752	42.1298683401	42.1473094302	42.1756586359	42.2201127431	42.2896932864	42.4002117533	42.5799682128	42.8809579124	43.1401490434
152	42.1099572770	42.1127612976	42.1216025155	42.1378778994	42.1643198591	42.2057573580	42.2705661319	42.3734110060	42.5405100076	42.8199733010	43.1302642620
153	42.1030148237	42.1056333076	42.1138882216	42.1290795478	42.1537487539	42.1923842542	42.2527644241	42.3484945699	42.5038712155	42.7634237133	43.1211120568
154	41.9653174205	41.9897755018	42.1066868948	42.1208698218	42.1438908313	42.1799229450	42.2361918116	42.3253234269	42.4698403866	42.7109705451	43.1126354212
155	41.9047618944	41.9276124940	41.9996279534	42.1132074519	42.1346956548	42.1683082446	42.2207592857	42.3037693141	42.4382227039	42.6623023105	43.1047820024
156	41.8481863450	41.8695401130	41.9368279152	42.1060541991	42.1261165250	42.1574798511	42.2063845947	42.2837138519	42.4088386123	42.6171323662	42.9750370320
157	41.7953168145	41.8152764278	41.8781616001	41.9937462252	42.1181101892	42.1473819631	42.1929917061	42.2650477459	42.3815225657	42.5751968346	42.9075631958
158	41.7458990854	41.7645598488	41.8233440281	41.9313586445	42.1106365757	42.1379629281	42.1805103146	42.2476700568	42.3561218819	42.5362527100	42.8449921041
159	41.6996971923	41.7171475922	41.7721107860	41.8730745378	42.1036585486	42.1291749193	42.1688753898	42.2314875312	42.3324956955	42.5000761282	42.7869499666
160	41.6564920508	41.6728142657	41.7242164745	41.8186112440	41.9714168281	42.1209736393	42.1580267623	42.2164139885	42.3105139997	42.4664607878	42.7330928704
161	41.6160801948	41.6313505653	41.6794332778	41.7677064830	41.9105405670	42.1133180470	42.1479087428	42.2023697598	42.2900567700	42.4352165063	42.6831042792
162	41.5782726119	41.5925620745	41.6375496457	41.7201168186	41.8536606195	42.1061701078	42.1384697733	42.1892811719	42.2710131613	42.4061679017	42.6366927502
163	41.5428936698	41.5562681566	41.5983690792	41.6756162417	41.8005022797	41.9949456240	42.1296621060	42.1770800757	42.2532807728	42.3791531859	42.5935898516
164	41.5097801258	41.5223009339	41.5617090107	41.6339948662	41.7508106051	41.9325871526	42.1214415088	42.1657034121	42.2367649747	42.3540230620	42.5535482597
165	41.4787802131	41.4905043453	41.5273997711	41.5950577258	41.7043489286	41.8743223958	42.1137669946	42.1550928143	42.2213782909	42.3306397139	42.5163400214
166	41.4497527980	41.4607332768	41.4952836372	41.5586236650	41.6608974894	41.8198699769	42.1066005716	42.1451942422	42.2070398327	42.3088758829	42.4817549658
167	41.4225666003	41.4328527590	41.4652139526	41.5245243165	41.6202521693	41.7689687581	41.9990701484	42.1359576474	42.1936747797	42.2886140207	42.4495992527
168	41.3970994755	41.4067372256	41.4370543158	41.4926031573	41.5822233286	41.7213763178	41.9365365535	42.1273366637	42.1812139037	42.2697455141	42.4196940438
169	41.3732377493	41.3822698294	41.4106778311	41.4627146378	41.5466347330	41.6768675481	41.8781018595	42.1192883246	42.1695931309	42.2521699743	42.3918742886
170	41.3508756049	41.3593418091	41.3859664161	41.4347233778	41.5133225621	41.6352333618	41.8234848282	42.1117728021	42.1587531409	42.2357945853	42.3659876112
171	41.3299145149	41.3378519050	41.3628101621	41.4085034237	41.4821344961	41.5962795003	41.7724244100	42.1047531671	42.1486389974	42.2205335063	42.3418932927
172	41.3102627172	41.3177058184	41.3411067434	41.3839375632	41.4529288717	41.5598254342	41.7246782287	41.9819516842	42.1391998096	42.2063073232	42.3194613379
173	41.2918347293	41.2988157121	41.3207608702	41.3609166910	41.4255739032	41.5257033493	41.6800211848	41.9206703027	42.1303884203	42.1930425455	42.2985716205
174	41.2745509001	41.2810997474	41.3016837836	41.3393392231	41.3999469626	41.4937572108	41.6382441684	41.8633926477	42.1221611198	42.1806711441	42.2791130998
175	41.2583369940	41.2644816567	41.2837927882	41.3191105553	41.3759339150	41.4638418987	41.5991528719	41.8098449988	42.1144773824	42.1691301269	42.2609831015
176	41.2431238067	41.2488903474	41.2670108193	41.3001425624	41.3534285038	41.4358224104	41.5625666949	41.7597732073	42.1072996234	42.1583611490	42.2440866592
177	41.2288468091	41.2342595353	41.2512660428	41.2823531346	41.3323317832	41.4095731239	41.5283177341	41.7129412331	42.1005929765	42.1483101539	42.2283359087
178	41.2154458176	41.2205274050	41.2364914841	41.2656657488	41.3125515923	41.3849771166	41.4962498500	41.6691297965	41.9432508833	42.1389270444	42.2136495334
179	41.2028646886	41.2076362957	41.2226246856	41.2500090718	41.2940020694	41.3619255362	41.4662178062	41.6281351344	41.8846592859	42.1301653792	42.1999522537
180	41.1910510354	41.1955324092	41.2096073881	41.2353165926	41.2766032027	41.3403170188	41.4380864739	41.5897678531	41.8298761633	42.1219820940	42.1871743589
181	41.1799559663	41.1841655405	41.1973852365	41.2215262825	41.2602804138	41.3200571510	41.4117300974	41.5538518698	41.7786425889	42.1143372452	42.1752512762
182	41.1695338404	41.1734888268	41.1859075067	41.2085802795	41.2449641725	41.3010579724	41.3870316147	41.5202234352	41.7307180386	42.1071937735	42.1641231757
183	41.1597420431	41.1634585158	41.1751268526	41.1964245961	41.2305896407	41.2832375147	41.3638820300	41.4887302311	41.6858790242	42.1005172859	42.1537346055
184	41.1505407758	41.1540337499	41.1649990712	41.1850088488	41.2170963409	41.2665193760	41.3421798335	41.4592305371	41.6439178328	41.9427585580	42.1440341578
185	41.1418928625	41.1451763668	41.1554828851	41.1742860072	41.2044278510	41.2508323258	41.3218304642	41.4315924606	41.6046413642	41.8843983803	42.1349741603
186	41.1337635693	41.1368507137	41.1465397403	41.1642121606	41.1925315201	41.2361099401	41.3027458138	41.4056932250	41.5678700569	41.8298169850	42.1265103927
187	41.1261204369	41.1290234754	41.1381336188	41.1547463026	41.1813582056	41.2222902623	41.2848437666	41.3814185119	41.5334368967	41.7787585728	42.1186018258
188	41.1189331255	41.1216635143	41.1302308648	41.1458501306	41.1708620294	41.2093154903	41.2680477743	41.3586618530	41.5011865019	41.7309854373	42.1112103809
189	41.1121732702	41.1147417222	41.1228000231	41.1374878597	41.1610001514	41.1971316854	41.2522864622	41.3373240670	41.4709742767	41.6862766291	42.1043007082
190	41.1058143474	41.1082308820	41.1158116887	41.1296260503	41.1517325599	41.1856885031	41.2374932639	41.3173127395	41.4426656299	41.6444267219	41.9783998258
191	40.9983154996	41.1021055400	41.1092383680	41.1222334478	41.1430218766	41.1749389430	41.2236060837	41.2985417407	41.4161352525	41.6052446744	41.9179771552
192	40.9420167113	40.9634188666	41.1030543488	41.1152808334	41.1348331761	41.1648391174	41.2105669832	41.2809307797	41.3912664490	41.5685527786	41.8614558121
193	40.8890299738	40.9091764578	40.9723558033	41.1087408864	41.1271338178	41.1553480362	41.1983218907	41.2644049914	41.3679505203	41.5341856885	41.8085725656
194	40.8391520801	40.8581197172	40.9175956111	41.1025880551	41.1198932904	41.1464274070	41.1868203323	41.2488945540	41.3460861910	41.5019895226	41.7590827336
195	40.7921928209	40.8100535357	40.8660523501	40.9679843786	41.1130830666	41.1380414505	41.1760151822	41.2343343343	41.3255790812	41.4718210345	41.7127588185
196	40.7479741183	40.7647952614	40.8175289448	40.9134967159	41.1066764690	41.1301567284	41.1658624310	41.2206635596	41.3063412160	41.4435468455	41.6693892484
197	40.7063292197	40.7221738704	40.7718409057	40.8622082890	41.1006485446	41.1227419833	41.1563209706	41.2078255130	41.2882905725	41.4170427360	41.6287772128
198	40.6671019469	40.6820291960	40.7288154913	40.8139232187	40.9497594932	41.1157679908	41.1473523950	41.1957672514	41.2713506596	41.3921929888	41.5907395888
199	40.6301459982	40.6442112101	40.6882909291	40.7684581274	40.8963683917	41.1092074217	41.1389208153	41.1844393432	41.2554501287	41.3688897822	41.5551059478
200	40.5953242972	40.6085793552	40.6501156896	40.7256413078	40.8461077023	41.1030347136	41.1309926871	41.1737956257	41.2405224133	41.3470326282	41.5217176370

$K_n(\frac{\pi}{2}\sqrt{q})$

q \ n	0	1	2	3	4	5	6	7	8	9	10
201	40.5625083873	40.5750019212	40.6141478109	40.6853119489	40.7987860496	40.9722595199	41.1235366514	41.1637929797	41.2265053950	41.3265278520	41.4904269314
202	40.5315778668	40.5433554655	40.5802542693	40.6473194161	40.7542242528	40.9175875971	41.1165233859	41.1543911203	41.2133410929	41.3072881105	41.4610962483
203	40.5024198632	40.5135242727	40.5483103935	40.6115225798	40.7122545161	40.8661219369	41.1099254674	41.1455524026	41.2009753769	41.2892319458	41.4335974214
204	40.4749285429	40.4853998508	40.5181993178	40.5777891914	40.6727196749	40.8176664936	41.1037172433	41.1372416416	41.1893577009	41.2722833719	41.4078110284
205	40.4490046537	40.4588804617	40.4898114739	40.5459953007	40.6354724942	40.7720377147	40.9787471252	41.1294259443	41.1784408551	41.2563714912	41.3836257693
206	40.4245550994	40.4338706833	40.4630441160	40.5160247136	40.6003750155	40.7290637116	40.9237541505	41.1220745544	41.1681807369	41.2414301396	41.3609378900
207	40.4014925419	40.4102810015	40.4378008785	40.4877684874	40.5672979477	40.6885834874	40.8719832846	41.1151587075	41.1585361376	41.2273975570	41.3396506496
208	40.3797350302	40.3880274293	40.4139913637	40.4611244588	40.5361201003	40.6504462185	40.8232377225	41.1086514968	41.1494685444	41.2142160814	41.3196738256
209	40.3592056552	40.3670311517	40.3915307571	40.4359968051	40.5067278547	40.6145105846	40.7773331854	41.1025277479	41.1409419567	41.2018318661	41.3009232564
210	40.3398322264	40.3472181938	40.3703394682	40.4122956346	40.4790146718	40.5806441451	40.7340970908	40.9676390299	41.1329227153	41.1901946159	41.2833204169
211	40.3215469706	40.3285191121	40.3503427960	40.3899366042	40.4528806328	40.5487227587	40.6933677789	40.9133791227	41.1253793439	41.1792573437	41.2667920252
212	40.3042862510	40.3108687052	40.3314706159	40.3688405631	40.4282320106	40.5186300412	40.6549937929	40.8622913367	41.1182824012	41.1689761433	41.2512696775
213	40.2879903039	40.2942057442	40.3136570885	40.3489332202	40.4049808708	40.4902568613	40.6188332083	40.8141823915	41.1116043446	41.1593099791	41.2366895100
214	40.2726029943	40.2784727209	40.2968403865	40.3301448333	40.3830446988	40.4635008698	40.5847530084	40.7688712763	41.1053194018	41.1502204908	41.2229918849
215	40.2580715857	40.2636156128	40.2809624408	40.3124099194	40.3623460523	40.4382660613	40.5526285020	40.7261884383	40.9940345291	41.1416718112	41.2101210991
216	40.2443465270	40.2495836629	40.2659687029	40.2956669844	40.3428122369	40.4144623642	40.5223427811	40.6859750279	40.9383391973	41.1336303980	41.1980251136
217	40.2313812516	40.2363291747	40.2518079224	40.2798582696	40.3243750029	40.3920052597	40.4937862152	40.6480821952	40.8858966338	41.1260648762	41.1866553025
218	40.2191319908	40.2238073203	40.2384319397	40.2649295164	40.3069702626	40.3708154253	40.4668559793	40.6123704343	40.8365088866	41.1189458932	41.1759662200
219	40.2075575992	40.2119759605	40.2257954926	40.2508297449	40.2905378267	40.3508184021	40.4414556149	40.5787089731	40.7899905514	41.1122459819	41.1659153839
220	40.1966193907	40.2007954778	40.2138560344	40.2375110485	40.2750211569	40.3319442849	40.4174946192	40.5469752040	40.7461679433	41.1059394355	41.1564630737
221	40.1862809857	40.1902286187	40.2025735647	40.2249284008	40.2603671360	40.3141274323	40.3948880628	40.5170541532	40.7048783259	41.1000021896	41.1475721446
222	40.1765081686	40.1802403476	40.1919104711	40.2130394757	40.2465258525	40.2973061962	40.3735562322	40.4888379864	40.6659691928	40.9441171324	41.1392078527
223	40.1672687536	40.1707977095	40.1818313807	40.2018044789	40.2334503992	40.2814226687	40.3534242970	40.4622255471	40.6292975985	40.8914690680	41.1313376940
224	40.1585324593	40.1618697011	40.1723030216	40.1911859904	40.2210966854	40.2664224468	40.3344219981	40.4371219265	40.5947295341	40.8418800767	41.1239312539
225	40.1502707921	40.1534271510	40.1632940932	40.1811488172	40.2094232607	40.2522544111	40.3164833579	40.4134380617	40.5621393463	40.7951650193	41.1169600675
226	40.1424569361	40.1454426072	40.1547751446	40.1716598558	40.1983911510	40.2388705201	40.2995464081	40.3910903617	40.5314091953	40.7511504229	41.1103974891
227	40.1350656506	40.1378902315	40.1467184613	40.1626879628	40.1879637042	40.2262256170	40.2835529370	40.3700003568	40.5024285488	40.7096737157	41.1042185719
228	40.1280731739	40.1307457013	40.1390979585	40.1542038345	40.1781064470	40.2142772502	40.2684482522	40.3500943731	40.4750937110	40.6705825139	40.9839995445
229	40.1214571330	40.1239861168	40.1318890816	40.1461798938	40.1687869497	40.2029855045	40.2541809595	40.3313032270	40.4493073826	40.6337339579	40.9291975657
230	40.1151964598	40.1175899147	40.1250687128	40.1385901846	40.1599747003	40.1923128433	40.2407027562	40.3135619407	40.4249782503	40.5989940926	40.8775748109
231	40.1092713115	40.1115367872	40.1186150841	40.1314102729	40.1516409871	40.1822239616	40.2279682374	40.2968094764	40.4020206035	40.5662372901	40.8289392314
232	40.1036629969	40.1058076061	40.1125076950	40.1246171536	40.1437587878	40.1726856480	40.2159347155	40.2809884881	40.3803539772	40.5353457112	40.7831108531
233	39.9835390655	40.1003843512	40.1067272359	40.1181891641	40.1363026664	40.1636666556	40.2045620513	40.2660450887	40.3599028179	40.5062088033	40.7399209869
234	39.9332744833	39.9525004416	40.1012555165	40.1121059027	40.1292486764	40.1551375811	40.1938124952	40.2519286338	40.3405961718	40.4787228314	40.6992114928
235	39.8856798587	39.9038868571	39.9607539802	40.1063481524	40.1225742703	40.1470707521	40.1836505401	40.2385915185	40.3223673935	40.4527904411	40.6608340932
236	39.8406078161	39.8578519691	39.9117073035	40.1008978094	40.1162582144	40.1394401209	40.1740427826	40.2259889876	40.3051538743	40.4283202506	40.6246497340
237	39.7979194309	39.8142536428	39.8652629265	39.9573781608	40.1102805095	40.1322211654	40.1649577931	40.2140789588	40.2888967879	40.4052264692	40.5905279870
238	39.7574837259	39.7729578816	39.8212773787	39.9085209832	40.1046223162	40.1253907963	40.1563659953	40.2028218562	40.2735408526	40.3834285421	40.5583464942
239	39.7191771999	39.7338383439	39.7796154065	39.8622550650	39.9926588519	40.1189272704	40.1482395522	40.1921804555	40.2590341095	40.3628508180	40.5279904482
240	39.6828833839	39.6967758880	39.7401494844	39.8184376031	39.9419449147	40.1128101087	40.1405522597	40.1821197386	40.2453277148	40.3434222386	40.4993521077
241	39.6484924258	39.6616581469	39.7027593568	39.7769339694	39.8939237323	40.1070200199	40.1332794475	40.1726067579	40.2323757459	40.3250760490	40.4723303457
242	39.6159006997	39.6283791278	39.6673316071	39.7376172249	39.8484467405	40.1015388295	40.1263978854	40.1636105088	40.2201350194	40.3077495267	40.4468302268
243	39.5850104400	39.5968388372	39.6337592543	39.7003676638	39.8053738901	39.9634941214	40.1198856964	40.1551018109	40.2085649216	40.2913837284	40.4227626138
244	39.5557293971	39.5669429278	39.6019413740	39.6650723850	39.7645731391	39.9143562865	40.1137222744	40.1470531964	40.1976272498	40.2759232531	40.4000437989
245	39.5279705143	39.5386023681	39.5717827419	39.6316248913	39.7259199782	39.8678226741	40.1078882077	40.1394388058	40.1872860630	40.2613160214	40.3785951606
246	39.5016516246	39.5117331312	39.5431935002	39.5999247116	39.6892969838	39.8237498876	40.1023652073	40.1322342898	40.1775075433	40.2475130681	40.3583428421
247	39.4766951655	39.4862559029	39.5160888433	39.5698770476	39.6545934002	39.7820027316	39.9713603892	40.1254167178	40.1682598653	40.2344683489	40.3392174512
248	39.4530279112	39.4620958073	39.4903887231	39.5413924406	39.6217047459	39.7424537248	39.9218446040	40.1189644922	40.1595130743	40.2221385593	40.3211537802
249	39.4305807210	39.4391821494	39.4660175722	39.5143864599	39.5905324447	39.7049826433	39.8749516209	40.1128572679	40.1512389720	40.2104829652	40.3040905434
250	39.4092883031	39.4174481724	39.4429040433	39.4887794093	39.5609834796	39.6694760911	39.8305371131	40.1070758765	40.1434110097	40.1994632445	40.2879701320

$K_n(\frac{\pi}{3}\sqrt{q})$

q \ n	0	1	2	3	4	5	6	7	8	9	10
1	50.3937175141	50.5559986033	51.1455596627	51.6115968163	52.3649751296	53.2849364289	54.2757439981	55.3188287106	56.4290000284	57.6586520482	59.1136429476
2	50.2191597957	50.2851016259	50.6041822640	51.1916967077	51.8370627579	52.4713424259	53.3266385850	54.2693836671	55.2579234221	56.2813490350	57.3445384553
3	50.1434347082	50.1792448413	50.3410804289	50.9314348257	51.3422242030	52.1602568217	52.9177645854	53.6232138443	54.4902117664	55.4386607972	56.4402255886
4	50.1014742298	50.1236424711	50.2195440925	50.5429408018	51.1774954916	51.7322769169	52.3673860222	53.2178194544	54.1492754403	55.1162162307	56.1013732474
5	49.7529048008	49.9011176652	50.1522562962	50.3502005553	51.1049590993	51.3936086417	52.1785894427	52.9545764511	53.5885816250	54.4117189047	55.3223755986
6	49.5772652897	49.6815938030	50.1108701798	50.2410496293	50.6747070545	51.2345317358	51.9817889264	52.4827517848	53.2732979050	54.1752991197	55.1257451256
7	49.4534857688	49.5297107456	49.8358622222	50.1736460032	50.4596299974	51.1500798150	51.5876453032	52.2695262016	53.1420683875	53.8473793393	54.5647263783
8	49.3630403718	49.4203367818	49.6468674190	50.1293914719	50.3267965619	51.1012052302	51.3743673564	52.1617925907	52.8021754089	53.4495062245	54.2811927611
9	49.2950868364	49.3391350309	49.5109869026	49.9897437621	50.2401258248	50.7104497679	51.2501557673	52.1026569622	52.4824897403	53.2559957031	54.1514996310
10	49.2428865180	49.2773764808	49.4104081948	49.7731089869	50.1811166977	50.5148530121	51.1735845485	51.6805041973	52.3050520716	53.1541941339	53.8686358886
11	49.2020522168	49.2294740134	49.3341935081	49.6143608339	50.1395521970	50.3828774047	51.1241940958	51.4673864766	52.2008186804	52.9718609077	53.5237583326
12	49.1696198775	49.1917067148	49.2753133288	49.4952831018	50.1094504985	50.2909012000	50.9113616848	51.3305661386	52.1366890817	52.6359417372	53.3292206582
13	49.1435253415	49.1615150737	49.2290798226	49.4042020861	49.8713969562	50.2250516803	50.6831886984	51.2396360645	51.9568648780	52.4294444138	53.2142975562
14	49.1222943210	49.1370904736	49.1922695997	49.3333713451	49.7027591798	50.1768212677	50.5215515302	51.1774118850	51.6860512972	52.2978868729	53.1437062380
15	49.1048509962	49.1171254888	49.1626083337	49.2774974880	49.5731299773	50.1407993056	50.4044702685	51.1337522207	51.5021416208	52.2114695111	52.9887395364
16	48.9039569469	49.1006563722	49.1384555723	49.2328717046	49.4720197183	50.1134362961	50.3180111807	51.1024471221	51.3742054016	52.1531806468	52.6956658823
17	48.7832438528	48.8696057671	49.1186053004	49.1968386437	49.3921375489	49.9234050908	50.2530784938	50.7957098086	51.2833137679	52.1129438704	52.4991808540
18	48.6817432868	48.7548828252	49.1021559949	49.1674609915	49.3283077894	49.7586227105	50.2035808800	50.6257238347	51.2175303702	51.8459569497	52.3644860171
19	48.5958656361	48.6581557190	48.8842377338	49.1433016387	49.2767873763	49.6284011616	50.1653462804	50.4975207154	51.1691273379	51.6425796203	52.2703053959
20	48.5227950311	48.5761174738	48.7688303341	49.1232787035	49.2348243278	49.5244126894	50.1354596256	50.3995355846	51.1329832374	51.4942854974	52.2032778312
21	48.4603002535	48.5061610528	48.6712507030	49.1065669283	49.2003653185	49.4405883135	50.1118475298	50.3237439619	51.1056324663	51.3845661125	52.1548097359
22	48.4065972024	48.4462115995	48.5882871472	48.9252930911	49.1718579037	49.3724400338	49.9301148526	50.2644803860	50.8468555978	51.3023084547	52.1192540350
23	48.3602474534	48.3946035007	48.5173916668	48.8066885753	49.1481142176	49.3166048508	49.7785270264	50.2176816688	50.6846691701	51.2398945606	51.9282727160
24	48.3200824895	48.3499891052	48.4565251824	48.7059403296	49.1282154308	49.2705323554	49.6555484612	50.1803919470	50.5578334303	51.1920155712	51.7294960129
25	48.2851464520	48.3112701330	48.4040428848	48.6199361602	49.1114437396	49.2322671075	49.5550412389	50.1504327925	50.4577317824	51.1549158088	51.5783344996
26	48.2546524294	48.2775455714	48.3586082966	48.5461820787	48.9723327169	49.2002947399	49.4723394800	50.1261795235	50.3780614661	51.1259015688	51.4622188307
27	48.2279487581	48.2480716979	48.3191281549	48.4826644621	48.8513418844	49.1734316144	49.4038603898	50.1064071225	50.3141575384	51.1030162475	51.3721907576
28	48.2044928131	48.2222311248	48.2847025786	48.4277462350	48.7478612637	49.1507446959	49.3468271537	49.9018255720	50.2625295229	50.8482197216	51.3017857090
29	48.1838304529	48.1995086251	48.2545865801	48.3800878903	48.6589833393	49.1314926853	49.2990690345	49.7678852219	50.2205393091	50.7025061287	51.2462845962
30	48.1655797784	48.1794721052	48.2281600880	48.3385868482	48.5823466581	49.1150823025	49.2588754873	49.6566876330	50.1861743005	50.5850072021	51.2022055069
31	48.1494182084	48.1617575197	48.2049044118	48.3023304946	48.5160214102	49.1010354925	49.2248885484	49.5638842715	50.1578857021	50.4896531409	51.1669536873
32	48.1350721255	48.1460568293	48.1843836304	48.2705595225	48.4584214270	48.8896459581	49.1960226624	49.4860499987	50.1344719366	50.4118068357	51.1385774831
33	48.1223085319	48.1321083259	48.1662297723	48.2426391005	48.4082359485	48.7855338536	49.1714043929	49.4204679541	50.1149937107	50.3478967942	51.1155961626
34	48.1109282840	48.1196888154	48.1501309397	48.2180360421	48.3643763188	48.6954246538	49.1503266914	49.3649688424	49.9871152803	50.2951512308	50.9687711760
35	48.1007605788	48.1086072636	48.1358217345	48.1963006060	48.3259340496	48.6171794340	49.1322139253	49.3178098214	49.8503929382	50.2514035614	50.8154738155
36	47.9165843609	47.9869960577	48.1230754964	48.1770519002	48.2921476070	48.5490257864	49.1165949285	49.2775824891	49.7350956822	50.2149488273	50.6892925989
37	47.8349498026	47.8982448533	48.1116979767	48.1599661095	48.2623759441	48.4894881902	49.1030820854	49.2431424409	49.6374733224	50.1844368013	50.5849307707
38	47.7616036479	47.8185973873	48.1015221566	48.1447669467	48.2360772831	48.4373328894	48.9135498645	49.2135549511	49.5545002895	50.1587917599	50.4982219288
39	47.6955921837	47.7469948323	47.9240398214	48.1312178700	48.2127920135	48.3915239964	48.8114757542	49.1880528025	49.4837226891	50.1371518078	50.4258689346
40	47.6360851506	47.6825169395	47.8421883895	48.1191157077	48.1921288338	48.3511883356	48.7223798007	49.1660033359	49.4231402984	50.1188226592	50.3652475739
41	47.5823579135	47.6243618011	47.7685862543	48.1082854113	48.1737534665	48.3155871375	48.6444042087	49.1468825466	49.3711149329	50.1032421900	50.3142578457
42	47.5337764798	47.5718288808	47.7022931304	47.9857572081	48.1573794248	48.2840931330	48.5759873759	49.1302546030	49.3262988524	49.8995307489	50.2712105561
43	47.4897848684	47.5243047360	47.6424890502	47.8985556555	48.1427604252	48.2561719266	48.5158118377	49.1157555636	49.2875784999	49.7858153442	50.2347402738
44	47.4498944227	47.4812509610	47.5884572222	47.8201106692	48.1296841243	48.2313667817	48.4627622018	49.1030803642	49.2540300429	49.6882073229	50.2037381079
45	47.4136747414	47.4421939748	47.5395695847	47.7494303107	48.1179669294	48.2092861378	48.4158909968	48.9197236585	49.2248840578	49.6041773225	50.1772994894
46	47.3807459575	47.4067163424	47.4952745926	47.6856484491	48.1074496814	48.1895933266	48.3743908227	48.8221492206	49.1994973347	49.5316319741	50.1546833801
47	47.3507721463	47.3744493791	47.4550868583	47.6280070412	47.9799405019	48.1719980664	48.3375715441	48.7362454181	49.1773302597	49.4688321402	50.1352802384
48	47.3234556824	47.3450668278	47.4185783389	47.5758411610	47.8947951458	48.1562494000	48.3048415373	48.6604532441	49.1579285889	49.4143277023	50.1185867344
49	47.2985323949	47.3182794417	47.3853708174	47.5285663120	47.8180082298	48.1421298106	48.2756922108	48.5934440998	49.1409086954	49.3669053069	50.1041856934
50	47.2757673977	47.2938303280	47.3551294693	47.4856676413	47.7486585208	48.1294503019	48.2496851805	48.5340824573	49.1259455797	49.3255463105	49.9173011481

$K_n\left(\frac{\pi}{3}\sqrt{q}\right)$

q \ n	0	1	2	3	4	5	6	7	8	9	10
51	47.2549514926	47.2714909374	47.3275573447	47.4466907459	47.6859379508	48.1180462707	48.2264416068	48.4813951023	49.1127630846	49.2893927887	49.8093037940
52	47.2358980579	47.2510576003	47.3023906218	47.4112338126	47.6291362434	48.1077740332	48.2056332987	48.4345457039	49.1011258803	49.2577199517	49.7154396592
53	47.2184403527	47.2323485291	47.2793945155	47.3789408818	47.5776278326	47.9850789291	48.1869752676	48.3928137172	48.9083287422	49.2299136712	49.6336715078
54	47.2024291738	47.2152012173	47.2583597407	47.3494960596	47.5308607004	47.9013765796	48.1702194760	48.3555768198	48.8171177304	49.2054521035	49.5628828167
55	47.1877308171	47.1994701788	47.2390994502	47.3226185313	47.4883468277	47.8256653364	48.1551495716	48.3222962459	48.7361458090	49.1838906066	49.4998230624
56	47.1742252988	47.1850249781	47.2214465756	47.2980582577	47.4496514042	47.7570932792	48.1415764409	48.2925044992	48.6641385969	49.1648493203	49.4450630516
57	47.1618048011	47.1717485110	47.2052515147	47.2755922499	47.4143987869	47.6949091983	48.1293344424	48.2657950311	48.5999961298	49.1480029021	49.3969583259
58	47.1503723109	47.1595355008	47.1903801156	47.2550213386	47.3822404321	47.6384494899	48.1182782078	48.2418135418	48.5427668152	49.1330720204	49.3546190775
59	47.1398404257	47.1482911806	47.1767119163	47.2361673676	47.3528756536	47.5871269129	48.1082799184	48.2202506320	48.4916256000	49.1198182796	49.3172853387
60	47.1301303041	47.1379301367	47.1641386038	47.2188707486	47.3260340864	47.5404209242	47.9922698050	48.2008355766	48.4458556180	49.1080283207	49.2843064548
61	47.1211707422	47.1283752914	47.1525626640	47.2029883287	47.3014743506	47.4978693485	47.9102003539	48.1833310364	48.4048327197	49.0975888596	49.2551240496
62	47.1128973589	47.1195570071	47.1418961950	47.1883915255	47.2789806313	47.4590611852	47.8357125368	48.1675285553	48.3680123974	48.8816268059	49.2292578485
63	47.1052518762	47.1114122958	47.1320938646	47.1749646943	47.2583596986	47.4236303824	47.7680286846	48.1532467173	48.3349187075	48.7979489128	49.2062938449
64	46.9818148333	47.1038843206	47.1229819903	47.1626036955	47.2394383089	47.3912504381	47.7064591179	48.1403178584	48.3053148599	48.7230825137	49.1858743970
65	46.9163827257	46.9692077742	47.1145977283	47.1512146355	47.2220609314	47.3616297088	47.6503912392	48.1286052475	48.2782952073	48.6560055973	49.1676899168
66	46.8557873911	46.9047534718	47.1068483560	47.1407127582	47.2060877585	47.3345073250	47.5992800967	48.1179806635	48.2540784072	48.5958257835	49.1514718782
67	46.7996333669	46.8450529014	46.9968063728	47.1310214679	47.1913929598	47.3096496286	47.5526402052	48.1083323097	48.2320215744	48.5417624650	49.1369869196
68	46.7475608222	46.7897160870	46.9304625913	47.1220714662	47.1778631478	47.2868470605	47.5100384428	47.9956103142	48.2124152686	48.4933276471	49.1240318587
69	46.6992420347	46.7383927251	46.8690133220	47.1137999886	47.1653960271	47.2659114353	47.4710878705	47.9157866965	48.1944991888	48.4493327647	49.1124296667
70	46.6543782491	46.6907606546	46.8120594614	47.1061501285	47.1538992046	47.2466735528	47.4354423454	47.8430689302	48.1782584673	48.4098380133	49.1020248799
71	46.6126968703	46.6465268456	46.7592377404	46.9907023733	47.1432891381	47.2289810995	47.4027918162	47.7767584762	48.1635204741	48.3741824225	49.0928254528
72	46.5739489532	46.6054238541	46.7102171967	46.9251339192	47.1334902068	47.2126968032	47.3728582097	47.7162322979	48.1501320552	48.3419559075	48.8428361416
73	46.5379069562	46.5672073749	46.6696960263	46.8643692060	47.1244338884	47.1976968060	47.3453918254	47.6609338199	48.1379571416	48.3127962067	48.7672371499
74	46.5043627262	46.5316540497	46.6223987698	46.8080198118	47.1160580291	47.1838692340	47.3201681730	47.6103651982	48.1268746769	48.2863828314	48.6991104524
75	46.4731256911	46.4985595014	46.5803739848	46.7557318464	47.1083061960	47.1711129213	47.2969851917	47.5640805637	48.1167768151	48.2624318404	48.6376473391
76	46.4440212356	46.4677365696	46.5464910402	46.7071825899	47.1011271003	47.1593362963	47.2756608036	47.5216801090	48.1075673537	48.2406913195	48.5821343356
77	46.4168892406	46.4390137249	46.5124399933	46.6620774896	46.9447408460	47.1484563839	47.2560307562	47.4828049034	47.9916036677	48.2209374649	48.5319410727
78	46.3915827677	46.4122336415	46.4807278739	46.6201474704	46.8830466558	47.1383979240	47.2379467181	47.4471323406	47.9147901197	48.2029711815	48.4865098185
79	46.3679668744	46.3872519126	46.4511780012	46.5811465258	46.8258012559	47.1290925880	47.2212745951	47.4143721356	47.8445448711	48.1866151262	48.4453464283
80	46.3459175444	46.3639358918	46.4236283252	46.5448495563	46.7726514806	47.1204782816	47.2058930403	47.3842627988	47.7802511610	48.1717111321	48.4080125068
81	46.3253207222	46.3421636472	46.3979301033	46.5110504284	46.7232749106	47.1124985240	47.1916921323	47.3565685273	47.7213554733	48.1581179613	48.3741166090
82	46.3060714400	46.3218230174	46.3739467075	46.4795602295	46.6773769510	47.1051018941	47.1785722033	47.3310764591	47.6673604938	48.1457093420	48.3433183330
83	46.2880730282	46.3028107570	46.3515524477	46.4502056977	46.6346882093	46.9824153579	47.1664427962	47.3075924449	47.6178189141	48.1343722503	48.3153031786
84	46.2712364000	46.2850317642	46.3306320987	46.4228278064	46.5949621434	46.9187471621	47.1552217377	47.2859478980	47.5723279740	48.1240054048	48.2897980666
85	46.2554794032	46.2683983804	46.3110790209	46.3972604893	46.5579729475	46.8596243013	47.1448343122	47.2659798888	47.5305246462	48.1145179457	48.2665574268
86	46.2407262324	46.2528297555	46.2927953643	46.3734294879	46.5235136498	46.8046904557	47.1352152546	47.2475474519	47.4920813836	48.1058282736	48.2453617789
87	46.2269068947	46.2382512722	46.2756908467	46.3511513118	46.4913944010	46.7536198593	47.1262944327	47.2305210826	47.4567023573	47.9786302758	48.2260147383
88	46.2139567248	46.2249540222	46.2596822008	46.3303322970	46.4614409299	46.7061144470	47.1180236088	47.2147831987	47.4241201255	47.9055618543	48.2083403918
89	46.2018159436	46.2117943316	46.2446925799	46.3108677550	46.4334931520	46.6619012894	47.1103485135	47.2002269477	47.3940926798	47.8384826879	48.1921809235
90	46.1904292565	46.1997933277	46.2306510196	46.2926612004	46.4074039111	46.6207302860	47.1032221236	47.1867551442	47.3664008230	47.7765641157	48.1773949391
91	46.1797454877	46.1885365455	46.2174919476	46.2756236517	46.3830378435	46.5823720872	46.9660145967	47.1742793197	47.3408458386	47.7201988315	48.1638549827
92	46.1697172466	46.1779735690	46.2051547382	46.2596729961	46.3602703491	46.5466162216	46.9044721620	47.1627188742	47.3172474171	47.6680726861	48.1514466663
93	46.1603006236	46.1680577038	46.1935833066	46.2447334132	46.3389666609	46.5132694060	46.8472342019	47.1520003168	47.2954418087	47.6200822124	48.1400669318
94	46.1514549125	46.1587456788	46.1827257392	46.2307348500	46.3190810007	46.4821540196	46.7939712439	47.1420565851	47.2752801761	47.5758693983	48.1296228972
95	46.1431423563	46.1499973735	46.1725339564	46.2176125447	46.3004558140	46.4531067248	46.7443813085	47.1328264358	47.2566271233	47.5351098410	48.1200307714
96	46.1353279157	46.1417755693	46.1629634051	46.2053065921	46.2830210750	46.4259772190	46.6981874188	47.1242539865	47.2393593817	47.4975093850	48.1112148953
97	46.1279790564	46.1340457209	46.1539727782	46.1937615480	46.2666936556	46.4006271047	46.6551353532	47.1162877743	47.2233646340	47.4628010744	48.1031068903
98	46.1210655553	46.1267757489	46.1455237571	46.1829260687	46.2513967513	46.3769288662	46.6149916173	47.1088812136	47.2085404614	47.4307424363	47.9564903210
99	46.1145593218	46.1199358481	46.1375807780	46.1727525815	46.2370593589	46.3547649399	46.5775416105	47.1019912972	47.1947933993	47.4011305146	47.8877293383
100	46.1084342354	46.1134983131	46.1301108165	46.1631969841	46.2236158007	46.3340268723	46.5425879677	46.9557868836	47.1820380907	47.3737124032	47.8244023944

$K_n(\frac{\pi}{3}\sqrt{q})$

q \ n	0	1	2	3	4	5	6	7	8	9	10
101	46.1026659953	46.1074373778	46.1230831909	46.1542183705	46.2110052915	46.3146145533	46.5099490588	46.8960730696	47.1701965255	47.3483579082	47.7660080156
102	45.9723198326	46.1017290683	46.1164693825	46.1457787790	46.1991715430	46.2964355208	46.4794576286	46.8404403754	47.1591973563	47.3248832121	47.7121285247
103	45.9211113769	45.9635106782	46.1102428700	46.1378429630	46.1880624029	46.2794043266	46.4509595641	46.7885846560	47.1489752835	47.3031366197	47.6623845208
104	45.8728383724	45.9128259281	46.1043789778	46.1303781802	46.1776295257	46.2634419600	46.4243127755	46.7402263921	47.1394705012	47.2829797028	47.6164310997
105	45.8273179438	45.8650427866	45.9885473733	46.1233540002	46.1678280715	46.2484753220	46.3993861807	46.6951085317	47.1306281974	47.2642860486	47.5739544761
106	45.7843795725	45.8199807502	45.9364875886	46.1167421271	46.1586164304	46.2344367463	46.3760587812	46.6529945367	47.1223981034	47.2469401342	47.5346689587
107	45.7438641929	45.7774714920	45.8874111406	46.1105162377	46.1499559705	46.2212635619	46.3542188231	46.6136666125	47.1147340873	47.2308363146	47.4983142424
108	45.7056233610	45.7373579734	45.8411322800	46.1046518327	46.1418108073	46.2088976938	46.3337630319	46.5769241012	47.1075937863	47.2158779124	47.4646529792
109	45.6695184870	45.6994936254	45.7974777971	45.9912609982	46.1341475922	46.1972852979	46.3145959171	46.5425820244	47.1009382736	47.2019763960	47.4334685984
110	45.6354201283	45.6637415939	45.7562861059	45.9391778792	46.1269353180	46.1863764281	46.2966291370	46.5104697585	46.9473175806	47.1890506405	47.4045633495
111	45.6032073371	45.6299740439	45.7174064011	45.8900709171	46.1201451418	46.1761247301	46.2797809199	46.4804298311	46.8894131150	47.1770262595	47.3777565412
112	45.5727670579	49.5980715170	45.6806978803	45.8437554525	46.1137502212	46.1664871628	46.2639755361	46.4523168258	46.8353662127	47.1658350014	47.3528829588
113	45.5439935718	45.5679223385	45.6460290272	45.8000592402	46.1077255641	46.1574237416	46.2491428150	46.4259963849	46.7848976629	47.1554142050	47.3297914374
114	45.5167879816	45.5394220700	45.6132769500	45.7588215479	46.1020478912	46.1488973041	46.2352177045	46.4013443016	46.7377501343	47.1457063055	47.3083435767
115	45.4910577374	45.5124730025	45.5823267703	45.7198923238	45.9669550877	46.1408732948	46.2221398670	46.3782456918	46.6936863258	47.1366583884	47.2884125822
116	45.4667161964	45.4869836892	45.5530710592	45.6831314308	45.9164819225	46.1333195673	46.2098533108	46.3565942386	46.6524872852	47.1282217848	47.2698822181
117	45.4436822162	45.4628685116	45.5254093154	45.6484079386	45.8688707858	46.1262062029	46.1983060517	46.3362915028	46.6139508797	47.1203517043	47.2526458618
118	45.4218797786	45.4400472794	45.4992474836	45.6155994705	45.8239456725	46.1195053440	46.1874498038	46.3172462932	46.5778904028	47.1130069029	47.2366056499
119	45.4012376398	45.4184448589	45.4744975081	45.5845916006	45.7815422912	46.1131910408	46.1772396948	46.2993740909	46.5441333057	47.1061493801	47.2216717038
120	45.3816890081	45.3979908294	45.4510769202	45.5552772963	45.7415072220	46.1072391100	46.1676340062	46.2825965227	46.5125200403	46.9974410445	47.2077614303
121	45.3631712431	45.3786191645	45.4289084557	45.5275564027	45.7036971405	46.1016270054	46.1585939336	46.2668408791	46.4829030040	46.9375876437	47.1947988865
122	45.3456255782	45.3602679364	45.4079197010	45.5013351664	45.6679781012	45.9633369781	46.1500833677	46.2520396731	46.4551455762	46.8816354051	47.1827142047
123	45.3289968626	45.3428790420	45.3880427647	45.4765257937	45.6342248749	45.9133956551	46.1420686919	46.2381302359	46.4291212386	46.8293089911	47.1714430702
124	45.3132333211	45.3263979482	45.3692139735	45.4530460428	45.6023203380	45.8662629228	46.1345185969	46.2250543464	46.4047127706	46.7803540360	47.1609262475
125	45.2962863324	45.3107734561	45.3513735897	45.4308188449	45.5721549058	45.8217677386	46.1274039101	46.2127578906	46.3818115136	46.7345354280	47.1511091491
126	45.2841102216	45.2959574809	45.3344655494	45.4097719540	45.5436260105	45.7797503152	46.1206974384	46.2011905499	46.3603166984	46.6916357421	47.1419414443
127	45.2706620684	45.2819048486	45.3184372188	45.3898376216	45.5166376161	45.7400613219	46.1143738234	46.1903055142	46.3401348283	46.6514538102	47.1333767024
128	45.2579015282	45.2685731060	45.3032391687	45.3709522952	45.4910997709	45.7025611477	46.1084094081	46.1800592186	46.3211791144	46.6138034142	47.1253720688
129	45.2457906660	45.2559223444	45.2888249645	45.3530563385	45.4669281922	45.6671192196	46.1027821140	46.1704111012	46.3033689580	46.5785120922	47.1178879688
130	45.2342938012	45.2439150359	45.2751509705	45.3360937714	45.4440438812	45.6336133724	45.9747132747	46.1613233800	46.2866294759	46.5454200465	47.1108878387
131	45.2233773641	45.2325158802	45.2621761691	45.3200120293	45.4223727669	45.6019292660	45.9245779534	46.1527608484	46.2708910641	46.5143791449	47.1043378797
132	45.2130097613	45.2216916628	45.2498619913	45.3047617382	45.4018453748	45.5719598454	45.8772352813	46.1446906858	46.2560889982	46.4852520056	46.9820683364
133	45.2031612505	45.2114111221	45.2381721597	45.2902965068	45.3823965202	45.5436048417	45.8325171083	46.1370822839	46.2421630651	46.4579111594	46.9246577824
134	45.1938038244	45.2016448266	45.2270725422	45.2765727327	45.3639650230	45.5167703085	45.7902662040	46.1299070864	46.2290572255	46.4322382819	46.8708793979
135	45.1849111016	45.1923650592	45.2165310156	45.2635494220	45.3464934436	45.4913681937	45.7503354946	46.1231384407	46.2167193027	46.4081234888	46.8204852200
136	45.1764582254	45.1835457102	45.2065173385	45.2511880214	45.3299278360	45.4673159412	45.7125873573	46.1167514620	46.2051006967	46.3854646900	46.7732454942
137	45.1684217690	45.1751621771	45.1970030328	45.2394522624	45.3142175205	45.4445361223	45.6768929677	46.1107229067	46.1941561208	46.3641669961	46.7289472407
138	45.1607796474	45.1671912715	45.1879612735	45.2283080155	45.2993148700	45.4229560931	45.6431316943	46.1050310564	46.1838433590	46.3441421732	46.6873929422
139	45.1535110347	45.1596111311	45.1793667855	45.2177231547	45.2851751133	45.4025076770	45.6111905393	45.9965561051	46.1741230423	46.3253081425	46.6483993398
140	45.1465962874	45.1524011392	45.1711957474	45.2076674313	45.2717561505	45.3831268690	45.5809636186	45.9457758632	46.1649584426	46.3075885193	46.6117963309
141	45.1400168718	45.1455418479	45.1634257017	45.1981123561	45.2590183821	45.3647535617	45.5523516813	45.8977922752	46.1563152827	46.2909121893	46.5774259565
142	45.1337552973	45.1390149072	45.1560354713	45.1890310893	45.2469245492	45.3473312904	45.5252616631	45.8524391895	46.1481615607	46.2752129189	46.5451414729
143	45.1277950531	45.1328029985	45.1490050810	45.1803983384	45.2354395855	45.3308069958	45.4996062718	45.8095610790	46.1404673875	46.2604289958	46.5148064986
144	45.1221205494	45.1268897726	45.1423156840	45.1721902618	45.2245304779	45.3151308035	45.4753036034	45.7690123113	46.1332048378	46.2465028981	46.4862942303
145	45.1167170626	45.1212597914	45.1359494941	45.1643843803	45.2141661384	45.3002558189	45.4522767846	45.7306564733	46.1263478112	46.2333809896	46.4594867232
146	45.1115706832	45.1158984732	45.1298897213	45.1569594929	45.2043172830	45.2861379359	45.4304536413	45.6943657450	46.1198719047	46.2210132379	46.4342742278
147	45.1066682680	45.1107920423	45.1241205121	45.1498955994	45.1949563194	45.2727356591	45.4097663904	45.6600203186	46.1137542937	46.2093529555	46.4105545803
148	45.1019973946	45.1059274809	45.1186268936	45.1431738269	45.1860572427	45.2600099377	45.3901513527	45.6275078594	46.1079736231	46.1983565599	46.3882326419
149	44.9754631933	45.1012924844	45.1133947209	45.1367763623	45.1775955368	45.2479240115	45.3715486871	45.5967230065	46.1025099058	46.1879833525	46.3672197811
150	44.9330393712	44.9687541985	45.1084106281	45.1306863878	45.1695480833	45.2364432664	45.3539021417	45.5675669078	45.9734442852	46.1781953140	46.3474333979

$K_n(\frac{\pi}{3}\sqrt{q})$

q \ n	0	1	2	3	4	5	6	7	8	9	10
151	44.8925974471	44.9266528636	45.1036619825	45.1248880221	45.1618930761	45.2255351000	45.3371588234	45.5399467893	45.9245966483	46.1689569159	46.3287964844
152	44.8540380553	44.8865167852	44.9913684116	45.1193662638	45.1546099415	45.2151687966	45.3212689827	45.5137755545	45.8783919473	46.1602349452	46.3112372198
153	44.8172671701	44.8482475181	44.9482391099	45.1141069396	45.1476792636	45.2053154099	45.3061658135	45.4889714118	45.8346762961	46.1519983434	46.2946885965
154	44.7821957986	44.8117519029	44.9071251061	45.1090966552	45.1410827144	45.1959476536	45.2918652662	45.4654575281	45.7933054293	46.1442180565	46.2790880756
155	44.7487396925	44.7769417616	44.8679253495	45.1043227494	45.1348029884	45.1870397998	45.2782658740	45.4431617073	45.7541440578	46.1368668965	46.2643772677
156	44.7168190777	44.7437336134	44.8305442200	44.9977325126	45.1288237418	45.1785675835	45.2653485906	45.4220160896	45.7170652706	46.1299194137	46.2505016384
157	44.6863583998	44.7120484064	44.7948912155	44.9543693976	45.1231295350	45.1705081131	45.2530766386	45.4019568736	45.6819499796	46.1233517771	46.2374102369
158	44.6572860853	44.6818112663	44.7608806589	44.9130280601	45.1177057792	45.1628397877	45.2414153687	45.3829240553	45.6486864033	46.1171416645	46.2250554436
159	44.6295343177	44.6529512609	44.7284314231	44.8736101784	45.1125386861	45.1555422189	45.2303321274	45.3648611869	45.6171695866	46.1112681605	46.2133927374
160	44.6030388266	44.6254011774	44.6974666721	44.8360188659	45.1076152210	45.1485961580	45.2197961342	45.3477151506	45.5873009552	46.1057116615	46.2023804806
161	44.5777386891	44.5990973145	44.6679136188	44.8001633590	45.1029230585	45.1419834277	45.2097783665	45.3314359489	45.5589879001	46.1004537876	46.1919797190
162	44.5535761439	44.5739792860	44.6397032966	44.7659577245	44.9845054150	45.1356868583	45.2002514519	45.3159765078	45.5321433916	45.9547730119	46.1821539973
163	44.5304964157	44.5499898366	44.6127703451	44.7333205847	44.9418664228	45.1296902283	45.1911895683	45.3012924943	45.5066856198	45.9076603089	46.1728691877
164	44.5084475505	44.5270746682	44.5870528085	44.7021748590	44.9012092610	45.1239782077	45.1825683495	45.2873421456	45.4825376594	45.8630480108	46.1640933312
165	44.4873802602	44.5051822771	44.5624919464	44.6724475217	44.8624351720	45.1185363061	45.1743647977	45.2740861094	45.4596271583	45.8207936635	46.1557964907
166	44.4672477765	44.4842638001	44.5390320550	44.6440693735	44.8254506675	45.1133508233	45.1665572009	45.2614872955	45.4378860464	45.7807635061	46.1479506139
167	44.4480057137	44.4642728700	44.5166202998	44.6169748277	44.7901672280	45.1084088035	45.1591250564	45.2495107364	45.4172502651	45.7428319036	46.1405294070
168	44.4296119384	44.4451654796	44.4952065578	44.5911017085	44.7565010204	45.1036979916	45.1520489986	45.2381234578	45.3976595145	45.7068808200	46.1335082168
169	44.4120264482	44.4268998532	44.4747432684	44.5663910615	44.7243726328	44.9920679298	45.1453107317	45.2272943567	45.3790570175	45.6727993269	46.1268639215
170	44.3952112563	44.4094363261	44.4551852941	44.5427869755	44.6937068259	44.9492423553	45.1388929663	45.2169940882	45.3613893000	45.6404831464	46.1205748292
171	44.3791302833	44.3927372304	44.4364897884	44.5202364147	44.6644322978	44.9083993372	45.1327793604	45.2071949591	45.3446059858	45.6098342257	46.1146205834
172	44.3637492546	44.3767667884	44.4186160717	44.4986890606	44.6364814650	44.8694405520	45.1269544639	45.1978708286	45.3286596045	45.5807603398	46.1089820756
173	44.3490356047	44.3614910104	44.4015255147	44.4780971639	44.6097902545	44.8322728931	45.1214036667	45.1889970155	45.3135054128	45.5531747221	46.1036413631
174	44.3349583859	44.3468776004	44.3851814274	44.4584154038	44.5842979095	44.7968081753	45.1161131496	45.1805502110	45.2991012268	45.5269957192	45.9858159367
175	44.3214881827	44.3328958653	44.3695489560	44.4396007569	44.5599468058	44.7629628566	45.1110698388	45.1725083970	45.2854072662	45.5021464694	45.9378693462
176	44.3085970308	44.3195166306	44.3545949845	44.4216123722	44.5366822799	44.7306577775	45.1062613630	45.1648507702	45.2723860075	45.4785546029	45.8924250701
177	44.2962583411	44.3067121601	44.3402880424	44.4044114548	44.5144524662	44.6998179155	45.1016760131	45.1575576702	45.2600020478	45.4561519612	45.8493432441
178	44.2844468271	44.2944560800	44.3265982173	44.3879611548	44.4932081445	44.6703721540	44.9730270404	45.1506105126	45.2482219766	45.4348743359	45.8084923584
179	44.2731384373	44.2827233082	44.3134970729	44.3722264639	44.4729025955	44.6422530658	44.9313093968	45.1439917260	45.2370142562	45.4146612245	45.7697487252
180	44.2623102908	44.2714899862	44.3009575714	44.3571741168	44.4534914661	44.6153967083	44.8915077924	45.1376846933	45.2263491097	45.3954556021	45.7329959830
181	44.2519406166	44.2607334162	44.2889539999	44.3427724991	44.4349326408	44.5897424317	44.8535280594	45.1316736962	45.2161984162	45.3772037084	45.6981246340
182	44.2420086961	44.2504320003	44.2774619015	44.3289915594	44.4171861216	44.5652326982	44.8172809755	45.1259438635	45.2065356124	45.3598548483	45.6650316127
183	44.2324948093	44.2405651840	44.2664580096	44.3158027276	44.4002139146	44.5418129112	44.7826819870	45.1204811222	45.1973356005	45.3433612056	45.6336198830
184	44.2233801829	44.2311134026	44.2559201866	44.3031788364	44.3839799228	44.5194312555	44.7496509479	45.1152721519	45.1885746624	45.3276776685	45.6037980625
185	44.2146469427	44.2220580302	44.2458273653	44.2910940486	44.3684498450	44.4980385459	44.7181118748	45.1103043418	45.1802303782	45.3127616669	45.5754800718
186	44.2062780670	44.2133813321	44.2361594936	44.2795237870	44.3535910811	44.4775880850	44.6879927169	45.1055657506	45.1722815510	45.2985730195	45.5485848062
187	44.1982573439	44.2050664189	44.2268974830	44.2684446696	44.3393726415	44.4580355287	44.6592251383	45.1010450684	45.1647081354	45.2850737912	45.5230358299
188	44.1905693299	44.1970972041	44.2180231584	44.2578344473	44.3257650628	44.4393387606	44.6317443143	44.9673158109	45.1574911711	45.2722281590	45.4987610895
189	44.1831993113	44.1894583632	44.2095192126	44.2476719454	44.3127403276	44.4214577718	44.6054887387	44.9261513704	45.1506127200	45.2600022868	45.4756926464
190	44.1761332676	44.1821352952	44.2013691614	44.2379370086	44.3002717888	44.4043545493	44.5804000433	44.8868611554	45.1440558078	45.2483642082	45.4537664270
191	44.1693578365	44.1751140866	44.1935573022	44.2286104487	44.2883340986	44.3879929693	44.5564228268	44.8493539724	45.1378043686	45.2372837162	45.4329219880
192	44.1628602812	44.1683814767	44.1860686746	44.2196739951	44.2769031404	44.3723386977	44.5335044941	44.8135433628	45.1318431930	45.2267322603	45.4131022979
193	44.1566284594	44.1619248251	44.1788890232	44.2111102482	44.2659559658	44.3573590953	44.5115951054	44.7793473412	45.1261578800	45.2166828494	45.3942535319
194	44.1506507934	44.1557320807	44.1720047620	44.2029026349	44.2554707338	44.3430231288	44.4906472328	44.7466881489	45.1207347904	45.2071099616	45.3763248800
195	44.1449162425	44.1497917527	44.1654029410	44.1950353674	44.2454266542	44.3293012869	44.4706158263	44.7154920217	45.1155610047	45.1979894586	45.3592683672
196	44.1394142765	44.1440928830	44.1590712147	44.1874934032	44.2358039339	44.3161655004	44.4514580862	44.6856889713	45.1106242822	45.1892985063	45.3430386852
197	44.1341348502	44.1386250193	44.1529978120	44.1802624076	44.2265837257	44.3035890675	44.4331333441	44.6572125799	45.1059130230	45.1810154992	45.3275930350
198	44.1290683805	44.1333781912	44.1471715078	44.1733287186	44.2177480804	44.2915465828	44.4156029494	44.6299998057	45.1014162325	45.1731199907	45.3128909786
199	44.1242057228	44.1283428857	44.1415815961	44.1666793132	44.2092799013	44.2800138705	44.3988301630	44.6039908006	44.9712348793	45.1655926265	45.2988943008
200	44.1195381505	44.1235100257	44.1362178642	44.1603017754	44.2011629010	44.2689679206	44.3827800565	44.5791287380	44.9302490611	45.1584150827	45.2855668791

$K_n(\frac{\pi}{3}\sqrt{q})$

q \ n	0	1	2	3	4	5	6	7	8	9	10
201	44.1150573342	44.1188709481	44.1310705692	44.1541842665	44.1933815608	44.2583868296	44.3674194176	44.5553596501	44.8911111427	45.1515700074	45.2728745620
202	44.1107553227	44.1144173842	44.1261304142	44.1483154962	44.1859210920	44.2482497436	44.3527166597	44.5326322754	44.8537322179	45.1450409658	45.2607850542
203	44.1066245248	44.1101414404	44.1213885273	44.1426846960	44.1787673995	44.2385368049	44.3386417381	44.5108979138	44.8180279382	45.1388123887	45.2492678101
204	44.1026576917	44.1060355802	44.1168364406	44.1372815931	44.1719070470	44.2292291016	44.3251660693	44.4901102908	44.7839182644	45.1328695241	45.2382939322
205	43.9884790105	44.1020926070	44.1124660707	44.1320963865	44.1653272247	44.2203086190	44.3122624556	44.4702254287	44.7513272326	45.1271983914	45.2278360771
206	43.9518854094	43.9830564780	44.1082697003	44.1271197238	44.1590157176	44.2117581954	44.2999050136	44.4512015256	44.7201827330	45.1217857385	45.2178683664
207	43.9167329534	43.9466813794	44.1042399604	44.1223426797	44.1529608768	44.2035614782	44.2880691070	44.4329988408	44.6904163027	45.1166190017	45.2083663037
208	43.8829612996	43.9117380614	44.1003698137	44.1177567347	44.1471515912	44.1957028839	44.2767312822	44.4155795867	44.6619629289	45.1116862675	45.1993066955
209	43.8505127894	43.8781666079	43.9665253877	44.1133537560	44.1415772614	44.1881675593	44.2658692083	44.3989078270	44.6347608646	45.1069762369	45.1906675782
210	43.8193323215	43.8459097658	43.9308171498	44.1091259788	44.1362277744	44.1809413457	44.2554616198	44.3829493798	44.6087514539	45.1024781916	45.1824281484
211	43.7893672320	43.8149128204	43.8965120817	44.1050659884	44.1310934800	44.1740107436	44.2454882626	44.3676717270	44.5838789675	44.9818196230	45.1745686980
212	43.7605671793	43.7851234753	43.8635515715	44.1011667036	44.1261651685	44.1673628809	44.2359298431	44.3530439280	44.5600904477	44.9407789903	45.1670705529
213	43.7328840363	43.7564917392	43.8318796075	43.9742136062	44.1214340489	44.1609854812	44.2267679795	44.3390365385	44.5373355618	44.9015684274	45.1599160155
214	43.7062717864	43.7289698181	43.8014426562	43.9382349832	44.1168917292	44.1548668351	44.2179851561	44.3256215335	44.5155664640	44.8641009886	45.1530883101
215	43.6806864256	43.7025120132	43.7721895457	43.9036694352	44.1125301968	44.1489957722	44.2095646800	44.3127722348	44.4947376646	44.8282941230	45.1465715323
216	43.6560858692	43.6770746228	43.7440713555	43.8704579748	44.1083418005	44.1433616343	44.2014906402	44.3004632420	44.4748059070	44.7940694378	45.1403506008
217	43.6324298628	43.6526158504	43.7170413109	43.8385442297	44.1043192330	44.1379542514	44.1937478684	44.2886703676	44.4557300511	44.7613524769	45.1344112122
218	43.6096798981	43.6290957160	43.6910546839	43.8078743199	44.1004555149	44.1327639170	44.1863219024	44.2773705756	44.4374709634	44.7300725101	45.1287397984
219	43.5877991327	43.6064759731	43.6660686977	43.7783967401	43.9674397839	44.1277813663	44.1791989511	44.2665419231	44.4199914130	44.7001623357	45.1233234864
220	43.5667523133	43.5847200284	43.6420424364	43.7500622494	43.9317825326	44.1229977547	44.1723658614	44.2561635054	44.4032559736	44.6715580931	45.1181500606
221	43.5465057035	43.5637928665	43.6189367595	43.7228237652	43.8975225227	44.1184046374	44.1658100870	44.2462154036	44.3872309303	44.6441990872	45.1132079272
222	43.5270270143	43.5436609775	43.5967142202	43.6966362635	43.8646015807	44.1139939505	44.1595196587	44.2366786356	44.3718841920	44.6180276210	45.1084860806
223	43.5082853386	43.5242922885	43.5753389875	43.6714566826	43.8329641041	44.1097579926	44.1534831561	44.2275351091	44.3571852085	44.5929888392	45.1039740716
224	43.4902510882	43.5056560984	43.5547767724	43.6472438332	43.8025569412	44.1056894075	44.1476896808	44.2187675773	44.3431048918	44.5690305792	44.9966197764
225	43.4728959345	43.4877230154	43.5349947575	43.6239583117	43.7733292766	44.1017811678	44.1421288315	44.2103595971	44.3296155419	44.5461032310	44.9554037482
226	43.4561927513	43.4704648985	43.5159615304	43.6015624184	43.7452325221	43.9802655957	44.1367906796	44.2022954893	44.3166907765	44.5241596047	44.9160031106
227	43.4401155613	43.4538548002	43.4976470195	43.5800200791	43.7182202135	43.9441916707	44.1316657463	44.1945603010	44.3043054646	44.5031548052	44.8783328118
228	43.4246394839	43.4378669138	43.4800224338	43.5592967711	43.6922479121	43.9095285903	44.1267449815	44.1871397698	44.2924356633	44.4830461137	44.8423120321
229	43.4097406867	43.4224765217	43.4630602048	43.5393594522	43.6672731107	43.8762177519	44.1220197426	44.1800202901	44.2810585586	44.4637928763	44.8078639606
230	43.3953963386	43.4076599468	43.4467339317	43.5201764939	43.6432551453	43.8442031356	44.1174817755	44.1731888810	44.2701524084	44.4453563975	44.7749155845
231	43.3815845651	43.3933945063	43.4310183289	43.5017176168	43.6201551099	43.8134311843	44.1131231960	44.1666331558	44.2596964897	44.4276998406	44.7433974901
232	43.3682844061	43.3796584673	43.4158891765	43.4839538301	43.5979357761	43.7838506881	44.1089364722	44.1603412932	44.2496710476	44.4107881328	44.7132436742
233	43.3554757752	43.3664310049	43.4013232722	43.4668573732	43.5765615167	43.7554126761	44.1049144076	44.1543020098	44.2400572472	44.3945878759	44.6843913673
234	43.3431394213	43.3536921619	43.3872983862	43.4504016605	43.5559982324	43.7280703121	44.1010501255	44.1485045347	44.2308371286	44.3790672613	44.6567808648
235	43.3312568919	43.3414228104	43.3737932183	43.4345612290	43.5362132825	43.7017787960	43.9733705402	44.1429385840	44.2219935635	44.3641959899	44.6303553692
236	43.3198104980	43.3296046156	43.3607873566	43.4193116876	43.5171754189	43.6764952706	43.9376891150	44.1375943381	44.2135102145	44.3499451960	44.6050608396
237	43.3087832805	43.3182200011	43.3482612382	43.4046296698	43.4988547233	43.6521787316	43.9033969315	44.1324624192	44.2053714962	44.3362873759	44.5808458500
238	43.2981589785	43.3072521152	43.3361961120	43.3904927879	43.4812225469	43.6287899431	43.8704365801	44.1275338704	44.1975625390	44.3231963194	44.5576614557
239	43.2879219989	43.2966847998	43.3245740028	43.3768795897	43.4642514536	43.6062913571	43.8387531669	44.1228001354	44.1900691536	44.3106470452	44.5354610657
240	43.2780573874	43.2865025598	43.3133776777	43.3637695171	43.4479151658	43.5846470361	43.8082941971	44.1182530398	44.1828777987	44.2986157404	44.5142003237
241	43.2685508008	43.2766905348	43.3025906133	43.3511428665	43.4321885124	43.5638225801	43.7790094639	44.1138847731	44.1759755490	44.2870797022	44.4938369936
242	43.2593884804	43.2672344711	43.2921969651	43.3389807517	43.4170473794	43.5437850573	43.7508509427	44.1096878711	44.1693500661	44.2760172831	44.4743308532
243	43.2505572272	43.2581206959	43.2821815379	43.3272650673	43.4024686632	43.5245029371	43.7237726910	44.1056552001	44.1629895699	44.2654078393	44.4556435917
244	43.2420443774	43.2493360920	43.2725297574	43.3159784553	43.3884302258	43.5059460278	43.6977307524	44.1017799413	44.1568828118	44.2552316809	44.4377387138
245	43.2338377799	43.2408680741	43.2632276439	43.3051042720	43.3749108515	43.4880854157	43.6726830660	43.9805557574	44.1510190498	44.2454700255	44.4205814488
246	43.2259257740	43.2327045659	43.2542617861	43.2946265570	43.3618902072	43.4708934083	43.6485893798	43.9447587085	44.1453880236	44.2361049541	44.4041386640
247	43.2182971686	43.2248339783	43.2456193170	43.2845300036	43.3493488028	43.4543434796	43.6254111684	43.9103486678	44.1399799325	44.2271193686	44.3883787835
248	43.2109412223	43.2172451888	43.2372878906	43.2747999304	43.3372679546	43.4384102178	43.6031115544	43.8772686390	44.1347854129	44.2184969524	44.3732717099
249	43.2038476241	43.2099275216	43.2292556593	43.2654222545	43.3256297498	43.4230692764	43.5816552340	43.8454641074	44.1297955182	44.2102221324	44.3587887522
250	43.1970064754	43.2028707285	43.2215112529	43.2563834653	43.3144170131	43.4082973265	43.5610084060	43.8148829257	44.1250016988	44.2022800432	44.3449025551

$K_n(\frac{\pi}{3}\sqrt{q})$

q \ n	0	1	2	3	4	5	6	7	8	9	10
251	43.1904082726	43.1960649709	43.2140437580	43.2476706004	43.3036132742	43.3940720118	43.5411387039	43.7854752049	44.1203957838	44.1946564932	44.3315870342
252	43.1840438900	43.1895008025	43.2068426990	43.2392712217	43.2932027379	43.3803719060	43.5220151315	43.7571932113	44.1159699629	44.1873379318	44.3188173127
253	43.1779045645	43.1831691527	43.1995890192	43.2311733933	43.2831702539	43.3671764717	43.5036080019	43.7299912675	44.1117167696	44.1803114194	44.3065696627
254	43.1719818800	43.1770613110	43.1932000633	43.2233656597	43.2735012899	43.3544660213	43.4858888786	43.7038256589	44.1076290654	44.1735645977	44.2948214492
255	43.1662677532	43.1711689118	43.1867395602	43.2158370257	43.2641819042	43.3422216601	43.4688305197	43.6786454446	44.1037000246	44.1670856626	44.2835510764
256	43.1607544194	43.1654839199	43.1805076073	43.2085769369	43.2551987209	43.3304253506	43.4524068254	43.6543787221	43.9992311925	44.1608633374	44.2727379375
257	43.1554344192	43.1599986167	43.1744956546	43.2015752605	43.2465328053	43.3190596787	43.4369278868	43.6311372968	43.9629210617	44.1548868481	44.2623623669
258	43.1503005863	43.1547055873	43.1686954902	43.1948222681	43.2381901406	43.3081080214	43.4213644379	43.6087161048	43.9260101329	44.1491458998	44.2524059944
259	43.1453460348	43.1495977075	43.1630992262	43.1883086185	43.2301406066	43.2975544163	43.4066988097	43.5871391396	43.8914412735	44.1436306541	44.2428497026
260	43.1405641480	43.1446681322	43.1576932849	43.1820253413	43.2223789574	43.2873835516	43.3925738863	43.5663727322	43.8621598207	44.1383117076	44.2336775852
261	43.1359485670	43.1399102833	43.1524883863	43.1759638212	43.2148943034	43.2775807386	43.3789685629	43.5463846347	43.8311134683	44.1332400715	44.2248729091
262	43.1314931803	43.1353178392	43.1474595355	43.1701157836	43.2076761863	43.2681318847	43.3658626062	43.5271439567	43.8012521592	44.1283471527	44.2164200766
263	43.1271921136	43.1308847942	43.1426060111	43.1644732800	43.2007145708	43.2590234678	43.3532666164	43.5086211051	43.7725279834	44.1236447347	44.2083041909
264	43.1230397200	43.1266059681	43.1379213536	43.1590266747	43.1939998175	43.2502425121	43.3410719907	43.4907877262	43.7448950805	44.1191249609	44.2005110227
265	43.1190305708	43.1224733467	43.1333993551	43.1537746317	43.1875226704	43.2417765645	43.3293568887	43.4736166513	43.7183095471	44.1147803174	44.1930269784
266	43.1151594466	43.1184840728	43.1290340486	43.1487041019	43.1812746403	43.2336136725	43.3180561997	43.4570818439	43.6927293483	44.1106036173	44.1858990706
267	43.1114213387	43.1146320870	43.1248196981	43.1438103121	43.1752459896	43.2257423631	43.3071715107	43.4411583500	43.6681142340	44.1065979858	44.1789348888
268	43.1078113911	43.1109133995	43.1207507894	43.1390867527	43.1694297172	43.2181516221	43.2966810769	43.4258222509	43.6446256587	44.1027268460	44.1723025729
269	43.1043249927	43.1073202120	43.1168220211	43.1345271676	43.1638175446	43.2108306753	43.2865697924	43.4110506172	43.6216267050	43.9901390474	44.1659307872
270	43.1009576694	43.1038509097	43.1130828956	43.1301255433	43.1584019027	43.2037699692	43.2768231633	43.3968214660	43.5996820113	43.9564314023	44.1598086960
271	42.9770512770	43.1005000541	43.1093647110	43.1258760992	43.1531755190	43.1969591541	43.2674278211	43.3831137195	43.5785577023	43.9200878939	44.1539259400
272	42.9456323729	42.9726337614	43.1058265532	43.1217732780	43.1481314050	43.1903896666	43.2583687981	43.3699071658	43.5582213230	43.8870533617	44.1482726146
273	42.9152802468	42.9413676875	43.1024092885	43.1178117366	43.1432628447	43.1840507136	43.2496349033	43.3571842409	43.5386417761	43.8552750037	44.1428392486
274	42.8859566692	42.9111628092	42.9910855598	43.1139863376	43.1385633816	43.1779354569	43.2412139997	43.3449208934	43.5197892614	43.8247022700	44.1376167841
275	42.8576248559	42.8819811122	42.9592016065	43.1102921404	43.1340268176	43.1720349983	43.2330921823	43.3331047500	43.5016352195	43.7952867613	44.1325965576
276	42.8302494102	42.8537860187	42.9284006694	43.1067243941	43.1296471829	43.1663413658	43.2252602179	43.3217168829	43.4841522765	43.7669821322	44.1277702819
277	42.8037962679	42.8265423300	42.8986439219	43.1032785289	43.1254187461	43.1608468997	43.2177065245	43.3107408787	43.4673141924	43.7397439939	44.1231300286
278	42.7782326444	42.8002161720	42.8698940059	42.9995014944	43.1213359950	43.1555442396	43.2104206529	43.3001609885	43.4510958114	43.7135298524	44.1186682120
279	42.7535269839	42.7747749422	42.8421149727	42.9673502767	43.1173936296	43.1504263126	43.2033925680	43.2899620996	43.4354730148	43.6882898738	44.1143775732
280	42.7296489110	42.7501872602	42.8152722277	42.9362909595	43.1135865531	43.1454863211	43.1966126321	43.2801297086	43.4204226756	43.6640123557	44.1102511654
281	42.7065691843	42.7264229184	42.7893324760	42.9062844076	43.1099098642	43.1407177313	43.1900715878	43.2706498951	43.4059226156	43.6406326254	44.1062823398
282	42.6842596515	42.7034528366	42.7642636713	42.8772929655	43.1063580488	43.1361142688	43.1837605424	43.2615092970	43.3919515642	43.6181239733	44.1024647319
283	42.6626932068	42.6812490173	42.7400349664	42.8492803980	43.1029289727	43.1316698782	43.1776709526	43.2526950871	43.3784891195	43.5964520836	43.9879224877
284	42.6418437499	42.6597845034	42.7166166661	42.8222118342	42.9961587418	43.1273787727	43.1717946102	43.2441949506	43.3655157104	43.5755840685	43.9529505685
285	42.6216861470	42.6390333373	42.6939801816	42.7960537128	42.9641535732	43.1232353654	43.1661236280	43.2359970629	43.3530125615	43.5554884054	43.9185557026
286	42.6021961924	42.6189705221	42.6720979873	42.7707737309	42.9332338510	43.1192342894	43.1606504270	43.2280900698	43.3409616583	43.5361348774	43.8858843976
287	42.5833505732	42.5995719839	42.6509435792	42.7463407937	42.9033607322	43.1153703840	43.1553677230	43.2204630672	43.3293457152	43.5174945163	43.8544054209
288	42.5651268342	42.5808145360	42.6304914346	42.7227249675	42.8744968397	43.1116386854	43.1502685152	43.2131055824	43.3181481440	43.4995395475	43.8241096998
289	42.5475033445	42.5626758447	42.6107169742	42.6998974333	42.8466062037	43.1080348197	43.1453460742	43.2060075564	43.3073530246	43.4822433359	43.7949502349
290	42.5304592662	42.5451343957	42.5915965252	42.6778304437	42.8196542062	43.1045299946	43.1405939309	43.1991593262	43.2969507163	43.4655803509	43.7668819588
291	42.5139745232	42.5281694631	42.5731072861	42.6564972807	42.7936075276	43.1011899924	43.1360058662	43.1925516087	43.2869096309	43.4495260892	43.7398617488
292	42.4980297723	42.5117610784	42.5552272931	42.6358732153	42.7684340948	42.9794116283	43.1315759002	43.1861754847	43.2772326066	43.4340570599	43.7136482438
293	42.4826063748	42.4958900019	42.5379353874	42.6159304694	42.7441030328	42.9480341667	43.1272926833	43.1800223843	43.2679004836	43.4191507260	43.6880018151
294	42.4676863697	42.4805376943	42.5212111844	42.5966481781	42.7205846169	42.9176981900	43.1231674862	43.1740840719	43.2589002802	43.4047854665	43.6646844803
295	42.4532524474	42.4656662900	42.5050350437	42.5780023550	42.6978502282	42.8883958320	43.1191781913	43.1683526328	43.2502195303	43.3909405374	43.6414598317
296	42.4392879252	42.4511855712	42.4893800407	42.5599708577	42.6758723097	42.8600806507	43.1153252842	43.1628304600	43.2418462619	43.3775960339	43.6190929672
297	42.4257767233	42.4371479436	42.4742513387	42.5425133552	42.6546843252	42.8327175717	43.1116038452	43.1574809415	43.2337689762	43.3647328545	43.5975504248
298	42.4127031419	42.4235684121	42.4596291614	42.5256662968	42.6340907190	42.8062728341	43.1080091419	43.1523849483	43.2259766281	43.3523326672	43.5768001197
299	42.4000528190	42.4103545383	42.4454427766	42.5093538820	42.6140168796	42.7807139385	43.1045366214	43.1473478230	43.2184586073	43.3403778765	43.5568112848
300	42.3878108094	42.3973615187	42.4317364526	42.4935730313	42.5950090971	42.7560095980	43.1011819034	43.1425423682	43.2112047204	43.3288515225	43.5375544138

$$K_{(n+1/2)}\left(\tfrac{\pi}{2}\sqrt{q}\right)$$

q \ n	0	1	2	3	4	5	6	7	8	9	10
1	50.2078795764	50.3402198249	50.8576515789	51.3070209589	52.1453954449	52.8637566311	53.6194125494	54.5212669254	55.5039673725	56.5506331790	57.6710732150
2	49.9119745717	50.1322507365	50.2697987010	50.7395111680	51.2600077598	52.1127352645	52.5842364652	53.3531719808	54.2443172372	55.1905000955	56.1653779994
3	49.5001901137	49.6840362889	50.1254488057	50.2969414494	50.8945817481	51.3258194052	52.1406771628	52.7047632755	53.4026240745	54.2586230238	55.1846356124
4	49.3055685465	49.4028340357	49.6902457146	50.1501395802	50.4035610602	51.1306256856	51.4977300244	52.2190246722	53.1095538780	53.6147278685	54.3827359077
5	49.1994519845	49.2562369653	49.4183078335	49.8517056602	50.2115707936	50.6272682642	51.2176084071	51.8681334957	52.3925037837	53.1986525891	54.1113840766
6	49.1362653725	49.1717057954	49.2701638319	49.5227822547	50.1221257686	50.3379414388	51.1088262584	51.4014839148	52.1674004879	52.7797709328	53.4017971534
7	48.9634412272	49.1195264125	49.1826253357	49.3392426405	49.7540246697	50.1972140622	50.5973918266	51.2065888874	51.8053793903	52.3501020799	53.1681125343
8	48.6993715467	48.8567854504	49.1277904987	49.2294933838	49.4893696151	50.1220815144	50.3511949047	51.1149687649	51.4232754462	52.1734566374	52.7841152885
9	48.5186505489	48.6287116137	48.9189007934	49.1603695637	49.3301104260	49.7908340402	50.2176132579	50.6794099825	51.2380424600	51.9266163106	52.3974071917
10	48.3914998212	48.4703153314	48.6755470221	49.1150310319	49.2296584958	49.5311381532	50.1405856146	50.4210431025	51.1412031671	51.5253561123	52.2150700867
11	48.2999781410	48.3575583703	48.5058760728	48.8430680838	49.1638653194	49.3673895145	49.9395821649	50.2711952461	50.8747893328	51.3125735557	52.1227438938
12	48.2328281691	48.2756164682	48.3847834921	48.6291868976	49.1194190966	49.2604362856	49.6459012787	50.1803553786	50.5617657862	51.1935422404	51.7319776329
13	48.1827467704	48.2150137383	48.2966394764	48.4766967924	48.8860676468	49.1884946010	49.4547070331	50.1232213316	50.3718221960	51.1239294532	51.4529363583
14	48.1448616941	48.1695090119	48.2313844117	48.3663521168	48.6677121777	49.1388815848	49.3266994504	49.8614980639	50.2525377648	50.8166012619	51.2892390813
15	48.1158440512	48.1348858614	48.1823534468	48.2847620926	48.5100128696	49.1039260171	49.2380119661	49.6144495289	50.1753909647	50.5155163440	51.1897950646
16	47.9337213659	48.1082327717	48.1450494794	48.2236594819	48.3942250641	48.7883452907	49.1774384613	49.4459573258	50.1240828939	50.5806579105	51.1275296458
17	47.7579732163	47.8750065354	48.1163284051	48.1773079123	48.3079668885	48.6052663889	49.1335970727	49.3286878490	49.8948527956	50.2677542715	50.8749834422
18	47.6193021077	47.7122300731	47.9399182855	48.1417416547	48.2428728737	48.4697352710	48.1018208476	49.2455939631	49.6540614779	50.1915414405	50.6115451140
19	47.5090052668	47.5833457875	47.7645992601	48.1141696661	48.1931817575	48.3680984571	48.7845527319	49.1857695542	49.4854315745	50.1391028227	50.4345481005
20	47.4206338577	47.4805121426	47.6258401845	47.9259617441	48.1548531025	48.2909897230	48.6105073902	49.1420784084	49.3644290071	50.1023993926	50.3134022988
21	47.3493544000	47.3978873503	47.5151801089	47.7557361514	48.1250097819	48.2318728970	48.4793440445	49.1097560431	49.2766470494	49.7631053574	50.2290874819
22	47.2915064399	47.3310719653	47.4263134400	47.6203848738	48.1015737722	48.1861159413	48.3794593946	48.8556336045	49.2121444827	49.5750596965	50.1695124552
23	47.2442915681	47.2767199055	47.3544906206	47.5120031271	47.8302494517	48.1503901806	48.3026229404	48.6726196843	49.1641920375	49.4377867146	50.1268352988
24	47.2055518101	47.2322631582	47.2960992309	47.4246528442	47.6823831058	48.1222730731	48.2430208379	48.5328186414	49.1281613314	49.3364083078	49.9587668562
25	47.1736097506	47.1957144306	47.2483671564	47.3538298732	47.5637242870	47.9998103222	48.1964022130	48.4250682158	49.1008222705	49.2607373547	49.7315863811
26	47.1471518874	47.1655240080	47.2091496045	47.2960871223	47.4679178660	47.8218689674	48.1596644353	48.3413331837	48.7989033708	49.2036984783	49.5630991369
27	47.1251426395	47.1404748068	47.1767745195	47.2487646964	47.3901207766	47.6789344101	48.1305115830	48.2757628832	48.6372984024	49.1603126753	49.4369109943
28	47.1067603442	47.1196046629	47.1499291936	47.2097944406	47.3266115256	47.5634456299	48.1072280043	48.2240521393	48.5115631208	49.1270335351	49.3415405854
29	46.9134919790	47.1021482556	47.1275762782	47.1775568866	47.2745083780	47.4696216992	47.8852000039	48.1830019382	48.4130299915	49.1013066043	49.2688507166
30	46.7838286919	46.8749333646	47.1088910090	47.1507755296	47.2315638430	47.3930082204	47.7340380984	48.1502135659	48.3352944098	48.8127270619	49.2130101670
31	46.6743673825	46.7514747422	46.9321388944	47.1284379883	47.1960133441	47.3301479857	47.6112547120	48.1238731491	48.2735808416	48.6556554499	49.1697969649
32	46.5816656505	46.6471260350	46.8001474485	47.1097367162	47.1664627814	47.2783395191	47.5110289958	48.1025982101	48.2249822295	48.5317193409	49.1361247775
33	46.5029198716	46.5586540943	46.6886521532	46.9402406519	47.1418042846	47.2354584532	47.4288361576	47.8532726751	48.1847247679	48.4333416591	49.1097170819
34	46.4358367304	46.4834211189	46.5941755994	46.8077797671	47.1211525916	47.1998242714	47.3611362048	47.7123964696	48.1527821387	48.3548108796	48.8888048130
35	46.3785326169	46.4192658993	46.5138821919	46.6957560550	47.1037966475	47.1701001090	47.3051428197	47.5969671348	48.1268722831	48.2917895719	48.7234533528
36	46.3294544009	46.3644105965	46.4454498970	46.6007291066	46.8916252635	47.1452166517	47.2586503780	47.5019843987	48.1057583362	48.2409606756	48.5915260494
37	46.2873167120	46.3173871773	46.3869696008	46.5198876842	46.7678484273	47.1243152385	47.2199035199	47.4235105572	47.8847704941	48.1997706589	48.4857276514
38	46.2510520375	46.2769790260	46.3368657050	46.4509252992	46.6628457135	47.1067014060	47.1874981161	47.3584277021	47.7427386353	48.1662414701	48.4004718654
39	46.2197708302	46.2421744333	46.2938331595	46.3919422948	46.5735173666	46.9181254307	47.1603055730	47.3043542550	47.6255441718	48.1388317757	48.3314541055
40	46.1927294750	46.2121293202	46.2567872843	46.3413683372	46.4973184766	46.7919019849	47.1371461242	47.2590053993	47.5284807446	48.1163338062	48.2753376491
41	46.1693044549	46.1861372633	46.2248236004	46.2979007899	46.4321515676	46.6845942229	47.1180862388	47.2210862357	47.4478031016	47.9779613277	48.2295213897
42	46.1489714330	46.1636523787	46.1971855308	46.2604554796	46.3762819969	46.5931237861	47.1017186767	47.1892095014	47.3805166922	47.8246547138	48.1919667677
43	46.1312884283	46.1440341848	46.1732383221	46.2281271891	46.3282701917	46.5149540721	46.8781997675	47.1623318465	47.3242163900	47.6974254783	48.1610679405
44	46.1158810422	46.1270026142	46.1524479048	46.2001578221	46.2869175910	46.4479875898	46.7598645673	47.1396042148	47.2769621679	47.5914842523	48.1355537730
45	46.1024328981	46.1121539515	46.1343639609	46.1759106464	46.2512231927	46.3904841567	46.6586567876	47.1203330100	47.2371827373	47.5029866637	48.1144133974
46	45.9067450964	45.9918563194	46.1186045261	46.1548493756	46.2203455222	46.3409954232	46.5742973832	47.1037495511	47.2036004755	47.4288339967	47.9683936718
47	45.8037648727	45.8784029109	46.1048417772	46.1365211174	46.1935891478	46.2983122485	46.4983094316	46.8998549410	47.1751726484	47.3665185965	47.8218398134
48	45.7134299869	45.7789857480	45.9281686629	46.1205424251	46.1703518087	46.2614222369	46.4345894695	46.7505593233	47.1510451743	47.3140033782	47.6992557705
49	45.6340694243	45.6917304108	45.8227945238	46.1065878501	46.1501353952	46.2294753430	46.3797031019	46.6783959401	47.1305160889	47.2696274687	47.5964237143
50	45.5642332034	45.6150320393	45.7303502174	45.9438051479	46.1325156439	46.2017559115	46.3323241968	46.5907118772	47.1130065509	47.2320319784	47.5099206853

$K_{(n+1/2)}\left(\frac{\pi}{2}\sqrt{q}\right)$

q \ n	0	1	2	3	4	5	6	7	8	9	10
51	45.5027006140	45.5475136586	45.6491242704	45.8368432720	46.1171324675	46.1776598686	46.2913440624	46.5152926129	46.9803773613	47.2001013505	47.4369588738
52	45.4484048087	45.4879914551	45.5776492648	45.7429753088	46.1036795336	46.1566760528	46.2558301646	46.4502878854	46.8521235243	47.1729168274	47.3752599754
53	45.4004295688	45.4354457134	45.5146641155	45.6604734651	45.9189565388	46.1383708856	46.2249961254	46.3941473500	46.7419979290	47.1497193804	47.3229559335
54	45.3579832727	45.3889364296	45.4590830299	45.5878550796	45.8155764828	46.1223757454	46.1981771761	46.3455685714	46.6472416922	47.1298800650	47.2785102085
55	45.3203807414	45.3478827985	45.4099693905	45.5238453355	45.7247441490	46.1083765368	46.1748100130	46.3034546002	46.5655463158	47.1128762263	47.2406550860
56	45.2870279112	45.3114459197	45.3665137955	45.4673460362	45.6448198875	45.9610504870	46.1544162140	46.2668792890	46.4949751187	46.9827233057	47.2083415672
57	45.2574088632	45.2791141832	45.3280155537	45.4174093928	45.5743941365	45.8533177571	46.1365885469	46.2350588479	46.4338992592	46.8570447272	47.1806991723
58	45.2310748239	45.2503908933	45.2938670544	45.3732159661	45.5122528467	45.7585993770	46.1209796342	46.2073284731	46.3809454739	46.7486781056	47.1570035838
59	45.2076348186	45.2248437657	45.2635405356	45.3340560637	45.4573484538	45.6752046589	46.1072925420	46.1831229269	46.3349532580	46.6550634232	47.1366505123
60	45.1867477126	45.2020959953	45.2365768605	45.2993140140	45.4087754496	45.6016792186	45.9527294745	46.1619608134	46.2949396778	46.5740456371	47.1191345192
61	45.1681154214	45.1818186455	45.2125759763	45.2684548448	45.3657497780	45.5367678887	45.8470260135	46.1434310975	46.2600703741	46.5038063911	47.1040318041
62	45.1514771066	45.1637241506	45.1911887883	45.2410129754	45.3275914178	45.4793872055	45.7533986051	46.1271822138	46.2296356012	46.4428079574	46.9098617079
63	45.1366042063	45.1475607587	45.1721102254	45.2165825976	45.2937096294	45.4285995283	45.6718510245	46.1129128634	46.2030303747	46.3897470915	46.7969755134
64	45.1232361714	45.1331077690	45.1550733105	45.1948094788	45.2635904308	45.3835222188	45.5993687185	45.9993687185	46.1003643432	46.1797379818	46.3435169434
65	45.1113768025	45.1201714450	45.1398440832	45.1753839619	45.2367854660	45.3436598441	45.5358863468	45.8931412026	46.1593162503	46.3031755383	46.6141693964
66	45.1006910959	45.1085814996	45.1262172417	45.1580349781	45.2129053280	45.3081890778	45.4785603826	45.7957043782	46.1413860873	46.2679196260	46.5402881521
67	44.9110252508	44.9818806805	45.1140123986	45.1425349154	45.1916070084	45.2766458655	45.4282853948	45.7096777610	46.1256218904	46.2370629323	46.4759378914
68	44.8249069295	44.8885909713	45.1030708563	45.1286452141	45.1725920693	45.2485644939	45.3836771038	45.6336302532	46.1117435072	46.2100180293	46.4198038870
69	44.7474930136	44.8047806890	44.9325828704	45.1162125789	45.1555985631	45.2235382639	45.3440502965	45.5663225197	45.9950947874	46.1862811860	46.3707647414
70	44.6778439247	44.7298214869	44.8443503166	45.1050657168	45.1403966378	45.2012115173	45.3088100303	45.5066796100	45.8871134888	46.1654196819	46.3278621749
71	44.6151282330	44.6616029345	44.7650862284	44.9506252244	45.1267843456	45.1812728095	45.2774368306	45.4537677327	45.7916886273	46.1470611606	46.2902758163
72	44.5586034065	44.6005198367	44.6937738583	44.8607764719	45.1145840335	45.1634490534	45.2494768956	45.4067745163	45.7072590631	46.1308846755	46.2573021203
73	44.5076342853	44.5454584755	44.6299617777	44.7800039460	45.1036392304	45.1475004870	45.2245332541	45.3649922009	45.6324706662	46.1166131437	46.2283366778
74	44.4616230423	44.4957857073	44.5716957172	44.7073289738	44.9381195822	45.1332163435	45.2022581878	45.3278033008	45.5661471183	46.1040069747	46.2028594765
75	44.4200604279	44.4509392861	44.5195067717	44.6419853512	44.8490840506	45.1204111185	45.1823467276	45.2946683530	45.5072650828	45.9285867880	46.1804222127
76	44.3824881235	44.4104194320	44.4724011252	44.5822055923	44.7703690997	45.1089213477	45.1645310624	45.2651154300	45.4543330522	45.8298829846	46.1606376916
77	44.3484980567	44.3737814361	44.4298510887	44.5277089648	44.6988621410	44.9860820486	45.1485757140	45.2387311484	45.4083732972	45.7423952737	46.1431721803
78	44.3177265485	44.3406292296	44.3913872734	44.4816910635	44.6344394143	44.8932817004	45.1342734036	45.2151529477	45.3669061356	45.6647640973	46.1277351988
79	44.2898491836	44.3106097243	44.3565917467	44.4381147147	44.5763527696	44.8098477805	45.1214414443	45.1940624486	45.3299382201	45.5958052706	46.1140758344
80	44.2645763100	44.2834078607	44.3250920399	44.3991020293	44.5233981527	44.7347296263	45.1099186483	45.1751797323	45.2969482060	45.5348859700	46.1019759684
81	44.2416490839	44.2587422600	44.2965559868	44.3636274530	44.4756055617	44.6670439772	44.9956263655	45.1582584043	45.2674800188	45.4799042007	45.9124593028
82	44.2208359929	44.2363614021	44.2706866640	44.3315116800	44.4328302751	44.6060073906	44.9024750752	45.1430813303	45.2411329793	45.4312712130	45.8172056441
83	44.2019297942	44.2160402642	44.2472192426	44.3024163167	44.3951451821	44.5509242613	44.8186181182	45.1294569466	45.2175548902	45.3878964203	45.7325587091
84	44.1847448159	44.1975773593	44.2259165265	44.2760391989	44.3601340677	44.5011763653	44.7430679081	45.1172160633	45.1964358103	45.3491744417	45.6572613372
85	44.1691145768	44.1807921260	44.2065662674	44.2521102756	44.3284257268	44.4562137225	44.6749484268	45.1062090912	45.1775026762	45.3145739551	45.5902146069
86	44.1548896835	44.1655226241	44.1889783109	44.2303879889	44.2996888005	44.4155466025	44.6134818490	44.9630363205	45.1605146478	45.2836280919	45.5304567342
87	44.1419359717	44.1516234997	44.1729821586	44.2106560863	44.2736272383	44.3787385222	44.5579768647	44.8738238332	45.1452590764	45.2559261504	45.4771494457
88	44.1301328615	44.1389641844	44.1584248143	44.1927208098	44.2499763089	44.3454001054	44.5078184731	44.7934131244	45.1315480057	45.2311064349	45.4295398828
89	44.1193719006	44.1274273028	44.1451688805	44.1764084161	44.2284990875	44.3151836919	44.4624590500	44.7208806530	45.1192151325	45.2088500602	45.3869921656
90	44.1095554727	44.1169072602	44.1330908738	44.1615629856	44.2089833597	44.2877785997	44.4214105224	44.6554057655	45.1081131638	45.1888755845	45.3489308008
91	44.1005956509	44.1073089907	44.1220797324	44.1480444858	44.1912388913	44.2629695641	44.3842375050	44.5962585478	45.0981151368	45.1709343533	45.3148531665
92	43.9241318019	43.9854684622	44.1120354930	44.1357270566	44.1750950158	44.2403200284	44.3505512731	44.5427891954	44.8909429638	45.1540864544	45.2841363488
93	43.8493657245	43.9054360891	44.1028681172	44.1244974916	44.1603985035	44.2197949834	44.3200046553	44.4941869944	44.8095857364	45.1402972016	45.2569296369
94	43.7810130097	43.8322961326	43.9449644844	44.1145238915	44.1470116743	44.2011320345	44.2922864213	44.4506306778	44.7361282301	45.1273407012	45.2323480148
95	43.7184908368	43.7654196482	43.8684728509	44.1049044689	44.1348107280	44.1841519165	44.2671190765	44.4109642033	44.6697559768	45.1154640329	45.2102665086
96	43.6612724412	43.7042384418	43.7985455563	43.9636648651	44.1236842630	44.1686936547	44.2446533408	44.3750074989	44.6097435249	45.1048512190	45.1904152726
97	43.6088814146	43.6482388665	43.7345858428	43.8856531340	44.1135319629	44.1546125896	44.2243659034	44.3423923911	44.5554441446	44.9527488856	45.1725551108
98	43.5608866172	43.5969562867	43.6760543640	43.8143358491	44.1042634290	44.1417786275	44.2045564096	44.3127894240	44.5062807902	44.8662764634	45.1564747494
99	43.5168776332	43.5499701365	43.6224633469	43.7491045474	43.9579714388	44.1300746893	44.1873496641	44.2859035522	44.4617361587	44.7881388285	45.1419855831
100	43.4765607064	43.5068995032	43.5733713803	43.6894092820	43.8805954864	44.1193953330	44.1716699214	44.2614703392	44.4213557030	44.7174840712	45.1289208341

$$K_{(n+1/2)}\left(\frac{\pi}{2}\sqrt{q}\right)$$

q \ n	0	1	2	3	4	5	6	7	8	9	10
101	43.4325551050	43.4673991780	43.5283787590	43.6347526747	43.8098422149	44.1096455314	44.1573859278	44.2392525997	44.3847214809	44.6535524661	45.1171320671
102	43.4055898661	43.4311561221	43.4871233217	43.5846846069	43.7451114592	44.1007395840	44.1443621857	44.2190374304	44.3514667318	44.5956659312	45.1064872144
103	43.3744068787	43.3978863008	43.4492767263	43.5387974758	43.6858605808	43.9260015006	44.1324809127	44.2006335824	44.3212610934	44.5432187571	44.9686866951
104	43.3457482679	43.3673318471	43.4145411161	43.4967219535	43.6315984419	43.8515738660	44.1216359727	44.1838691336	44.2938083761	44.4956694471	44.8817161519
105	43.3194140484	43.3392585176	43.3824661313	43.4581231918	43.5818812034	43.7834818072	44.1117316596	44.1685894251	44.2688428294	44.4525335272	44.8030255493
106	43.2952000166	43.3134534081	43.3533462305	43.4226974241	43.5363056744	43.7211546457	44.1026816144	44.1546552301	44.2461258368	44.4133772048	44.7317802232
107	43.2729258573	43.2897229036	43.3264182862	43.3901689202	43.4945071517	43.6640760395	43.9440786084	44.1419411273	44.2254299907	44.3778117712	44.6672344541
108	43.2524274410	43.2678908346	43.3016594270	43.3602872561	43.4561546964	43.6117785210	43.8683994673	44.1303340560	44.2066014986	44.3454886551	44.6087214645
109	43.2335552918	43.2477968197	43.2788850974	43.3328248632	43.4209479975	43.5638386139	43.7991417705	44.1197320291	44.1894278830	44.3160950483	44.5556440021
110	43.2161732083	43.2292947736	43.2579273144	43.3075748284	43.3886143813	43.5198724644	43.7357293008	44.1100429891	44.1737659387	44.2893500338	44.5074695554
111	43.2001570212	43.2122515642	43.2386330984	43.2843489168	43.3589061283	43.4795319294	43.6776404625	44.1011837874	44.1594749185	44.2650011553	44.4637175031
112	43.1853934731	43.1965458016	43.2208630606	43.2629757938	43.3319806848	43.4425010720	43.6244028190	43.9307927460	44.1464279185	44.2428213755	44.4239589997
113	43.1717792083	43.1820667474	43.2044901306	43.2432994259	43.3064853991	43.4084930193	43.5755882047	43.8566148888	44.1345104426	44.2226063766	44.3878086420
114	43.1592198607	43.1687133297	43.1893984093	43.2251776401	43.2833817765	43.3772471427	43.5308083504	43.7886893070	44.1236191221	44.2041721629	44.3549202911
115	43.1476292306	43.1563932546	43.1754821341	43.2084808267	43.2621175298	43.3485265267	43.4897109625	43.7264591493	44.1136605762	44.1873529297	44.3249828585
116	43.1369285403	43.1450222031	43.1626447454	43.1930907694	43.2425381045	43.3221156949	43.4519762095	43.6694199116	44.1045503938	44.1719991673	44.2977165659
117	43.1270457614	43.1345231056	43.1507980429	43.1788995908	43.2245026405	43.2978185652	43.4173135682	43.6171142503	43.9621222584	44.1579759729	44.2728696248
118	43.1179150063	43.1248254861	43.1396142940	43.1658087997	43.2078826937	43.2754566103	43.3854589940	43.5691273352	43.8857697315	44.1451615473	44.2502152861
119	43.1094759770	43.1158648679	43.1297611945	43.1537284311	43.1925610836	43.2548672023	43.3561723775	43.5250826852	43.8158206146	44.1334458530	44.2295492170
120	43.1016734661	43.1075822367	43.1204299455	43.1425762695	43.1784308528	43.2359021209	43.3292352589	43.4846384332	43.7517079206	44.1227294183	44.2106871673
121	42.9445690501	42.9992355350	43.1118059895	43.1322771460	43.1653943283	43.2184262094	43.3044487720	43.4474839733	43.6929176063	44.1129222685	44.1934628905
122	42.8777995353	42.9283931320	43.1038329491	43.1227623029	43.1533622728	43.2023161622	43.2816317932	43.4133369502	43.6389833656	44.1039429710	44.1777262919
123	42.8160012834	42.8628414476	42.9645879434	43.1139688179	43.1422531182	43.1874594312	43.2606192751	43.3819405535	43.5894819611	43.9571778126	44.1633417761
124	42.7587846529	42.8021644802	42.8963644277	43.1058390837	43.1319922718	43.1737532374	43.2412607440	43.3530610843	43.5440290354	43.8817987883	44.1501867733
125	42.7057921303	42.7459806424	42.8332227893	42.9832033511	43.1225114887	43.1611036791	43.2234189454	43.3264857653	43.5022753518	43.8126868287	44.1381504219
126	42.6566955445	42.6939397676	42.7747650873	42.9136422161	43.1137483038	43.1494249245	43.2069686219	43.3020207702	43.4633034159	43.7492923900	44.1271323919
127	42.6111935366	42.6457203912	42.7206254565	42.8492641858	43.1056455165	43.1386384827	43.1917954099	43.2794804469	43.4286244396	43.6911166936	44.1170418321
128	42.5690092579	42.6010272778	42.6704682575	42.7896627502	42.9815074255	43.1286725431	43.1778948426	43.2587307162	43.3961756101	43.6377067925	44.1077962684
129	42.5298882749	42.5595891728	42.6239852853	42.7344649350	42.9121590063	43.1194613771	43.1648714494	43.2399976284	43.3661176320	43.5886511406	43.9932155950
130	42.4935966639	42.5211567559	42.5808934135	42.6833283939	42.8479700843	43.1109447971	43.1529379409	43.2229560586	43.3388325134	43.5435756127	43.9154954135
131	42.4599192737	42.4855007783	42.5409324501	42.6359387657	42.7885365404	43.1030676649	43.1419144716	43.2076835303	43.3135215715	43.5021399257	43.8441894862
132	42.4286581439	42.4524103655	42.5038611860	42.5920072707	42.7334876936	42.9577944659	43.1317279729	43.1906681513	43.2902036341	43.4640344203	43.7787400639
133	42.3996310629	42.4216914709	42.4694561867	42.5512685240	42.6824832437	42.8903380858	43.1223115482	43.1768076525	43.2687134167	43.4289771627	43.7186404374
134	42.3726702523	42.3931654660	42.4375373314	42.5134785452	42.6352106557	42.8278825056	43.1136039247	43.1640085173	43.2489000582	43.3967113357	43.6634300283
135	42.3476211671	42.3666785644	42.4078920191	42.4784129447	42.5913827797	42.7700377236	43.1055489573	43.1521851948	43.2306257978	43.3670028867	43.6126899753
136	42.3243414002	42.3420470983	42.3803581406	42.4458652730	42.5507356858	42.7164457116	42.9809517684	43.1412593865	43.2137647795	43.3396384069	43.5660391640
137	42.3026996820	42.3191635473	42.3547776916	42.4156455140	42.5130266926	42.6667776616	42.9119538168	43.1311594006	43.1982019710	43.3144232184	43.5231306531
138	42.2825749668	42.2978884598	42.3310050833	42.3875787125	42.4780325707	42.6207314814	42.8480626568	43.1218195660	43.1838321859	43.2911796469	43.4836484552
139	42.2638559971	42.2781031092	42.3089061185	42.3615037212	42.4455479061	42.5780295150	42.7888808068	43.1131797016	43.1705591984	43.2697454616	43.4473046363
140	42.2464385402	42.2596979665	42.2883570572	42.3372720573	42.4153836083	42.5384164680	42.7340432952	43.1051846341	43.1582949415	43.2499724655	43.4138367004
141	42.2302886895	42.2425719532	42.2692437609	42.3147468579	42.3873655483	42.5016575169	42.6832148687	43.0977837609	43.1469587807	43.2317252000	43.3830052293
142	42.2153182648	42.2266317574	42.2514609122	42.2938019265	42.3613333169	42.4675365863	42.6360874521	42.9093064961	43.1364768549	43.2148798924	43.3545917525
143	42.2010860278	42.2117912084	42.2349112990	42.2743208609	42.3371390906	42.4358547780	42.5923778357	42.8458268352	43.1267814798	43.1993232110	43.3283668233
144	42.1879971450	42.1979707033	42.2195051610	42.2561962557	42.3146465955	42.4064289387	42.5518255691	42.7870072625	43.1178106049	43.1849515203	43.3043282800
145	42.1758022976	42.1850966828	42.2051595909	42.2393289737	42.2937301610	42.3790903519	42.5141910420	42.7324882649	43.1095073220	43.1716699236	43.2819496735
146	42.1644374304	42.1731011498	42.1917975854	42.2236274782	42.2742738547	42.3536835447	42.4792537348	42.6813994543	43.1018194174	43.1593915065	43.2613788457
147	42.1538433000	42.1619212292	42.1793495435	42.2090072224	42.2561706909	42.3300651973	42.4468106230	42.6350570920	42.9469896589	43.1480366327	43.2423866412
148	42.1439650952	42.1514987632	42.1677488056	42.1953900896	42.2393219071	42.3081031468	42.4166747215	42.5915618340	42.8810196119	43.1375323039	43.2248547423
149	42.1347520904	42.1417799406	42.1569352310	42.1827036811	42.2236363012	42.2876754767	42.3886737552	42.5511966755	42.8198797971	43.1278115800	43.2086396126
150	42.1261573260	42.1327149569	42.1[illegible]38528115	42.1708818460	42.2090296249	42.2686696839	42.3626489465	42.5137250777	42.7631987463	43.1188130515	43.1936615392

$K_{(n+1/2)}\left(\frac{\pi}{2}\sqrt{q}\right)$

q \ n	0	1	2	3	4	5	6	7	8	9	10
151	42.1181373162	42.1242577013	42.1374497149	42.1598622509	42.1954240282	42.2509819170	42.3384539057	42.4789292587	42.7106349739	43.1104803601	43.1798137643
152	42.1106517794	42.1163654701	42.1286779597	42.1495879846	42.1827475502	42.2345162790	42.3159536182	42.4466086340	42.6618744390	43.1027617634	43.1670066975
153	42.1036633913	42.1089987033	42.1204931153	42.1400061956	42.1709336523	42.2191841886	42.2950235181	42.4165783930	42.6166282329	42.9560973815	43.1551582003
154	41.9713755751	42.1021207417	42.1128540264	42.1310679593	42.1599207904	42.2049037958	42.2755486407	42.3886681987	42.5746304707	42.8898061986	43.1441929360
155	41.9104220464	41.9569760505	42.1057225610	42.1227279727	42.1496520220	42.1915994458	42.2574228470	42.3627209997	42.5356363681	42.8283427424	43.1340417797
156	41.8534758792	41.8969778643	41.9906337719	42.1149442736	42.1400746458	42.1792011878	42.2405481138	42.3385919444	42.4994204865	42.7713379806	43.1246412814
157	41.8002611431	41.8409206425	41.9284370990	42.1076779824	42.1311398714	42.1676443247	42.2248338838	42.3161473878	42.4657751307	42.7184524660	43.1159331776
158	41.7505217969	41.7885332866	41.8703317410	42.1008930656	42.1228025150	42.1568689997	42.2101964696	42.2952639836	42.4345088858	42.6693738510	43.1078639474
159	41.7040201883	41.7395642189	41.8160358392	41.9455611726	42.1150207203	42.1468198174	42.1965585083	42.2758278525	42.4054452801	42.6238146211	43.1003844077
160	41.6605356723	41.6937799123	41.7652878614	41.8863615878	42.1077557024	42.1374454952	42.1838484607	42.2577338214	42.3784215632	42.5815100264	42.9344934509
161	41.6198633385	41.6509635352	41.7178450680	41.8310445421	42.1009715114	42.1286985441	42.1720001522	42.2408847263	42.3532875886	42.5422161939	42.8701718042
162	41.5818128372	41.6109137033	41.6734820997	41.7793434042	41.9463481596	42.1205349749	42.1609523521	42.2251907734	42.3299047917	42.5057084030	42.8104966252
163	41.5462072979	41.5734433289	41.6319896757	41.7310107071	41.8871470351	42.1129140278	42.1506483863	42.2105689542	42.3081452536	42.4717795109	42.7551158945
164	41.5128823311	41.5383785592	41.5931733944	41.6858167071	41.8318249665	42.1057979249	42.1410357830	42.1969425085	42.2878908458	42.4402385125	42.7037055398
165	41.4816851073	41.5055577979	41.5568526268	41.6435480563	41.7801158415	41.9915164171	42.1320659461	42.1842404322	42.2690324447	42.4109092243	42.6559671124
166	41.4524735077	41.4748308016	41.5228594966	41.6040065789	41.7317726517	41.9294269704	42.1236938561	42.1723970252	42.2514692139	42.3836290804	42.6116256670
167	41.4251153394	41.4460578461	41.4910379390	41.5670081434	41.6865660586	41.8714096001	42.1158777943	42.1613514774	42.2351079450	42.3582480309	42.5704278236
168	41.3994876109	41.4191089570	41.4612428318	41.5323816214	41.6442830718	41.8171847214	42.1085790897	42.1510474873	42.2198624539	42.3346275333	42.5321399979
169	41.3754758628	41.3938631980	41.4333391934	41.4999679283	41.6047258304	41.7664928348	42.1017618864	42.1414329124	42.2056530270	42.3126396289	42.4965467823
170	41.3529735494	41.3702080151	41.4072014429	41.4696191370	41.5677104796	41.7190930177	41.9539292877	42.1324594482	42.1924059127	42.2921660972	42.4634494662
171	41.3318814672	41.3480386288	41.3827127151	41.4411976600	41.5330661341	41.6747615338	41.8944136468	42.1240823320	42.1800528550	42.2730976800	42.4326646818
172	41.3121072262	41.3272574736	41.3597642292	41.4145754945	41.5006339218	41.6332905514	41.8387856359	42.1162600719	42.1685306654	42.2553333708	42.4040231648
173	41.2935647611	41.3077736787	41.3382547042	41.3896335242	41.4702661015	41.5944869614	41.7867794937	42.1089541967	42.1577808290	42.2387797631	42.3773686197
174	41.2761738793	41.2895025887	41.3180898188	41.3662608753	41.4418252477	41.5581712873	41.7381484622	42.1021290257	42.1477491431	42.2233504524	42.3525566807
175	41.2598598422	41.2723653194	41.2991817120	41.3443543203	41.4151834978	41.5241766796	41.6926633658	41.9575145751	42.1383853851	42.2089654866	42.3294539591
176	41.2445529782	41.2562883470	41.2814485210	41.3238177273	41.3902218573	41.4923479870	41.6501113018	41.8979077471	42.1296430069	42.1955508633	42.3079371707
177	41.2301883235	41.2412031277	41.2648139531	41.3045615506	41.3668295570	41.4625408999	41.6102944332	41.8421846465	42.1214788536	42.1830380657	42.2878923358
178	41.2167052907	41.2270457454	41.2492068910	41.2865023595	41.3449034594	41.4346211584	41.5730288744	41.7900805394	42.1138529052	42.1713636382	42.2692140443
179	41.2040473606	41.2137565861	41.2345610251	41.2695624021	41.3243475091	41.4084638215	41.5381436634	41.7413495609	42.1067280384	42.1604687957	42.2518047829
180	41.1921617971	41.2012800350	41.2208145150	41.2536692020	41.3050722253	41.3839525918	41.5054798124	41.6957633091	42.1000698075	42.1502990637	42.2355743164
181	41.1809993831	41.1895641970	41.2079096748	41.2387551843	41.2869942318	41.3609791900	41.4748894323	41.6531095495	41.9384624271	42.1408039484	42.2204391197
182	41.1705141755	41.1785606367	41.1957926819	41.2247573298	41.2700358221	41.3394427786	41.4462349230	41.6131910195	41.8802766410	42.1319366327	42.2063218571
183	41.1606632778	41.1682241379	41.1844133068	41.2116168543	41.2541245572	41.3192494273	41.4193882261	41.5758243250	41.8258651023	42.1236536964	42.1931509023
184	41.1514066294	41.1585124805	41.1737246631	41.1992789117	41.2391928923	41.3003116191	41.3942301336	41.5408389218	41.7749718022	42.1159148585	42.1808598984
185	41.1427068100	41.1493862331	41.1636829749	41.1876923185	41.2251778322	41.2825477933	41.3706496493	41.5080761755	41.7273588805	42.1086827404	42.1693873528
186	41.1345288580	41.1408085611	41.1542473622	41.1768092988	41.2120206113	41.2658819220	41.3485433983	41.4773884931	41.6828052822	42.1019226474	42.1586762648
187	41.1268401024	41.1327450480	41.1453796402	41.1665852474	41.1996663971	41.2502431189	41.3278150807	41.4486385200	41.6411055173	41.9560236738	42.1486737826
188	41.1196100056	41.1251635303	41.1370441347	41.1569785104	41.1880640158	41.2355652758	41.3083749657	41.4216983991	41.6020685163	41.8969198513	42.1393308883
189	41.1128100189	41.1180339435	41.1292075096	41.1479501816	41.1771656973	41.2217867268	41.2901394247	41.3964490847	41.5655165738	41.8416371157	42.1306021072
190	41.1064134469	41.1113281788	41.1218386071	41.1394639130	41.1669268394	41.2088499371	41.2730304973	41.3727797091	41.5312843723	41.7899172583	42.1224452405
191	41.1003953222	41.1050199514	41.1149082992	41.1314857401	41.1573057881	41.1967012136	41.2569754910	41.3505869957	41.4992180810	41.7415202973	42.1148211187
192	40.9473228892	40.9908467627	41.1083893502	41.1239839182	41.1482636349	41.1852904378	41.2419066096	41.3297747170	41.4691745227	41.6962231348	42.1076933748
193	40.8940249410	40.9349935391	41.1022562880	41.1169287717	41.1397640279	41.1745708175	41.2277606091	41.3102531923	41.4410204036	41.6538183170	42.1010282349
194	40.8438548704	40.8824246377	40.9648528554	41.1102925529	41.1317729965	41.1644986563	41.2144784786	41.2919388229	41.4146316011	41.6141128889	41.9479432518
195	40.7966212547	40.8329386511	40.9105404969	41.1040493120	41.1242587886	41.1550331402	41.2020051452	41.2747536620	41.3898925059	41.5769273370	41.8896249387
196	40.7521448831	40.7863470477	40.8594171856	40.9817477523	41.1171917201	41.1461361392	41.1902891996	41.2586250156	41.3666954123	41.5420946119	41.8350564709
197	40.7102579450	40.7424733140	40.8112876566	40.9264623240	41.1105440339	41.1377720234	41.1792826417	41.2434850739	41.3449399545	41.5094592259	41.7839859721
198	40.6708032744	40.7011521568	40.7659691082	40.8744243158	41.1042897698	41.1299074920	41.1689406454	41.2292705683	41.3245325849	41.4788764174	41.7361792290
199	40.6336336466	40.6622287595	40.7232903728	40.8254348169	40.9840464317	41.1225114144	41.1592213393	41.2159224549	41.3053860910	41.4502113796	41.6914183993
200	40.5986111228	40.6255580908	40.6830911462	40.7793076169	40.9286593231	41.1155546830	41.1500856039	41.2033856197	41.2874191479	41.4233385459	41.6495008180

$$K_{(n+1/2)}\left(\frac{\pi}{2}\sqrt{q}\right)$$

q \ n	0	1	2	3	4	5	6	7	8	9	10
201	40.5656064405	40.5910042604	40.6452212684	40.7358683606	40.8765237353	41.1090100763	41.1414968828	41.1916086064	41.2705559035	41.3981403296	41.6102378938
202	40.5344984448	40.5584399187	40.6095400557	40.6943537618	40.8274406367	41.1026521311	41.1334210077	41.1805433628	41.2547255951	41.3745095126	41.5734540904
203	40.5051735569	40.5277456979	40.5759156773	40.6564108712	40.7812236946	40.9705702434	41.1256260361	41.1701450064	41.2398621924	41.3523426788	41.5398859838
204	40.4775252907	40.4988096909	40.5442245754	40.6200963945	40.7376984305	40.9160246395	41.1186820997	41.1603716063	41.2259040685	41.3315459606	41.5066813905
205	40.4514537721	40.4715269660	40.5143509242	40.5858760582	40.6967014347	40.8646758254	41.1119612642	41.1511839807	41.2127936929	41.3120302031	41.4763985615
206	40.4268653308	40.4457991138	40.4861861266	40.5536240176	40.6580796348	40.8163284942	41.1056377992	41.1425455095	41.2004773484	41.2937138145	41.4480054364
207	40.4036720894	40.4215338257	40.4596283437	40.5232223059	40.6216896147	40.7707997484	40.9968605618	41.1344219591	41.1889048669	41.2765196494	41.4213789528
208	40.3817915927	40.3986444994	40.4345820575	40.4945603210	40.5873969799	40.7279183104	40.9408435606	41.1267813210	41.1780293858	41.2603759722	41.3960440073
209	40.3611464592	40.3770498724	40.4109576625	40.4675343465	40.5550757668	40.6875237473	40.8881088426	41.1195936606	41.1678071202	41.2452158291	41.3729748637
210	40.3416640564	40.3566736789	40.3886710842	40.4420471053	40.5246078918	40.6494657559	40.8384559297	41.1128309776	41.1581971531	41.2309767159	41.3509906047
211	40.3232761974	40.3374443303	40.3676434244	40.4180073437	40.4958826382	40.6136034963	40.7916971028	41.1064670754	41.1491612389	41.2176002700	41.3303586241
212	40.3059188574	40.3192946166	40.3478006289	40.3953294432	40.4687961776	40.5798049719	40.7476565563	41.1004774402	41.1406636223	41.2050319839	41.3109921558
213	40.2895319099	40.3021614274	40.3290731786	40.3739330577	40.4432511236	40.5479464510	40.7061696108	41.0948393873	41.1326708689	41.1932209405	41.2928102382
214	40.2740588796	40.2859854922	40.3113958000	40.3537427765	40.4191561160	40.5179119279	40.6670819797	40.8953066286	41.1251517085	41.1821195663	41.2757373089
215	40.2594467114	40.2707111373	40.2947071955	40.3346878081	40.3964254327	40.4895926210	40.6302490861	40.8453193262	41.1180768895	41.1716834029	41.2597028299
216	40.2456455551	40.2562860581	40.2789497918	40.3167016860	40.3747786273	40.4628865041	40.5955354269	40.7982410528	41.1114190423	41.1618708945	41.2446409398
217	40.2326085645	40.2426611079	40.2640695039	40.2997219938	40.3547401915	40.4376978703	40.5628139800	40.7538954089	41.1051525542	41.1526431902	41.2304901301
218	40.2202917082	40.2297900989	40.2500155159	40.2836901084	40.3356392393	40.4139369239	40.5319656512	40.7121171361	40.9925345120	41.1439639611	41.2171929464
219	40.2086535946	40.2176296172	40.2367400749	40.2685509603	40.3176092131	40.3915194012	40.5028787597	40.6727513850	40.9369928929	41.1357992296	41.2046957096
220	40.1976553066	40.2061388495	40.2241982991	40.2545258092	40.3005876083	40.3703662153	40.4754485575	40.6356530323	40.8846905257	41.1281172108	41.1929482574
221	40.1872602483	40.1952794213	40.2123479987	40.2407470351	40.2845157168	40.3504031255	40.4495767817	40.6006860451	40.8354305872	41.1208881653	41.1819037049
222	40.1774340008	40.1850152449	40.2011495073	40.2279879421	40.2693383668	40.3315604279	40.4251712364	40.5677228880	40.7890287087	41.1140842622	41.1715182214
223	40.1681441875	40.1753123781	40.1905655255	40.2159325758	40.2550037992	40.3137726677	40.4021454034	40.5366439710	40.7453121561	41.1076794515	41.1617508229
224	40.1593603462	40.1661388917	40.1805609739	40.2045405524	40.2414632576	40.2969783690	40.3804180779	40.5073371343	40.7041190654	41.1016493454	41.1525631802
225	40.1510538214	40.1574647447	40.1711028554	40.1937738383	40.2286709931	40.2811197837	40.3599130291	40.4796971676	40.6652977307	40.9597110827	41.1439194395
226	40.1431976335	40.1492616691	40.1621601273	40.1835969010	40.2165839809	40.2661426561	40.3405586835	40.4536253624	40.6287059412	40.9062335325	41.1357860562
227	40.1357663956	40.1415030605	40.1537035804	40.1739759686	40.2051617694	40.2519960034	40.3222878289	40.4290290941	40.5941203623	40.8558604705	41.1281316398
228	40.1287362071	40.1341638767	40.1457057269	40.1648794995	40.1943663202	40.2386319104	40.3050373376	40.4058214314	40.5616859597	40.8084042062	41.1209268103
229	40.1220845643	40.1272205422	40.1381406944	40.1562777594	40.1841618583	40.2260053374	40.2887479087	40.3839207726	40.5310154612	40.7636888619	41.1141440640
230	40.1157902765	40.1206508588	40.1309841280	40.1481427668	40.1745147323	40.2140739409	40.2733638266	40.3632505058	40.5020888958	40.7215495985	41.1077576489
231	40.1098333856	40.1144339223	40.1242130970	40.1404481854	40.1653932832	40.2027979058	40.2588327355	40.3437386913	40.4748029260	40.6818318953	41.1017434483
232	40.1041950919	40.1085500441	40.1178060090	40.1331692238	40.1567677216	40.1921397885	40.2451054290	40.3253177655	40.4490608111	40.6443908777	40.9607687338
233	39.9885766438	40.1029806774	40.1117425283	40.1262825412	40.1486100135	40.1820643696	40.2321356530	40.3079242638	40.4247716005	40.6090906909	40.9074776183
234	39.9380447507	39.9770834871	40.1060035001	40.1197661593	40.1408937723	40.1725385174	40.2198799215	40.2914985624	40.4018499532	40.5758039160	40.8571528457
235	39.8901973766	39.9271659338	40.1005708794	40.1135993797	40.1335941582	40.1635310586	40.2082973441	40.2759846363	40.3802157429	40.5444110248	40.8097785822
236	39.8448864994	39.8798969456	39.9542766386	40.1077627060	40.1266877845	40.1550126581	40.1973494663	40.2613298335	40.3597937272	40.5147998717	40.7651306372
237	39.8019723987	39.8351362815	39.9055783151	40.1022377720	40.1201526286	40.1469557065	40.1870001163	40.2474846640	40.3405132373	40.4868652198	40.7230457048
238	39.7613233941	39.7927400657	39.8594628189	39.9700727313	40.1139679498	40.1393432148	40.1772152663	40.2344026024	40.3223078895	40.4605082980	40.6833706562
239	39.7228151449	39.7525803182	39.8157878106	39.9205490289	40.1081142115	40.1321237150	40.1679628995	40.2220399032	40.3051153150	40.4356363880	40.6459618804
240	39.6863306546	39.7145344723	39.7744190994	39.8736529304	40.1025730089	40.1253011682	40.1592128866	40.2103554282	40.2888769074	40.4121624390	40.6106846689
241	39.6517594025	39.6784869375	39.7352301585	39.8292395750	39.9732700053	40.1188448774	40.1509368705	40.1993104851	40.2735375866	40.3900047070	40.5774126421
242	39.6189971761	39.6443286878	39.6981016712	39.7871723980	39.9235984473	40.1127344069	40.1431081577	40.1888686761	40.2590455786	40.3690864187	40.5460272137
243	39.5879456573	39.6113568743	39.6629211034	39.7473226371	39.8765613959	40.1069505055	40.1357016170	40.1789957568	40.2453522091	40.3493354576	40.5164170911
244	39.5585120764	39.5812744621	39.6295823042	39.7095688706	39.8320136693	40.1014750354	40.1286935844	40.1696595039	40.2324117105	40.3306840702	40.4884778094
245	39.5306088871	39.5521898889	39.5979851294	39.6737965793	39.7898183962	39.9629090567	40.1220617744	40.1608295907	40.2201810417	40.3130685913	40.4621112954
246	39.5041534613	39.5246167448	39.5680350888	39.6398977455	39.7498465217	39.9138200900	40.1157851964	40.1524774717	40.2086197195	40.2964291883	40.4372254618
247	39.4790678020	39.4984734714	39.5396430152	39.6077704637	39.7119763440	39.8673316318	40.1098440764	40.1445762739	40.1976896601	40.2807096209	40.4137338270
248	39.4552782744	39.4736830790	39.5127247525	39.5773185847	39.6760930792	39.8233005587	40.1042197841	40.1371006944	40.1873550320	40.2658570174	40.3915551608
249	39.4327153525	39.4501728807	39.4872008641	39.5484513772	39.6420884535	39.7815912894	39.9889476393	40.1300269059	40.1775821171	40.2518216648	40.3706131529
250	39.4113133810	39.4278742437	39.4629963575	39.5210832112	39.6098603193	39.7420784946	39.9385247077	40.1233324669	40.1683391814	40.2385568127	40.3508361031

$$K_{(n+1/2)}\left(\frac{\pi}{3}\sqrt{q}\right)$$

q \ n	0	1	2	3	4	5	6	7	8	9	10
1	50.4297872341	50.8402038108	51.2836793849	52.1438489672	52.9899274542	53.8651648740	54.9186880320	56.1149118832	57.1655178361	58.2698475331	59.4912574623
2	50.2342151315	50.3923659098	51.1029035350	51.3866580844	52.1930505091	53.1211859840	53.9194272301	54.8191995518	55.8389253353	56.9711971589	58.1254387377
3	50.1517197997	50.2353673093	50.5410141956	51.1726751104	51.7205068646	52.3747801395	53.2344949010	54.1718167606	55.1444362662	56.1370923757	57.1450520400
4	50.1066464481	50.1575663763	50.3323436570	50.9509784135	51.3510754878	52.1603733622	52.8774065887	53.5606473594	54.4103081595	55.3386495897	56.3113202918
5	49.7876930926	50.1124083356	50.2227837864	50.5881157989	51.1980898733	51.8201735210	52.4050963896	53.2331010357	54.1533722914	55.1136789556	55.9377388464
6	49.6018651389	49.8365013006	50.1580191221	50.3916676402	51.1226856144	51.4696258790	52.2136597490	53.1129796437	53.6320399756	54.4633146936	55.3500031351
7	49.4715245152	49.6417116157	50.1166362444	50.2746584598	50.8105626000	51.2907661937	52.1235463278	52.6087662819	53.3419371838	54.2158935227	55.1514718141
8	49.3766402854	49.5038010583	49.8869181373	50.2001001440	50.5615945530	51.1906543139	51.7642123620	52.3544814499	53.1871614298	54.1109664262	54.7305384420
9	49.3055685465	49.4028340357	49.6902467146	50.1501395802	50.4035610602	51.1306256856	51.4977300244	52.2190246722	53.1095538780	53.6147278684	54.3827359077
10	49.2511115420	49.3269410183	49.5472958514	50.1153290088	50.2985151473	50.9266267457	51.3376517153	52.1418174769	52.6761457401	53.3612865478	54.2140507046
11	49.2086040065	49.2686657154	49.4406684179	49.9030566527	50.2260738353	50.6761305975	51.2367476380	51.9537565401	52.4355861789	53.2227428927	54.1262078152
12	49.1749057986	49.2231211089	49.3594254704	49.7185252278	50.1745928491	50.5050138947	51.1705950989	51.6618524379	52.2907332900	53.1428647385	53.7773451844
13	49.1478371190	49.1869917555	49.2964113254	49.5795142079	50.1370801020	50.3847022017	51.1257851561	51.4715545312	52.1999152249	52.9472631950	53.4966682733
14	49.1258453964	49.1579631156	49.2467893914	49.4728857353	50.1091604394	50.2980236819	50.9458239436	51.3436082074	52.1409995462	52.6461108525	53.3274054417
15	49.1078004357	49.1343799027	49.2071992787	49.3898170151	49.8799971120	50.2342579885	50.7233494380	51.2552812191	52.1016473812	52.4515882247	53.2217190894
16	48.9286395203	49.1150335875	49.1752506904	49.3242236899	49.7170696210	50.1864913549	50.5614438081	51.1928944223	51.7468966488	52.3224137910	53.1537131499
17	48.8040396377	48.9902588050	49.1492084710	49.2718126184	49.5898795770	50.1501381295	50.4414872249	51.1479393473	51.5580999156	52.2345332665	53.1087870059
18	48.6993715467	48.8567854504	49.1277904987	49.2294933838	49.4893696150	50.1220815144	50.3511949047	51.1149687649	51.4232754462	52.1734566374	52.7841152884
19	48.6108918720	48.7447235516	49.1100344793	49.1950018617	49.4090759220	50.1001569901	50.2822693897	50.9040564151	51.3253123824	52.1301963328	52.5744659064
20	48.5356683020	48.6500488919	48.9520807094	49.1666531973	49.3443048284	49.8283240543	50.2289885946	50.7184758730	51.2530217561	51.9903137715	52.4270770774
21	48.4713803775	48.5696079100	48.8274697407	49.1431759950	49.2915948125	49.6900459169	50.1873325026	50.5764837628	51.1989271454	51.7623490822	52.3217274500
22	48.4161748598	48.5009046016	48.7221148988	49.1235987555	49.2483572441	49.5786699888	50.1544293638	50.4665939504	51.1579349108	51.5932813896	52.2452890934
23	48.3685592324	48.4419454930	48.6325552818	49.1071706772	49.2126317530	49.4882172792	50.1281965555	50.3806605344	51.1265134016	51.4663116620	52.1890670846
24	48.3273222766	48.3911253096	48.5560416411	48.9330551707	49.1829166872	49.4141995179	50.1071029295	50.3128203392	51.1021746746	51.3698594186	52.1471971151
25	48.2914741454	48.3471416066	48.4903716349	48.8154120245	49.1580497212	49.3532086617	49.9000864599	50.2587958727	50.8314042090	51.2958166500	52.1156579973
26	48.2602006688	48.3089302991	48.4337673933	48.7151038268	49.1371225459	49.3026296146	49.7605541551	50.2154276648	50.6812254855	51.2384252694	51.9165028791
27	48.2328281691	48.2756164682	48.3847834921	48.6291868976	49.1194190966	49.2604362856	49.6459012786	50.1803553786	50.5617657861	51.1935422404	51.7319776328
28	48.2087961263	48.2464764654	48.3422370619	48.5552850818	49.1043702717	49.2250448962	49.5511096336	50.1517971052	50.4660213461	51.1581504284	51.5888730851
29	48.1876357649	48.2209084619	48.3051541972	48.4914673062	48.9152036694	49.1952071843	49.4722887374	50.1283945042	50.3887441043	51.1300279841	51.4769638793
30	48.1689531511	48.1984093735	48.2727284983	48.4361543123	48.8050193050	49.1699317787	49.4063971899	50.1091027581	50.3259633509	51.1075216923	51.3887688861
31	48.1524157541	48.1785566456	48.2442887352	48.3880469754	48.7101674598	49.1484257111	49.3510388785	49.9311144869	50.2746476565	50.8938953878	51.3187582916
32	48.1377416909	48.1609937706	48.2192734325	48.3460707539	48.6282131870	49.1300504862	49.3043123788	49.7978703984	50.2324631641	50.7469001248	51.2628053353
33	48.1246910643	48.1454186989	48.1972107514	48.3093323047	48.5571570644	49.1142887885	49.2646985942	49.6863063987	50.1975989014	50.6270337895	51.2178026444
34	48.1130589476	48.1315745080	48.1777024580	48.2770853531	48.4953485619	49.1007190381	49.2309761685	49.5924668641	50.1686392515	50.5287509179	51.1813907282
35	48.1026696695	48.1192418450	48.1604110684	48.2487036613	48.4414183532	48.8899579098	49.2021572708	49.5131952184	50.1444699679	50.4477470983	51.1517638179
36	47.9337213658	48.1082327737	48.1450494794	48.2236594819	48.3942250641	48.7883452907	49.1774384613	49.4459572357	50.1242082938	50.3806579105	51.1275296467
37	47.8503598455	47.9838573860	48.1313725591	48.2015062799	48.3528131060	48.6999977589	49.1561628146	49.3887067009	50.1071505692	50.3248363561	51.1076072422
38	47.7754839791	47.8956142382	48.1191702908	48.1818648002	48.3163790831	48.6229574859	49.1377905186	49.3397825115	49.9273263875	50.2781869463	50.9115177406
39	47.7081147022	47.8163933167	48.1082621559	48.1644117710	48.2842448760	48.5555896004	49.1218759004	49.2978293108	49.8049971172	50.2390410539	50.7749883966
40	47.6474000409	47.7451494428	47.9849251001	48.1488707007	48.2558359565	48.4965232979	49.1080493627	49.2617358622	49.7008325502	50.2060625716	50.6612283667
41	47.5925967044	47.6809735885	47.8972676052	48.1350043418	48.2306638275	48.4446047020	48.9600309624	49.2305868995	49.6118316068	50.1781760067	50.5660563120
42	47.5430546276	47.6230730999	47.8184819330	48.1226084938	48.2083117332	48.3988589340	48.8547971702	49.2036252822	49.5355389701	50.1545113113	50.4861280997
43	47.4982039435	47.5707550959	47.7475532741	48.1115068847	48.1884229763	48.3584594394	48.7626317984	49.1802220805	49.4699368890	50.1343612848	50.4187556097
44	47.4575439685	47.5234124844	47.6835970209	48.1015469252	48.1706913250	48.3227030660	48.6817147643	49.1598528031	49.4133601674	50.1171484875	50.3617676111
45	47.4206338577	47.4805121425	47.6258401845	47.9259617440	48.1548531025	48.2909897230	48.6105073902	49.1420784084	49.3644290071	50.1023993926	50.3134022988
46	47.3870846539	47.4415848946	47.5736057376	47.8453938603	48.1406806379	48.2628057082	48.5477045698	49.1265300634	49.3219956816	49.8972408456	50.2722238081
47	47.3565525029	47.4062169886	47.5262993788	47.7727603133	48.1279768230	48.2377099853	48.4921957943	49.1128968524	49.2851019839	49.7880023022	50.2370570032
48	47.3287328459	47.3740428251	47.4833983091	47.7071821448	48.1165705723	48.2153228454	48.4430332652	49.1009158228	49.2529451107	49.6936036038	50.2069362727
49	47.3033554375	47.3447387381	47.4444416856	47.6478891289	48.1063130230	48.1953165027	48.3994056993	48.9036388634	49.2248501881	49.6118173044	50.1810651231
50	47.2801800588	47.3180176606	47.4090224787	47.5942048690	47.9707434344	48.1774072675	48.3606167284	48.8105120602	49.2002480501	49.5407820023	50.1587841402

$K_{(n+1/2)}\left(\frac{\pi}{3}\sqrt{q}\right)$

q \ n	0	1	2	3	4	5	6	7	8	9	10
51	47.2589928205	47.2936245372	47.3767805076	47.5455341412	47.8874104404	48.1613490085	48.3260670226	48.7281577299	49.1786571919	49.4789370273	50.1395454693
52	47.2396029671	47.2713323702	47.3473964671	47.5013521122	47.8121370508	48.1469276748	48.2952394420	48.6551894375	49.1596690548	49.4249696870	50.1228923992
53	47.2218401073	47.2509388024	47.3205867919	47.4611951312	47.7440505048	48.1339566907	48.2676866640	48.5904175410	49.1429359831	49.3777724872	50.1084429586
54	47.2055518101	47.2322631582	47.2960992308	47.4246528442	47.6823831058	48.1222730731	48.2430208379	48.5328186414	49.1281613314	49.3364083078	49.9587668561
55	47.1906015114	47.2151438745	47.2737090227	47.3913614232	47.6264582670	48.1117341482	48.2209049096	48.4815101802	49.1150913093	49.3000819476	49.8492391201
56	47.1768666898	47.1994362666	47.2532155853	47.3609977402	47.5756785865	48.1022147666	48.2010453236	48.4357292484	49.1035082368	49.2681167934	49.7535705460
57	47.1642372720	47.1850105807	47.2344396422	47.3332743403	47.5295156313	47.9360493638	48.1831858666	48.3948148558	48.9322494760	49.2399356225	49.6698351019
58	47.1526142373	47.1717502934	47.2172207244	47.3079350965	47.4875011630	47.8580780451	48.1671024595	48.3581930503	48.8408012996	49.2150447556	49.5963983978
59	47.1419083935	47.1595506227	47.2014149932	47.2847514437	47.4492195857	47.7873793168	48.1525987396	48.3253643949	48.7593443750	49.1930209337	49.5318699172
60	47.1320393018	47.1483172243	47.1868933396	47.2635191094	47.4143014298	47.7231981459	48.1395023042	48.2958933993	48.6866723231	49.1735004163	49.4750636573
61	47.1229343301	47.1379650452	47.1735397213	47.2440552688	47.3824177174	47.6648661672	48.1276615078	48.2693995767	48.6217385024	49.1561698994	49.4249655949
62	47.1145278187	47.1284173160	47.1612497064	47.2261960645	47.3532750813	47.6117907608	48.1169427245	48.2455498579	48.5636329852	49.1407589275	49.3807067152
63	47.1067603442	47.1196046629	47.1499291936	47.2097944406	47.3266115256	47.5634456299	48.1072280043	48.2240521393	48.5115631208	49.1270335351	49.3415405854
64	46.9957806721	47.1114643234	47.1394932878	47.1947182470	47.3021927383	47.5193626564	47.9841305940	48.2046497831	48.4648370860	49.1147909063	49.3068246558
65	46.9293215617	47.1039394540	47.1298653095	47.1808485777	47.2798088777	47.4791248471	47.9040553295	48.1871169180	48.4228499305	49.1038548761	49.2760046266
66	46.8677827509	46.9697851596	47.1209759203	47.1680783117	47.2592717651	47.4423602110	47.8312350555	48.1712544150	48.3850717089	48.9407213245	49.2486013423
67	46.8107612910	46.9053473186	47.1127623507	47.1563108298	47.2404124301	47.4087364362	47.7649420527	48.1568864333	48.3510373660	48.8530900086	49.2241997780
68	46.7578906013	46.8456560236	47.1051677163	47.1454588832	47.2230789585	47.3779562525	47.7045289074	48.1438574501	48.3203380954	48.7744871731	49.2024397600
69	46.7088368668	46.7903247683	46.9814041240	47.1354435965	47.2071346038	47.3497533832	47.6494188251	48.1320297011	48.2926139418	48.7038910873	49.1830081299
70	46.6632958267	46.7390017093	46.9163357572	47.1261935855	47.1924561268	47.3238890075	47.5990972122	48.1212809694	48.2675474552	48.6404061652	49.1656321103
71	46.6209899059	46.6913662575	46.8560460687	47.1176441768	47.1789323326	47.3001486613	47.5531043483	48.1115026736	48.2448582347	48.5832460848	49.1500736778
72	46.5816656505	46.6471260349	46.8001474484	47.1097367162	47.1664627814	47.2783395191	47.5110289958	48.1025982101	48.2242982294	48.5317193409	49.1361247775
73	46.5450914317	46.6060141549	46.7482868798	47.1024179547	47.1549566488	47.2582880054	47.4725028164	47.9448151378	48.2056476836	48.4852168561	49.1236032458
74	46.5110553889	46.5677867880	46.7001425578	46.9563950264	47.1443317180	47.2398376939	47.4371954868	47.8707580569	48.1887116296	48.4432013356	49.1123493290
75	46.4793635830	46.5322209820	46.6554208667	46.8935734444	47.1345134871	47.2228474545	47.4048104171	47.8031250228	48.1733168512	48.4051981020	49.1022227055
76	46.4498383386	46.4991127055	46.6138536777	46.8353140550	47.1254343768	47.2071898194	47.3750809925	47.7413026302	48.1593092485	48.3707871917	48.9309993160
77	46.4223167527	46.4682750922	46.5751959283	46.7812516623	47.1170330273	47.1927495379	47.3477672691	47.6847415783	48.1465515466	48.3395965245	48.8487224956
78	46.3966493521	46.4395368619	46.5392234520	46.7310531714	47.1092536722	47.1794222976	47.3226530651	47.6329493821	48.1349213023	48.3112959921	48.7744370024
79	46.3726988845	46.4127409000	46.5057310308	46.6844145032	47.1020455815	47.1671135911	47.2995433957	47.5854839787	48.1243091640	48.2855923320	48.7072949686
80	46.3503392269	46.3877429778	46.4745306446	46.6410578317	46.9536256450	47.1557377101	47.2782622078	47.5419481128	48.1146173534	48.2622246757	48.6465462044
81	46.3294544009	46.3644105985	46.4454498970	46.6007291085	46.8916252634	47.1452168517	47.2586503780	47.5019843986	48.1057583362	48.2409606756	48.5915260493
82	46.3099376820	46.3426219555	46.4183305980	46.5631958400	46.8340707152	47.1354803227	47.2405639389	47.4652709694	47.9765365803	48.2215931311	48.5416448462
83	46.2916907946	46.3222649916	46.3930274859	46.5282450910	46.7806114906	47.1264638317	47.2238725080	47.4315176411	47.9023292303	48.2039370431	48.4963788057
84	46.2746231827	46.3032365477	46.3694070747	46.4956816895	46.7309273469	47.1181088569	47.2084578914	47.4004625236	47.8343289621	48.1878270410	48.4552620658
85	46.2586513490	46.2854415929	46.3473466129	46.4653266100	46.6847254584	47.1103620819	47.1942128448	47.3718690234	47.7719671382	48.1731151299	48.4178797790
86	46.2436982554	46.2687925260	46.3267331425	46.4370155170	46.6417378573	47.1031748912	47.1810399692	47.3455231902	47.7147318752	48.1596687158	48.3838620845
87	46.2296927788	46.2532085431	46.3074626474	46.4105974512	46.6017191337	46.9650291937	47.1688507279	47.3212313636	47.6621619056	48.1473688732	48.3528788461
88	46.2165692171	46.2386150633	46.2894392821	46.3859336428	46.5644443674	46.9030564578	47.1575645701	47.2988180842	47.6138411548	48.1361088214	48.3246350491
89	46.2042668389	46.2249432066	46.2725746731	46.3628964396	46.5297072641	46.8454603252	47.1471081474	47.2781242370	47.5693939443	48.1257925836	48.2988667714
90	46.1927294750	46.2121293202	46.2567872843	46.3413683372	46.4973184766	46.7919019848	47.1374146142	47.2590053993	47.5284807445	48.1163338062	48.2753376491
91	46.1819051452	46.2001145466	46.2420018418	46.3212411005	46.4671040891	46.7420712676	47.1284230010	47.2413303690	47.4907944077	48.1076547152	48.2538357739
92	46.1717457192	46.1888444309	46.2281488102	46.3024149684	46.4389042494	46.6956840132	47.1200776537	47.2249798519	47.4560568245	47.9968519616	48.2341709654
93	46.1622066063	46.1782685628	46.2151639174	46.2847979319	46.4125719312	46.6524796997	47.1123277302	47.2098452898	47.4240159526	47.9236197846	48.2161723694
94	46.1532464727	46.1683402502	46.2029877208	46.2683050790	46.3879718158	46.6122193061	47.1051267484	47.1958278130	47.3944431721	47.8562791434	48.1996863413
95	46.1448269834	46.1590162211	46.1915652136	46.2528580000	46.3649792783	46.5746833846	46.9843218105	47.1828373033	47.3671309308	47.7943133880	48.1845745778
96	46.1369125657	46.1502563519	46.1808454646	46.2383842459	46.3434794693	46.5396703198	46.9220508997	47.1707915542	47.3418906435	47.7372550165	48.1707124666
97	46.1294701934	46.1420234184	46.1707812908	46.2248168362	46.3233664821	46.5069947552	46.8640979782	47.1596155189	47.3185508176	47.6846806284	48.1579876261
98	46.1224691690	46.1342828685	46.1613289574	46.2120938110	46.3045425964	46.4764861699	46.8101359183	47.1492406343	47.2969553780	47.6362064332	48.1462986122
99	46.1158810422	46.1270026141	46.1524479048	46.2001578220	46.2869175910	46.4479875898	46.7598645672	47.1396042148	47.2769621679	47.5914842522	48.1355537720
100	46.1096732444	46.1201528408	46.1441004978	46.1889557604	46.2704081196	46.4213544204	46.7130083357	47.1306489069	47.2584416076	47.5501979523	48.1256702259

$K_{(n+1/2)}\left(\frac{\pi}{3}\sqrt{q}\right)$

q \ n	0	1	2	3	4	5	6	7	8	9	10
101	46.1038391363	46.1137058327	46.1362517977	46.1784384162	46.2549371423	46.3964533875	46.6693140196	47.1223221978	47.2412754919	47.5120602643	48.1165729633
102	45.9833776770	46.1076358127	46.1288693523	46.1685601685	46.2404334078	46.3731615763	46.6285488299	47.1145759738	47.2253559109	47.4768099402	48.1081940384
103	45.9315376954	46.1019187954	46.1219230041	46.1592787011	46.2268309817	46.3513655586	46.5904986097	47.1073661212	47.2105842814	47.4442092109	48.1004718537
104	45.8826723586	45.9653245245	46.1153847145	46.1505547433	46.2140688169	46.3309605992	46.5549662191	47.1006521666	47.1968704765	47.4140415113	47.9335052198
105	45.8365961534	45.9145598811	46.1092284028	46.1423518320	46.2020903601	46.3118499342	46.5217700714	46.9439695235	47.1841320417	47.3861094412	47.8677929609
106	45.7931361152	45.8667002574	46.1034297978	46.1346360949	46.1908431944	46.2939441135	46.4907428051	46.8856634243	47.1722934900	47.3602329371	47.8071206067
107	45.7521309096	45.8215650287	45.9796630187	46.1273760503	46.1802787107	46.2771604027	46.4617300775	46.8312895712	47.1612856664	47.3362476316	47.7510687721
108	45.7134299869	45.7789857480	45.9281686629	46.1205424251	46.1703518087	46.2614222369	46.4345894694	46.7805593232	47.1510451743	47.3140033781	47.6992557704
109	45.6768928019	45.7388052574	45.8796187616	46.1141079866	46.1610206225	46.2466587227	46.4091894886	46.7332070169	47.1415138585	47.2933629262	47.6513339692
110	45.6423880959	45.7008768707	45.8338304484	46.1080473890	46.1522462696	46.2328041839	46.3854086635	46.6889879903	47.1326383371	47.2742007277	47.6069865225
111	45.6097932330	45.6650636184	45.7906331663	46.1023370316	46.1439926207	46.2197977460	46.3631347173	46.6476767895	47.1243695796	47.2564018623	47.5659244391
112	45.5789935885	45.6312375529	45.7498677722	45.9695492891	46.1362260892	46.2075829565	46.3422638156	46.6090655405	47.1166625235	47.2398610684	47.5278839502
113	45.5498819833	45.5992791057	45.7113857110	45.9188059147	46.1289154374	46.1961074375	46.3226998810	46.5729624688	47.1094757289	47.2244818696	47.4926241426
114	45.5223581618	45.5690764952	45.6750482547	45.8709491537	46.1220315987	46.1853225682	46.3043539662	46.5391905542	47.1027710637	47.2101757846	47.4599248303
115	45.4963283093	45.5405251788	45.6407257998	45.8258008120	46.1155475150	46.1751831931	46.2871436830	46.5075863048	46.9651341958	47.1968616147	47.4295846380
116	45.4717046049	45.5135273469	45.6082972195	45.7831946073	46.1094379865	46.1656473556	46.2709926800	46.4779986425	46.9067045340	47.1844647983	47.4014192745
117	45.4484048086	45.4879914551	45.5776492648	45.7429753087	46.1036795336	46.1566760528	46.2558301646	46.4502878854	46.8521235242	47.1729168273	47.3752599754
118	45.4263518790	45.4638317907	45.5486760115	45.7049979437	45.9825027029	46.1482330114	46.2415904666	46.4243248211	46.8011162117	47.1621547183	47.3509520978
119	45.4054736182	45.4409680725	45.5212783493	45.6691270664	45.9312978750	46.1402844812	46.2282126381	46.3999898603	46.7534288735	47.1521205333	47.3283538514
120	45.3857023443	45.4193250793	45.4953635083	45.6352360817	45.8829904523	46.1327990455	46.2156400868	46.3771722643	46.7088272532	47.1427609450	47.3073351512
121	45.3669745863	45.3988323059	45.4708446220	45.6032066214	45.8374027358	46.1257474474	46.2038202406	46.3557694388	46.6670949525	47.1340268424	47.2877765798
122	45.3492308020	45.3794236450	45.4476403220	45.5729279674	45.7943688130	46.1191024292	46.1927042395	46.3356862886	46.6280319655	47.1258729722	47.2695684484
123	45.3324151163	45.3610370908	45.4256743628	45.5442965182	45.7537337146	46.1128385855	46.1822466530	46.3168346268	46.5914533427	47.1182576131	47.2526099460
124	45.3164750773	45.3436144656	45.4048752743	45.5172152963	45.7153526363	46.1069322268	46.1724052205	46.2991326343	46.5571879704	47.1111422794	47.2368083681
125	45.3013614310	45.3271011645	45.3851760395	45.4915934910	45.6790902196	46.1013612551	46.1631406130	46.2825043643	46.5250774578	47.1044914517	47.2220784170
126	45.2870279112	45.3114459197	45.3665137954	45.4673460362	45.6448198875	45.9610504869	46.1544162140	46.2668792889	46.4949751187	46.9827233056	47.2083415671
127	45.2734310444	45.2966005808	45.3488295561	45.4443932188	45.6124232310	45.9114435533	46.1461979178	46.2521918826	46.4667450415	46.9245461347	47.1955254881
128	45.2605299685	45.2825199105	45.3320679550	45.4226603158	45.5817894409	45.8646119473	46.1384539442	46.2383812402	46.4402612379	46.8701029017	47.1835635201
129	45.2482862639	45.2691613954	45.3161770055	45.4020772578	45.5528147822	45.8203876787	46.1311546677	46.2253907264	46.4154068641	46.8191345661	47.1723941976
130	45.2366637966	45.2564850692	45.3011078797	45.3825783170	45.5254021080	45.7786137341	46.1242724604	46.2131676537	46.3920735070	46.7714014485	47.1619608148
131	45.2256285720	45.2444533485	45.2868147012	45.3641018177	45.4994604091	45.7391433049	46.1177815466	46.2016629863	46.3701605305	46.7266816768	47.1522110307
132	45.2151485985	45.2330308804	45.2732543533	45.3465898675	45.4749043961	45.7018390733	46.1116578695	46.1908310680	46.3495744757	46.6847697662	47.1430965087
133	45.2051937609	45.2221843999	45.2603863006	45.3299881075	45.4516541127	45.6665725515	46.1058789676	46.1806293713	46.3302285115	46.6454753195	47.1345725883
134	45.1957357021	45.2118825974	45.2481724230	45.3142454802	45.4296345774	45.6332234714	46.1004238614	46.1710182673	46.3120419288	46.6086218390	47.1265979855
135	45.1867477126	45.2020959953	45.2365768604	45.2993140140	45.4087754496	45.6016792185	45.9527294744	46.1619608134	46.2949396777	46.5740456371	47.1191345192
136	45.1782046280	45.1927968325	45.2255658694	45.2851486228	45.3890107214	45.5718343080	45.9040790201	46.1534225570	46.2788519408	46.5415948390	47.1121468609
137	45.1700827329	45.1839589576	45.2151076884	45.2717069191	45.3702784303	45.5435898993	45.8581159084	46.1453713558	46.2637137416	46.5111284685	47.1056023072
138	45.1623596709	45.1755577280	45.2051724131	45.2589490405	45.3525203926	45.5168533466	45.8146798628	46.1377772109	46.2494645841	46.4825156086	46.9947056983
139	45.1550143619	45.1675699170	45.1957318794	45.2468374884	45.3356819560	45.4915377809	45.7736209048	46.1306121135	46.2360481215	46.4556346325	46.9372358549
140	45.1480269230	45.1599736262	45.1867595549	45.2353369768	45.3197117690	45.4675617231	45.7347986426	46.1238499029	46.2234118503	46.4303724960	46.8833534027
141	45.1413785960	45.1527482039	45.1782304373	45.2244142926	45.3045615667	45.4448487249	45.6980816132	46.1174661359	46.2115068292	46.4066240889	46.8328170955
142	45.1350516791	45.1458741692	45.1701209599	45.2140381646	45.2901859718	45.4233270346	45.6633466720	46.1114379653	46.2002874199	46.3842916376	46.7854031111
143	45.1290294630	45.1393331404	45.1624089028	45.2041791416	45.2765423086	45.4029292878	45.6304784278	46.1057440284	46.1897110479	46.3632841566	46.7409037036
144	45.1232961714	45.1331077690	45.1550733105	45.1948094788	45.2635904308	45.3835922188	45.5993687184	46.1003643432	46.1797379818	46.3435169434	46.6991259677
145	45.1178369049	45.1271816769	45.1480944147	45.1859030315	45.2512925602	45.3652563932	45.5699161250	45.9528021282	46.1703311298	46.3249111135	46.6598907040
146	45.1126375890	45.1215393986	45.1414535623	45.1774351563	45.2396131368	45.3478659585	45.5420255202	45.9047413687	46.1614558516	46.3073931726	46.6230313766
147	45.1076849249	45.1161663265	45.1351331474	45.1693826185	45.2285186794	45.3313684128	45.5156076496	45.8592972909	46.1530797849	46.2908946216	46.5883931561
148	45.1029663439	45.1110486598	45.1291165491	45.1617235059	45.2179776546	45.3157143889	45.4905787428	45.8163164144	46.1451726845	46.2753515937	46.5558320387
149	44.9846996444	45.1061733570	45.1233880717	45.1544371477	45.2079603558	45.3008574534	45.4668601517	45.7756549353	46.1377062742	46.2607045183	46.5252140369
150	44.9418455164	45.1015280910	45.1179328900	45.1475040395	45.1984387894	45.2867539200	45.4443780150	45.7371780719	46.1306541092	46.2468978119	46.4964144341

$K_{(n+1/2)}\left(\frac{\pi}{3}\sqrt{q}\right)$

q \ n	0	1	2	3	4	5	6	7	8	9	10
151	44.9009947992	44.9710120723	45.1127369971	45.1409057726	45.1893865690	45.2733626748	45.4230629451	45.7007594580	46.1239914491	46.2338795923	46.4693170987
152	44.8620469744	44.9288168427	45.1077871565	45.1346249678	45.1807788164	45.2606450144	45.4028497383	45.6662805799	46.1176951404	46.2216014150	46.4438138523
153	44.8249069295	44.8885909712	45.1030708563	45.1286452141	45.1725920692	45.2485644939	45.3836771038	45.6336302531	46.1117435072	46.2100180293	46.4198038870
154	44.7894846471	44.8502358260	44.9857626710	45.1229510107	45.1648041946	45.2370867858	45.3654874123	45.6027041370	46.1061162503	46.1990871528	46.3971932289
155	44.7556949127	44.8136580697	44.9429220184	45.1175277131	45.1573943085	45.2261795483	45.3482264617	45.5734042834	46.1007943537	46.1887692635	46.3758942427
156	44.7234570404	44.7787693547	44.9020807856	45.1123614820	45.1503427000	45.2158123021	45.3318432584	45.5456387171	45.9575999768	46.1790274066	46.3558251751
157	44.6926946157	44.7454860386	44.8631388540	45.1074392365	45.1436307611	45.2059563156	45.3162898142	45.5193210458	45.9099647827	46.1698270164	46.3369097322
158	44.6633352533	44.7137289151	44.8260014771	45.1027486091	45.1372409201	45.1965844973	45.3015209563	45.4943700972	45.8648813244	46.1611357510	46.3190766910
159	44.6353103703	44.6834229634	44.7905789720	44.9827790432	45.1311565804	45.1876712958	45.2874941506	45.4707095815	45.8222026871	46.1529233396	46.3022595382
160	44.6085549725	44.6544971110	44.7567864302	44.9401605967	45.1253620622	45.1791926062	45.2741693365	45.4482677767	45.7817910268	46.1451614400	46.2863961384
161	44.5830074536	44.6268840116	44.7245434453	44.8995260878	45.1198425483	45.1711256820	45.2615087732	45.4269772363	45.7435169713	46.1378235081	46.2714284260
162	44.5586094064	44.6005198367	44.6937738582	44.8607764718	45.1145840334	45.1634490533	45.2494768956	45.4067745162	45.7072590630	46.1308846755	46.2573021203
163	44.5353054456	44.5753440786	44.6644055170	44.8238180001	45.1095732767	45.1561424506	45.2380401802	45.3875999210	45.6729032413	46.1243216363	46.2439664625
164	44.5130430404	44.5512993663	44.6363700515	44.7885619172	45.1047977568	45.1491867321	45.2271670198	45.3693972665	45.6403423609	46.1181125426	46.2313739714
165	44.4917723576	44.5283312915	44.6096026616	44.7549241764	45.1002456304	45.1425638175	45.2168276061	45.3521136592	45.6094757435	46.1122369069	46.2194802175
166	44.4714461134	44.5063882452	44.5840419179	44.7228251730	44.9590569246	45.1362566244	45.2069938205	45.3356992903	45.5802087603	46.1066755114	46.2082436138
167	44.4520194343	44.4854212638	44.5596295747	44.6921894929	44.9176734005	45.1302490096	45.1976391314	45.3201072430	45.5524524442	46.1014103243	46.1976252215
168	44.4334497261	44.4653838845	44.5363103931	44.6629456773	44.8782053733	45.1245257142	45.1887384984	45.3052933129	45.5261231269	45.9642442123	46.1875885704
169	44.4156965499	44.4462320087	44.5140319760	44.6350260007	44.8405578324	45.1190723111	45.1802682829	45.2912158409	45.5011421024	45.9170191305	46.1780994913
170	44.3987215058	44.4279237738	44.4927446112	44.6083662628	44.8046408111	45.1138751573	45.1722061640	45.2778355562	45.4774353121	45.8722787788	46.1691259617
171	44.3824881235	44.4104194320	44.4724011252	44.5829055923	44.7703690996	45.1089213477	45.1645310603	45.2651154300	45.4549330521	45.8298829845	46.1606379615
172	44.3669617584	44.3936812363	44.4529567443	44.5585862627	44.7376619771	45.1041986730	45.1572230560	45.2530205387	45.4335696993	45.7897000346	46.1526073399
173	44.3521094946	44.3776733332	44.4343689645	44.5353535187	44.7064429585	44.9969557937	45.1502633322	45.2415179362	45.4132834564	45.7516061313	46.1450076908
174	44.3379000523	44.3623616612	44.4165974288	44.5131554132	44.6766395575	44.9540113068	45.1436341024	45.2305765343	45.3940161140	45.7154848844	46.1378142377
175	44.3243037016	44.3477138552	44.3996038112	44.4919426531	44.6481830631	44.9130497357	45.1373185519	45.2201669906	45.3757128277	45.6812268380	46.1310037265
176	44.3112921802	44.3336991568	44.3833517091	44.4716684549	44.6210083300	44.8739730409	45.1313007812	45.2102616041	45.3583219109	45.6487290302	46.1245543256
177	44.2988386166	44.3202883286	44.3678065347	44.4522884085	44.5950535807	44.8366883662	45.1255657528	45.2008342167	45.3417946407	45.6178945817	46.1184455335
178	44.2869174565	44.3074535746	44.3529354290	44.4337603483	44.5702602197	44.8011077458	45.1200992411	45.1918601221	45.3260850762	45.5886323128	46.1126580919
179	44.2755043949	44.2951684643	44.3387071597	44.4160442326	44.5465726589	44.7671478300	45.1148877859	45.1833159793	45.3111498892	45.5608563854	46.1071739058
180	44.2645763100	44.2834078607	44.3250920399	44.3991020293	44.5239381527	44.7347296262	45.1099186483	45.1751797323	45.2969482060	45.5344859699	46.1019759683
181	44.2541112025	44.2721478537	44.3120618460	44.3828976082	44.5023066430	44.7037782560	45.1051797695	45.1674305344	45.2834414585	45.5094449331	45.9704829137
182	44.2440881375	44.2613656955	44.2995897407	44.3673966399	44.4816306130	44.6742227265	45.1006597319	45.1600486779	45.2705932458	45.4856615473	45.9237584011
183	44.2344871892	44.2510397411	44.2876502002	44.3525665000	44.4618649500	44.6459957153	44.9634772298	45.1530155271	45.2583692044	45.4630682190	45.8794447277
184	44.2252893897	44.2411493906	44.2762189461	44.3383761787	44.4429668150	44.6190333683	44.9223350092	45.1463134566	45.2467368864	45.4416012346	45.8374088403
185	44.2164766794	44.2316750362	44.2652728805	44.3247961958	44.4248955213	44.5932751087	44.8830736251	45.1399257927	45.2356656456	45.4212005229	45.7975255235
186	44.2080318612	44.2225980107	44.2547900245	44.3117985202	44.4076124188	44.5686634578	44.8456011295	45.1338367587	45.2251265314	45.4018094336	45.7596769077
187	44.1999385561	44.2139005400	44.2447494611	44.2993564940	44.3910807852	44.5451438664	44.8098303744	45.1280314233	45.2150921878	45.3833745295	45.7237520107
188	44.1921811624	44.2055656970	44.2351312800	44.2874447611	44.3752657241	44.5226645553	44.7756787451	45.1224956522	45.2055367610	45.3658453925	45.6896463089
189	44.1847448159	44.1975773593	44.2259165265	44.2760391989	44.3601340676	44.5011763653	44.7430679080	45.1172160633	45.1964358103	45.3491744417	45.6572613371
190	44.1776153530	44.1899201679	44.2170871522	44.2651168550	44.3456542856	44.4806326163	44.7119235750	45.1121799833	45.1877662268	45.3333167635	45.6265043152
191	44.1707792758	44.1825794893	44.2086259691	44.2546558865	44.3317963992	44.4609889738	44.6821752803	45.1073754083	45.1795061554	45.3182299525	45.5972877982
192	44.1642237183	44.1755413784	44.2005166061	44.2446355028	44.3185319000	44.4422033234	44.6537561710	45.1027909658	45.1716349227	45.3038739621	45.5695293504
193	44.1579364154	44.1687925446	44.1927434674	44.2350359118	44.3058336726	44.4242356525	44.6266028100	44.9841587950	45.1641329689	45.2902109647	45.5431512393
194	44.1519056729	44.1623203188	44.1852916936	44.2258382687	44.2936759227	44.4070479383	44.6006549896	44.9423993577	45.1569817838	45.2772052214	45.5180801508
195	44.1461203392	44.1561126227	44.1781471247	44.2170246281	44.2820341084	44.3906040428	44.5758555569	44.9025345260	45.1501638468	45.2648229586	45.4942469216
196	44.1405697785	44.1501579392	44.1712962648	44.2085778977	44.2708848751	44.3748696128	44.5521502483	44.8644725003	45.1436625709	45.2530322533	45.4715862895
197	44.1352438455	44.1444452851	44.1647262496	44.2004817957	44.2602059951	44.3598119867	44.5294875345	44.8281262244	45.1374622492	45.2418029250	45.4500366591
198	44.1301328615	44.1389641844	44.1584248143	44.1927208098	44.2499763089	44.3454001053	44.5078184731	44.7934131243	45.1315480056	45.2311064349	45.4295398827
199	44.1252275912	44.1337046437	44.1523802642	44.1852801583	44.2401756713	44.3316044285	44.4870965711	44.7602548632	45.1259057482	45.2209157902	45.4100410554
200	44.1205192216	44.1286571282	44.1465814467	44.1781457538	44.2307848993	44.3183968558	44.4672776538	44.7285771093	45.1205221245	45.2112054558	45.3914883225

$K_{(n+1/2)}(\frac{\pi}{3}\sqrt{q})$

q \ n	0	1	2	3	4	5	6	7	8	9	10
201	44.1159993410	44.1238125398	44.1410177243	44.1713041681	44.2217857232	44.3057506520	44.4483197424	44.6983093185	45.1153844811	45.2019512699	45.3738326995
202	44.1116599201	44.1191621956	44.1356789492	44.1647425999	44.2131607405	44.2936403768	44.4301829372	44.6693845289	45.1104808241	45.1931303658	45.3570279031
203	44.1074932929	44.1146978076	44.1305554398	44.1584488434	44.2048933721	44.2820418174	44.4128293085	44.6417391667	45.1057997828	45.1847210982	45.3410301929
204	44.1034921400	44.1104114640	44.1256379577	44.1524112590	44.1969678206	44.2709319261	44.3962227929	44.6153128648	45.1013305751	45.1767029732	45.3257982232
205	43.9964947122	44.1062956107	44.1209176860	44.1466187451	44.1893690316	44.2602887605	44.3803290958	44.5900482900	44.9706297528	45.1690565840	45.3112929032
206	43.9595861040	44.1023430344	44.1163862090	44.1410607120	44.1820826561	44.2500914273	44.3651155988	44.5658909809	44.9298728336	45.1617635489	45.2974772665
207	43.9241318018	43.9854684621	44.1120354930	44.1357270566	44.1750950158	44.2403200284	44.3505512731	44.5427891954	44.8909429637	45.1548064544	45.2843163488
208	43.8900708787	43.9490046599	44.1078578674	44.1306081389	44.1683930693	44.2309556111	44.3366065966	44.5206937657	44.8537528129	45.1481688003	45.2717770719
209	43.8573451193	43.9139760786	44.1038460079	44.1256947591	44.1619643810	44.2219801204	44.3232534766	44.4995579628	44.8182194952	45.1418349493	45.2598281367
210	43.8258988920	43.8803226614	43.9999291928	44.1209781366	44.1557970909	44.2133763531	44.3104651757	44.4793373672	44.7842643285	45.1357900789	45.2484399204
211	43.7956790271	43.8479870211	43.9629192024	44.1164498894	44.1498798865	44.2051279159	44.2982162428	44.4599897481	44.7518126083	45.1300201362	45.2375843822
212	43.7666347012	43.8169143140	43.9273662806	44.1121020151	44.1442019757	44.1972191844	44.2864824471	44.4414749486	44.7207933933	45.1245117956	45.2272349728
213	43.7387173275	43.7870521209	43.8932094460	44.1079268727	44.1387530620	44.1896352650	44.2752407157	44.4237547775	44.6911393047	45.1192524186	45.2173665505
214	43.7118804511	43.7583503323	43.8603904284	44.1039171648	44.1335233193	44.1823619584	44.2644690755	44.4067929069	44.6627863357	45.1142300165	45.2079553021
215	43.6860796502	43.7307610417	43.8288535404	44.1000659220	44.1285033701	44.1753857256	44.2541465967	44.3905547758	44.6356736725	45.1094332146	45.1989786680
216	43.6612724412	43.7042384418	43.7985455563	43.9636648650	44.1236842630	44.1686936547	44.2442533407	44.3750074989	44.6097435249	45.1048512190	45.1904152725
217	43.6374181894	43.6787387275	43.7694155964	43.9281249775	44.1190574528	44.1622734306	44.2347703101	44.3601197799	44.5849409665	45.1004737849	45.1822448578
218	43.6144780239	43.6542200030	43.7414150176	43.8939787819	44.1146147803	44.1561133054	44.2256794015	44.3458618305	44.5612137844	44.9629118724	45.1744482215
219	43.5924147556	43.6306421935	43.7144973088	43.8611681997	44.1103484543	44.1502020708	44.2169633607	44.3322052927	44.5385123368	44.9229419252	45.1670071589
220	43.5711928010	43.6079669614	43.6886179920	43.8296377221	44.1062510336	44.1445290317	44.2086057407	44.3191231663	44.5167894180	44.8847403243	45.1599044078
221	43.5507781081	43.5861576264	43.6637345282	43.7993342897	44.1023154105	44.1390839815	44.2005908614	44.3065897396	44.4960001323	44.8482237900	45.1531235963
222	43.5311380869	43.5651790893	43.6398062273	43.7702071774	43.9853479517	44.1338571780	44.1929037717	44.2945805244	44.4761017735	44.8133132117	45.1466491947
223	43.5122415427	43.5449977603	43.6167941633	43.7422078862	43.9490270006	44.1288393213	44.1855302134	44.2830721937	44.4570537115	44.7799334257	45.1404664693
224	43.4940586128	43.5255814898	43.5946610934	43.7152900388	43.9141292604	44.1240215324	44.1784565875	44.2720425240	44.4388172856	44.7480130068	45.1345614388
225	43.4765607063	43.5068995032	43.5733713802	43.6894092819	43.8805954863	44.1193953330	44.1716699213	44.2614703391	44.4213557030	44.7174840711	45.1289208340
226	43.4597204468	43.4889223382	43.5528909191	43.6645231922	43.8483690513	44.1149526264	44.1651578384	44.2513354585	44.4046339428	44.6882820890	45.1235320594
227	43.4435116174	43.4716217862	43.5331870679	43.6405911874	43.8173958236	44.1106856789	44.1589085290	44.2416186471	44.3886186659	44.6603457105	45.1183831564
228	43.4279091093	43.4549708352	43.5142285806	43.6175744416	43.7876240497	44.1065871033	44.1529107229	44.2323015685	44.3732781290	44.6336165979	45.1134627695
229	43.4128888717	43.4389436162	43.4959855441	43.5954358046	43.7590042440	44.1026498415	44.1471536631	44.2233667405	44.3585821037	44.6080392697	45.1087601143
230	43.3984278646	43.4235153521	43.4784293180	43.5741397256	43.7314890835	43.9886714974	44.1416270811	44.2147974928	44.3445017998	44.5835609523	45.1042649464
231	43.3845040143	43.4086623088	43.4615324771	43.5536521797	43.7050333073	43.9523258332	44.1363211733	44.2065779269	44.3310097929	44.5601314392	44.9996753335
232	43.3710961699	43.3943617488	43.4452687572	43.5339405992	43.6795936215	43.9173998267	44.1312265788	44.1986928786	44.3180799554	44.5377029595	44.9585862724
233	43.3581840629	43.3805918866	43.4296130024	43.5149738069	43.6551286087	43.8838346002	44.1263343580	44.1911278816	44.3056873915	44.5162300520	44.9192943918
234	43.3457482678	43.3673318471	43.4145411160	43.4967219535	43.6315986418	43.8515738659	44.1216359727	44.1838691336	44.2938083761	44.4956694471	44.8817161518
235	43.3337701657	43.3545616247	43.4000300136	43.4791564576	43.6089658021	43.8205638062	44.1171232670	44.1769034641	44.2824202958	44.4759799547	44.8457721332
236	43.3222319080	43.3422620452	43.3860575771	43.4622499488	43.5871938010	43.7907529579	44.1127884490	44.1702183038	44.2715015942	44.4571223584	44.8113868226
237	43.3111163834	43.3304147295	43.3726026131	43.4459762133	43.5662479060	43.7620921038	44.1086240737	44.1638016550	44.2610317191	44.4390593152	44.7784884085
238	43.3004071852	43.3190020583	43.3596448109	43.4303101422	43.5460948702	43.7345341686	44.1046230266	44.1576420648	44.2509910733	44.4217552609	44.7470085892
239	43.2900885809	43.3080071392	43.3471647044	43.4152276818	43.5267028646	43.7080341198	44.1007785081	44.1517285984	44.2413609675	44.4051763198	44.7168823912
240	43.2801454827	43.2974137747	43.3351436344	43.4007057876	43.5080414142	43.6825488745	43.9708401896	44.1460508144	44.2321235755	44.3892902204	44.6880479971
241	43.2705634197	43.2872064322	43.3235637135	43.3867223783	43.4900813372	43.6580372094	43.9353334592	44.1405987411	44.2232618923	44.3740662146	44.6604465840
242	43.2613285111	43.2773702149	43.3124077923	43.3732562942	43.4727946870	43.6344596764	43.9012054860	44.1353628543	44.2147596937	44.3594750013	44.6340221689
243	43.2524274410	43.2678908346	43.3016594270	43.3602872560	43.4561546963	43.6117785209	43.8683994672	44.1303340560	44.2066014986	44.3454886551	44.6087214644
244	43.2438474337	43.2587545849	43.2913028489	43.3477958261	43.4401357251	43.5899576056	43.8368610809	44.1255036540	44.1987725327	44.3320805568	44.5844937408
245	43.2355762308	43.2499483169	43.2813229351	43.3357633716	43.4247132099	43.5689623365	43.8065383708	44.1208633430	44.1912586948	44.3192253296	44.5612906963
246	43.2276020692	43.2414594143	43.2717051803	43.3241720293	43.4098636163	43.5487595938	43.7773816375	44.1164051863	44.1840465236	44.3068987772	44.5390663338
247	43.2199136594	43.2332757715	43.2624356703	43.3130046718	43.3955643930	43.5293176647	43.7493433346	44.1121215983	44.1771231677	44.2950778261	44.5177768451
248	43.2125001661	43.2253857711	43.2535010568	43.3022448756	43.3817939289	43.5106061808	43.7223779701	44.1080053283	44.1704763557	44.2837404699	44.4973804998
249	43.2053511881	43.2177782633	43.2448885323	43.2918768904	43.3685315110	43.4925960573	43.6964420123	44.1040494445	44.1640943689	44.2728657175	44.4778375418
250	43.1984567406	43.2104425463	43.2365858078	43.2818856101	43.3557572853	43.4752594358	43.6714938002	44.1002473197	44.1579660151	44.2624335433	44.4591100900

$$K_{(n+1/2)}\left(\frac{\pi}{3}\sqrt{q}\right)$$

q \ n	0	1	2	3	4	5	6	7	8	9	10
251	43.1918072371	43.2033683466	43.2285810900	43.2722565446	43.3434522190	43.4585696298	43.6847934591	43.9659261654	44.1520860629	44.2524248403	44.4411620448
252	43.1853934731	43.1965458015	43.2208630606	43.2629757938	43.3315980647	43.4425010720	43.6644028189	43.9307927459	44.1464279185	44.2428213755	44.4239589996
253	43.1792066093	43.1899654418	43.2134208557	43.2540300216	43.3201773261	43.4270292652	43.6021853372	43.8970149719	44.1409982013	44.2336057475	44.4074681568
254	43.1732381571	43.1836181744	43.2062440468	43.2454064322	43.3091732950	43.4121307442	43.5808060261	43.8645373948	44.1357821318	44.2247613467	44.3916582480
255	43.1674799634	43.1774952677	43.1993226223	43.2370927465	43.2985696706	43.3977829832	43.5602313819	43.8333069676	44.1307707917	44.2162721167	44.3764994589
256	43.1619241966	43.1715883352	43.1926469698	43.2290771806	43.2883512296	43.3839644475	43.5404293188	43.8032729353	44.1259556647	44.2081235184	44.3619633576
257	43.1565633336	43.1658893222	43.1862078594	43.2213484241	43.2785030976	43.3706544582	43.5213691052	43.7743867297	44.1213286074	44.2003004958	44.3480228666
258	43.1513901465	43.1603904911	43.1799964276	43.2138956206	43.2690110720	43.3578331996	43.5030213034	43.7466018702	44.1168818346	44.1927894434	44.3346519992
259	43.1463976907	43.1550844087	43.1740041617	43.2067083478	43.2598615267	43.3454816731	43.4853577120	43.7198738686	44.1126079021	44.1855771749	44.3218261978
260	43.1415792929	43.1499613934	43.1682288858	43.1997765999	43.2510413866	43.3335816616	43.4683513110	43.6941601390	44.1084996913	44.1786510941	44.3095218764
261	43.1369285402	43.1450222030	43.1626447454	43.1930907694	43.2425381045	43.3221156949	43.4519762094	43.6694199116	44.1045503938	44.1719991672	44.2977165659
262	43.1324392693	43.1402526235	43.1572621960	43.1866416306	43.2343396386	43.3110670180	43.4362075954	43.6456141507	44.1007534974	44.1656098958	44.2863888217
263	43.1281055561	43.1356488577	43.1520679886	43.1804203235	43.2264344309	43.3004195599	43.4210216889	43.6227054774	43.9710277212	44.1594722918	44.2755181748
264	43.1239217059	43.1312048147	43.1470551580	43.1744183388	43.2188113865	43.2901579039	43.4063956961	43.6006580943	43.9359225770	44.1535758539	44.2650850842
265	43.1198822442	43.1269146401	43.1422170110	43.1686275028	43.2114598544	43.2802672600	43.3923077661	43.5794377156	43.9021625095	44.1479105443	44.2550708932
266	43.1159819078	43.1227727058	43.1375471155	43.1630399636	43.2043696084	43.2707334374	43.3787369500	43.5590114992	43.8696929415	44.1426667672	44.2454577866
267	43.1122156358	43.1187736013	43.1330392894	43.1576481779	43.1975308293	43.2615428191	43.3656631614	43.5393479825	43.8384616385	44.1373534485	44.2362287507
268	43.1085785617	43.1149121243	43.1286875904	43.1524448979	43.1909340878	43.2526823375	43.3530671390	43.5204170214	43.8084186025	44.1322075158	44.2273675353
269	43.1050660055	43.1111832729	43.1244863063	43.1474231593	43.1845703282	43.2441394508	43.3409304106	43.5021897315	43.7795159711	44.1273748802	44.2188586175
270	43.1016734661	43.1075822367	43.1204299455	43.1425762695	43.1784308528	43.2359021209	43.3292352588	43.4846384331	43.7517079205	44.1227294183	44.2106871672
271	42.9839661408	43.1041043897	43.1165132282	43.1378977965	43.1725073068	43.2279587915	43.3179646892	43.4677365975	43.7249505746	44.1182634555	44.2028390147
272	42.9523128478	43.1007452824	43.1127310774	43.1333815580	43.1667916643	43.2202983687	43.3071023983	43.4514587969	43.6992019167	44.1139696502	44.1953006191
273	42.9217347180	42.9750063503	43.1090786112	43.1290216115	43.1612762143	43.2129102003	43.2966327443	43.4357806557	43.6744217069	44.1098409779	44.1880590396
274	42.8921913054	42.9436613054	43.1055511345	43.1248122441	43.1559535479	43.2057840582	43.2865407189	43.4206788050	43.6505714025	44.1058707176	44.1811019066
275	42.8636512220	42.9133840818	43.1021441313	43.1207479635	43.1508165457	43.1989101202	43.2768119198	43.4061308384	43.6276140822	44.1020524372	44.1744173957
276	42.8360732792	42.8841325668	42.9885325831	43.1168234887	43.1458583660	43.1922789527	43.2674325251	43.3921152703	43.6055143746	43.9837998077	44.1679942022
277	42.8094244327	42.8558661305	42.9567433700	43.1130337416	43.1410724332	43.1858814952	43.2583826887	43.3786114957	43.5842383889	43.9484745598	44.1618215167
278	42.7836722287	42.8285553902	42.9260334764	43.1093738388	43.1364524270	43.1797090438	43.2496694165	43.3655997523	43.5637536499	43.9144922213	44.1558890024
279	42.7587845528	42.8021644801	42.8963642276	43.1058390837	43.1319922718	43.1737532374	43.2412607440	43.3530610842	43.5440290354	43.8817987882	44.1501867733
280	42.7347310615	42.7766606872	42.8676984102	43.1024249588	43.1276861269	43.1680060426	43.2331515147	43.3409773069	43.5250347166	43.8503425517	44.1447053735
281	42.7114820345	42.7520155530	42.8400002145	42.9912711895	43.1235283769	43.1624597407	43.2253304596	43.3293309744	43.5067421016	43.8200739949	44.1394357573
282	42.6890091303	42.7281897955	42.8132351788	42.9594138377	43.1195136223	43.1571069143	43.2177867576	43.3181053474	43.4891237811	43.7909456949	44.1343692704
283	42.6672650428	42.7051632622	42.7873701354	42.9286373158	43.1156366711	43.1519404352	43.2105100166	43.3072843631	43.4721534768	43.7629122293	44.1294976323
284	42.6462834602	42.6829048864	42.7623731597	42.8989029284	43.1118925300	43.1469534525	43.2034902557	43.2968526065	43.4558059322	43.7359300871	44.1248129190
285	42.6259790449	42.6613876442	42.7382135211	42.8701734412	43.1082763967	43.1421393808	43.1967178879	43.2867958284	43.4400571656	43.7099575841	44.1203075469
286	42.6063473959	42.6405855137	42.7148616360	42.8424130229	43.1047836521	43.1374918901	43.1901837036	43.2770831905	43.4248838251	43.6849547816	44.1159745572
287	42.5873650122	42.6204734361	42.6922690225	42.8155871893	43.1014098529	43.1330048945	43.1838788555	43.2677476976	43.4102637460	43.6608834094	44.1118061018
288	42.5690092578	42.6010272777	42.6704682574	42.7896627501	42.9815072453	43.1286725431	43.1777948426	43.2587307162	43.3961756101	43.6377067924	44.1077964283
289	42.5512583282	42.5822237945	42.6493729346	42.7646077577	42.9500215449	43.1244892096	43.1719234970	43.2500346802	43.3825989662	43.6153897804	44.1039388678
290	42.5340912184	42.5640405973	42.6289776254	42.7403914582	42.9196018576	43.1204941839	43.1662569692	43.2416475234	43.3695141935	43.5938986812	44.1002273214
291	42.5174876918	42.5464561187	42.6092578405	42.7169842444	42.8902101668	43.1165481632	43.1607877155	43.2335576581	43.3569024654	43.5732011966	44.0965594825
292	42.5014282505	42.5294495811	42.5901899931	42.6943576106	42.8618096501	43.1127802432	43.1555084856	43.2257539557	43.3447457163	43.5532663622	43.9321915443
293	42.4859941074	42.5130009669	42.5717513646	42.6726841099	42.8343652219	43.1091409106	43.1504123099	43.2182257270	43.3330266087	43.5340648886	43.8991158151
294	42.4710671585	42.4970909883	42.5539200700	42.6513373121	42.8078428794	43.1056255354	43.1454924868	43.2109627044	43.3217285021	43.5155671063	43.8672809628
295	42.4563299569	42.4817010602	42.5366750264	42.6308917647	42.7822099500	43.1022296630	43.1407425813	43.2039550236	43.3108354242	43.4977469132	43.8366378076
296	42.4422656877	42.4668132727	42.5199959220	42.6111229544	42.7574349814	43.0989400790	43.1361563943	43.1971932079	43.3003320417	43.4805777236	43.8071392268
297	42.4286581439	42.4524103655	42.5038631860	42.5920072706	42.7334876935	43.0957944658	43.1317279729	43.1906681513	43.2902036340	43.4640340202	43.7787400638
298	42.4154917031	42.4384757028	42.4882579604	42.5735219707	42.7103389325	43.0927701103	43.1274515907	43.1843711037	43.2804360672	43.4480929086	43.7513970421
299	42.4027513956	42.4249932500	42.4731620728	42.5556541464	42.6879606266	43.0897701103	43.1233217404	43.1782936560	43.2710157692	43.4327300727	43.7250686824
300	42.3904224336	42.4119475505	42.4585580100	42.5383556910	42.6663257439	42.8689838638	43.1193331249	43.1724277263	43.2619297067	43.4179237333	43.6997152242

In general, for a given argument, this formula was used to calculate two of the functions, with orders differing by unity, and the recursion formula

$$K_{n+1}(z) = K_{n-1}(z) + \frac{2n}{z} K_n(z) \tag{3}$$

was then used to compute the other orders required.

For half-integral orders, the series in equation (2) is exact, and no difficulty arose in the calculation of the corresponding tables. For integral orders the terms of the series eventually diverge; and in order to cope with this, three separate ranges of the argument were considered as follows:

(i) $z \geqslant 10$

In this range the computer calculated $K_0(z)$ and $K_1(z)$ and built up the other orders using equation (3). The asymptotic series was summed up to the point where the terms began to diverge, and the series was then rounded off by adding to the sum one half of the first divergent term. Within its range this approximation gave almost 12-figure accuracy in the results.

(ii) $3.6 \leqslant z < 10$

Over this range a method due to Dingle (1958*a*, 1959) was employed to calculate a more accurate converging factor than the crude value 0.5 used in the first range of z. Generally, in this method, the asymptotic series is allowed to run on for a number of terms beyond the first divergent one, and is cut off after p terms, where p depends upon the values of n and z in $K_n(z)$. The converging factor Σ_t, which is applied to the last term calculated, may be written

$$\Sigma_t = \sum_{t=0}^{\infty} \frac{\Gamma(n+\frac{1}{2})\Gamma(n+p+\frac{1}{2}-t)}{\Gamma(n+\frac{1}{2}-t)\Gamma(n+p+\frac{1}{2})} (-2z)^t \Lambda^{(t)}_{p-n-\frac{1}{2}}(2z) \tag{4}$$

where the $\Lambda^{(t)}_{p-n-\frac{1}{2}}$ are defined in the form

$$\Lambda^{(t)}_s(s+\theta) = \sum_{r=t}^{\infty} \sum_{q=0}^{r-t} a_{t,r} s^{-r} b_{t,r,q} \theta^q. \tag{5}$$

The numerical factors $a_{t,r}$ and $b_{t,r,q}$ are given by Dingle (1958*b*, 1959) up to terms in $t = 3$.* Values of p and θ were found from the relationship

$$p - n - \tfrac{1}{2} = s \tag{6}$$

$$2z = s + \theta \tag{7}$$

where in accordance with the derivation of equation (5), θ is restricted to small values; $|\theta| < 0.5$. Since p and n must be integers, s was chosen to be the half-integer nearest to $2z$; p was then obtained from equation (6). Because the series for the converging factor is itself asymptotic, it was necessary to insert into the computer program a test which was arranged to cut off Σ_t correctly at its least term. For this range of z, the best results were obtained by calculating $K_2(z)$ and $K_3(z)$ and using the recursion formula to obtain the

*In the calculation of the tables, the expressions in equations (4) and (5) were used up to terms in $t = 4$ and a minor error in Dingle's expression for $\Lambda^{(1)}_s$ was corrected.

other orders. Above $z = 5$ the method gave results accurate to at least 11 figures; but from this point down to $z = 3.6$ the accuracy fell off steadily. In the region $z = 3.6$–4.5 the error in the tables may amount to ± 1 unit in the 10th figure.

(iii) $0 < z < 3.6$

This is the only range in which a method independent of equation (2) was used to calculate the Bessel functions. The method is adequately described by Aldis (1899) and will not be repeated here; it makes use of series which occur in the calculation of the modified Bessel functions of the first kind. In this range $K_0(z)$ and $K_1(z)$ were calculated as a basis for the application of equation (3). The accuracy of the method is limited essentially by the fact that the two basic $K_n(z)$ are derived as the differences of other series each of which could only be calculated on the computer to a limited number of figures. Once again in the region of $z = 3.6$ the absolute value of the error in $K_n(z)$ may approach one unit in the 10th place; on going to lower values of z, however, the accuracy improves until, in the region of $z = 0.1$, 12-figure accuracy is obtained.

In order to estimate the limits of the various ranges of the argument, and to decide the magnitude of the errors within the ranges, sets of values of $K_0(z)$ and $K_1(z)$ were computed by the various methods described above, for values of z increasing by 0.1 in the range $0 < z \leqslant 6$, and by 1.0 in the range $6 \leqslant z \leqslant 12$; these were compared with a table of more accurate values of $K_0(z)$ and $K_1(z)$ over the same range, given by Aldis (1899). These computations served also to compare Dingle's method of calculating the converging factor for the asymptotic series with a simpler method due to Burnett (1930); this work forms the basis of a separate note (Dempsey and Benson, unpublished).

ACKNOWLEDGMENT

We wish to thank Dr. D. C. Baxter, of the Analysis and Computation Group of the Division of Mechanical Engineering, N.R.C., for the preparation of a rounding program used in the calculations.

REFERENCES

ALDIS, W. S. 1899. Proc. Roy. Soc. (London), A, **64**, 203.
BENSON, G. C., BALK, P., and WHITE, P. 1959. J. Chem. Phys. **31**, 109.
BENSON, G. C., DEMPSEY, E., and BALK, P. Unpublished.
BURNETT, D. 1930. Proc. Cambridge Phil. Soc. **26**, 145.
DEMPSEY, E. and BENSON, G. C. Unpublished.
DINGLE, R. B. 1958*a*. Proc. Roy. Soc. (London), A, **244**, 456.
——— 1958*b*. Proc. Roy. Soc. (London), A, **244**, 476.
——— 1959. Proc. Roy. Soc. (London), A, **249**, 270.
DURHAM, G. S. and SODERBERG, B. A. 1958. J. Chem. Phys. **28**, 1201.
HARTMAN, P. 1956. Acta Cryst. **9**, 569.
VAN DER HOFF, B. M. E. and BENSON, G. C. 1953. Can. J. Phys. **31**, 1087.
HOVE, J. and KRUMHANSL, J. A. 1953. Phys. Rev. **92**, 569.
LENNARD-JONES, J. E. and DENT, B. M. 1928. Trans. Faraday Soc. **24**, 92.
MADELUNG, E. 1918. Physik. Z. **19**, 524.
SCHREIBER, H. P. and BENSON, G. C. 1955. Can. J. Phys. **33**, 534.
SHUTTLEWORTH, R. 1949. Proc. Phys. Soc. (London), A, **62**, 167.
WATSON, G. N. 1948. A treatise on the theory of Bessel functions, 2nd ed. (Cambridge University Press, London), p. 78.
VAN ZEGGEREN, F. and BENSON, G. C. 1957. J. Chem. Phys. **26**, 1077.

AN ANALYSIS OF SOME STATISTICAL PROPERTIES OF AURORAL RADAR REFLECTIONS AND THEIR RELATIONSHIPS TO THE DETECTION CAPABILITIES OF THE RADAR[1]

A. G. McNAMARA

ABSTRACT

A statistical model of auroral echo occurrence has been made from an analysis of observations at 48.5 Mc/s obtained over a number of years of continuous operation. The probability density distribution of auroral target cross sections (σ) has been examined experimentally, and the resulting curve fitted by simple mathematical relations. Both an inverse power law and an exponential law have been derived, of the forms

$$p(\sigma)d\sigma = k\sigma^{-1.67}d\sigma$$

and

$$p(\sigma)d\sigma = \frac{1}{\sigma_m} e^{-\sigma/\sigma m}d\sigma.$$

These models have been interpreted in terms of distributed and localized targets, and used to analyze the echo occurrence indices and the effect which variation of radar parameters will have upon them. Both forms of the target law are useful although it is considered that the exponential form yields better agreement with observations over a wider range of the variables.

1. INTRODUCTION

A previous paper (McNamara 1958) has given the details of an auroral radar designed for continuous unattended monitoring of radar echoes from aurora. Two complementary forms of record are obtained from the radar and are scaled to give measures of echo occurrence. This paper examines the parameters involved in the design of equipment for auroral detection, and their relationship to the performance, echoes obtained, range distribution, scaling procedure, and indices derived from the data.

2. A RADAR EQUATION FOR AURORAL ECHOES

For the jth single elementary target, of small dimensions, the received power at time t_0 is given by (Kerr 1951)

$$P_{rj} = \frac{p(R_j)G_tG_r\lambda^2F_t^2(\theta,\phi)F_r^2(\theta,\phi)A(\theta,\phi)\sigma_j}{64\pi^3R_j^4} \tag{1}$$

where t, r refer to the transmitting and receiving parameters respectively and

$p(R_j)$ = a function proportional to the magnitude of the Poynting vector of the incident wave at R at such time that the reflected signal from the scatterer returns to the receiver at the instant t_0 under consideration,

G = power gain of the antenna over an isotropic radiator,

λ = radio-frequency wavelength,

[1]Manuscript received October 7, 1959.
Contribution from the Division of Radio and Electrical Engineering, National Research Council, Ottawa, Canada.
Issued as N.R.C. No. 5559.

$F(\theta,\phi)$ = pattern propagation factor of the field strength,
$= f(\theta,\phi) \cdot g(\theta)$,
$f(\theta,\phi)$ = antenna pattern function expressing the relative free space field strength in the direction specified by elevation and azimuth angles θ and ϕ,
$g(\theta)$ = interference function, between the direct and ground-reflected rays, giving the field strength in the specified elevation relative to the maximum field strength in free space,
σ_j = equivalent backscattering area of the elementary target,
R = range to the target,
$A_j(\theta,\phi)$ = the aspect function of the target cross section, giving the factor by which the effective target area is reduced when the target is located in the direction θ,ϕ.

From a consideration of the characteristics of auroral echoes, the actual targets are thought to be represented by a number of scatterers which scatter in a non-coherent manner relative to each other. The received power is the arithmetic sum of the powers from individual scatterers, and is averaged over a short period of time (the integration time of the eye, the camera viewing the cathode ray tube, or other recording device). Observations (Currie, Forsyth, and Vawter 1953; McNamara and Currie 1954; Unwin and Gadsden 1957) also indicate that the auroral echoing region is a relatively thin layer, over which the elementary targets will be considered to be distributed.

For non-isotropically scattering targets, the returned signal is modified by an 'aspect attenuation' function which is dependent upon the angle of incidence of the radiation on asymmetrical targets and hence upon the geometry of the radar case. The aspect function will be denoted by $A(\psi)$ where ψ is the angle of intersection with the major axis of the target, which is assumed to have axial symmetry about the earth's magnetic field, and by $A(\theta,\phi)$ relative to the radar. At a constant height of reflection, the aspect function can be expressed in terms of range and azimuth from the radar by the function $A(R,\phi)$, or along a specified beam direction by $A(R)$.

Radar observations at 50 Mc/s show that echoes can be received at angles deviating by as much as 15° from orthogonality to the magnetic field. Hence the length of field-aligned concentrations generally will not be greater than several tens of meters if such a beam width is to be observed in the scattering pattern of the target. This dimension is much less than a Fresnel zone and the range dependence of the scattered power from such elementary targets will still be as R^{-4} as in equation (1).

The horizontal distribution of targets may now be classified under the two conditions:

Case (*i*): The scattering region completely fills the azimuthal beam width.

Case (*ii*): The scattering region is more localized in space, occupying only a fraction of the azimuthal beam width.

In both cases the extent in range of the scattering region will be assumed to be appreciable, i.e., greater than the pulse lengths commonly employed.

The scatterers are considered independent and the received power, averaged over many pulse periods, is the sum of the average powers from each contributing scatterer.

For case (*i*), the density function $n(R,\phi,\bar{\sigma})RdRd\phi d\bar{\sigma}$ is now introduced. This is the number of scatterers per unit area of cross section $\bar{\sigma}$ to $\bar{\sigma}+d\bar{\sigma}$. If the scatterers are uniformly distributed horizontally, then the density function separates in the integration yielding

$$\int_0^\infty \bar{\sigma} n(\bar{\sigma}) d\bar{\sigma} \equiv \sigma m^2/m^2,$$

the average cross section per unit area of the ionosphere. Hence the signal-to-noise ratio is

$$\frac{P_r}{P_n} = \frac{G_t G_r \lambda^2 \sigma}{64\pi^3 k T_e B} \int_0^\infty \int_{-\pi}^{\pi} F_t^2(\theta,\phi) F_r^2(\theta,\phi) A(\theta,\phi) d\phi \frac{p(R)}{R^3} dR. \tag{2}$$

Now a "beam width" Φ may be defined by

$$\int_{-\pi}^{\pi} F_t^2(\theta,\phi) F_r^2(\theta,\phi) A(\theta,\phi) d\phi = \Phi F_t^2(\theta,0) F_r^2(\theta,0) A(\theta,0). \tag{3}$$

Within the next integral, $p(R)$ is non-zero only over a short interval roughly equivalent to the pulse length. Over this small interval the other factors in the integrand are substantially constant and may be moved outside the integral. There remains

$$\int_0^\infty p(R) dR = P_t \cdot \frac{\tau c}{2} \tag{4}$$

where the definition is in terms of the conventional values

P_t = peak power transmitted,
τ = pulse duration,
c = velocity of propagation of the electromagnetic energy.

Also

P_n = total noise power referred to the receiver input terminals,
$= kT_e B$,
k = Boltzmann's constant,
T_e = effective absolute temperature of the source, including the effects of system noise, atmospheric noise, and cosmic noise,
B = noise bandwidth of the receiver.

Collecting all the parts

$$\frac{P_r}{P_n} = \frac{P_t G_t G_r \lambda^2}{64\pi^3 k T_e B} \frac{\tau c}{2} \Phi \frac{F_t^2(\theta,0) F_r^2(\theta,0) A(\theta,0)}{R^3} \sigma. \tag{5}$$

Turning now to case (*ii*) and starting with equation (1), the ensemble of scatterers may be replaced by equivalent scatterers of time and azimuthal average cross section $\sigma(m^2/m)$ located at the centers of the active region.

$$\frac{P_r}{P_n} = \frac{P_t G_t G_r \lambda^2}{64\pi^3 k T_e B} \frac{\tau c}{2} \frac{F_t^2(\theta,\phi) F_r^2(\theta,\phi) A(\theta,\phi)}{R^4} \cdot \sigma. \tag{6}$$

Since we shall be interested in following the long-term variations of σ through P_r, we shall introduce the approximation that the propagation patterns and aspect factor are broad and flat in the azimuthal direction and cut off sharply beyond some critical azimuth. Then for a fixed broad beam radar, equation (6) reduces to the approximate form

$$\frac{P_r}{P_n} = \frac{P_t G_t G_r \lambda^2}{64\pi^3 k T_e B} \frac{\tau c}{2} \frac{F_t^2(\theta,0) F_r^2(\theta,0) F(\theta,0)}{R^4} \sigma. \tag{7}$$

This formulation will also be applicable to a rotating narrow beam.

Other factors being constant, it will be noted that the signal-to-noise ratio is proportional to $P_t\tau/B$ where the factor τ arises from spatial integration of the distributed target by the pulse length. For optimum signal-to-noise in the receiver, the bandwidth should be approximately equal to the inverse of the pulse length and the signal-to-noise ratio becomes proportional to $P_t\tau^2$. Hence peak power may be traded for narrow bandwidth and a large high-power radar may be replaced by a compact, reliable, low-power equipment. As an example, for a completely distributed target, a 1-kilowatt 300-μsec pulse radar can approach the detection sensitivity of a 100-kilowatt 30-μsec pulse radar.

For any given radar the received power sensitivity is determined by the antenna system through a fourth-degree propagation pattern. Since in practice all propagation patterns, both for horizontal and vertical polarization, have a null at zero degrees elevation, the detection of echoes at low elevation is sharply dependent on F and hence on antenna height. If antenna height is made too great, however, nulls in the pattern may appear at important echo elevations.

3. DEFINITIONS AND INDICES OF ECHO OCCURRENCE

The most complete and detailed description of echo occurrence conveniently obtainable from a range–time recording with a fixed beam radar is obtained by a method whereby the range–time record is searched in units which are one equivalent pulse length of range ($\tau c/2$) by one unit of time, and an occurrence is defined if an auroral echo is detectable in this cell. These can also be grouped under either the range intervals or time to obtain statistics on variation of occurrence with range or percentage time of occurrence of echoes respectively. The latter quantity, the occurrence of any auroral signal at any range in a unit time interval, is advantageous in that it applies uniformly to any equivalent pulse or continuous wave system and it is much more quickly read from the film record. Moreover, this index can also be obtained directly and immediately from the chart record produced by the signal integrator (McNamara 1958). The integrator also yields another index which is a measure of intensity of the disturbance. For daily measures the area under the trace of the time variation of signal amplitude, integrated over all ranges, may be scaled. On the daily basis, plots of the experimental data of percentage occurrence and integrated area, both derived from the integrator charts, show a fairly well-defined statistical relation between the two indices, although these indices, on occasion, may be expected to differ considerably. The relationship

is demonstrated in Fig. 1, where 423 daily points from the period 4 April 1956 to 31 May 1957 have been used. The data is well fitted by the parabola (solid line) of Fig. 1. The dashed lines give the values of the first-order standard deviations.

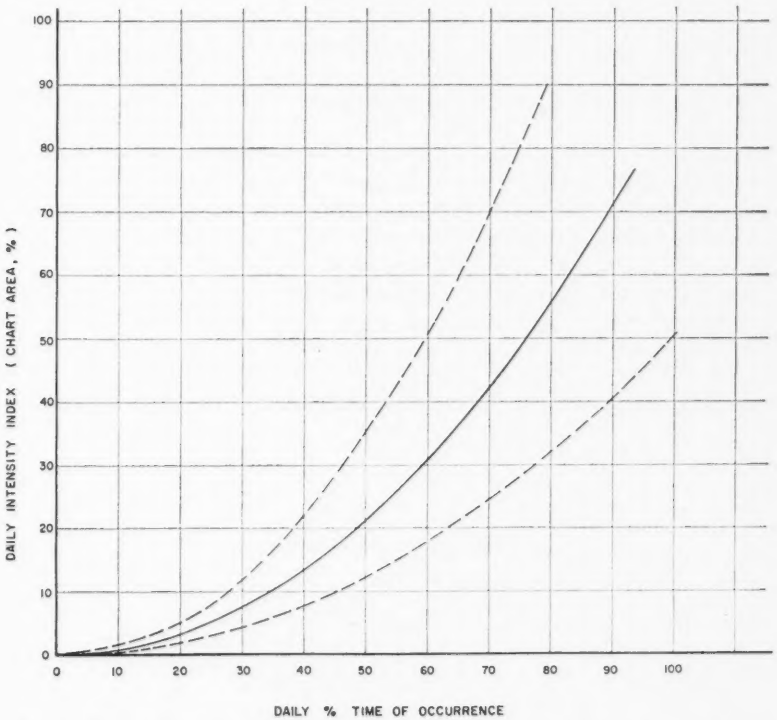

FIG. 1. The statistical relationship between 423 daily indices of echo intensity and duration of occurrence. The solid line is the line of best fit and the dashed lines are the first-order standard deviations.

4. DERIVATION OF ECHO OCCURRENCE FORMULAS

As discussed in Section 2, observations indicate that the auroral echoing region is a relatively thin layer over which we will consider the long-term unit-area target cross-section probability density function to be given by $p(\sigma)$ where $p(\sigma)$ is defined as

$$p(\sigma) = \frac{\left(\begin{array}{c}\text{number of time units in which a target occurs} \\ \text{with cross section between } \sigma \text{ and } \sigma+\Delta\sigma\end{array}\right) \Big/ \Delta\sigma}{(\text{total number of time units} = n)} \tag{8}$$

$$\Delta\sigma \to 0,$$

$$n \to \infty.$$

It will be implicitly assumed here that the probability density function is independent of the geographical position over the ionosphere. This is at least reasonable over the limited region viewed by a radar. Geographical variations in the frequency of occurrence are accounted for by a multiplicative factor $N(R,\phi)$, which represents the average rate of occurrence of all targets per unit area of the ionosphere. Therefore, the number of targets observable per unit area over an extended period of time is proportional to

$$N(R,\phi)\cdot\int_{\sigma_L}^{\infty}p(\sigma)d\sigma \tag{9}$$

where σ_L is the limiting cross section for threshold detection on the radar.

For the geometry of a thin auroral echoing layer at height h over a curved earth, it may be shown that the occurrence of targets in a range interval R_1 to R_2 is approximated closely for case (*i*) by

$$D=\int_{R_1}^{R_2}\int_{\sigma_L}^{\infty}\left(\frac{1+(h/\rho)}{\cos\alpha}\right)N(R,\phi)p(\sigma)d\sigma dR\approx\int_{R_1}^{R_2}N(R,\phi)dR\int_{\sigma_L}^{\infty}p(\sigma)d\sigma \tag{10}$$

and for case (*ii*) by

$$D=\int_{R_1}^{R_2}\int_{\sigma_L}^{\infty}\left(\frac{1+(h/\rho)}{\cos\alpha}\right)N(R,\phi)p(\sigma)Rd\sigma dR\approx\int_{R_1}^{R_2}N(R,\phi)RdR\int_{\sigma_L}^{\infty}p(\sigma)d\sigma \tag{11}$$

where ρ = radius of the earth,

α = angle subtended at the center of the earth by the arc from the radar to the subtarget point,

and $(h/\rho)\ll 1$, $\cos\alpha\approx 1$ for ranges at which echoes occur.

From this point onward, we shall only carry out the development of case (*ii*). Case (*i*) is then obtainable from any of the case (*ii*) equations by deleting the multiplicative R factor and by changing the R^{-4} to an R^{-3}.

The minimum detectable signal is taken to be a constant given by $P_{r_{min}}/P_n = 1/b$. (In practice, a nominal threshold value of $b = 1$ is often used.)

From equation (7)

$$\frac{1}{\sigma_L}=\frac{bP_tG_tG_r\lambda^2}{kT_eB}\cdot\frac{F_t^2(\theta,0)F_r^2(\theta,0)}{64\pi^3R^4}\cdot\frac{\tau c}{2}\,\Phi A(\theta,0). \tag{12}$$

But

$$\int_{\sigma_L}^{\infty}p(\sigma)d\sigma=f\{\sigma_L\}\text{ since the integral goes to zero at the upper limit} \tag{13a}$$

$$=f\left\{\frac{1}{b}\cdot\frac{kT_eB}{P_tG_tG_r\lambda^2}\cdot\frac{64\pi^3R^4}{F_t^2(\theta,0)F_r^2(\theta,0)}\cdot\frac{2}{\tau c}\cdot\frac{1}{\Phi A(\theta,0)}\right\} \tag{13b}$$

and therefore

$$D=\int_{R_1}^{R_2}f\{\sigma_L\}\cdot N(R,\phi)\cdot R\cdot dR. \tag{14}$$

To predict the range distribution, small range segments are taken. If the range segments are all equal and sufficiently small, then by the mean value theorem the range distribution D' is well represented by the integrand

$$D' = f\{\sigma_L\} \cdot N(R,\phi) \cdot R. \tag{15}$$

The term which is most uncertain is $f\{\sigma_L\}$ due to the aspect factor A contained within it. In principle it should be possible to plot the distribution D' by setting $A = 1$ and estimating values of N from other sources, and by using the difference between this curve and the observed range distribution to derive the aspect function A.

From radar observations, the aspect factor appears to be tolerant of small departures from normality but falls rapidly with increasing departures producing a rather sharp cutoff of echo occurrence at some minimum range. Theoretical derivations of an aspect function have been made by several authors on the bases of definite scattering models, and these could be substituted in the above relations. However, for determination of certain statistical properties of total echo occurrence no assumptions need be made of a physical model, and a simple linear approximation can be used to represent the attenuation. For illustrative purposes, A will be represented here by the ramp-like function

$$\begin{aligned} A(R) &= 0 && R < R_0, \\ &= \frac{R-R_0}{R_1-R_0} && R_0 < R < R_1, \\ &= 1 && R > R_1. \end{aligned} \tag{16}$$

The cutoff range R_0 and the 'full-signal' range R_1 are suitably chosen with reference to the observed range distribution or by examination of the aspect angle ψ (for example, Figs. 4 or 3 of McNamara 1958). Although this results in inaccuracies in range distribution near the cutoff, the integral or total occurrence is not greatly in error if R_0 or R_1 are well selected.

The function $N(R)$ expressing the true geographical variation of mean auroral occurrence is not well established at present. It is necessary to know the zenithal occurrence at each point. Again, we shall make a simplification by setting $N(R) = 1$.

5. EXPERIMENTAL AND THEORETICAL PROBABILITY DENSITY FUNCTIONS FOR TARGET CROSS SECTIONS

The law which governs the distribution of target size is required to specify the nature of the function $f\{\sigma_L\}$ used in the preceding section. To this end, calibration of the over-all receiving–recording system was made with a random noise generator on the receiver input since this type of signal is most representative of auroral signals. The recording characteristic was thus established as nearly linear with noise power input, and hence linear with echo cross section σ. Echo data were derived from 469 days of consecutive operation, 1 January 1957 to 14 April 1958. The function scaled was actually the inte-

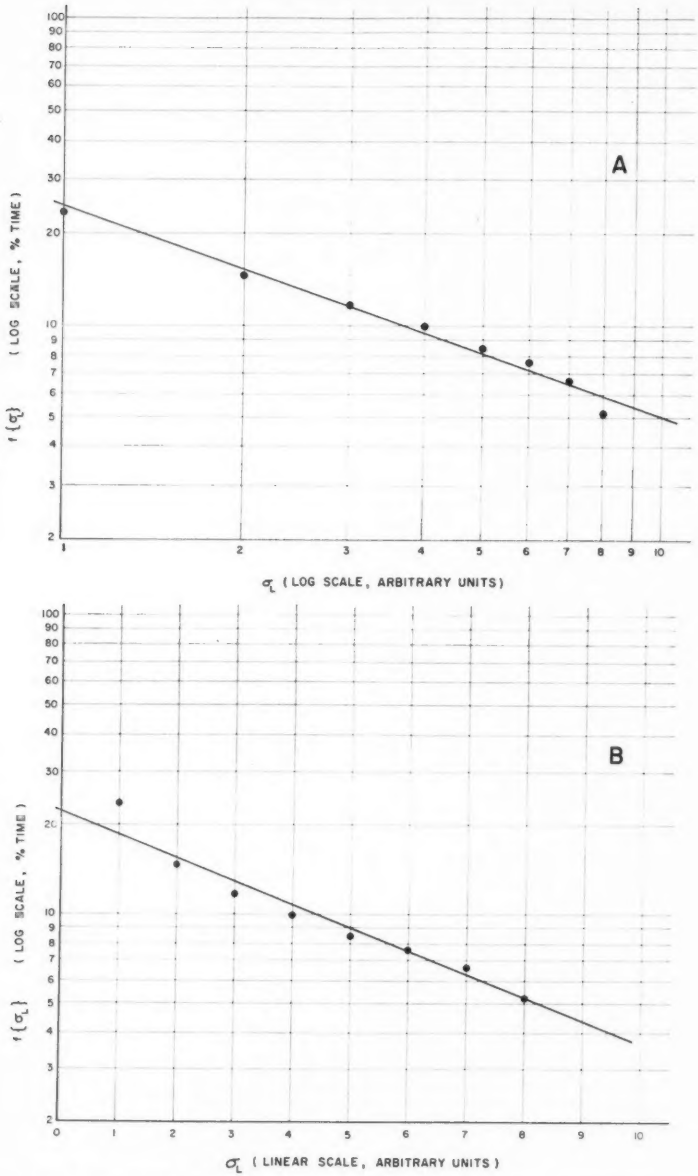

FIGS. 2A and 2B. Experimentally derived target cross-section distributions fitted to a power law (A) and to an exponential law (B); Fig. 2A yields the slope $m-1 = 0.68$ and Fig. 2B yields the mean cross section $\sigma_m = 5.3$.

grated probability density, $f\{\sigma_L\}$, defined by equation (13*a*). This was obtained by determining the time that the signal level was above a series of selected levels on the chart.

Mathematical description of the cross-section distribution was obtained by fitting simple expressions to the data. Figures 2A and 2B show the results of assuming an inverse power law and an exponential law. Reasonably good fits are obtained over the dynamic recording range for both forms. In the following the consequences of both approximations will be examined. Further discussion of the applicability of the laws will then be given.

(*a*) The inverse power law:

$$p(\sigma)d\sigma = \frac{K}{\sigma^m}d\sigma. \tag{17}$$

Hence

$$\int_{\sigma_L}^{\infty} p(\sigma)d\sigma = \frac{K'}{\sigma_L^{m-1}} \equiv f\{\sigma_L\} \qquad \text{provided } m > 1 \tag{18}$$

and

$$D' = \left\{\frac{K'}{(\sigma_L)^{m-1}}\right\} \cdot R \cdot N(R) \tag{19a}$$

$$= K''\left\{b\frac{P_t G_t G_r \lambda^2}{kT_e B}\frac{F_t^2 \cdot F_r^2}{64\pi^3 R^4}\frac{\tau c}{2}\Phi A\right\}^{m-1} \cdot R \cdot N. \tag{19b}$$

(*b*) The exponential law:

$$p(\sigma)d\sigma = \frac{1}{\sigma_m} e^{-\sigma/\sigma_m} d\sigma \tag{20}$$

where σ_m = mean cross section. Hence

$$\int_{\sigma_L}^{\infty} p(\sigma)d\sigma = e^{-\sigma_L/\sigma_m} \equiv f\{\sigma_L\} \tag{21}$$

and

$$D' = e^{-\sigma_L/\sigma_m} \cdot R \cdot N(R) \tag{22a}$$

$$= \left\{\exp -\left[\frac{1}{b\sigma_m}\frac{kT_e B}{P_t G_t G_r \lambda^2}\frac{64\pi^3 R^4}{F_t^2 F_r^2}\frac{2}{\tau c}\frac{1}{\Phi A}\right]\right\} \cdot R \cdot N. \tag{22b}$$

The slope of the best-fitting straight line in Fig. 2A yields the value of $m-1$. From several selected periods, the quantity $m-1$ is found to lie in the region 0.5 to 0.9, and a representative value of 0.67 will be adopted. This result, $m = 1.67$, is consistent with earlier work by the author (McNamara 1954) at Saskatoon where the value $m = 1.5$ was obtained using a much different method of analysis on data obtained from a high-power short-pulse radar at 56 Mc/s. In the present instance, additional checks were also made by shorter periods of operation with simultaneous recordings of 50-km gate length

covering the interval 700–750 km and the standard 800-km gate length covering 300–1100 km. The distributions obtained over the period 1 December 1958 to 30 January 1959 with short and long gates are shown in Fig. 3. The close correspondence of the slopes of the two curves supports the validity of the application of the long-gate statistics to the general analysis. A further check on the exponent was made using a logarithmic receiver recording a 30-db range of signal, yielding the value of $m = 1.5$.

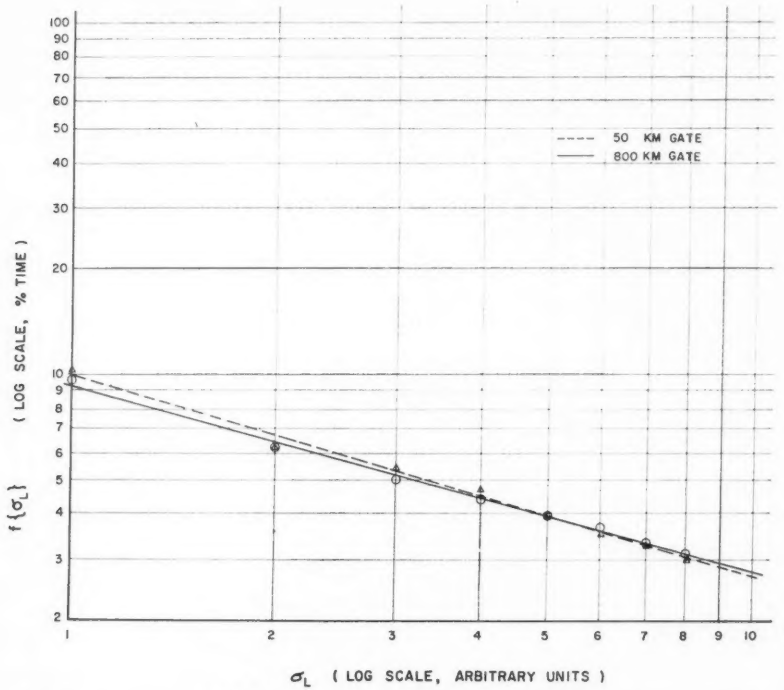

FIG. 3. Comparison of cross-section distributions obtained from simultaneous operation of narrow and wide gates centered at a range of 700 km. The slopes $m-1$ of the lines are 0.58 and 0.53 respectively.

Equation 19 or 22 may thus be taken as giving the variation of echo occurrence with range, and giving a measure of the functional dependence of occurrence rate on the geometry, equipment parameters, and antenna patterns. Plots of equations 19 and 22 for two different combinations of antenna heights are shown in Fig. 5, corresponding to case (*ii*). Modification of equations 19 and 22, by deleting the multiplicative R factor and changing the R^{-4} to R^{-3}, results in equations appropriate to case (*i*). These are plotted in Fig. 4. For all sample calculations the values $N(R) = 1$, $R_0 = 300$ km, $R_1 = 500$ km were used. In each figure, the A curves correspond to the

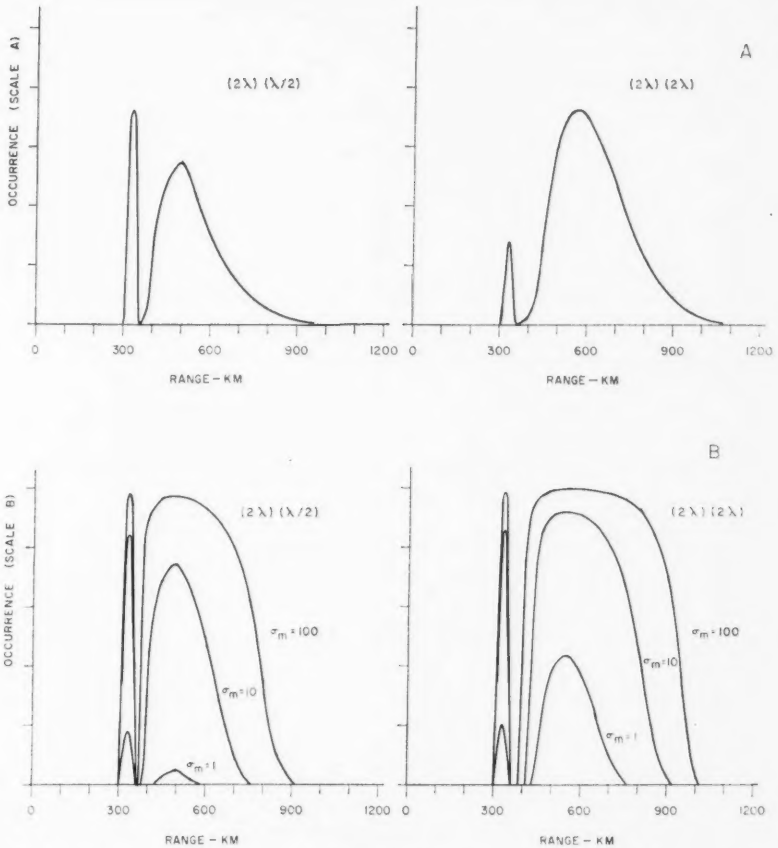

FIG. 4. Theoretical echo range distributions for two radar systems differing only in the heights of their transmitting–receiving antenna configurations above the ground. Calculations are based on the assumptions of completely distributed targets, and for a power law (A) and an exponential law (B) of target cross sections.

inverse power law distribution of target cross sections, and the *B* curves correspond to the exponential law.

For the inverse power law, the shape of the echo distribution is independent of the radar sensitivity factors, the vertical scale varying as the 0.67 power of the sensitivity. For the exponential law, the shape as well as the vertical scale varies with the sensitivity, and also with the mean of the target cross section distribution.

As indicated in Tables I and II both forms yield distributions and occurrences not unlike the observational data, provided an appropriate choice is made for σ_m in the exponential law. Additional data from a (2λ) (λ/2) system

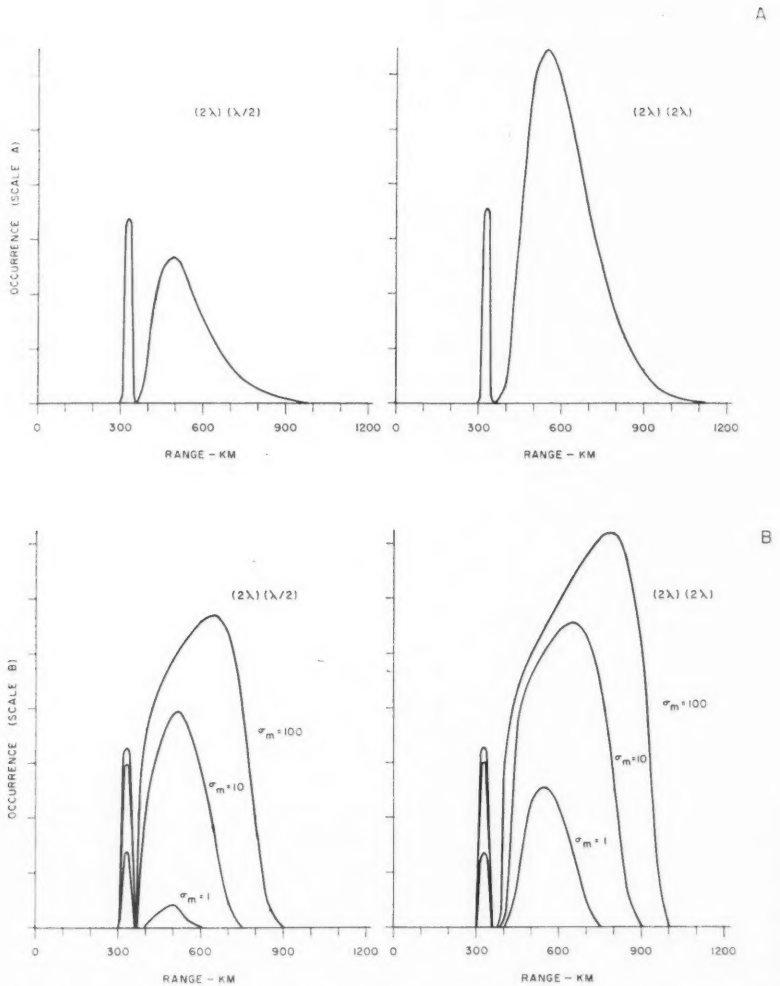

FIG. 5. Theoretical echo range distributions for two radar systems differing only in the heights of their transmitting–receiving antenna configurations above the ground. Calculations are based on the assumptions of localized targets, and for a power law (A) and an exponential law (B) of target cross sections.

TABLE I

Echo occurrences derived from Fig. 4 for the case of completely distributed targets (case (*i*))*

Relative mean target cross section	Area under curve*			Peak value of first lobe*		
	(2λ) $(\lambda/2)$ configuration	Ratio →	(2λ) (2λ) configuration	(2λ) $(\lambda/2)$ configuration	Ratio →	(2λ) (2λ) configuration
			A. Power law for cross section			
	100	2.9	290	100	2.6	260
			B. Exponential law for cross section			
$\sigma_m = 1$	3.7	14	52	6.7	10	67
$\sigma_m = 10$	100	2.2	220	100	1.5	150
$\sigma_m = 100$	240	1.5	360	150	1.3	200

*Normalized to the value 100 for the reference configuration (A) (2λ) $(\lambda/2)$, (B) (2λ) $(\lambda/2)$ with $\sigma_m = 10$.

TABLE II

Echo occurrences derived from Fig. 5 for the case of localized targets (case (*ii*))*

Relative mean target cross section	Area under curve*			Peak value of first lobe*		
	(2λ) $(\lambda/2)$ configuration	Ratio →	(2λ) (2λ) configuration	(2λ) $(\lambda/2)$ configuration	Ratio →	(2λ) (2λ) configuration
			A. Power law for cross section			
	100	2.4	240	100	2.4	240
			B. Exponential law for cross section			
$\sigma_m = 1$	9.1	5.7	52	11	6	66
$\sigma_m = 10$	100	1.8	180	100	1.4	140
$\sigma_m = 100$	210	1.6	330	150	1.2	180

*Normalized to the value 100 for the reference configuration (A) (2λ) $(\lambda/2)$, (B) (2λ) $(\lambda/2)$ with $\sigma_m = 10$.

with a 20-db variability in sensitivity suggests that the exponential law can be fitted more accurately over a larger dynamic range. Mathematically, the exponential law may be more convenient since all its moments are finite and it can be normalized. On the other hand, the inverse power formulation may often be convenient for comparison of system parameters since no assumptions nor measurements need be made concerning the magnitude of the cross-section scale.

It should be noted that although the equations contain a radio wavelength term (λ^2), they do not give the frequency dependence of the echo occurrence. The λ^2 term arises from the conversion of effective area of receiving antenna into antenna gain; the true wavelength dependence of the echoes is hidden in the cross-section term, σ, and is not considered in this paper.

6. INTEGRATED ECHO OCCURRENCE

The formulas of the preceding section were developed in terms of the detailed echo occurrence defined by the range and time division discussed in Section 3. Also of interest, is the description of occurrence in terms of time alone, any echo or echoes present at a given time satisfying the definition of an occurrence. The formulas may be used as a guide in deriving these indices but cannot be confidently applied because of the unknown correlation of echo occurrence in space and time. In fact, the geographical correlation distance of

target occurrence is often large and the probability of echo occurrence in adjacent range increments is not independent. If the echoes in each range increment were statistically independent in time, the range-integrated echo probability would be proportional to the area under the D' curve.

This may be seen from the following argument. Assume that echoes in adjacent range increments occur independently in time and let the probability that range increment i will have an echo be D'_i, and the probability that all increments will simultaneously fail to have an echo is $\Pi_{i=1}^{n}(1-D'_i)$. Our definition of an echo occurrence on a purely time basis is that at least one increment does contain an echo. This probability is $1-\Pi_{i=1}^{n}(1-D'_i)$, which, for small probabilities, $D_i \ll 1$, may be expanded

$$1-\prod_{i}^{n}(1-D'_i) = 1-(1-\Sigma D'_i+\text{higher-order terms}) \approx \Sigma D'_i.$$

This is simply the area under the distribution curve of equations 19 and 22, for which examples are plotted in Figs. 4 and 5. The areas under these curves are tabulated in Tables I and II and may be taken as an approximation to the relative amount of echo which will be observed.

7. NUMERICAL EXAMPLES

In Tables I and II, corresponding to cases (*i*) and (*ii*) of distributed and localized targets, are given the areas under the curves and the heights of the peak of the main lobe. The tabulated values have been normalized to 100 for the reference configuration (2λ) $(\lambda/2)$ with $\sigma_m = 10$. It should be noted that the computations were made on the basis of a uniform occurrence of targets all over the ionosphere, $N(R,\phi) = 1$.

Experimentally, for two such radar systems operating simultaneously at Ottawa over a period of 2 years, the occurrence ratio was found to be 2.5 to 1. Although no allowance has been made for small system gain differences, nor for the naturally increasing occurrence of aurora with range toward the auroral zone, the agreement with the tabular values is satisfactory.

CONCLUSION

Expressions have been derived relating the radar parameters to the auroral echo statistics observed. For this to be done, it was necessary to adopt practical definitions of 'echo occurrences' and to interpret the appropriate activity indices. The sensitivity of the indices is demonstrated by equations 19 and 22 and Figs. 4 and 5, and indicates the necessity for caution in the comparison of indices from different systems and the need for accuracy in determination and stabilization of the radar parameters.

REFERENCES

CURRIE, B. W., FORSYTH, P. A., and VAWTER, F. E. 1953. J. Geophys. Research, **58**, 179.
KERR, D. E. 1951. Propagation of short radio waves, M.I.T. Radiation Laboratory Series, Vol. 13.
MCNAMARA, A. G. 1954. Ph.D. Thesis, University of Saskatchewan, Saskatoon, Saskatchewan.
——— 1958. Can. J. Phys. **36**, 1.
MCNAMARA, A. G. and CURRIE, B. W. 1954. J. Geophys. Research, **59**, 279.
UNWIN, R. S. and GADSDEN, M. 1957. Nature, **180**, 1469.

LIQUID–SOLID INTERFACE SHAPE OBSERVED IN SILICON CRYSTALS GROWN BY THE CZOCHRALSKI METHOD[1]

W. D. Edwards

ABSTRACT

A study has been made of the macroscopic structure of the liquid–solid interface which exists during growth of silicon crystals by the Czochralski method. In two crystals the interface was seen to contain a (111) facet. The development of such facets is discussed with reference to current crystal growth theories.

INTRODUCTION

The shape and structure of the liquid–solid interface during growth of silicon single crystals is of great importance and has been discussed by a number of authors (Cressell and Powell 1957; Rosi 1958; and Tiller 1958). For example, Cressell (1957) and Rosi (1958) have observed that an interface which is planar or slightly convex towards the liquid leads to crystals with a minimum dislocation density. In this laboratory interfaces have been observed which are parallel, over macroscopic distances, to the (111) planes lying normal to the growth direction.

The interface shape may be observed in a number of ways. It may be viewed directly by rapidly separating the growing crystal from the melt during growth (Elbaum and Chalmers 1955). The possibility that liquid adhering to the crystal will solidify after decantation and the fact that the interface shape is observed at one position only are the limitations of this method. A second method of revealing interface shape requires the addition of volatile impurities to a melt under vacuum from which a crystal is being grown by the Czochralski technique. For example, a silicon crystal grown from a melt containing boron as an impurity will be *P*-type, but when an excess of antimony is added to the melt the growing crystal becomes *N*-type. Under vacuum, antimony evaporates rapidly compared with boron and the growing silicon crystal reverts to *P*-type (Bradshaw and Mlavsky 1956). The grown crystal may be sectioned longitudinally, i.e. parallel to the growth axis, ground and etched to reveal the *P*–*N* and *N*–*P* junctions. The interface shape at the time of the addition of the antimony is shown by the shape of the *P*–*N* junction. In this way the interface shape at a number of times during the growth of the crystal may be studied. Rate-grown junctions (Tanenbaum *et al.* 1955) may also be used to give a continuous record of the interface shape during crystal growth. However, this method imposes stringent conditions on the growth rate of the crystal and on the impurities added to the melt.

The most useful and convenient method of interface examination makes use of the variations in crystal composition which occur during growth. Unless special precautions are taken during growth, Czochralski-type silicon crystals

[1]Manuscript received October 7, 1959.
Contribution from the Electronics Laboratory, Defence Research Telecommunications Establishment, Defence Research Board, Montreal Road, Ottawa, Ontario.

exhibit variations in resistivity and oxygen content both radially and longitudinally. The longitudinal variations are closely related to the rotation rate and in many instances their period equals the growth per revolution of the crystal. If a crystal is cut longitudinally and if the exposed face is ground and etched these variations or striations are revealed as corrugations on the surface. The striations give a revolution-by-revolution macroscopic picture of the interface shape during crystal growth. Striations with a separation of 0.001 cm have been resolved. In a variation of this method Camp (1954) has used a copper-plating technique to delineate resistivity striations in germanium and has successfully resolved striations with a separation of just less than 1 mm.

EXPERIMENTAL

Six crystals were examined; these were grown by the Czochralski method with the solid–liquid interface convex towards the liquid. Each crystal was cut longitudinally and then the newly exposed faces were ground and etched as described in the Appendix. The corrugations produced on the flat surface by the etch had a separation equal to the growth per revolution of the crystal and a curvature as expected for an interface which was convex towards the liquid.

Two crystals examined had two distinct breaks in each of the striations and the sections of the striations between the breaks were straight lines (Figs. 1*a* and 1*b*). Typical straight line sections were 0.45 cm long on striations with a radius of curvature of 2.5 cm. Near to the top of the crystal, as shown in Fig. 1*a*, the reduced radius of curvature of the interface restricted the development of these 'flats' on the interface and caused an increase in the change of direction at the breaks in the striations to an observed maximum of $7\frac{1}{2}°$. These straight line sections of the striations were observed to be perpendicular to the [111] direction which was near to the growth axis of the crystal. Each of the two crystals was cut again to bisect the straight line striations and to reveal a second face normal to the original section. These second faces were also ground and etched in order to reveal the striations. The two flat faces of each crystal were masked with 'Halo' wax and the remaining crystal surface was etched in hot caustic soda which is a structure-sensitive etch for silicon. An optical goniometer was used to show that the (111) planes approximately normal to the axis of growth would give traces in the two sectioned faces parallel to the straight line sections of the striations.

The growth axis of one crystal was 4.5° from the [111] direction and this angle is shown as θ in Fig. 1*a*. The growth and rotation rates of this crystal were 8.4×10^{-4} cm/sec and 4.6 r.p.m., respectively, which gave a striation separation of 1.1×10^{-2} cm. The crystal was *P*-type with a resistivity of approximately 0.4 ohm-cm. The exact growth conditions of the second crystal* are not known. This second crystal was *N*-type with a resistivity of approxi-

*Kindly donated by D.R.B. to Northern Electric Co. Ltd.

FIG. 1*a*. The form of the striations seen after etching a section of a silicon crystal which had been cut parallel to the [111] growth axis. The lines x and y indicate the extent of the (111) flats.

FIG. 1*b*. Photograph of the striations taken at the approximate position of the inset marked near the top left corner of Fig. 1*a*.

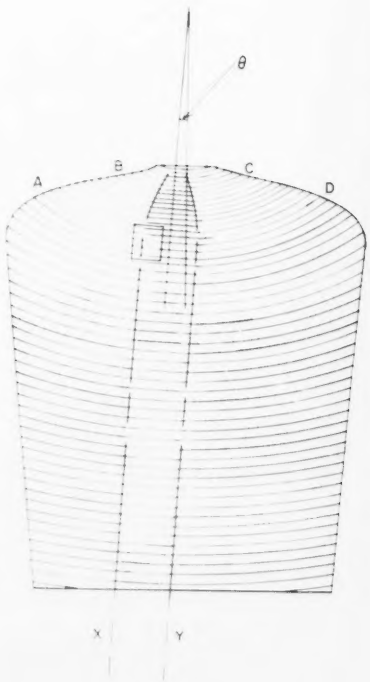

FIG. 1*a*.

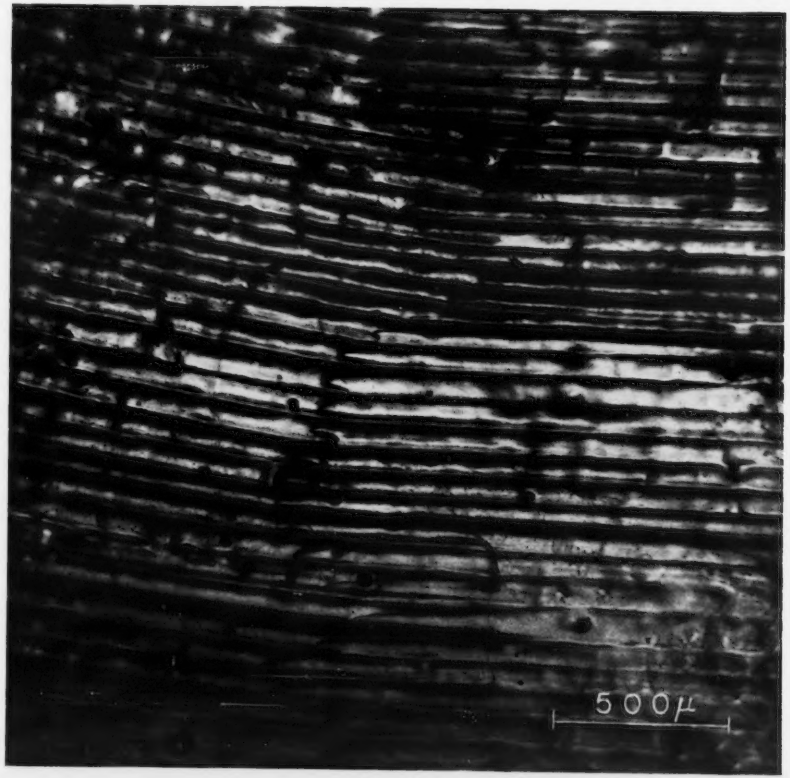

FIG. 1*b*.

mately 20 ohm-cm and the growth axis was 4° from the [111] direction. The striation separation varied between 0.001 cm and 0.01 cm.

On this second crystal it was observed that where the diameter was increasing rapidly, i.e. in the sections *AB* and *CD* (Fig. 1*a*), the striations abruptly changed direction within approximately 0.1 mm from the edge of the section (Fig. 2). These were probably traces of other {111} planes but unfortunately poor masking of the sample led to their loss during etching and before measurements were made.

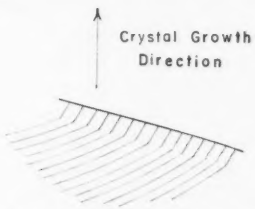

FIG. 2. An enlarged drawing of the crystal-section edge in the region *CD* of Fig. 1*a*. The abrupt change in striation direction near to the surface is indicated.

DISCUSSION

With crystals grown by the Czochralski method the {111} planes often give rise to facets on the crystal (Billig 1955). Crystals pulled in the ⟨111⟩ direction have three such facets spaced symmetrically around the circumference of the crystal; the fourth {111} plane which is normal to the growth direction lies approximately parallel to the liquid–solid interface. The {111} planes are the most closely packed in the silicon structure. Growth in a direction normal to these planes is slow because of the low accommodation coefficient (Chalmers 1954) whereas growth by lateral extension of the {111} planes is preferred (Tiller 1958; Billig 1955). The preferred directions of lateral growth in the (111) plane are the $[2\bar{1}\bar{1}]$, $[\bar{1}2\bar{1}]$, and $[\bar{1}\bar{1}2]$ directions (Billig 1955) which give rise to the three symmetrically placed spikes commonly observed when a crystal is pulled in the [111] direction.

It is the (111) set of planes lying perpendicular to the growth axis of a [111] crystal which has been detected on a macroscopic scale by the etching experiments and which normally does not give rise to any visual characteristics of a crystal. In two crystals the interface was found to be limited over macroscopic distances by the densely packed (111) planes which are approximately normal to the growth axis.

The temperature gradient existing at the interface during crystal growth can be estimated only approximately. Calculations made by Billig (1955, 1956) are inapplicable because the considerable radiation received by the ingot from the adjacent melt and susceptor is ignored; this leads to values of temperature gradient which are much too high. With growth from a crucible the temperature gradient decreases as crystal growth proceeds. Observations made with a pyrometer, at pertinent times during crystal growth, indicated a temperature drop of 150° C in the first centimeter from the liquid–solid interface. If it is assumed that

(*a*) the gradient actually existing at the interface is 150°/cm,
(*b*) the curved portions of the liquid–solid interface are coincident with the freezing point isotherm, and
(*c*) the liquid–solid interface has an approximately constant radius of curvature,

then in the two crystals considered there is approximately 1.5° C of supercooling at the center of the (111) flats.

Nucleation of (111) planes will occur at this point. With an interface slightly convex towards the liquid these (111) planes will grow outwards in a stepwise manner (Tiller 1958; Elbaum and Chalmers 1955) to the limiting diameter of the crystal. If the interface is appreciably curved, as in Fig. 1*a*, the completion of a (111) layer will take several revolutions of the growing crystal. However, if the interface is concave towards the liquid there is the possibility of nucleation at several points around the interface periphery. With nucleation at the periphery the (111) planes grow inwards in a stepwise manner to completion. At the interface periphery there is a liquid–gas and a liquid–solid interface. Twinning and heterogeneous nucleation are likely to occur here, possibly because the lattice spacing is not quite normal in the last few atomic layers near to the solid–gas interface and also because of the presence of minute particles of oxide or other impurity, for example, silicon carbide if a carbon susceptor and heater are used. The growth of strays and twins into the main body of the crystal is thus encouraged by the concave interface and this has been discussed by Chalmers (1953) and Bolling *et al.* (1956).

In conclusion, lattice misfits and twinning are more likely to occur if (111) planes nucleate at the crystal periphery and grow inwards rather than if nucleation occurs near the crystal center with growth outwards to completion as is the case with an interface which is slightly convex to the melt. Results have been given which suggest that the (111) planes normal to the crystal growth axis do play an important role in the growth mechanism. In equilibrium the interface will be composed of {111} planes as they have the lowest accommodation coefficient and equilibrium temperature. Consequently, an interface limited by the (111) plane normal to the growth axis is most likely to occur in crystals which are pulled slowly from a melt in which the temperature gradients are small. This picture of crystal growth, which especially applies to the two instances cited, is in agreement with the observations of Cressell and Powell (1957), Rosi (1958), Bolling *et al.* (1956), and Billig (1956) that the least twinning, lineage, and the lowest density of dislocations occur when the interface is planar or slightly convex towards the liquid during crystal growth.

APPENDIX

The etching of silicon by a mixed nitric acid–hydrofluoric acid etch is basically a two-step process. The HNO_3 oxidizes the silicon and the HF dissolves the oxide re-exposing the silicon surface to the action of the HNO_3 (Robbins and Schwartz 1959). The oxidation is the structure-sensitive step and suitable control of the HNO_3 content leads to maximum information regarding the structure and composition of the silicon.

For the delineation of striations the sample surfaces to be studied were first ground and then chemically polished in a mixture of 3 parts HNO_3 (70%) and 1 part HF (48%). The sample was then placed in 40 cc of HF (48%) and approximately 0.03 cc (one drop) of HNO_3 (70%) was added to the solution every 30 seconds for a total time of from 5 to 15 minutes. Illumination of the specimen during the etching process greatly enhanced the delineation of the striations. The rate of addition of drops and time of etch were not critical and the most suitable conditions for silicon of a given resistivity were experimentally determined. A slow oxidation step appeared to be essential and if the sample was immersed in a comparable HNO_3–HF mixture a fast reaction took place with evolution of considerable heat and very poor, if any, delineation of striations.

REFERENCES

BILLIG, E. 1955. Proc. Roy. Soc. **229**, 346.
——— 1956. Proc. Roy. Soc. **235**, 37.
BOLLING, G. F., TILLER, W. A., and RUTTER, J. W. 1956. Can. J. Phys. **34**, 234.
BRADSHAW, S. E. and MLAVSKY, A. I. 1956. J. Electronics, **2**, 134.
CAMP, P. R. 1954. J. Appl. Phys. **25**, 459.
CHALMERS, B. 1953. Can. J. Phys. **31**, 132.
——— 1954. Trans. AIME, **200**, 519.
CRESSELL, L. G. and POWELL, J. A. 1957. Progress in Semiconductors, **2**, 139.
ELBAUM, C. and CHALMERS, B. 1955. Can. J. Phys. **33**, 196.
ROBBINS, H. and SCHWARTZ, B. 1959. J. Electrochem. Soc. **106**, 505.
ROSI, F. D. 1958. R. C. A. Rev. **19**, 349.
TANENBAUM, M., VALDES, L. B., BUEHLER, E., and HANNAY, N. B. 1955. J. Appl. Phys. **26**, 686.
TILLER, W. A. 1958. J. Appl. Phys. **29**, 611.

AN EMISSION SYSTEM OF THE IO MOLECULE[1]

R. A. DURIE,[2] F. LEGAY,[3] AND D. A. RAMSAY

ABSTRACT

The "methyl iodide flame bands", lying in the region 4100 to 6300 Å, have been photographed using a 21-ft concave grating spectrograph. The bands are shown to arise from an $A^2\Pi \rightarrow X^2\Pi$ transition of the IO molecule. Rotational and vibrational analysis of the bands has been carried out and the molecular constants of IO obtained.

INTRODUCTION

A number of red-degraded bands, now known as the "methyl iodide flame bands", was first observed by Vaidya (1937) in emission from a flame of methyl iodide mixed with methyl alcohol or coal gas. The bands were analyzed into two systems, A and B, and were tentatively assigned to the IO or CI molecule. Coleman, Gaydon, and Vaidya (1948) obtained the bands in emission from an oxyhydrogen flame to which iodine was added, thus supporting the assignment to IO. These authors observed approximately 40 bands in the region 4100 to 6300 Å and showed that all the bands could be arranged into one system instead of two. Vibrational constants were given but no rotational analysis was attempted since the bands were observed only with low resolution.

Durie and Ramsay (1958) observed six bands of the same system in absorption during the flash photolysis of mixtures of iodine vapor and oxygen. The bands were observed with high resolution but no rotational analysis of the absorption bands was attempted since the same bands, extending to much higher J values, were also observed in emission from an oxyhydrogen flame to which methyl iodide was added. Most of the bands reported by Coleman, Gaydon, and Vaidya were rephotographed under high resolution by Durie and Ramsay. The rotational and vibrational analysis of these bands forms the main subject of the present paper and confirms the assignment of the bands to the IO molecule.

EXPERIMENTAL

The source used to excite the methyl iodide flame bands consisted of a diffusion flame of hydrogen, saturated with methyl iodide vapor at room temperature, burning in an atmosphere of oxygen. The bands were photographed using the second order of a 21-ft concave grating spectrograph and Eastman Kodak 103a0, 103aD, 103aB, and 103aF plates. The exposure times varied from 1 to 5 hours. An iron arc was used to provide a reference spectrum.

[1]Manuscript received December 10, 1959.
Contribution from the Division of Pure Physics, National Research Council, Ottawa, Canada.
Issued as N.R.C. No. 5554.

[2]N.R.C. Postdoctorate Fellow 1955. Present address: C.S.I.R.O. Coal Research Section, Sydney, Australia.
[3]N.R.C. Postdoctorate Fellow 1959. Present address: Laboratoire d'Infrarouge, 12 rue Cuvier, Paris V, France.

PLATE I

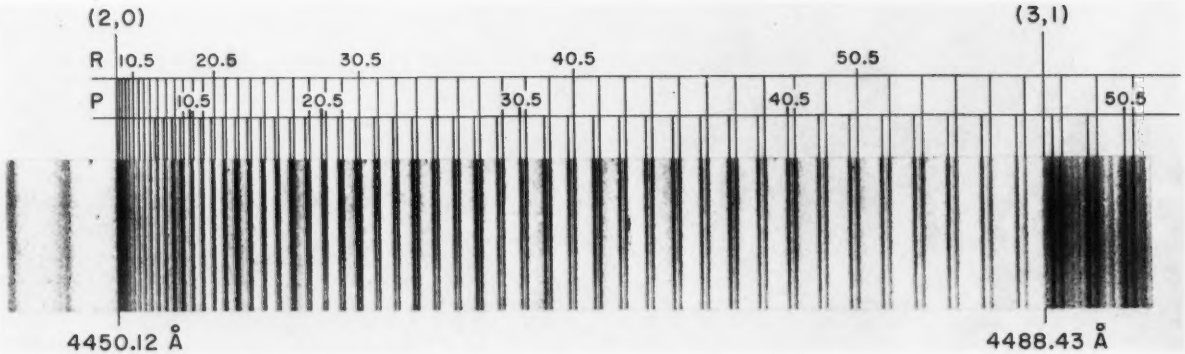

FIG. 1. Enlargement of the (2,0) band of IO showing the assignments of the rotational lines.

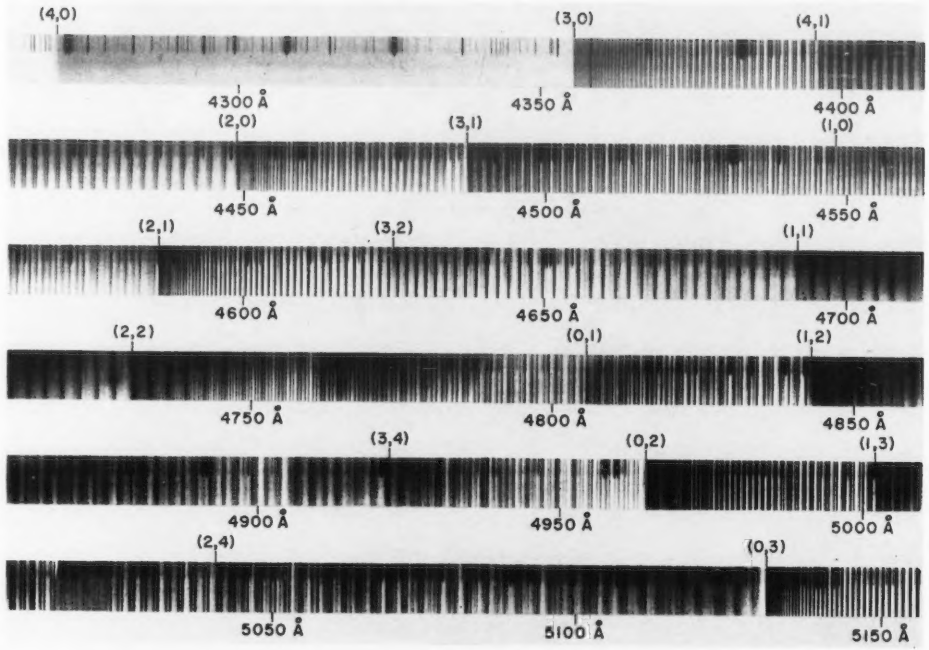
(4,0)
(3,0)
(4,1)
4300 Å
4350 Å
4400 Å
(2,0)
(3,1)
(1,0)
4450 Å
4500 Å
4550 Å
(2,1)
(3,2)
(1,1)
4600 Å
4650 Å
4700 Å
(2,2)
(0,1)
(1,2)
4750 Å
4800 Å
4850 Å
(3,4)
(0,2)
(1,3)
4900 Å
4950 Å
5000 Å
(2,4)
(0,3)
5050 Å
5100 Å
5150 Å

FIG. 2

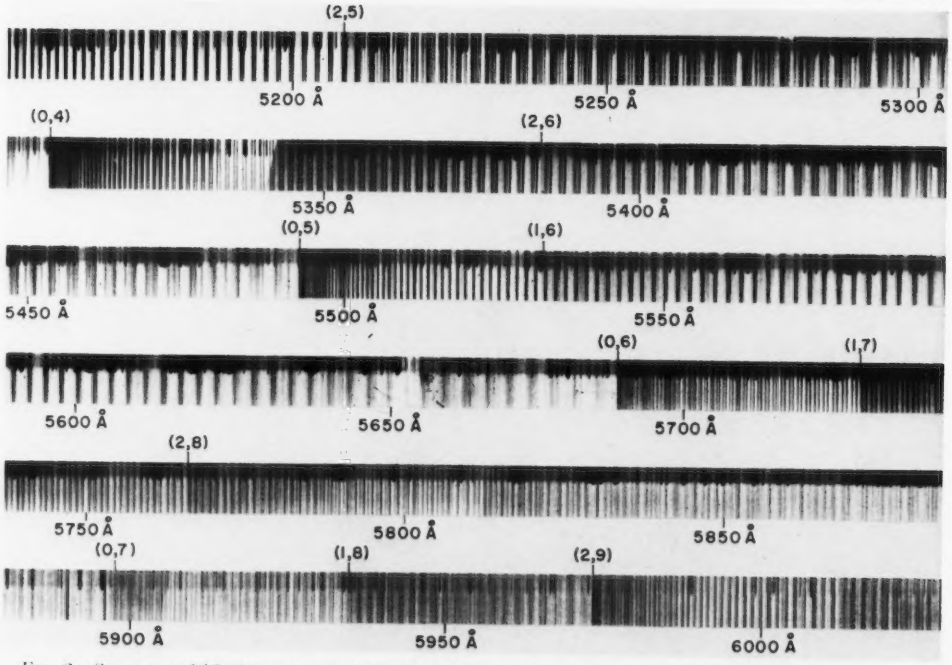

FIG. 2. Spectrum of IO observed in emission from an oxyhydrogen flame to which methyl iodide was added. The bands were photographed using the second order of a 21-ft concave grating spectrograph. (The discontinuities near 5020, 5340, and 5650 Å are due to plate joins.)

A reproduction of the spectrum is given in Fig. 2; an enlargement showing the rotational structure of one of the bands and the rotational assignments is given in Fig. 1. It may be seen from Fig. 2 that many of the bands have discrete and well-resolved rotational structures while others are completely diffuse or show a distinct broadening of the rotational lines. The presence of diffuseness in certain bands is due to predissociation in the excited state. Using the vibrational assignments of Coleman, Gaydon, and Vaidya we find that bands with $v' = 1, 4$, and 5 are completely diffuse, bands with $v' = 3$ have rotational lines which are slightly broader than the slit width, while bands with $v' = 0$ and 2 have rotational lines which are sharp. These different types of rotational structure may be seen (Fig. 2) by comparing the rotational structures of the (4,0), (3,0), and (2,0) bands.

Wavelength measurements were carried out using a comparator equipped with a photoelectric scanning device of the type described by Tomkins and Fred (1951). Standard wavelengths were taken from the M.I.T. wavelength tables (Harrison 1939) and were combined with the vacuum corrections of Edlén (1953). The rotational lines of eight bands were measured and the vacuum wavenumbers and assignments are given in Table I. The wavelengths of the sharp band heads are given in Table II; the band head measurements of Coleman, Gaydon, and Vaidya are also given. Both sets of measurements are compared with the wavelengths of the band heads calculated from our final molecular constants.

ANALYSIS

The electronic transition responsible for the IO bands is expected to be of the type $^2\Pi_i(a)$–$^2\Pi_i(a)$ by analogy with the known transitions for ClO and BrO (Durie and Ramsay 1958). For Hund's case (*a*) coupling, each band splits into two well-defined subbands, viz. $^2\Pi_{3/2}$–$^2\Pi_{3/2}$ and $^2\Pi_{\frac{1}{2}}$–$^2\Pi_{\frac{1}{2}}$, and each subband consists predominantly of a single P and R branch and a very weak Q branch. For IO, the discrete bands show single P and R branches but no Q branches were detected. Moreover, for each band, only one of the subbands was observed, presumably due to a large spin splitting in the upper state. This is not surprising in view of the large doublet splitting in the ground state of the iodine atom, viz. 7598 cm^{-1}. It has been assumed that the observed subbands are of the type $^2\Pi_{3/2}$–$^2\Pi_{3/2}$ although it should be pointed out that it was not possible to verify this assumption by observation of the P and R branches to the lowest J values.

The various molecular constants were determined by the following standard procedures (Herzberg 1950).

1. Determination of B_v and D_v

The rotational constants B_v and D_v were obtained from the combination differences $\Delta_2F'(J) = R(J) - P(J)$ and $\Delta_2F''(J) = R(J-1) - P(J+1)$ by plotting $\Delta_2F/(J+\frac{1}{2})$ against $(J+\frac{1}{2})^2$. The values of B and D for $v' = 0$ and 2 and $v'' = 0$ and 2 were obtained using data from more than one band. These values are considered to be more accurate than those obtained for the other vibrational levels and are given in Table III. The other B and D values were refined in the manner described in Sections 2 and 3.

TABLE I

Vacuum wavenumbers and rotational assignments for the $^2\Pi_{3/2}$–$^2\Pi_{3/2}$ subbands of IO

	(0,2)		(2,2)		(2,0)		(3,0)	
J	$R(J)$	$P(J)$	$R(J)$	$P(J)$	$R(J)$	$P(J)$	$R(J)$	$P(J)$
2.5								
3.5				21130.25				
4.5				129.10				
5.5				127.88				
6.5		20130.74	21134.09	126.49	22470.76			
7.5		129.27	133.65	125.00	470.24			
8.5	20137.65	127.74	133.09	123.38	469.64	22459.86		
9.5	137.03	126.10	132.46	121.64	468.87	458.02	22951.26	
10.5	136.46	124.22	131.63	119.77	467.95	456.05	948.86	22937.25
11.5	135.56	122.40	130.72	117.77	466.89	453.93	947.77	935.10
12.5	134.67	120.34	129.67	115.63	465.71	451.66	946.46	932.69
13.5	133.59	118.26	128.48	113.38	464.39	449.26	944.99	930.27
14.5	132.45	115.98	127.18	110.99	462.92	446.71	943.49	927.52
15.5	131.14	113.62	125.74	108.46	461.32	444.04	941.83	924.85
16.5	129.83	111.15	124.16	105.85	459.57	441.22	939.96	921.86
17.5	128.32	108.57	122.49	103.07	457.70	438.27	—	918.80
18.5	126.74	105.88	120.69	100.18	455.67	435.18	935.84	915.64
19.5	124.98	103.02	118.72	097.16	453.52	431.95	933.55	912.27
20.5	123.15	100.07	116.66	094.02	451.21	428.58	931.15	908.81
21.5	121.17	097.00	114.46	090.73	448.80	425.07	928.57	905.17
22.5	119.08	093.83	112.15	087.34	446.24	421.43	925.83	901.40
23.5	116.91	090.53	109.68	083.81	443.51	417.65	922.98	897.46
24.5	114.57	087.15	107.11	080.16	440.66	413.73	919.99	893.36
25.5	112.13	083.61	104.40	076.40	437.66	409.66	916.87	889.21
26.5	109.60	079.99	101.55	072.47	434.55	405.46	913.58	884.87
27.5	106.90	076.22	098.60	068.44	431.29	401.14	910.11	880.34
28.5	104.11	072.34	095.51	064.27	427.89	396.66	906.57	875.70
29.5	101.23	068.32	092.29	059.98	424.36	392.05	902.85	870.93
30.5	098.23	064.19	088.95	055.56	420.67	387.30	898.97	866.00
31.5	095.09	059.98	085.48	051.03	416.86	382.41	894.94	860.92
32.5	091.78	055.66	081.87	046.35	412.91	377.38	890.78	855.71
33.5	088.42	051.17	078.15	041.55	408.81	372.22	886.49	850.32
34.5	084.97	046.59	074.30	036.63	404.58	366.93	882.03	844.85
35.5	081.32	041.88	070.31	031.57	400.21	361.49	877.44	839.18
36.5	077.62	037.05	066.19	026.41	395.71	355.90	872.71	833.38
37.5	073.79	032.15	061.96	021.11	391.06	350.20	867.81	827.45
38.5	069.83	027.12	057.60	015.67	386.27	344.35	862.77	821.35
39.5	065.73	021.95	053.09	010.11	381.34	338.50	857.60	815.13
40.5	061.56	016.69	048.48	004.42	376.29	332.24	852.27	808.76
41.5	057.27	011.28	043.70	20998.60	371.08	325.98	846.81	802.25
42.5	052.83	005.76	038.86	992.69	365.74	319.56	841.20	795.57
43.5	048.29	000.16	033.86	986.61	360.26	313.03	835.43	788.76
44.5	043.64	19994.38	028.73	980.41	354.65	306.35	829.50	781.77
45.5	038.86	988.56	023.46	974.07	348.90	299.53	823.45	774.69
46.5	033.98	982.58	018.09	967.65	343.01	292.57	817.26	767.45
47.5	028.97	976.49	012.58	961.06	336.97	285.48	810.91	760.04
48.5	023.84	970.24	006.93	954.38	330.80	278.25	804.42	752.52
49.5	018.57	963.97	001.15	947.55	324.51	270.92*	797.79	744.82
50.5	013.26	957.50	20995.26	940.60	318.05	263.41*	791.00	737.00
51.5	007.77	950.99	989.26	933.50	311.47		784.05	729.02
52.5	002.24	944.30	983.09	926.35	304.73		776.97	720.90
53.5	19996.47	937.56	976.83	919.01	297.90		769.74	712.63
54.5	990.62	930.62	970.41	911.50	290.88		762.38	704.23
55.5	984.70	923.59	963.89	903.91	283.75		754.85	695.67
56.5	978.63	916.45	957.21	896.24	276.49*		747.17	686.95
57.5	972.46	909.16	950.44	888.40	269.05*		739.37	678.12
58.5	966.18	901.86	943.52	880.44	261.65*		731.40	669.12
59.5	959.74	894.42	936.48	872.34			723.26	659.97
60.5	953.22	886.60	929.32	864.12			715.01	650.66
61.5	946.58	879.01	922.00	855.78			706.59	641.23
62.5	939.81	871.21	914.56	847.29			698.04	631.63
63.5	932.95	863.26	907.04	838.72			689.34	621.90
64.5	925.95	855.24	899.36	830.05			680.47	612.03
65.5	918.85	847.02	891.55	821.23			671.45	601.99
66.5	911.70	838.68	883.49	812.16			662.30	591.83
67.5	904.21	830.37*	875.50	802.66*			653.00	581.50
68.5	896.81	822.00*	867.40	793.63*			643.56	570.99
69.5	889.25		859.03	784.16*			633.90	560.41
70.5	881.56		850.57				624.17	549.67
71.5	873.83		841.94				614.27	538.77
72.5	865.92		833.29				604.22	527.64
73.5	857.66		824.41				594.00	516.50
74.5	849.55		815.45				583.63	505.08
75.5	841.56		806.22				573.10	493.56
76.5	832.75		797.14*				562.47	481.97
77.5	824.57*		786.37*				551.67	470.34
78.5	815.43*						540.72	458.75
79.5							529.48	446.16
80.5							518.28	

*Denotes overlapped line.

TABLE I (*Concluded*)

Vacuum wavenumbers and rotational assignments for the $^2\Pi_{3/2}$–$^2\Pi_{3/2}$ subbands of IO

	(2,9)		(0,6)		(0,4)		(0,3)	
J	$R(J)$	$P(J)$	$R(J)$	$P(J)$	$R(J)$	$P(J)$	$R(J)$	$P(J)$
2.5								
3.5								
4.5								
5.5						18830.38		
6.5						829.09		
7.5		16727.65			18836.69	827.77		
8.5	16736.02	726.36			836.39	826.32	19482.54	19472.37*
9.5	735.76	724.97	17570.51	17559.21	835.74	824.79	481.92	470.75*
10.5	735.37	723.52	569.72	557.67	835.14	823.24	481.32	469.02*
11.5	734.91	721.97	569.18	556.06	834.54	821.35	480.56	467.18*
12.5	734.31	720.31	568.55	554.31	833.80	819.48	479.73	465.24*
13.5	733.70	718.60	567.82	552.39	832.87	817.52	478.78	463.20*
14.5	732.95	716.74	566.94	550.52	831.85	815.35	477.72	461.01*
15.5	732.07	714.86	566.17	548.45	830.78	813.24	476.53	458.72*
16.5	731.23	712.88	565.09	546.38	829.59	810.85	475.27	456.33*
17.5	730.18	710.80	564.06	544.16	828.25	808.51	473.89	453.83*
18.5	729.11	708.62	562.73	541.86	826.83	806.03	472.37*	451.21*
19.5	727.92	706.39	561.45	539.42	825.34	803.38	470.75*	448.63
20.5	726.68	704.05	560.05	536.94	823.69	800.64	469.02*	445.83
21.5	725.32	701.62	558.56	534.38	821.97	797.82	467.18*	442.86
22.5	723.87	699.10	556.97	531.73	820.16	794.90	465.24*	439.80
23.5	722.34	696.47	555.28	528.96	818.20	791.85	463.20*	436.63
24.5	720.73	693.82	553.56	526.05	816.14	788.73	461.01*	433.35
25.5	719.04	691.06	551.67	523.06	814.02	785.47	458.72*	429.97
26.5	717.24	688.18	549.71	520.06	811.77	782.09	456.33*	426.50
27.5	715.35	685.23	547.67	516.90	809.39	778.65	453.83*	422.87
28.5	713.38	682.16	545.47	513.66	806.94	775.08	451.21*	419.15
29.5	711.35	679.05	543.23	510.31	804.33	771.43	448.33	415.32
30.5	709.21	675.83	540.98	506.88	801.64	767.66	445.50	411.38
31.5	707.01	672.54	538.49	503.35	798.84	763.74	442.52	407.33
32.5	704.63	669.16	535.93	499.71	795.96	759.79	439.44	403.16
33.5	702.23	665.61	533.31	496.00	792.97	755.69	436.28	398.89
34.5	699.79	662.10	530.56	492.20	789.86	751.54	432.99	394.50
35.5	697.14	658.47	527.75	488.30	786.63	747.18	429.56	389.99
36.5	694.44	654.71	524.86	484.28	783.32	742.78	426.03	385.41
37.5	691.76	650.91	521.84	480.16	779.86	738.29	422.42	380.67
38.5	688.89	646.95	518.74	476.03	776.36	733.61	418.66	375.86
39.5	685.96	643.01	515.55	471.77	772.74	728.97	414.81	370.91
40.5	682.92	638.89	512.29	467.37	768.99	724.07	410.85	365.86
41.5	679.81	634.71	508.83	462.89	765.12	719.15	406.76	360.69
42.5	676.67	630.42	505.40	458.33	761.20	714.11	402.56	355.42
43.5	673.28	626.10	501.79	453.68	757.13	708.97	398.29	350.02
44.5	670.01	621.68*	498.13	448.94	752.97	703.69	393.86	344.54
45.5	666.53	617.19*	494.41	444.09	748.69	698.38	389.32	338.93
46.5	662.90	612.66*	490.54	439.13	744.33	692.97	384.69	333.22
47.5	659.41*	607.84*	486.60	434.11	739.81	687.32	379.94	327.38
48.5	655.60*	602.97*	482.60	428.97	735.23	681.69	375.10	321.44
49.5	651.65*	598.11*	478.40	423.78	730.57	675.89	370.11	315.40
50.5	647.94	593.17*	474.18	418.37	725.75	670.00	365.04	309.24
51.5	644.00*	588.22*	469.91	413.06	720.85	664.03	359.86	302.98
52.5	639.79*	583.00*	465.46	407.47	715.83	657.95	354.54	296.59
53.5	635.60	577.75*	460.92	401.96	710.67	651.76	349.12	290.12
54.5	631.44*		456.31	396.26	705.52	645.46	343.60	283.50
55.5			451.64	390.47	700.24	639.05	337.98	276.80
56.5	622.74*		446.85	384.64	694.71	632.56	332.22	269.77
57.5			441.90	378.66	689.21	625.93	326.34	263.06
58.5	613.48*		436.97	372.60	683.56	619.21	320.37	256.01
59.5	609.21*		431.86	366.44	677.82	612.38	314.30	248.85
60.5	604.26*		426.64	360.18	671.96	605.48	308.11	241.59
61.5			421.46	353.83	665.98	598.44	301.82	234.24
62.5			416.08	347.47	659.91	591.32	295.39	226.74
63.5	589.42*		410.63	340.98	653.75	584.07	288.87	219.16
64.5			405.12	334.40	647.46	576.74	282.21	211.45
65.5			399.45		641.09	569.28	275.49	203.64
66.5			393.72		634.60	561.72	268.63	
67.5			387.90		628.03	554.07	261.67	
68.5			381.78*		621.31	546.27	254.58	
69.5			375.82*		614.51	538.52*	247.40	
70.5			369.81*		607.60	530.54*	240.10	
71.5			363.63*		600.60	522.36*	232.69	
72.5			357.25		593.46	514.26*	225.17	
73.5			350.83*		586.28	505.93*	217.54	
74.5			344.53*		578.96	497.59*	209.82	
75.5			337.95*		571.54	489.11*	201.93	
76.5					564.06*	480.53*		
77.5					556.40*	471.81*		
78.5					548.48*	463.04*		
79.5					540.85*	454.15*		
80.5					532.83*	445.20*		
81.5					524.79*	436.06*		
82.5					516.47*	426.78*		
83.5					508.23*	417.55*		
84.5					499.74*			
85.5					491.49*			
86.5					482.85*			
87.5					474.16*			
88.5					465.44*			
89.5					456.36*			

*Denotes overlapped line.

TABLE II

Band heads and band origins for IO

		Band head, Å in air		λ_{Head} (obs. − calc.), Å	
(v', v'')	ν_0, cm^{-1}	Coleman, Gaydon, and Vaidya	Our measurements	Coleman, Gaydon, and Vaidya	Our measurements
(5,0)		4189.0		3.0	
(4,0)		4268.2*		0.1	
(3,0)	22951.52	4355.9	4355.59	0.3	0.05
(4,1)		4396.7		2.4	
(2,0)	22470.07	4448.7	4448.87	−0.2	0.02
(3,1)		4487.7	4487.17	0.6	0.10
(1,0)		4548.1		−0.5	
(2,1)		4586.7	4586.16	0.5	0.01
(3,2)		4624.9		0.0	
(4,3)		4668.3		3.5	
(1,1)		4693.5		1.3	
(2,2)	21133.11	4731.2	4730.29	1.0	0.01
(3,3)		4763.3		−6.2	
(0,1)		4806.1	4805.73†	0.4	0.02
(1,2)		4844.5		1.4	
(3,4)		4920.9	4921.36	−0.4	0.04
(0,2)	20137.11	4963.6	4964.23	−0.6	0.04
(1,3)		5002.3		0.4	
(2,4)		5049.8	5040.76†	9.0	0.00
(0,3)	19481.63	5131.0	5131.21	−0.1	0.05
(2,5)		5208.8	5208.52†	0.6	0.33
(3,6)		5248.7		0.3	
(0,4)	18835.25	5307.5	5307.27	0.2	0.02
(1,5)		5345		−0.3	
(2,6)		5385.5	5384.45	1.0	−0.01
(3,7)		5422		−2.8	
(0,5)		5495	5493.18	1.8	0.01
(1,6)		5533		1.8	
(4,9)		5655.5		3.4	
(0,6)	17569.10	5692	5689.67	2.3	0.01
(1,7)		5730		2.5	
(2,8)		5767	5766.35†	0.6	−0.06
(0,7)		5900		2.4	
(1,8)		5939		4.0	
(2,9)	16734.46	5976	5973.37	2.6	0.02
(1,9)		6152.5		−2.0	
(2,10)		6193	6192.18†	0.7	−0.22
(3,11)		6231.5		0.3	
(4,12)		6273		1.9	

*Coleman, Gaydon, and Vaidya quote 4286.2 Å which apparently is due to a misprint.
†Overlapped.

2. Determination of ν_0, $(B'-B'')$ and $(D'-D'')$

The band origins ν_0 were determined from the equation

$$(1) \qquad R(J-1)+P(J) = 2\nu_0+2(B'_v-B''_v)J^2-2(D'_v-D''_v)J^2(J^2+1)$$

by plotting $R(J-1)+P(J)-2(B'_v-B''_v)J^2$ against J^2, using approximate values of $(B'_v-B''_v)$, and extrapolating to $J = 0$. The values obtained are given in Table II. More accurate values for the differences $(B'_v-B''_v)$ and $(D'_v-D''_v)$ were next determined by plotting $[R(J-1)+P(J)-2\nu_0]/2J^2$ against (J^2+1). These values were then combined with the B and D values determined in Section 1, to obtain B and D values for the other vibrational levels. The rotational constants obtained in this manner are given in Table III.

TABLE III

Rotational constants for IO

A. Upper $^2\Pi_{3/2}$ state

v'	Bands	B_v, cm^{-1} (measured)	D_v, cm^{-1} (measured)	B_v, cm^{-1} (calculated)
0	(0,2) (0,3) (0,4) (0,6)	0.27491	0.33×10^{-6}	0.27498
2	(2,0) (2,2) (2,9)	0.26974	0.35	0.26952
3	(3,0)	0.26665	0.38	0.26679

B. Lower $^2\Pi_{3/2}$ state

v''	Bands	B_v, cm^{-1} (measured)	D_v, cm^{-1} (measured)	B_v, cm^{-1} (calculated)
0	(2,0) (3,0)	0.33890	0.36×10^{-6}	0.33891
2	(0,2) (2,2)	0.33347	0.36	0.33346
3	(0,3)	0.33068	0.36	0.33070
4	(0,4)	0.32794	0.36	0.32793
6	(0,6)	0.32234	0.36	0.32233
9	(2,9)	0.31377	0.37	0.31377

3. Determination of ΔG, $(B_{v_1}-B_{v_2})$, *and* $(D_{v_1}-D_{v_2})$

To provide a check on the molecular constants derived in Sections 1 and 2 the quantities ΔG, $(B_{v_1}-B_{v_2})$, and $(D_{v_1}-D_{v_2})$ were determined from the appropriate combination relations between corresponding lines of pairs of bands having one state in common (Herzberg 1950, p. 188). The evaluation of these quantities was carried out in two stages in a manner similar to that discussed in Section 2. First, approximate values of $(B_{v_1}-B_{v_2})$ were assumed and the data used to determine accurate values of ΔG. Second, these values of ΔG were combined with the experimental data to determine more accurate values for $(B_{v_1}-B_{v_2})$ and $(D_{v_1}-D_{v_2})$. The values of ΔG, $(B_{v_1}-B_{v_2})$ and $(D_{v_1}-D_{v_2})$ were found to be in good agreement with those derived by method 2.

4. Determination of B_e, D_e, α_e, γ_e, *and* r_e

The variation of B with v for the upper and lower states is shown in Fig. 3. For the lower state a marked curvature is observed, but the variation is very regular and it was found that the B values could be fitted to the quadratic equation

$$B_v = B_e-\alpha_e(v+\tfrac{1}{2})+\gamma_e(v+\tfrac{1}{2})^2 \qquad (2)$$

to within ±0.00002 cm^{-1}. Final values for B_e, α_e, and γ_e were determined by the method of least squares and are given in Table IV. The values of B_v calculated from these constants are given in Table III.

For the upper state it is apparent that one or more of the B values is perturbed. This is perhaps not surprising in view of the predissociations observed near $v' = 1$ and $v' = 4$. Since the magnitudes of the perturbations are not known, a linear dependence of B on v was assumed and values for B_e and α_e were determined by the method of least squares. The constants are given in Table IV and the calculated values for B_v are given in Table III. It may be

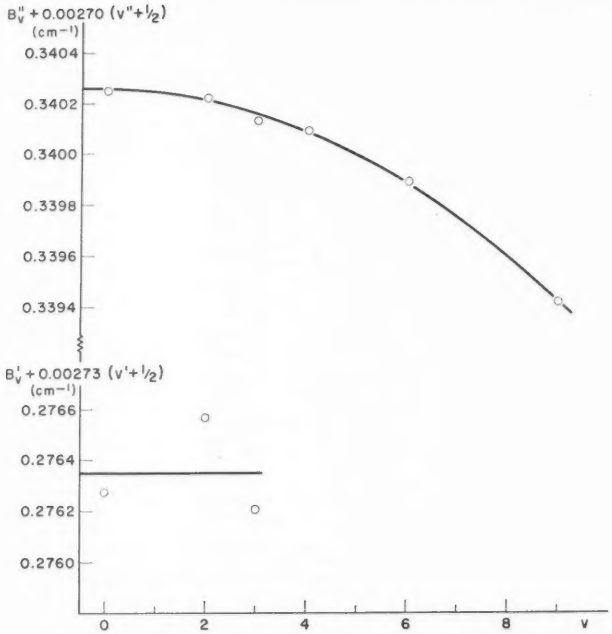

FIG. 3. Variation of B with v for the ground and excited states of IO.

noted that while the theoretical value of α, calculated assuming a Morse potential function (Herzberg 1950, p. 108) and our final molecular constants (Table IV), agrees well with the experimental values for the lower state ($\alpha''_{calc} = 0.00260\ cm^{-1}$, $\alpha''_{obs} = 0.00269_6\ cm^{-1}$), the agreement is less satisfactory for the upper state ($\alpha'_{calc} = 0.00309\ cm^{-1}$, $\alpha'_{obs} = 0.0027_3\ cm^{-1}$).

TABLE IV

Molecular constants for IO

$X\ ^2\Pi_{3/2}$	$A\ ^2\Pi_{3/2}$
$B_e = 0.34026\ cm^{-1}$	$B_e = 0.2763_5\ cm^{-1}$
$\alpha_e = 0.00269_6\ cm^{-1}$	$\alpha_e = 0.0027_3\ cm^{-1}$
$\gamma_e = -0.000009_7\ cm^{-1}$	$D_e = 0.32\times10^{-6}\ cm^{-1}$
$D_e = 0.36\times10^{-6}\ cm^{-1}$	$r_e = 2.072_3$ Å
$r_e = 1.8676$ Å	$\omega_e = 514.5_7\ cm^{-1}$
$\omega_e = 681.4_7\ cm^{-1}$	$\omega_e x_e = 5.5_2\ cm^{-1}$
$\omega_e x_e = 4.2_9\ cm^{-1}$	$T_e = 21557.8_1\ cm^{-1}$
$\omega_e y_e = -0.01_3\ cm^{-1}$	

From the graphical procedures used in Section 3, it was found that the D values for the lower state showed a very slight increase with increasing v. The magnitude of this effect was comparable to the accuracy of the measurements, hence no accurate value for β'' could be determined experimentally. Theoretically, the value of β'' derived from our final molecular constants and the

equation given by Herzberg (1950, p. 108) is $\beta'' = 0.002\times10^{-6}$ cm^{-1}. Combining this value with the D'' values given in Table III we obtain $D''_e = 0.36\times10^{-6}$ cm^{-1}. For the upper state the values of $(D'_{v_1}-D'_{v_2})$ cannot be considered as highly significant owing to the perturbations present. The theoretical value for β' is 0.009×10^{-6} cm^{-1}. Combining this value with the D' values given in Table III we obtain $D'_e = 0.32\times10^{-6}$ cm^{-1} (see Table IV). The experimental values of D''_e and D'_e are in good agreement with the values calculated from the equation $D_e = 4B_e^3/\omega_e^2$, viz. $D''_{e\ \mathrm{calc}} = 0.339\times10^{-6}$ cm^{-1}, $D'_{e\ \mathrm{calc}} = 0.319\times10^{-6}$ cm^{-1}.

Values for r_e were calculated from the equation r_e^2 (Å^2) $= 16.8630/\mu B_e$ where μ is the reduced mass of the IO molecule in atomic mass units (I = 126.9453, O = 16.0000). The values are given in Table IV.

5. *Determination of* ω_e, $\omega_e x_e$, $\omega_e y_e$, *and* T_e

The vibrational constants for the upper and lower states and the electronic term value T_e for the excited state were determined by fitting the band origins given in Table II to the equation

$$(3)\quad \nu_0 = T_e+\omega'_e(v+\tfrac{1}{2})-\omega'_e x'_e(v+\tfrac{1}{2})^2-[\omega''_e(v+\tfrac{1}{2})-\omega''_e x''_e(v+\tfrac{1}{2})^2+\omega''_e y''_e(v+\tfrac{1}{2})^3].$$

Only two vibrational constants could be derived for the excited state owing to the limited data available; for the lower state it was found that a cubic expansion fitted the data to within the experimental error. The constants were obtained by the method of least squares and are given in Table IV.

DISCUSSION

From the rotational analysis of the bands it is clear that the carrier must be a diatomic or a linear polyatomic molecule. Since the bands have been observed in absorption during the flash photolysis of mixtures of iodine and oxygen, the carrier can only contain one or both of these elements. The only possibility, consistent with the rotational constants, is IO and it is interesting to note that the ground-state bond length obtained on the basis of this conclusion is consistent with the ground-state bond lengths of related molecules. Thus $r_0(\mathrm{IO})-r_0(\mathrm{ClO}) = 0.325$ Å is in good agreement with $\frac{1}{2}[r_0(\mathrm{I_2})-r_0(\mathrm{Cl_2})] = 0.338$ Å and $r_0(\mathrm{HI})-r_0(\mathrm{HCl}) = 0.331$ Å (Herzberg 1950). It should be pointed out that the alternative carrier proposed by Vaidya (1937), viz. CI, cannot be eliminated on the basis of the rotational analysis alone. This possibility is excluded, however, by the flash photolysis experiments and the observation by Coleman, Gaydon, and Vaidya of the bands in emission from an oxyhydrogen flame to which iodine is added.

Our results confirm the vibrational assignments of Coleman, Gaydon, and Vaidya. The wavelengths of the band heads calculated from our final molecular constants are found to be in satisfactory agreement with the measured values (see Table II). The vibrational constants of the ground and excited states are now known with greater precision, but it is not possible to improve significantly the earlier estimates for the dissociation energy since considerable extrapolations are needed for both states. The values quoted by Coleman, Gaydon, and

Vaidya (1948) and by Durie and Ramsay (1958) are $D_0'' = 44$ kcal/mole and 42 ± 5 kcal/mole respectively.

It is interesting to note that several diffuse bands were observed in emission from the flame source used even under conditions of high-resolving power. This result is in marked contrast to the general absence of such bands in emission from discharge tube sources. The appearance of diffuse bands from flame sources may be attributed to the higher pressures prevalent in flames and to the fact that conditions in hydrogen diffusion flames approximate to thermal equilibrium (Durie 1952; Gaydon and Wolfhard 1953).

REFERENCES

COLEMAN, E. H., GAYDON, A. G., and VAIDYA, W. M. 1948. Nature, **162**, 108.
DURIE, R. A. 1952. Proc. Phys. Soc. A, **65**, 125.
DURIE, R. A. and RAMSAY, D. A. 1958. Can. J. Phys. **36**, 35.
EDLÉN, B. 1953. J. Opt. Soc. Am. **43**, 339.
GAYDON, A. G. and WOLFHARD, H. G. 1953. Flames, their structure, radiation, and temperature (Chapman & Hall, Ltd., London), p. 142.
HARRISON, G. R. 1939. M.I.T. wavelength tables (John Wiley & Sons, Inc., New York).
HERZBERG, G. 1950. Spectra of diatomic molecules (D. Van Nostrand Co., Inc., Princeton, N.J.).
TOMKINS, F. S. and FRED, M. 1951. J. Opt. Soc. Am. **41**, 641.
VAIDYA, W. M. 1937. Proc. Indian Acad. Sci. A, **6**, 122.

AN ANALYSIS OF A SPECTROGRAM OF THE RED AURORA OF FEBRUARY 10/11, 1958, IN THE WAVELENGTH RANGE 7300–8700 Å[1]

A. VALLANCE JONES

ABSTRACT

A high-dispersion photographic infrared spectrum covering the 7300–8700 Å region was obtained from the great red aurora of February 10/11, 1958. This spectrum shows the λλ7774 and 8446 OI lines to have been enhanced at least five times relative to normal aurora. The most striking feature of the spectrum was the appearance with high intensity of the forbidden ^2D–^2P multiplet of OII. The measured wavelengths and relative intensities of the features of the spectrum are listed.

1. INTRODUCTION

The great type-A red aurora of February 10/11, 1958, was observed simultaneously over a very wide geographical area. Spectra of the display have been obtained in Alaska by Belon and Clark (1959), at Yerkes Observatory by Wallace (1959), and near Moscow by Mironov, Prokudina, and Shefov (1959). At Saskatoon, a high-dispersion spectrogram was obtained in the region 7300–8700 Å. In addition, a set of nine low-dispersion (330 Å/mm) spectra (over the range 3750–7000 Å) were obtained with a Perkin–Elmer patrol spectrograph. In common with the results obtained by other investigators, these spectra show unusual enhancements of some atomic lines of oxygen and nitrogen. In particular the infrared spectrum shows the forbidden [OII] ^2D–^2P doublet with very high relative intensity. The presence of this feature was tentatively assumed by Omholt (1957) in low-dispersion spectra obtained from the higher-altitude portions of auroral forms. Dufay (1959) obtained further evidence of its appearance by just resolving the doublet in a photoelectric spectrum of a low-latitude aurora. Wallace (1959) provided very good evidence for the appearance of the doublet in a high-dispersion spectrum obtained at Yerkes Observatory on December 5, 1958; in his spectrum the lines appear superposed on the almost coincident $P_1(1)$ and $P_2(2)$ lines of the underlying (8–3) OH night airglow band. While the spectra of Dufay and Wallace leave little doubt of the identification of the multiplet, the spectrum obtained at Saskatoon puts the matter beyond question since the lines of the doublet are completely separated and the night airglow lines are absent.

2. EXPERIMENTAL

The infrared auroral spectrum was obtained with a dispersion of 66 Å/mm in the first order of the 9-in. $f/0.8$ auroral spectrograph at Saskatoon. The spectral slit width was 5.4 Å. A Kodak spectroscopic I–N plate, hypersensitized

[1]Manuscript received December 23, 1959.
Contribution from the Department of Physics, University of Saskatchewan, Saskatoon, Saskatchewan. The research reported in this paper has been sponsored by the Geophysics Research Directorate of the Air Force Cambridge Research Center, Air Research and Development Command under Contract No. AF 19(604)-1831.

in an ammonia–ethanol bath, was used. A Wratten 23 filter eliminated the second- and third-order spectra. The plate was exposed to the red aurora of February 10/11 for 9 hours 40 minutes, between 1820 and 0420 hours Mountain Standard Time. The plate remained in the spectrograph and subsequently received a further 5-hour 53-minute exposure to aurora over a period lasting until February 23. Some of this later aurora was also type-A red aurora; from past experience with this spectrograph it is believed that the spectrum obtained is almost entirely to be attributed to the very intense display of February 10/11.

A print of the spectrogram is reproduced in Fig. 1 together with a night

TABLE I

Wavelengths and relative intensities of auroral features 7300–8700 Å

Feature	Observed wavelength	Laboratory wavelength	Relative peak intensity		
			Feb. 10/11 aurora	Normal aurora (Meinel)	Normal aurora (Saskatoon)
OII, (2*F*) $2\frac{1}{2}$–$1\frac{1}{2}$	7319.7	7319.4	17.0	0	0
$1\frac{1}{2}$–$\frac{1}{2}$, $1\frac{1}{2}$–$1\frac{1}{2}$	7330.1	7330.0	11.8	0	0
	7341.6				
	7350.1				
N_2, 1*P* (5–3)	7360.7				
	7373.0				
	7384.2		2.7	1.5	
	7466.6		8.9	5.1	9
	7480.1				
N_2, 1*P* (4–2)	7490.0				
	7503.1		8.5	4.6	9
	7586.9		9.0	6.7	9.2
N_2, 1*P* (3–1)	7619.6				
	7625.8				
O_2 (atmos.) (1–1) *R*-branch	7687.1		27	12	20
	7703.1				
	7713.2				
N_2, 1*P* (2–0)	7726.9				
	7738.5				
	7751.7		10.9	8.6	14
OI, (1)	7773.7	7773.4	>100	8.2	13
	7826.9		8.9	8.8	11
N_2^+, Meinel, (2–0)	7860.8		7.6	8.2	8.6
	7875.9		9.7	13	19
N_2^+, 2–0?	7913.6				
OI, (19)	7994.8	7995.1	3.1	1.3	2.6
	8054.7		4.6	4.6	4.6
N_2^+, Meinel, (3–1)	8090.8				
	8105.9		4.8	6.5	7.2
NI, (2) ($1\frac{1}{2}$–$2\frac{1}{2}$) ($\frac{1}{2}$–$1\frac{1}{2}$)	8185.9	8186.6	2.7	1.3	1.4
NI, (2) ($2\frac{1}{2}$–$2\frac{1}{2}$)	8216.4	8216.3	4.2	1.9	2.8
Unidentified feature	8241.9		v.w.		
	8296.6		v.w.	1.0	
N^+, Meinel (4–2)	8346.0		v.w.	1.7	
OH, 6–2, $P_1(2)$?	8399.2	8399.7	v.w.		
Unidentified	8411.8		3.0		
Unidentified	8423.2		v.w.		
OH, 6–2 $P_1(3)$?	8429.6	8430.7	v.w.		
OI, (4)	8446.2	8446.5	>100	12	17
O_2, atmos. (0–1) *R*-max.	8628.6		3.7	23	27
Origin	8642.9				
P-max.	8656.4				

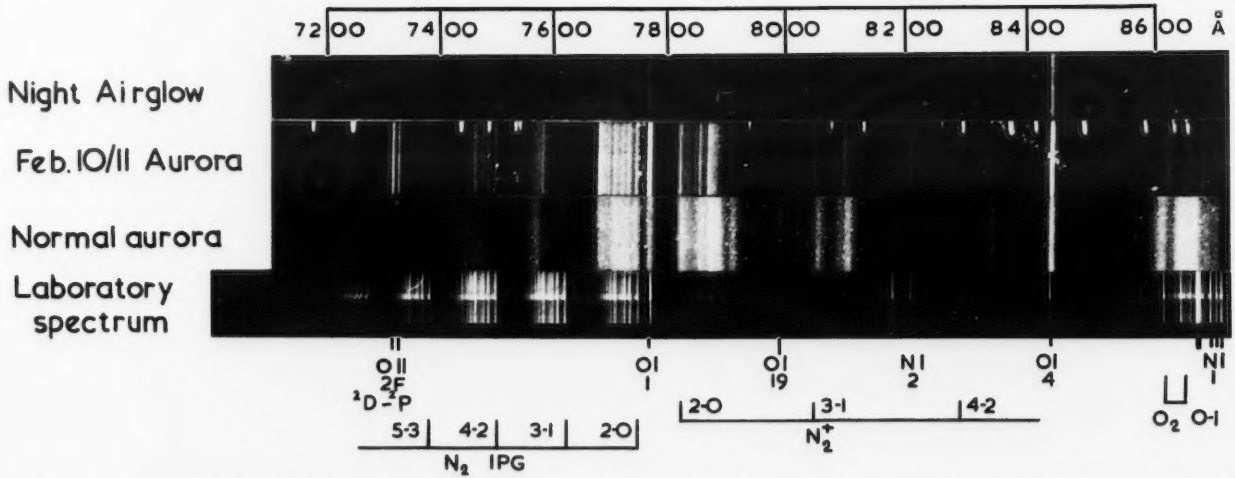

FIG. 1. Spectra in 7200–8700 Å region of night airglow, February 10–11 type-A red aurora, normal aurora (October 19, 1953), and a N_2 hollow-cathode discharge. The night airglow spectrum is slightly contaminated by aurora.

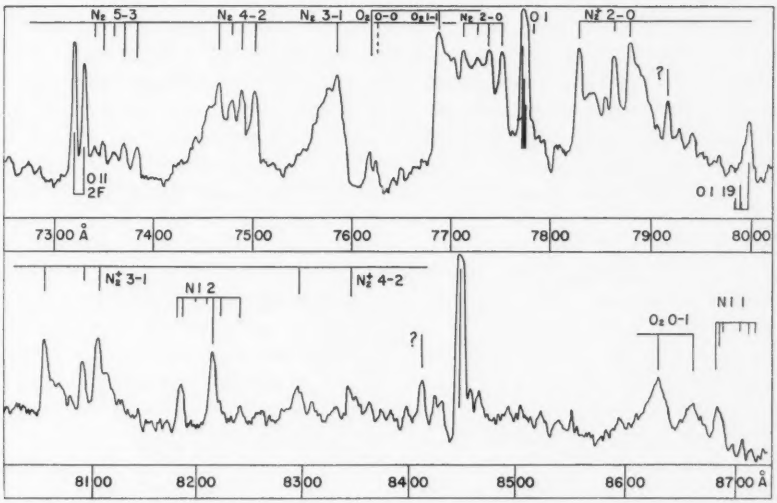

FIG. 2. Microphotometer tracing of the February 10/11 red aurora spectrum. The positions of the principal molecular bands and atomic multiplets are indicated. The atomic multiplets are identified by the numbers adopted by Moore (1945) and by Chamberlain and Oliver (1953).

airglow spectrum obtained with a 45-hour exposure on the same plate. For comparison, a spectrum of normal aurora obtained at Saskatoon with a spectrograph of dispersion 132 Å/mm and spectral slit width 9.3 Å is reproduced in the same figure. The fourth spectrum in Fig. 1 is that obtained from a N_2 hollow-cathode discharge, with a spectrograph of still higher dispersion (20 Å/mm).

The wavelengths of the features of the auroral spectrogram were measured by setting up an interpolation based on the Ne comparison spectrum superposed on the auroral spectrum. Unfortunately, the wavelengths of the principal atomic features obtained in this way showed a systematic difference of 1.4 ± 0.6 Å from the accepted laboratory values. This was attributed to the fact that the comparison spectrum was not applied until the plate was about to be removed from the spectrograph 12 days after the principal auroral exposure; it can only be supposed that some slight mechanical shock or thermal effect led to the observed shift. The final wavelengths, corrected for this displacement, are listed in Table I. The wavelengths should be accurate within ± 0.6 Å.

The relative peak intensities of some of the features listed in Table I were calculated with the help of an intensity calibration photographed on the same plate. This calibration was produced by exposing the spectrograph to a low-brightness source (Shepherd 1954), with a rotating step sector at the slit. The low-brightness source was calibrated against a black-body standard. The relative intensities so obtained are set out in column 4 of Table I.

These relative intensities may be compared with those listed by Meinel (1951) whose values are listed in column 5 of Table I. The spectral slit width employed by Meinel seems to have been about 12 to 15 Å compared with about 5 to 6 Å for the present study. Consequently, in his spectrum, lines and sharp band heads may appear weaker by a factor of up to 2.5 in comparison with unresolved bands and continuum.

A further comparison may be made with the relative brightnesses listed in column 6 of Table I. These values were obtained from a normal auroral display observed from Saskatoon during the night of April 5/6, 1957. The spectrum was photographed with a 5-in. $f/0.8$ spectrograph (Petrie and Small 1952) on a I–N plate. The plate was developed together with a similar plate on which an intensity calibration had been applied as described above. The spectral slit width for this exposure was about 9.3 Å. For this spectrum, the relative intensities of the features do not differ significantly from the values reported by Meinel.

3. GENERAL FEATURES OF SPECTRUM

In comparison with the spectrum of normal aurora the most striking points are:

(*i*) The λλ7774 and 8446 OI multiplets belonging to the $3s$–$3p$ transition array are from 5 to 10 times more intense relative to the N_2^+ bands than in normal low-level aurora.

(*ii*) The $3p^3P$–$3s'^3D^0$, OI, multiplet (19)* is definitely present; its relative intensity may be slightly enhanced in comparison with normal aurora.

(*iii*) The $3s^4P$–$3p^4P^0$, NI, multiplet (2) is present with a somewhat enhanced intensity relative to the normal auroral spectrum.

(*iv*) The relative intensities of the first positive N_2 bands and the Meinel N_2^+ bands do not seem much different.

(*v*) The ^2D–^2P, OII, multiplet ($2F$) lines are present with extraordinary intensity. The measured wavelengths agree to within 0.3 Å with the theoretical values. The intensity ratio between the lines was found to be 1.4. This is in fair agreement with the theoretical values of Seaton and Osterbrock (1957), who predict the range of values of ratio to be 1.24 to 1.31.

(*vi*) The 0–1 O_2 atmospheric band appears to be particularly weak in comparison with the N_2^+ bands. This is possibly due to the increased dispersion of the spectrograph. However, the spectral slit width of the 9-in. spectrograph is about half that of the lower-dispersion spectrograph while the relative intensity of the O_2 band is about 8 times less than for the normal auroral spectrum.

The sharp maximum at 7687.1 Å attributed by Chamberlain, Fan, and Meinel (1954) to the R-branch head of 1–1 O_2 band appears clearly. Strangely, its intensity relative to that of the neighboring 2–0 first positive N_2 band is not very different from its value in normal aurora; if anything its relative intensity is greater. This observation might appear to raise some doubt as to the correctness of the identification of the 7687-Å peak; however, it must be borne in

*The multiplet numbers are those adopted by Moore (1945); see also Chamberlain and Oliver (1953).

mind that the sharp head of the 1–1 band would be less affected by the reduction in spectral slit width than the headless branches of the 0–1 band. Moreover, the rapid drop in emulsion sensitivity beyond 8600 Å makes the intensity calibration liable to considerable error in the region of the 0–1 band.

A comparison between the auroral and the laboratory spectra in Fig. 1 shows that all the measured intensity maxima within the N_2 and N_2^+ bands correspond to heads or lines occurring in the laboratory spectrum. The maximum at 7687.1 Å in the auroral spectrum does not, of course, appear in the laboratory spectrum.

There are a few unidentified features listed in Table I. The most intense is the line-like emission at 8411.8 Å. This is not an OH night airglow line as may be seen by comparing the auroral and night airglow spectra in Fig. 1.

4. CONCLUSIONS

The most striking feature of the spectrum of the February 10/11 red aurora in this spectral region was the great enhancement of the forbidden ^2D–^2P multiplet of OII. This observation may be an important one in an understanding of the mechanism of type-A red aurora. The enhancement of this multiplet is very beautifully paralleled by the enhancement of the related ^2D–^4S multiplet at λλ3729–3726 observed by Wallace for the same aurora. The intensification of these transitions may very well be a height effect.

The other notable peculiarity of this spectrum is the generally enhanced relative brightnesses of its atomic lines in comparison with those of the molecular bands. This effect, which has been noted by other observers for the same aurora, is probably also a height effect.

ACKNOWLEDGMENTS

It is a pleasure to acknowledge the invaluable part played by Mr. H. J. Koenig in operating the spectrographic equipment, and to Mr. D. Strelioff for computing the relative intensities of the spectra. I am also indebted to Drs. L. Wallace and K. C. Clark for providing preprints of their papers on the February 10/11 aurora.

REFERENCES

Belon, A. E. and Clark, K. C. 1959. J. Atmospheric and Terrest. Phys. **16**, 220.
Chamberlain, J. W., Fan, C. Y., and Meinel, A. B. 1954. Astrophys. J. **120**, 560.
Chamberlain, J. W. and Oliver, N. J. 1953. J. Geophys. Research, **58**, 457.
Dufay, M. 1959. Ann. géophys. **15**, 134.
Meinel, A. B. 1951. Astrophys. J. **113**, 583.
Mironov, A. V., Prokudina, V. S., and Shefov, N. N. 1959. Spectral, electrophotometrical and radar researches of aurora and airglow (Academy of Sciences, Moscow).
Moore, C. E. 1945. A multiplet table of astrophysical interest. Contribution No. 20 from the Princeton University Observatory.
Omholt, A. 1957. J. Atmospheric and Terrest. Phys. **10**, 320.
Petrie, W. and Small, R. 1952. Astrophys. J. **116**, 433.
Seaton, M. J. and Osterbrock, E. E. 1957. Astrophys. J. **125**, 66.
Shepherd, G. G. 1954. Scientific Report No. AR-16, Contract AF 19(122)-152, University of Saskatchewan, Saskatoon, Saskatchewan.
Wallace, L. 1959. J. Atmospheric and Terrest. Phys. **17**, 46.

ROTATIONAL AND VIBRATIONAL INTENSITY DISTRIBUTION OF THE FIRST NEGATIVE N_2^+ BANDS IN SUNLIT AURORAL RAYS[1]

A. Vallance Jones and D. M. Hunten

ABSTRACT

Spectra of sunlit auroral rays were obtained from Saskatoon during the auroras of September 3/4 and 4/5, 1958. The resolution of these spectra was sufficiently high to enable measurements to be made of the relative intensities of the lines of the 0–0 first negative N_2^+ band as well as the relative intensities of bands of the $\Delta v = -1$ sequence of this system. An analysis of the rotational line intensities shows they are consistent with an excitation process in which N_2^+ ions in thermal equilibrium with the atmosphere at 2200° K fluoresce under the influence of solar radiation. The vibrational intensity distribution also is consistent with a fluorescent excitation from a state of thermal equilibrium at about 2050° K. It is shown that the results are not consistent with a fluorescent excitation process in which the rotational and vibrational degrees of freedom of the N_2^+ ions come into radiative equilibrium with the solar radiation. Earlier conclusions that radiative equilibrium did hold for vibration are shown to be in error as a result of the high rotational temperature and the low dispersion used. It is concluded that the destruction of N_2^+ ions as a result of dissociative recombination proceeds sufficiently fast to prevent any significant approach to radiative equilibrium. This investigation provides a strong indication that the kinetic temperature of a sunlit auroral ray (perhaps in the 400–500 km region) is in the neighborhood of 2000° K. This may be somewhat higher than the temperature of the normal atmosphere at this height.

1. INTRODUCTION

One of the principal objectives of the study of aurora is the determination of the properties of the upper atmosphere. The emission from the most common forms of aurora is concentrated between 80 and 120 km. While the summits of some auroral rays may occasionally reach as high as 600 km the work of Störmer (1955) has shown that the forms occurring at the greatest heights are the sunlit auroral rays. The highest measured points for these rays lie near 1100 km while the lower ends are generally found between 200 and 400 km. Consequently, spectroscopic observations of sunlit aurora should enable information to be obtained about conditions in the 400 to 600 km height range.

Spectra of sunlit rays have been obtained by Störmer (1939). These spectra which were obtained from parts of the rays at heights between 400 and 650 km showed the first negative N_2^+ bands to be particularly strong and to exhibit an unusually great development of the vibrational sequences.

These results were interpreted by Bates (1949*a*) in a classic paper in which it was shown that the experimental data were consistent with the excitation by sunlight of N_2^+ by a resonance fluorescence process in which a special equilibrium distribution was set up among the vibrational levels of the ion. This distribution reflects the tendency of the vibrational degree of freedom to come

[1]Manuscript received December 1, 1959.
Contribution from the Department of Physics, University of Saskatchewan, Saskatoon. Supported by the Geophysics Research Directorate of the Air Force Cambridge Research Center, Air Research and Development Command, under Contract No. AF 19(604)-1831.

into radiative equilibrium with the solar black-body radiation. For N_2^+ such a steady state can arise for the case when collisions are unimportant since pure vibrational and rotational transitions are forbidden. Bates also calculated the population rates for fluorescent excitation of the upper state of N_2^+ for the case where the collision rate is high enough to maintain thermal equilibrium in the ground state. The results of the latter calculation did not seem to fit Störmer's data unless an atmospheric temperature of 5000° K was assumed; this temperature appeared to be too high even for a height of 650 km. However, in view of the high rotational temperatures reported for sunlit rays in the present work, it seems that Störmer's data require reinterpretation.

Swings (1949) pointed out that the rotational structure of sunlit aurora should exhibit irregularities of the same kind as were found in the spectra of comets by Swings (1941) and McKellar (1942). These irregularities were shown by Swings and McKellar to arise from the presence of Fraunhofer lines in the exciting solar continuum. The observation of such irregularities in the spectra of sunlit aurora would provide definite evidence for the operation of the fluorescent mechanism in the excitation of sunlit aurora.

On the nights of September 3/4 and 4/5, 1958, high- and medium-dispersion spectra were obtained at Saskatoon of sunlit auroral rays. The analysis of these spectra, to which this paper is devoted, shows definitely that the sunlit rays were excited by resonance fluorescence and provides strong evidence to support the view that the rotational degree of freedom of the N_2^+ ion remained in thermal equilibrium with the atmosphere at a temperature of approximately 2200° K. The observed vibrational intensities of the $\Delta v = -1$ sequence of bands also appear to be close to that which would result from fluorescent excitation of ions in the distribution for thermal equilibrium at approximately 2050° K. This differs significantly from the distribution which would result from equilibrium with the solar radiation, which corresponds approximately to a vibrational temperature of 4200° K.

2. OBSERVATIONS

Displays of aurora exhibiting sunlit auroral rays were observed from Saskatoon on September 3/4 and 4/5, 1958. These rays showed the greyish-blue color described by Störmer (1955) and at times exhibited the characteristic intensity minimum where the rays crossed the boundary between the sunlit and dark regions of the atmosphere. The spectrographs were directed towards the sunlit, upper parts of rays. The sunlit portions of the rays were recognized, in general, by their unusual color. The characteristics of the spectra obtained show that this procedure was successful.

Three separate plates were obtained from the sunlit aurora. Two of these plates (one on each evening) were obtained using the 5-in. $f/0.8$ spectrograph described by Petrie and Small (1952). This instrument has a linear dispersion of 40 Å/mm. These two exposures were made on Kodak 103a–O plates and covered the regions 3500–3950 Å and 3500–4280 Å respectively. A third, higher-dispersion spectrum was obtained using a 9-in. $f/0.8$ spectrograph having a dispersion of 20Å/mm. This exposure covered the sunlit parts of the display on both September 3/4 and 4/5; the spectral region covered was 3400–4000 Å.

A reproduction of the 3914-Å N_2^+ band from the high-dispersion plate is shown in Fig. 1; a reproduction of the same band as obtained from a normal aurora is also shown. Microphotometer tracings of the band have been published in a preliminary report of our results (Hunten, Koenig, and Vallance Jones 1959). A reproduction of one of the lower-dispersion plates is shown in Fig. 2 together with a spectrum of aurora obtained after dark the same night (September 4/5, 1958). These two spectra were obtained using a step slit having 11 segments with widths ranging from 0.2 to 2.0 mm in geometrical progression. Such a slit provides a means of determining the characteristic curve of the emulsion from a region where the spectrum is continuous.

3. RESULTS

The rotational structure of the 0–0 N_2^+ band for the sunlit auroral spectrum in Fig. 1 clearly corresponds to a much higher rotational temperature than does the normal spectrum. The relative intensities of the lines of the R branch were derived from the microphotometer tracing with the help of an intensity calibration applied to another part of the auroral plate; this calibration was made by photographing the spectrum of a standard low-brightness source (Shepherd 1954) with a rotating step sector at the slit of the spectrograph. The relative intensities of the R branch lines obtained in this way must then be corrected by subtracting the contributions of the higher lines of the P branch which coincide almost exactly with the R branch lines. The correction was made by assuming that the P branch line would have the same intensity as the corresponding R branch line from the same K' level. The results are given in Table I.

As a first approximation the corrected R branch line intensities were then used to derive a rotational temperature according to the usual graphical method (Section 6) of plotting log (I/K') against $K'(K'+1)$. The B_0 value for the $X^2\Sigma_g^-$ state of N_2^+ was used in the relation between the slope of the plot and the rotational temperature. The temperature obtained was 2100° K. This result must be regarded as a preliminary one only since no account has been taken of the nature of the excitation mechanism. A more correct treatment is given in Section 6.

It is clear from Fig. 1 that irregular fluctuations are present in the line intensities of the R branch; such irregularities are to be expected for fluorescent excitation of the band system by sunlight.

As was found by Störmer (1939) the relative intensities of the vibrational bands of the first negative system of N_2^+ are also abnormal in the sunlit auroral spectrum. This is particularly evident for the 4278-Å ($\Delta v = -1$) sequence of bands as may be seen by comparing the two spectra reproduced in Fig. 2. Figure 3(*a*) shows an intensity plot of this region derived from the spectrum of Fig. 2. This intensity plot was obtained from a microphotometer tracing across the fourth step in the spectrum (counting from the strongest step). A characteristic curve for the plate was derived by scanning across the spectrum at 3775 Å and 4260 Å where the auroral spectrum is quasi-continuous. Near the edge of its field the spectrograph suffers from severe vignetting which was

PLATE I

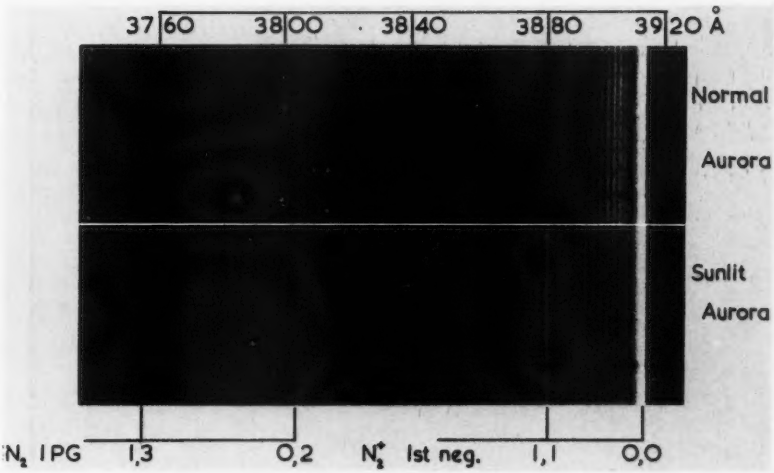

FIG. 1. The high-dispersion spectrum of sunlit aurora compared with that of a normal aurora later in the night; the rotational temperature of the former is much higher. The N_2 second positive bands are abnormally weak in the sunlit spectrum because they are not enhanced by resonance.

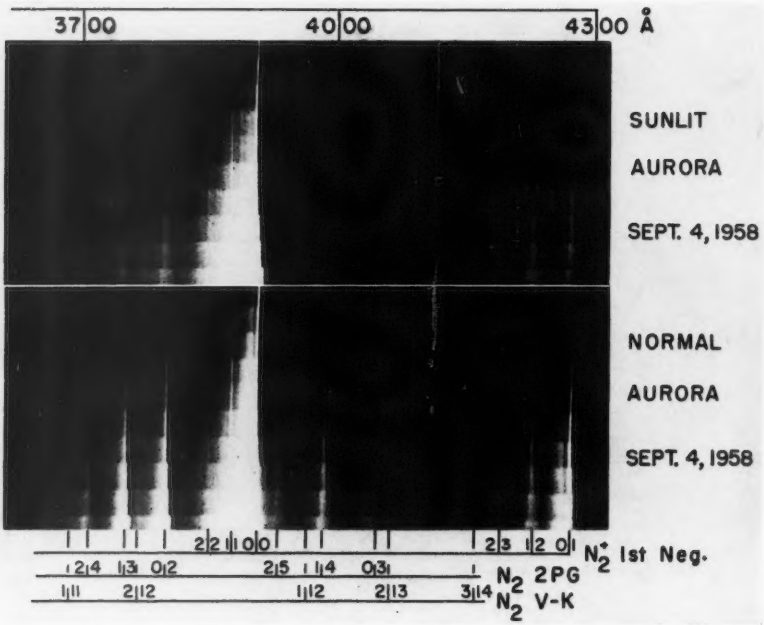

FIG. 2. The ow-dispersion spectra of sunlit and normal aurora, taken with a step slit. The enhancement of the negative system with respect to the rest of the spectrum is again noticeable.

taken into account by calibrating the sensitivity of the instrument from 4200–4300 Å with the help of a low-brightness source. Figure 3 also shows a plot of the band sequence as obtained from the non-sunlit auroral spectrum of Fig. 2. In order to keep the peak density of the P branch of the 0–1 band within the range of accurate microphotometry the intensity plot for the non-sunlit aurora was derived from the seventh step of the spectrum. The consequent differences between the spectral slit widths for the two traces of Fig. 3

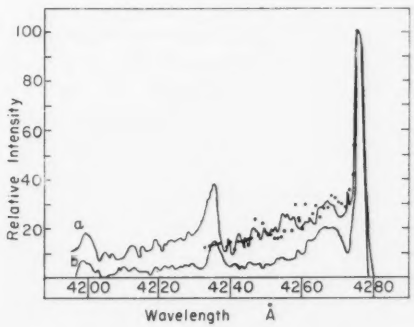

FIG. 3. (*a*) Intensity tracing of the 4278-Å group in the sunlit spectrum of Fig. 2. The dots show the synthetic spectrum for the 0–1 band at a rotational temperature of 2200° K. (*b*) A similar tracing for the normal auroral spectrum of Fig. 2.

will not seriously affect the measurements of the intensity ratios of the bands since the shapes of the bands are very similar. The vibrational sequence appears to be very much more strongly developed for the sunlit auroral spectrum. The significance of this result is considered further in the next section.

4. VIBRATIONAL INTENSITY DISTRIBUTION

Bates (1949*a*) has shown that the relative intensities of the 4278-Å (0–1), 4236-Å (1–2) and 4200-Å (2–3) first negative bands are of fundamental importance in the theoretical interpretation of the spectrum. The relative intensities required, however, cannot be taken directly from the curve of Fig. 3 because the high rotational temperature leads to overlapping of the bands. This effect is not very important for normal aurora but is of major significance in the case of the sunlit aurora which has been shown above to have a rotational structure corresponding to a temperature of over 2000° K. A similar difficulty in a more acute form was encountered by Clark and Belon (1959) in the analysis of somewhat lower-dispersion spectra of the $\Delta v = -2$ sequence of the bands.

The correction to the intensity of the 1–2 band was made by calculating a synthetic spectrum for the 0–1 band. The wavelengths of the rotational lines were taken from the data of Childs (1932). A value of 2200° K was adopted as an approximation to the rotational temperature. The synthetic spectrum was then derived for a spectral slit width of 4 Å by summing the contributions of all lines within a range of ±2 Å of each wavelength at which the spectrum was

required. The synthetic spectrum was calculated at 4-Å intervals for the range 4236 Å–4284 Å. The 4-Å spectral slit width corresponds to the value for the segment of the slit which produced the spectrum from which the intensity plot of Fig. 3 was derived. This procedure supposes that the resolution function of the spectrograph was rectangular; in fact for this slit width it was found to be distinctly trapezoidal (as determined from the profile of the 4047-Å mercury line). As a consequence it is to be expected that the synthetic spectrum would tend to exhibit a somewhat "sharper" structure than the observed spectrum.

The synthetic spectrum so obtained is shown superimposed on the experimental curve in Fig. 3. The two curves fit well within the limits of experimental error set by the grain "noise" of the emulsion.

The relative intensities of the 0–1 and 1–2 bands may now be calculated on the assumption that the ratio will be equal to that of the peak intensities of the P branches after the contribution of the R branch of the 0–1 band has been subtracted. The result obtained is $I(0\text{–}1):I(1\text{–}2) = 100:26$. The result which would have been obtained if no correction had been made for the R branch contribution to the peak of the 1–2 band is 100:39. The ratio derived from the intensity trace for the non-sunlit aurora (where the correction is negligible) is 100:11. This agrees with the usual value of the ratio for normal aurora (Hunten 1955). For the sunlit aurora, the relative intensity of the third band (2–3) was estimated by extrapolating the background under its head as about 10; the full set of intensity ratios is thus 100:26:10.

To discuss the excitation mechanism we need the relative population rates $g(v')$ rather than the intensities. The relation between them is well known (Bates 1949*a*) and need not be repeated. It is no longer necessary to use Franck–Condon factors instead of relative transition probabilities in the calculation since a table of the latter has been given by Wallace and Nicholls (1955). The factors multiplying the relative intensities to convert them to relative population rates are then 0.93 for 1–2 and 1.06 for 2–3. We thus find $g(0):g(1):g(2) = 100:24:11$; the third is very uncertain. Reference to Bates' Table 12 (1949*a*) gives a vibrational "temperature" of about 2050° K. This "temperature" is not far from the rotational temperature 2200° K found in Section 6, and is certainly lower than the 4200° K given by Bates for the case of radiative equilibrium with sunlight.

5. THEORY OF THE ROTATIONAL ENERGY DISTRIBUTION

The work of Bates (1949*a*) on the vibrational intensity distribution showed that it could apparently be explained by assuming that the molecules are in equilibrium with the solar radiation. If it were not for the Fraunhofer lines in the sunlight, the molecules would have a vibrational temperature equal to the temperature of the sun's surface; Bates' result corresponds to a vibrational temperature of about 4200° K, suggesting that the Fraunhofer lines do have an appreciable effect. Since the N_2^+ molecule is homonuclear, it has no rotation–vibration nor pure rotational spectra; thus the only transitions governing the equilibrium are electronic. This effect is illustrated by McKellar's results

(1942) on comet spectra, in which the C_2 molecule gives a very high temperature while the CN gives a temperature about equal to that of the cometary gas (Swings 1943).

The new observations of sunlit auroral rays at high dispersion show what appears to be the analogous effect on the rotational energy distribution; although the temperature is lower, about 2100° K, this might be explained by the presence of Fraunhofer lines in the exciting sunlight. The spectrum to be expected on this mechanism was calculated and found indeed to be in fair agreement with the observations. However, it was thought best to calculate another spectrum on the assumption that the N_2^+ ground state had a Boltzmann distribution corresponding to the temperature of 2100°; to our surprise, this gave much better agreement. The methods used will now be described; the two cases will be called "radiative equilibrium" and "thermal equilibrium".

A complete calculation for radiative equilibrium should take into account the absorption and emission by all the bands of the first negative and other systems, allowing for the intensity of the sunlight at each individual line. This would yield a new version of Bates' result for the vibrational distribution, as well as the rotational distribution of each rotational level of ground and excited states. However, it is not practical for several reasons: far too much work would be required; probably the wavelengths of all the lines have not been measured; and the theory would be almost impossibly complicated. Consideration was therefore restricted to the first negative system and the first two vibrational levels of each state; the 0–0 band (3914 Å) is the most important, and the 0–1 band (4278 Å) next. The 1–1 can be ignored because the transition probability is small, and the 1–0 because the solar continuum is much weaker in the ultraviolet (3582 Å); moreover, these bands go to the level $v' = 1$ which does not directly concern us. Only two bands were thus included; the calculated spectrum may be expected to exaggerate the effects of individual Fraunhofer lines and allowance must be made for this in the comparison with observation.

Let us first consider the simple case in which only the levels $v' = 0$ and $v'' = 0$ are included. Figure 4(*a*) shows the rotational levels numbered with the quantum number K which is convenient to use when the spin splitting of each level can be neglected. Some of the possible transitions are indicated; it will be seen that there are two independent sets of levels since neither the absorbing nor the emitting transitions join them. The odd levels of the one state are in equilibrium with the even levels of the other. The equations describing the equilibrium may be set up with the aid of the principle of detailed balance: the probability of a transition and its inverse is proportional to the statistical weight of the final level. We use A and B to represent transition probabilities for emission and absorption, n for the population of a state, and I for the flux of radiation at the wavelength of a line. Then

$$A\nu^4 n'(K-1)(2K+1) = B\nu I_\nu n''(K)(2K-1)$$

and

$$A\nu^4 n'(K+1)(2K+1) = B\nu I_\nu n''(K)(2K+3).$$

The first of these expresses the fact that in equilibrium the number of transitions per unit time must be the same for both absorption and emission between an upper level numbered $K-1$ and a lower level numbered K; this is a transition in the P branch and so the flux is called I_p. The second equation expresses the same fact for the R transition having the same lower level. Dividing the second equation by the first gives

$$\frac{n'(K+1)}{n'(K-1)} = \frac{2K+3}{2K-1}\frac{I_r}{I_p} = \frac{r(K)}{p(K)} = s(K). \tag{1}$$

The quantities p and r represent radiation fluxes multiplied by the statistical weight of the upper level concerned; their use will allow later equations to be written more compactly.

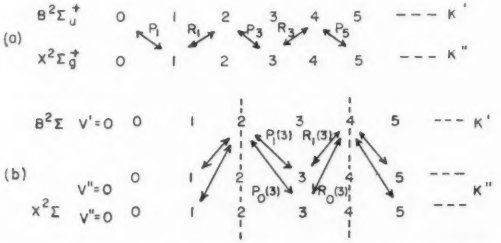

FIG. 4. (*a*) Rotational levels and transitions for part of the 0–0 band.
(*b*) The same, but including both 0–0 and 0–1 bands. (The vibrational numbers v'' of the X state should be 0 and 1, reading upwards.)

When we include the level $v'' = 1$ the situation becomes much more complicated; it is shown in Fig. 4(*b*). Because of the assumption of equilibrium it is possible to consider the transitions between the dotted lines by themselves. But within these lines there is now a loop, so that equilibrium is possible without having each absorption transition individually equal in rate to the corresponding emission. Instead, we must equate the number of transitions reaching each level to the number leaving; of the four equations thus found, one is redundant. Quantities relating to the 0–0 band will be given the subscript 0, and 1 will be used for the 0–1 band. The relative transition probabilities of these bands will be called q_0 and q_1. The result will first be worked out for the specific levels shown in Fig. 4(*b*) and then generalized.

If $n_0''(3)$ is constant,

$$B\nu_0 q_0 n_0''(3)[p_0(3)+r_0(3)] = 7.1\nu_0^4 q_0[n_0'(2)+n_0'(4)];$$

no statistical weights appear on the left because they are included in the quantities p and r. For $n_1''(3)$ constant,

$$B\nu_1 q_1 n_1''(3)[p_1(3)+r_1(3)] = 7.1\nu_1^4 q_1[n_0'(2)+n_0'(4)].$$

Finally, for $n_0'(2)$ constant,

$$B\nu_0 q_0 n_0''(3)p_0(3)+B\nu_1 q_1 n_1''(3)p_1(3) = 7.1n_0'(2)[q_0\nu_0^4+q_1\nu_1^4].$$

If the first two equations are substituted in the third so as to eliminate the populations of the lower levels, the result is

$$\frac{n_0'(4)}{n_0'(2)} = \frac{q_0\nu_0^4 r_0(3)[p_1(3)+r_1(3)]+q_1\nu_1^4 r_1(3)[p_0(3)+r_0(3)]}{q_0\nu_0^4 p_0(3)[p_1(3)+r_1(3)]+q_1\nu_1^4 p_1(3)[p_0(3)+r_0(3)]}.$$

A more convenient form is obtained by dividing top and bottom by $q_0\nu_0^4 p_0 p_1$, using $s(K)$ as defined in (1) and writing q for $q_1\nu_1^4/q_0\nu_0^4$; at the same time we may replace the particular values of K by general ones:

$$\frac{n'(K+1)}{n'(K-1)} = \frac{s_0(K)[1+s_1(K)]+qs_1(K)[1+s_0(K)]}{[1+s_1(K)]+q[1+s_0(K)]}. \tag{2}$$

It is seen that (2) reduces to (1), as it should, if q is taken equal to zero. It is interesting to consider the special case in which the illuminating flux has a black-body spectrum; the ratio I_r/I_p depends on the wave-number difference of the R and P lines with the same K'', and this is just the difference ΔF between the energy levels $K+1$ and $K-1$. From the definition of $s(K)$ in (1) it follows that

$$s_0(K) = s_1(K) = \frac{2K+3}{2K-1}\exp\left(-\Delta F\frac{hc}{kT}\right) = \frac{n'(K+1)}{n'(K-1)};$$

thus in this case the rotational temperature is equal to the temperature of the black body as would be expected from more general reasoning. The solar spectrum in the blue and ultraviolet deviates considerably from that of a black body; the detailed calculations show that the Fraunhofer lines happen to lie in such a way as to simulate a much lower temperature near 1200° K.

Equation (2) is not suitable for calculation for two reasons: first, its complexity, and second, because it gives only the ratio of adjacent odd or even levels and a large error could accumulate over the whole width of the band unless an unreasonable number of extra digits were carried. If (2) is examined it is seen to produce a weighted mean of s_0 and qs_1, with the quantities in square brackets acting as weights. The value of the mean will not be greatly changed if all the weights are taken equal to 2; then we may write approximately

$$\frac{n'(K+1)}{n'(K-1)} \doteqdot \frac{s_0(K)+qs_1(K)}{1+q} \doteqdot 0.77s_0(K)+0.23s_1(K). \tag{3}$$

The numbers follow from the values of $q_0(0.54)$ and $q_1(0.23)$ given by Wallace and Nicholls (1955) and the definition of q just before equation (2). The radiation fluxes I_r and I_p may be found as fractions of the continuum from the Utrecht Atlas (Minnaert *et al.* 1940) and we will call their ratio $U(K)$; then

$$s_1(K) = \frac{2K+3}{2K-1}\frac{I_r}{I_p} = \frac{2K+3}{2K-1}U_1\exp\left(-\Delta F\frac{hc}{kT}\right),$$

where we have again used the Wien approximation to the black-body law. When these are substituted into (3) the Boltzmann factors are common; and

when a whole series of ratios as given by (3) is multiplied together, all the Boltzmann factors combine:

$$(4)\quad \frac{n'(K)}{n'(0)} = \prod_{m=2,4}^{K} [0.77U_0(m)+0.23U_1(m)]\,(2K+1)\exp\left(-F\frac{hc}{kT}\right)$$

(even levels).

A similar expression holds for the ratio of odd levels to $K' = 1$. Build-up of error has now been eliminated from the Boltzmann factor but not from the term involving U; thus, one must be careful in estimating the U's from the Atlas and in making the calculations. F can be taken equal to $B''K(K+1)$.

The case of "thermal equilibrium" is much simpler. The question of what the molecules are in thermal equilibrium with will be considered later; for the present, the term will be taken to imply that the N_2^+ ground state has a Boltzmann distribution of the rotational levels, instead of a distribution determined by the radiative equilibrium as just discussed. This distribution will be

$$(5)\qquad n''(K) = (2K+1)\exp\left(-B''K\,(K+1)\frac{hc}{kT}\right);$$

T no longer represents the temperature of the sun, but rather that of the ground-state distribution. If absorption of the 0–0 band alone is considered, the distribution in the upper state is

$$n'(K) = I_r(K-1)n''(K-1)+I_p(K+1)n''(K+1).$$

This will be altered very little if both the n'' are replaced by what is nearly their average, $n''(K)$; then

$$(6)\quad n'(K) \doteq (2K+1)\exp\left(-B''K(K+1)\frac{hc}{kT}\right)\left(I_r(K-1)+I_p(K+1)\right).$$

Throughout this development, normalizing constants have been omitted since only the distribution among levels is of interest. In (6), I_r and I_p can be taken as the fractional intensities u_r and u_p from the Utrecht Atlas with little error: the variation of the continuum cancels to first order since the P and R branches go in opposite directions. To second order, however, there is an appreciable variation in the mean wavelength of corresponding P and R lines; this is what causes the head in the P branch and the increasing spacing of the lines in the R branch. An approximate calculation of this effect showed that the measured temperature would be about 50° too low if it is 2100° K and the sun's color temperature 7150° K. This small correction is hardly significant in view of the other errors of measurement and interpretation, but it is included in our final result; it was not included in our preliminary announcement (Hunten, Koenig, and Vallance Jones 1959).

The 0–1 band can be included by adding to the last term of (6) the amount $q(I_r'+I_p')$ where the primed fluxes refer to this band. The fact that the first vibrational level is less populated than the zeroth is balanced by the greater solar flux at the longer wavelength; thus, only the ratio of the transition

probabilities enters as long as the vibration of the molecule is in radiative equilibrium. Actually, the vibration is somewhat less than this, but use of the full factor q will help to compensate the omission of other bands. Replacing the I's by u's as suggested above, we finally get from (6)

$$(7) \qquad n'(K) \doteqdot (2K+1) \exp\left(-B''K(K+1)\frac{hc}{kT}\right) [u_r+u_p+q(u'_r+u'_p)].$$

In the next section the abbreviation $\bar{u}$ is used for the quantity at the end of (7).

6. NUMERICAL CALCULATIONS AND RESULTS

The biggest part of the labor of calculation is the reading of the fractional intensity of sunlight at the position of each line of the 0–0 and 0–1 bands. As already mentioned, the solar spectrum used was that of the Utrecht Atlas, which gives intensity tracings on a large scale for the light from the center of the sun's disk. It would be better to have a spectrum of integrated sunlight, but this is much more difficult to obtain and is not available. The finite resolution of the spectrograph used to obtain the Atlas fills in the narrow lines appreciably; however, the lines for the whole sun must be somewhat filled in also because of the rotation and the resulting Doppler shift; thus, these two errors tend to cancel. The wavelengths of the N_2^+ lines are given by Childs (1932); they were marked lightly on the tracings of the Atlas and the fractional intensities estimated as closely as possible. Because the Fraunhofer lines are often narrow and the rotational lines may fall on their steep sides, some of these results are rather uncertain, perhaps by 5 or even sometimes 10%. (Those who have no Utrecht Atlas available may find a reproduction of one of its pages in just this wavelength region in the paper by McKellar (1942).) The radial component of the earth's orbital motion and its rotation cause a Doppler shift of the whole spectrum which may have an appreciable further effect; it was not taken into account and thus provides another source of error. With cometary spectra a considerable change in radial velocity is required to affect the spectrum seriously; thus, this error should be small. Each branch of each band was followed a little beyond $K'' = 40$; for those lines with a measured spin splitting both intensities were read and then averaged.

The tracings in the Utrecht Atlas were supposed to be adjusted so that the continuum was at the 100% level. It has since been discovered by Chalonge and co-workers that in the near ultraviolet the continuum is well above 100% in places, primarily because of the wings of Balmer lines (Canavaggia and Chalonge 1946; Canavaggia, Chalonge, Egger-Moreau, and Oziol-Peltey 1950; brief summary by Minnaert 1953). The best estimate of the corrections by Michard (1950) are as follows: the continuum taken as having a color temperature of 7150° K is at 114% from 3926 to 3892 Å, and at 124% from 3893 to 3793 Å. The discontinuity occurs in the middle of the 0–0 band and must be taken into account, especially in the case of radiative equilibrium.

Calculations for radiative equilibrium were made by means of (4) except that the weights used were 0.70 and 0.30 because of a numerical error. It was not thought worth while to repeat the calculation, especially since the result

neglects all the other bands of the system and a slightly too large weight for the 0–1 band would help to compensate for this. B'' was taken as 1.922 cm^{-1} (Childs 1932; Herzberg 1950). Separate calculations were made for odd and even levels and the results are shown separately in Fig. 5(*b*) by means of lines joining the plotted points; the observations are shown by the dots. The two sets could be combined by assuming them to be populated according to the ratio of their statistical weights, but there did not seem to be any advantage to this. Since the ordinate scale is logarithmic, the various sets of points can be moved up and down without change of shape; this procedure was used to fit the corresponding ones together as well as possible. The vertical displacement between the odd and even lines is arbitrary. While there is agreement in some places, the general fit between theory and observation is poor.

Equation (7) was used to calculate the results for thermal equilibrium. The temperature assumed was 2100° K as found in Section 3 from the observations; another calculation using 1700° was also made, but this temperature was obviously too low. The weights used for the two bands were the ones in (4); this result is given in Fig. 5(*a*) along with the observations. The 2:1 intensity alternation has been removed by doubling the measured intensities of the weak lines; this gives a smoother plot which is easier to interpret. The agreement between calculation and observation is considered to be good and to show that the distribution of rotational levels in the ground state is close to a Boltzmann

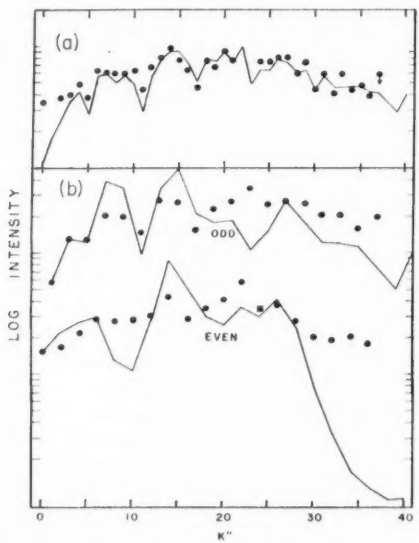

FIG. 5. (*a*) The synthetic spectrum of the 0–0 band for thermal equilibrium, indicated by lines joining the calculated points. The observations are shown by the dots. Since the ordinate scale is logarithmic, the spectrum can be displaced vertically by any desired amount. The observed intensities of the weak lines have been doubled.

(*b*) Similar plots for radiative equilibrium. An arbitrary displacement has been used to separate the lines of odd and even K''.

one. The biggest disagreements are found at the ends of the branch where the lines are faintest and the measurements least certain; in addition, the first few lines ride above an intense series of P lines which must be subtracted. The possible errors in the calculations have already been discussed; the principal ones are the errors in the fractional intensities of the sunlight and the omission of the weaker bands of the system.

TABLE I

Observed intensities of the R lines in the sunlit spectrum, corrected for the presence of the P branch. Also included are the calculated Fraunhofer correction factors $\bar{u}$ defined in the text after equation (7)

K''	Observed intensity	K'	$\bar{u}$	K''	Observed intensity	K'	$\bar{u}$
0	299	1	182	23	215	24	105
1	74	2	177	24	631	25	143
2	315	3	178	25	318	26	144
3	169	4	199	26	676	27	188
4	406	5	195	27	331	28	180
5	163	6	108	28	496	29	153
6	537	7	206	29	318	30	174
7	256	8	193	30	368	31	125
8	513	9	147	31	257	32	165
9	255	10	158	32	343	33	149
10	533	11	126	33	254	34	149
11	184	12	71	34	366	35	165
12	574	13	132	35	200	36	178
13	345	14	181	36	323	37	169
14	826	15	201	37	241	38	180
15	328	16	193	38		39	161
16	533	17	157	39	<100	40	147
17	195	18	110	40	234	41	215
18	646	19	167	41	200	42	153
19	288	20	156	42	190	43	143
20	764	21	188	43	100		
21	326	22	158	44	186		
22	(1–1 head)	23	214				

Once it has been established that excitation is from a ground state with a Boltzmann energy distribution, a more accurate temperature for this distribution can be found by modifying the standard plot of $\log(I/K')$ vs. $K'(K'+1)$ to take account of the Fraunhofer lines. As is well known (Herzberg 1950), this follows from an equation similar to (5); $(2K+1)$ is replaced by K' to take into account a slight dependence of transition probability on K'. Since the excitation is now described by (7), the ordinate must be changed to $\log(I/K'\bar{u})$, where $\bar{u}$ is the average residual intensity defined after (7). Such a plot is shown in Fig. 6 along with what is thought to be the most probable straight line; it gives a temperature of 2150° K. Adding the correction of 50° for the slope of the solar continuum, we find 2200° K as the final result; it could probably be in error by ±200°. The line was drawn to favor the points from $K'' = 15$ to 21 and 30 to 35; the points at the ends are uncertain for the reasons already discussed, and the ones between 22 and 29 appear to be raised by the presence of the 1–1 band. The values of $\bar{u}$ used are given in Table I along with the measured line intensities.

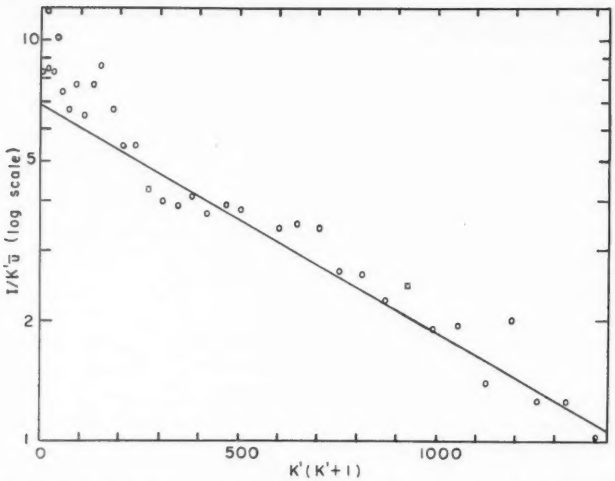

FIG. 6. Plot of log $I/K'\bar{u}$ against $K'(K'+1)$ for finding the rotational temperature. Intensities of the weak lines have been doubled.

For later discussion it will be convenient to have an estimate of the rotational "temperature" corresponding to the distribution for radiative equilibrium. The representation by a temperature is not very good, but a plot of the synthetic spectrum according to (7) gave 1200° K for the strongest part of the band. This is much lower than the solar "continuum" temperature because of a number of strong, wide absorption lines in the region of the R branch of the 0–0 band; prominent among these is H-zeta.

7. DISCUSSION

In this section we wish to discuss the relation between the rotational and vibrational temperatures of the ions and the kinetic temperature of the atmosphere. Since the term "temperature" is used in a somewhat specialized sense, it will be best to review this first. It may be assumed that the N_2 molecules are in thermal equilibrium, so that it is strictly correct to speak of rotational and vibrational temperatures which are equal to the kinetic temperature T. But we observe N_2^+ ions, not neutral molecules, and the observed rotational and vibrational "temperatures" may differ from T; in such a case it is not strictly correct to use the term temperature, but it is convenient to use it as a parameter which specifies the distribution among the states. We will use the term RT to represent the rotational "temperature", and VT the vibrational "temperature", of the ground state of the ion $X^2\Sigma$. The observed intensities actually give the distributions in the excited state $B^2\Sigma$, but since the excitation mechanism is known the ground-state distributions can be deduced. This was done for the rotation in Section 6, and for the vibration in Section 4.

The processes that control RT and VT will now be considered. First we have the original ionization process

$$N_2+X(\text{fast})\rightarrow N_2^++X+e; \tag{8}$$

X will usually be an electron even if the primary particles are fast protons because of the large number of fast secondaries (Omholt 1959; Bates, McDowell, and Omholt 1957). The measured cross sections indicate that most of the N_2^+ ions are produced in their ground electronic state (Omholt 1959). Franck–Condon factors for this process are given by Bates (1949*a*) and from these it is easy to calculate VT as a function of T. (In general there is no guarantee that the vibrational distribution resulting from excitation or ionization can be represented by a temperature, but in this case a good representation is possible.) The result is shown in Fig. 7. For low T, VT is about 1400° K,

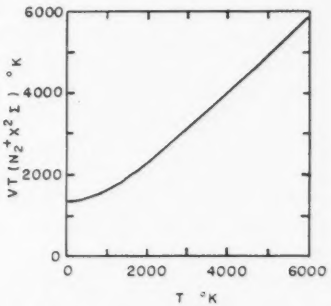

FIG. 7. Effective vibrational temperature of the ground state of the N_2^+ ion resulting from electron impact on N_2 at temperature T.

reflecting the transition probabilities from the lowest vibrational level; for the range 2000° to 3000° which interests us most, VT is about 250° higher than T. To a first approximation, RT is unchanged by ionization because of the restriction of the selection rule and the small change in internuclear distance. However, the actual effect is easily found since the RT's are in the same ratio as the B values; thus, RT = 0.96 T.

If X in (8) is a slow proton the most probable reaction is charge exchange in which the electron after the collision is bound to X. Experiments bearing on this process have been made most recently by Fan (1956), Carleton (1957), and Roesler, Fan, and Chamberlain (1958). They seem to show that there is no change in RT at any energy, but a considerable increase in VT around a bombarding energy of 20 kev. The effect on VT when the initial temperature is high is not known, but there would probably still be some increase. Thus one would expect to find VT greater than RT if charge-exchange excitation were affecting VT appreciably, but RT would still be nearly the same as T. No significant difference was observed for either the sunlit or the non-sunlit aurora.

The life of an ion is ended by recombination

$$N_2^+ + e \rightarrow N + N \tag{9}$$

which has a large coefficient; the value 4.0×10^{-7} cm^3/sec has been measured (Faire and Champion 1959). A lower value may be more appropriate for our purpose, since the molecules in the laboratory afterglow may well be vibrationally excited; we adopt 4×10^{-8} cm^3/sec which may be as much as an order of magnitude too small. In the presence of aurora, the electron density is probably rather higher than normal; we assume $n(e) = 5 \times 10^5$/cm^3.

The mean life of an ion is thus only about 50 seconds; a smaller electron density will give a longer life, but it is unlikely to exceed 200 seconds and may be as short as 5 seconds. In this short time RT and VT are not able to depart very far from their original values; thus, the cycle (8) and (9) is effective in keeping the ions close to thermal equilibrium and is by far the most effective process at high altitudes.

As the ion scatters solar radiation, its vibrational and rotational distributions are altered; the final result for the latter is discussed in Sections 5 and 6, and for the former by Bates (1949*a*). As we have seen, the rotational distribution, for the case of radiative equilibrium, can be represented roughly by RT = 1200° K. The corresponding VT may be found by comparing Bates' Tables 12 and 13, and is about 4200° K. Both temperatures differ from the sun's color temperature because of the effect of Fraunhofer lines. The speed at which radiative equilibrium is approached depends first of all on the rate of scattering, which was calculated by Bates (1949*b*). Lytle and Hunten (1960) have revised the result to agree with more recent measurements, and find 0.11 quantum/ion sec for the whole negative system; thus, the mean time between scatterings is 9 seconds. If the estimate of the lifetime of an ion given above is correct, it can scatter only 5.5 quanta, on the average, before recombining; even the longest reasonable life of 200 seconds permits only 22 quanta. Because of the selection rule ($\Delta K = \pm 1$) and the large number of rotational levels, the rotational distribution can be affected only slightly in this time; neither restriction operates on the VT which may rise rather rapidly towards 4200° K. The observed value will be a time average and will lie between (T+250°) and 4200°, probably closer to the lower limit. If T is near 2200° as it appears to be, RT may be slighly less than its original value 0.96 T.

Let us now consider the effect of collisions with other gas molecules. It is known (Massey and Burhop 1952) that rotational energy is easily transferred; but vibrational energy transfer is essentially impossible on the time scale we are concerned with. For N_2^+ in the atmosphere there are, however, two special processes which effectively do cause rapid transfer of both types of energy:

$$N_2^+ + N_2 \rightarrow N_2 + N_2^+ \quad \text{(charge exchange)}, \tag{10}$$

and

$$N_2^+ + N \rightarrow N + N_2^+ \quad \text{(atom exchange)}. \tag{11}$$

Charge exchange creates a new ion for which RT and VT are both equal to T. The effect of atom exchange is not so obvious, but it seems likely to cause

equipartition among rotational, vibrational, and translational degrees of freedom; thus, if VT was large before the reaction, RT will be increased after it. This seems to be the only mechanism by which RT can become greater than T.

The coefficients for (10) and (11) may be of the order of gas-kinetic, or 3×10^{-10} cm^3/sec. If they are to compete effectively with (8) and (9) the mean time between reactions must be less than about 30 seconds, so that the density of N_2 or N must be at least 10^8 particles/cm^3. The corresponding height may be estimated with the aid of Nicolet's model of the thermosphere (1959): 250 to 300 km for N_2 and not far above 100 km for N. Rotational energy can be transferred to atomic oxygen, presumably again with about a gas-kinetic cross section requiring as before a density of 10^8 atoms/cm^2 which is found in the 400- to 500-km region.

Finally, the possibility of direct excitation by electrons should be considered. Excitation accompanies only a few per cent of ionizations, but each ionization is followed by the scattering of five or six photons. Similarly, excitation of the ion by electron impact during its short life is improbable. Photon excitation is always much more important than electron excitation, with the latter serving only to produce the ions so that they may scatter light.

We conclude that above about 300 km the only important reactions are (8) and (9); RT is approximately equal to T and VT somewhat higher. Below 300 km, exchange reactions become more important and RT and VT should not differ appreciably from T. Our aurora was probably well above 300 km, perhaps at 400 or 500 km, and gave RT as 2200° K and VT about 2050° K. Thus it appears that T was not far below 2200° K. Whether this should be taken as the temperature of the normal atmosphere is another question, since considerable energy was being deposited by reactions such as (8) and by the action of solar radiation in raising VT. That VT is found to be less than RT instead of greater is not significant, since neither is accurate to better than ±200°.

Some accepted conclusions about sunlit and "low-latitude" aurora must be reviewed in the light of our results. In Section 4 it was shown that VT cannot be found from the spectrum without first making a substantial correction for the overlapping of bands which occurs when RT is high. Since this high RT was not suspected previously, many erroneous VT have been derived.

The measurements of Störmer (1939, 1955) on blue sunlit rays were used by Bates (1949*a*) to deduce that VT corresponded with the value expected from radiative equilibrium as closely as would be expected. Study of Störmer's microphotometer tracing shows that the appearance of the 4278-Å group is very similar to that of Fig. 4, though of much lower dispersion. Störmer gives the intensity ratio (0–1):(1–2) as 100:59; this is to be compared with our uncorrected result of 100:39. It is highly probable that the true intensity ratio is close to our 100:26 and the VT close to 2050° K. The lower resolution of Störmer's spectrum would be expected to raise the uncorrected intensity of the 1–2 band as observed.

A curious type of auroral spectrum has sometimes been observed from low latitudes (Rayleigh 1922; Barbier 1947), and more recently from the latitude

of Moscow (Mironov, Prokudina, and Shefov 1959). Its characteristics are the very high apparent VT shown by the N_2^+ first negative bands and the almost complete absence of the N_2 second positive bands. Both these facts strongly suggest that the aurora is sunlit, an idea which is by no means new (Seaton 1956; notice in particular his statement that Barbier's aurora may have been sunlit despite earlier statements to the contrary). Sunlit aurora should be observable for long distances because of its great height, and its spectrum observed from far away is less likely to be contaminated by light from ordinary aurora than when it is observed from below (Chamberlain and Meinel 1954). On the other hand, it seems likely to be more contaminated by other high-altitude emissions than the spectrum of Störmer which was produced by guiding on visible rays. All the "low-latitude" spectra mentioned were produced by long unguided exposures, though in some cases the sunlit phase must have been rather short. It would seem that "high-altitude" rather than "low-latitude" is the important characteristic of this aurora, although the latter name has the advantage of established usage.

All the "low-latitude" spectra appear to show an even greater development of the negative system than Störmer's; this is particularly evident in the 4709 Å sequence in which the 1–3 band is brighter than the 0–2 and the 2–4 as bright. Unfortunately, our spectrum did not cover this region, but one of the plates by Mironov, Prokudina, and Shefov (1959, Fig. 5) covers it very well. Fortunately, the resolution of this spectrum is just good enough to show some lines of certain multiplets of OII whose other lines must be blended with the heads of the two anomalously intense bands. A rough allowance for these lines brings the relative intensities into reasonable agreement with Störmer's. The 0–1 and 1–2 bands are the most likely to be free of blends; they appear very similar to ours. Their Fig. 6 shows a 0–0 band whose appearance strongly suggests a high RT.

It is suggested that some of the exposure to the atomic lines may have accumulated during the night before the visible aurora appeared, and that the latter then provided the sunlit N_2^+ bands. A rough calculation of the shadow-height during the visible aurora, using the times and pointing data given, shows that it varied between 410 and 330 km. This is consistent with the hypothesis that the display was sunlit.

8. CONCLUSIONS

The spectra taken of the sunlit auroral rays occurring on September 3, 4, and 5, 1958, have been described. Even by inspection it was clear that the rotational and vibrational "temperatures" of the first negative N_2^+ bands were unusually high. A preliminary value of the former was 2100° K; the latter was found to be about 2050° K by comparison with calculations of Bates. Detailed calculations of the rotational structure resulting from fluorescent excitation by sunlight were made on either of two assumptions: first, that the rotational distribution was determined by the fluorescence process itself ("radiative equilibrium"); and second, that the ground state of the N_2^+ ion had a rotational distribution of the Boltzmann type ("thermal equilibrium"). The second case

gave better agreement with the observed spectrum. It was then possible to derive an improved rotational temperature by a method which took account of the solar Fraunhofer lines, and the result was $2200 \pm 200°$ K.

It thus appears that both the rotational and vibrational degrees of freedom of the ion were near thermal equilibrium with the atmosphere. A discussion of the possible mechanisms of thermal relaxation showed that the most important at high altitudes seems to be the short lifetime of the ion against recombination, after which it is replaced by a new ion. The new ion has a rotational temperature slightly less than the kinetic, and a vibrational "temperature" slightly higher. As photons are scattered the vibrational "temperature" rises rather quickly but the rotation is affected only very slowly. After scattering only a few photons (as few as five or six on reasonable assumptions) the ion recombines. The kinetic temperature in the auroral rays cannot have been much below 2200° K, but the rays may possibly have been hotter than the normal atmosphere.

This work reverses the accepted conclusion that the vibration of the ions is in radiative equilibrium in sunlit auroral rays. Earlier spectra did not have high enough dispersion to show the large rotational temperature which causes neighboring bands to overlap. It appears that "low-latitude" aurora requires the same correction, and also others for blending with atomic lines. With these corrections this type of aurora gives results very similar to those found in this paper.

ACKNOWLEDGMENTS

This investigation was greatly aided by a number of people whose contributions are appreciated. H. J. Koenig operated the spectrographs and the unique spectra resulted from his excellent guiding. The synthetic spectrum of Fig. 4 was calculated by A. E. Johanson. Contributions to the interpretation were made by J. F. Noxon, J. W. Chamberlain, and especially D. R. Bates.

REFERENCES

BARBIER, D. 1947. Ann. géophys. **3**, 227.
BATES, D. R. 1949*a*. Proc. Roy. Soc. (London), A, **196**, 217.
——— 1949*b*. Proc. Roy. Soc. (London), A, **196**, 562.
BATES, D. R., MCDOWELL, M. R. C., and OMHOLT, A. 1957. J. Atmospheric and Terrest. Phys. **10**, 51.
CANAVAGGIA, R. and CHALONGE, D. 1946. Ann. astrophys. **9**, 143.
CANAVAGGIA, R., CHALONGE, D., EGGER-MOREAU, M., and OZIOL-PELTEY, H. 1950. Ann. astrophys. **13**, 355.
CARLETON, N. P. 1957. Phys. Rev. **107**, 110.
CHAMBERLAIN, J. W. and MEINEL, A. B. 1954. The earth as a planet, *edited by* G. P. Kuiper (University of Chicago Press).
CHILDS, W. H. J. 1932. Proc. Roy. Soc. (London), A, **137**, 641.
CLARK, K. C. and BELON, A. E. 1959. J. Atmospheric and Terrest. Phys. **16**, 205.
FAIRE, A. C. and CHAMPION, K. S. 1959. Phys. Rev. **113**, 1.
FAN, C. Y. 1956. Phys. Rev. **103**, 1740.
HERZBERG, G. 1950. Spectra of diatomic molecules (D. Van Nostrand Co., Inc., New York).
HUNTEN, D. M. 1955. J. Atmospheric and Terrest. Phys. **7**, 141.
HUNTEN, D. M., KOENIG, H. J., and VALLANCE JONES, A. 1959. Nature, **183**, 453.
LYTLE, E. A. and HUNTEN, D. M. 1960. Can. J. Phys. **38**, 477.
MASSEY, H. S. W. and BURHOP, E. H. S. 1952. Electronic and ionic impact phenomena (Oxford University Press).

McKELLAR, A. 1942. Revs. Modern Phys. **14**, 179.
MICHARD, R. 1950. Bull. Astron. Inst. Netherlands, **11**, 227.
MINNAERT, M. 1953. The sun, *edited by* G. P. Kuiper (University of Chicago Press).
MINNAERT, M., MULDERS, G. F. W., and HOUTGAST, J. 1940. Photometric atlas of the solar spectrum (Sonneborg Observatory, Utrecht).
MIRONOV, A. V., PROKUDINA, V. S., and SHEFOV, N. N. 1959. Spectral electro-photometrical and radar researches of aurora and airglow (Academy of Sciences, Moscow).
NICOLET, M. 1959. Ann. géophys. **15**, 1.
OMHOLT, A. 1959. Geofys. Publikasjoner (Oslo), **20**, No. 11.
PETRIE, W. and SMALL, R. G. 1952. Astrophys. J. **116**, 433.
RAYLEIGH, Lord. 1922. Proc. Roy. Soc. A, **101**, 114.
ROESLER, F. L., FAN, C. Y., and CHAMBERLAIN, J. W. 1958. J. Atmospheric and Terrest Phys. **12**, 200.
SEATON, M. J. 1956. The airglow and the aurorae, *edited by* E. B. Armstrong and A. Dalgarno (Pergamon Press, London).
SHEPHERD, G. G. 1954. Scientific Report No. AR-16, U.S.A.F. Contract AF 19(122)-152. (University of Saskatchewan).
STÖRMER, C. 1939. Terrestrial Magnetism and Atmospheric Elec. **44**, 7.
——— 1955. The polar aurora (Oxford University Press).
SWINGS, P. 1941. Lick Observatory Bull. **19**, 131.
——— 1943. Monthly Notices Roy. Astron. Soc. **103**, 86.
——— 1949. The atmospheres of the earth and planets, *edited by* G. P. Kuiper (University of Chicago Press).
WALLACE, L. V. and NICHOLLS, R. W. 1955. J. Atmospheric and Terrest. Phys. **7**, 101.

DAWN ENHANCEMENT OF AURORAL N_2^+ EMISSION[1]

E. A. Lytle and D. M. Hunten

ABSTRACT

The 0–0 band at 3914 Å was observed once per minute with a scanning spectrometer as sunlight illuminated the upper atmosphere on the morning of September 5, 1958. It is reasonable to assume that the density of N_2^+ ions was maintained constant during this time, and that the observed rise of intensity was due to resonance scattering of sunlight. The ions were found to be distributed between 180 and 320 km with peak at 250; density here was 12×10^4 ions/cm^3. There was some evidence for another layer at 120 km. Rotational temperatures measured while the main layer was fully illuminated agreed well and gave an average of $1060\pm100°$ K.

1. INTRODUCTION

Measurement of rotational temperature of N_2^+ bands in aurora has been carried out for many years. This experience has shown that it is difficult to find measurable aurora much above 100 km, most temperatures being below 400° K. Sunlit auroral rays are much higher (Störmer 1955) and are bright enough to give a good spectrum of the 0–0 band (3914 Å) in a short time. An accompanying paper (Vallance Jones and Hunten 1960) gives details of the measurements of high sunlit rays on September 4, 5, and 6, 1958, with a high-dispersion spectrograph. During the same display it was possible to observe continuously the dawn enhancement on September 5 with a scanning spectrometer at 1 spectrum/minute. There is reason to suppose that the N_2^+ density was maintained constant during the half-hour required for this enhancement; its vertical distribution can then be found by well-established methods used for twilight analysis. The ions were found to occupy a layer about 100 km thick; measurement of intensity gave a peak density of 12×10^4 ions/cm^3 at 250 km. The measured rotational temperature of 1060° K presumably applies to this mean height and should be essentially equal to the kinetic temperature of the atmosphere.

2. OBSERVATIONS

The spectrometer was used with a resolution of 2 Å, normal for rotational-temperature work with this instrument (Shepherd and Hunten 1955). It is usual to make scans lasting 10 seconds on aurora, but on this occasion the amplifier for the high-speed recorder was not working and it was necessary to use a slower one at 1 scan/minute. Fortunately, the aurora was unusually quiet, especially during the dawn enhancement; thus, the slow scans were no disadvantage and in fact gave improved sensitivity. The typical spectrum shown in Fig. 1 illustrates the low dispersion and appreciable noise level; but

[1]Manuscript received December 1, 1959.
Contribution from the Department of Physics, University of Saskatchewan, Saskatoon, Saskatchewan. Supported by the Geophysics Research Directorate of the Air Force Cambridge Research Center, Air Research and Development Command, under Contract No. AF 19(604)-1831.

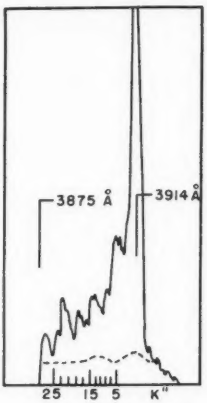

FIG. 1. Sample spectrum taken at a shadow height of 150 km. The estimated solar background is shown also.

the results are consistent from scan to scan and appear reliable. The region covered was from 3875 Å to somewhat past the head at 3914 Å; while this normally includes the whole of the 0–0 band, it did not do so this time because of the high temperature which was not recognized until later; lines with K'' greater than 26 were missed. It is now obvious that the filling in of the zero gap by the returning P branch indicates the high temperature immediately; normal aurora shows the gap clearly at the resolution used (Shepherd and Hunten 1955).

Towards morning the aurora was observed to be rather faint but with constant and fairly uniform intensity all over the sky. Scattered clouds were present but had no observable effect on the intensity, presumably because they were well illuminated by auroral light. The sky was fairly clear in the north; the spectrometer was left pointing in this direction at a zenith angle of 55°. Since the sun rises almost exactly in the east at this time of year, the shadow height for observations to the north is the same as in the zenith. The intensity as a function of shadow height is shown in Fig. 2, with an indication of time

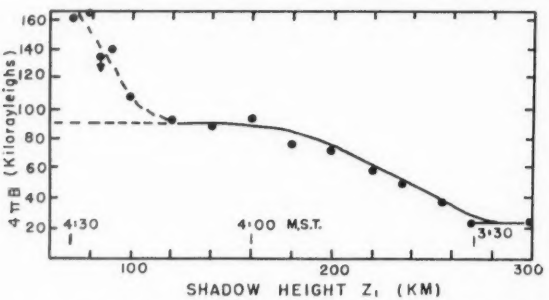

FIG. 2. Band intensity as a function of geometrical shadow height z_1. Mountain Standard Time (105th meridian) is also shown. Each point is an average of about five individual spectra.

as well. The intensity remained at 24 kilorayleighs (kR) for at least 20 minutes, until the shadow reached the 280-km level; it then steadily rose to 86 kR between 170 and 120 km. The further rise starting at 120 km seems to be real, but the measurements in this region are unreliable because a large continuous background had to be subtracted; it was equal to the band intensity at 90 km. The assumption that the enhancement was entirely due to resonance is seen to be reasonable, but it cannot be proved. Proof might have been obtained by measuring some other emission which does not come from a resonance transition, but this was not feasible.

Rotational temperatures were measured for the region 200 to 140 km when the intensity was nearly constant. The unresolved profiles were corrected for convergence of the lines as described by Shepherd and Hunten (1955). The plots of $\log(I/K')$ vs. $K'(K'+1)$ gave the expected straight line for K'' between 15 and 25; below 15 the returning P branch raises the intensity and this was observed. The effect is illustrated by Hunten, Koenig, and Vallance Jones (1959) for a higher temperature obtained during the same display. The spectra were averaged in four groups of 5 giving temperatures of 1100, 1125, 1000, and 1025° K; the average of these is 1060° K. As the shadow fell still more, the temperature seemed to rise still higher, but this measurement is even more unreliable than the intensity one at low shadow-heights, because even a small error in estimating the continuous background could give a large error in the temperature. The measurements given for the greater shadow-heights are not appreciably affected by this difficulty.

3. N_2^+ DENSITY AND DISTRIBUTION

To find the vertical distribution of N_2^+ ions we must differentiate the curve of Fig. 2; this can only be done roughly but at least the heights at which the derivative goes to zero are reasonably well defined. The symmetrical curve chosen is shown in Fig. 3. As for any twilight investigation, we also need to calculate the transmission of the lower atmosphere as a function of height above and below the geometrical shadow, since this gives the form of the shadow imposed on the incident sunlight. The calculation was done essentially as described by Hunten (1954) using an extinction coefficient of 0.040 per atmosphere (Allen 1955); this includes a small contribution from ozone which was lumped in with the rest since it is so small. Dust in the lowest atmosphere was represented by a coefficient of 0.042 per atmosphere falling off with a scale height of 1.0 km. Numerical differencing of the final table of T gave dT/dz_1 which we call $\dot{T}(z_1+x)$; z_1 is the geometrical shadow-height used in Section 2. $\dot{T}$ is plotted in Fig. 3; the center of mass is 29 km above the geometrical shadow and the second moment is 62 km^2. It has recently been shown (Hunten 1959) that the brightness derivative plotted against (z_1+29 km) as in Fig. 3 may be regarded as the ion distribution broadened by a "slit function" $\dot{T}$. From the relative breadths of these two curves it may be seen that the broadening is negligible considering the uncertainties in the observations, and this is confirmed by trying the sharpening procedure used for twilight sodium observations. Figure 3 thus gives the ion distribution directly. If the lower layer is really present, its height would be about $90+29\doteq 120$ km, a common height for aurora.

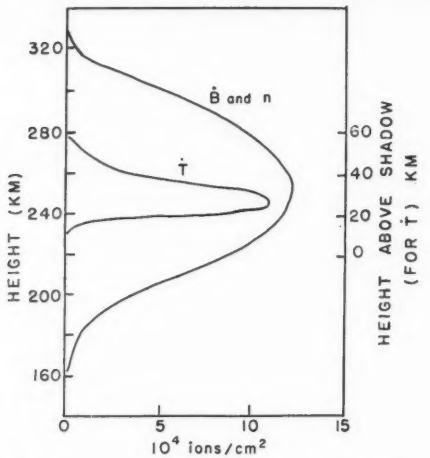

FIG. 3. $\dot{B}$, estimated derivative of Fig. 2 plotted against (z_1+29 km). $\dot{T}$, derivative of the transmission function plotted against the height above the geometrical shadow; this height is shown at the right. n, N_2^+ ion density (units of 10^4 ions/cm^3).

To find the total amount of N_2^+ we use the observation that resonance produced a brightness of 86−24 = 62 kR at a zenith angle of 55°. Presumably the same layer seen in the zenith would be fainter by the van Rhijn factor 0.616 calculated for a height of 250 km; this gives a zenith brightness of 38 kR. According to the Appendix, N_2^+ illuminated by sunlight scatters 0.068 quantum/ion sec; thus we have $(38/.068)\times10^9 = 5.6\times10^{11}$ ions/cm^2 (column). The half-thickness of the layer shown in Fig. 3 is about 90 km; thus, the average density is about 6×10^4 ions/cm^3 and the peak 12×10^4. This gives the ion-density scale in Fig. 3.

4. DISCUSSION

It should be repeated that most of this analysis rests on the assumption that the ion density remained constant during the 30 or 40 minutes taken by the shadow to sweep over the 200- to 300-km region. While this is plausible, there is no way of being sure without other measurements which were not made. The height distribution found is similar to that of high auroral rays, though we do not suggest that the observations were of ray structures, rather, of a sort of afterglow remaining from a night of unusually strong and high aurora. The high sunlit rays observed in the evenings of September 4 and 5 were presumably a somewhat different phenomenon; this is confirmed by their higher temperature of about 2300° K which suggests a higher altitude of around 500 km.

Our rotational temperature of 1060±100° K does not depend on the above assumption and seems reliable. This temperature is a reasonable one for a height of 250 km, and probably agrees with the kinetic temperature there as

suggested by the analysis of Vallance Jones and Hunten (1960). The N_2^+ ions apparently occupied a layer between 180 and 320 km with peak at 250. Their abundance was 5.6×10^{11} ions/cm^2 (column) and the peak density 12×10^4 ions/cm^3. These numbers were deduced from a brightness $4\pi B = 62$ kR for the dawn enhancement observed at a zenith angle of 55°.

If another opportunity comes to observe high sunlit aurora with a scanning spectrometer, the scan should if possible be extended to 3840 Å to include the lines of higher rotation. Since this type of aurora is not very bright but is rather quiet, 1-minute scans can be used and perhaps wider slits, 4 or 5 Å instead of 2 Å, preferred for normal aurora. The better resolution is required only for the region near the origin which is useless in high-temperature aurora because of the presence of high lines of the *P* branch.

If at all possible, a twilight series of the kind discussed here should be accompanied by measurements of a bright line or band which shows no resonance enhancement. This would allow a check on our assumption that the N_2^+ density remained constant during the twilight. A bright band of the N_2 second positive system would probably be best.

REFERENCES

Allen, C. W. 1955. Astrophysical quantities (Athlone Press, London), p. 116.
Bates, D. R. 1949. Proc. Roy. Soc. (London), A, **196**, 562.
Dalby, F. W. and Bennett, R. G. 1959. Symposium on molecular structure and spectroscopy, Ohio State University, Columbus.
Hunten, D. M. 1954. J. Atmospheric and Terrest. Phys. **5**, 44.
——— 1959. J. Atmospheric and Terrest. Phys. In press.
Hunten, D. M., Koenig, H. J., and Vallance Jones, A. 1959. Nature, **183**, 453.
Shepherd, G. G. and Hunten, D. M. 1955. J. Atmospheric and Terrest. Phys. **6**, 328.
Shull, H. 1950. Astrophys. J. **112**, 352.
——— 1951. Astrophys. J. **114**, 546.
Störmer, C. 1955. The polar aurora (Oxford University Press).
Vallance Jones, A. and Hunten, D. M. 1960. Can. J. Phys. **38**, 458.

APPENDIX

Scattering Power for the 0–0 Band of an N_2^+ Ion

The fundamental calculation of this quantity was made by Bates (1949). The ions were taken as having a rotational temperature of 273° K, and the exciting intensities at each line were found from the Utrecht Atlas of the solar spectrum. For the case in which collisions could be neglected, he found 0.13 quantum scattered per ion per second for the whole band system, and 60% of this in the 3914-Å band. An oscillator strength $f = 0.04$ was calculated and used. A rather larger value was calculated later by Shull (1950, 1951), but a recent measurement by Dalby and Bennett (1959) agrees better with Bates' result: $f = 0.0348\pm0.002$. Combining this with Bates' figure given above, we find a scattering power for the 0–0 band of 0.068 quantum/ion sec. This is not strictly correct for our much higher rotational temperature, but should not be greatly in error.

ROTATIONAL SPECTRUM OF $K^{39}F$ BY THE MOLECULAR BEAM ELECTRIC RESONANCE METHOD[1]

G. W. GREEN[2] AND H. LEW

ABSTRACT

Transitions between the $J = 0$ and $J = 1$ rotational states of $K^{39}F$ have been measured by means of the molecular beam electric resonance method. The following rotational constants have been determined (all frequencies in Mc/sec):

$$\begin{aligned} Y_{01} &\approx B_e & 8392.312 \pm 0.006 \\ -Y_{11} &\approx \alpha_e & 69.991 \pm 0.010 \\ Y_{21} &\approx \gamma_e & 0.204 \pm 0.005 \\ B_e & & 8392.482 \pm 0.070 \end{aligned}$$

The quadrupole interaction constants eqQ as measured in the $J = 1$ state are found to be

$$\begin{aligned} v = 0 \quad & -7.932 \pm 0.003 \text{ Mc/sec}, \\ v = 1 \quad & -7.835 \pm 0.010 \text{ Mc/sec}. \end{aligned}$$

The equilibrium internuclear distance obtained directly from B_e is

$$r_e = (2.17144 \pm 0.00005) \times 10^{-8} \text{ cm}.$$

The electric dipole moment in the $v = 0$ state is

$$\mu_E = (8.60 \pm 0.09) \times 10^{-18} \text{ e.s.u.}$$

INTRODUCTION

When the rotational spectrum of RbF was obtained in this laboratory (Lew *et al.* 1958), the remaining alkali halides for which the rotational constants were unknown were LiF, NaF, KF, and LiCl: these had all proved unsuitable for microwave absorption methods (Honig *et al.* 1954). Since KF was expected to have the lowest rotational frequencies among these molecules, it was the next one chosen for investigation. From the equilibrium internuclear distances calculated by Honig *et al.*, the $J = 1 \leftarrow J = 0$ frequency was estimated to be $17{,}400 \pm 175$ Mc/sec.

Potassium fluoride has been studied twice previously by beam methods: each time by observations of the radio-frequency transitions between Stark sublevels of particular rotational states. Grabner and Hughes (1950) obtained values for the quadrupole interaction energy eqQ_K* in the vibrational states $v = 0, 1, 2, 3, 4$, an estimate of the dipole moment and of the moment of inertia in the zeroth vibrational state, and also the vibrational constant ω_e from intensity measurements in several vibrational states. Schlier (1957)

[1]Manuscript received September 17, 1959.
Contribution from the Division of Pure Physics, National Research Council, Ottawa, Canada.
Issued as N.R.C. No. 5563.

[2]National Research Council Postdoctorate Fellow 1957–59. Now at the Department of Physics, University of Reading, Reading, England.

*In this work, the quadrupole interaction constant will be denoted by eqQ rather than eqQ/h, for instance, regardless of the units in which the quantity is expressed. This is consistent with the practice of using B_e for the equilibrium rotational constant no matter whether it is given in ergs, cm^{-1}, or Mc/sec.

obtained more accurate values for the quadrupole interaction using a multipole version of the electric resonance apparatus to refocus $J = 1, 2$, and 3 states and also obtained values for the spin–rotation $(I.J)$ interaction constants C, for both the F and K nuclei.

In the present experiment, through the observation of $J = 1 \leftarrow J = 0$ transitions, we have obtained the molecular rotational constants B_e and α_e and the electric dipole moment μ_E and also obtained quadrupole interaction constants in agreement with those of Grabner and Hughes and Schlier.

THEORY

The rotational spectrum obtained in this experiment is analyzed by means of Dunham's expressions for the energy levels of a vibrating rotator. The frequencies of the rotational transitions in the first four vibrational states in the absence of hyperfine structure (h.f.s.) are given in terms of the Dunham coefficients by Dunham (1932) and are restated by Lew *et al.* (1958). In order to use these expressions, the h.f.s. of the $J = 1$ state must be taken into account. The major contribution to h.f.s. in KF is due to the quadrupole moment of the K^{39} nucleus which has a spin of 3/2; fluorine, with spin 1/2, has no quadrupole moment. The h.f.s. pattern due to the K^{39} quadrupole was determined with the aid of the table of Casimir's function given by Townes and Schawlow (1955, Appendix I, p. 517) and with the aid of the experimental results of Schlier (1957) or of Grabner and Hughes (1950). First-order separations were found to be 1.5 to 2 Mc/sec; second-order energies were in no case greater than 0.1 kc/sec and were quite negligible (Townes and Schawlow 1955, Appendix II, p. 517). Further h.f.s. arises from the spin–rotation $(I.J)$ interactions for both nuclei. Schlier's values for these interaction constants are

$$C_F = +10.55 \pm 0.07 \text{ kc/sec},$$

$$C_K = 0.380 \pm 0.097 \text{ kc/sec}.$$

Neglecting the potassium $I.J$ interaction, we find for the h.f.s. of the $J = 1$ state the pattern shown in Fig. 1. The magnitude of the $I_F.J$ splitting has been calculated from eq. 8 of Nierenberg, Rabi, and Slotnick (1948). This shows that the maximum splitting occurs in line Y and is approximately 12.7 kc/sec. It was expected that such a splitting would be observed and although a splitting did appear in some traces it was not reproducible consistently and could not be attributed unambiguously to the $I.J$ interaction.

The electric dipole moment may be determined by observing the change in transition frequencies on application of a static voltage to the C field. The most suitable line for this measurement is line Z (Fig. 1). From eq. 10-31 of Townes and Schawlow (1955, p. 261), the $F_1 = 1/2$ level of $J = 1$ is neither split nor shifted by a weak field. Thus the only change in the transition frequency arises from a shift of the $J = 0$ level. This is given by (eq. 10-19, Townes and Schawlow)

$$\Delta W_{J=0} = -\mu_E^2 E^2 / 6B_e. \tag{1}$$

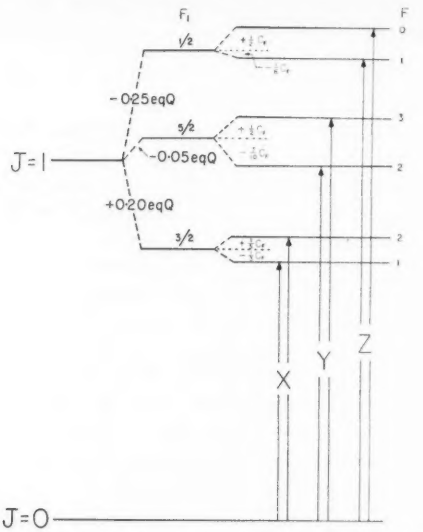

FIG. 1. Energy levels of the $J = 0$ and $J = 1$ rotational states of $K^{39}F$. $F_1 = J + I_K$, $F = F_1 + I_F$.

Using Grabner and Hughes' estimate of μ_E it is seen that C fields of up to 30 volts/cm produce shifts of less than 0.5 Mc/sec and satisfy the "weak field" condition that

$$\mu_E^2 E^2 / B_e \ll eqQ.$$

APPARATUS

The apparatus has been described by Lew *et al.* (1958). The previously used FP-54 d-c. amplifier was replaced by an Applied Physics Corporation vibrating reed electrometer (model 31) using a 5×10^{10}-ohm input resistor and taking the electrometer output via an integrating circuit to a Leeds and Northrup 20-millivolt pen recorder. This system gave an over-all sensitivity of 1 inch per 5×10^{-14} ampere although it was usually employed at 1/3 or 1/10 of this sensitivity. The surface ionization detector was a specially treated tungsten wire* in which the potassium contamination had been largely removed. The background ion current from the special wire, though still appreciable, was much less than that from commercial tungsten wires. Under our experimental conditions the best signal-to-noise ratio was obtained with an oxidized tungsten wire at a temperature of about 1150° K. The absolute detection efficiency at this temperature is not known. After oxidation the efficiency was found to decrease slowly over the course of several hours. Hence a capillary supply of air to the filament was provided to permit periodic re-oxidation without loss of vacuum.

*This wire was kindly supplied by Mr. E. P. Kilroy, General Electric Company, Cleveland, Ohio.

An attempt was made to improve the signal-to-noise ratio by chopping the beam at 15 cycles/sec and using a tuned a-c. amplifier, integrator, and recording system. This had very poor sensitivity except at high-filament temperatures where filament noise was prohibitive. The poor efficiency was attributed to the filament time constant being greater than the chopping period and the inverse dependence of this time constant on the filament temperature.

ELECTRONIC EQUIPMENT

Two modifications were made to the arrangement described by Lew *et al.* (1958). The first was the replacement of the Varian X-12 klystron by a Sperry 2K39 for measurements on the $v = 0$ transitions. This change was necessary because the Varian klystron had a large bandwidth at the higher frequency end of its range. Since the Sperry klystron had a frequency range of 7,500 to 10,300 Mc/sec, it was necessary to feed the output into a crystal rectifier and use the second harmonic for the inducement of transitions. The second modification was the conversion of the frequency multiplier chain to give an output at 540 Mc/sec instead of 270 Mc/sec. The sequence of multiplications is then 1–5–10–30–60–180–540 Mc/sec. The 31st harmonic and associated markers could then be used for klystron stabilization and frequency measurement rather than the much weaker 62nd harmonic of 270 Mc/sec.

The klystron control remained the same as that used by Lew *et al.* but since a recording system was used, the tuning condenser of the frequency modulation receiver was driven by a synchronous motor rather than being set manually as previously.

EXPERIMENT

The production of a beam of KF molecules presented no difficulties: an oven temperature of 875° to 900° C as measured by an iron–constantan thermocouple produced an ion current at the detector of 2 to 3×10^{-9} ampere. Commercial KF:$2H_2O$ was used; a load of several grams filled the oven up to the bottom of the slit and was sufficient for a month's work.

The refocussed beam was found to be 2 or 3 times greater than the predicted fraction (1 part in 10^4) of the main beam; part of this is accounted for by states other than $J = 0$ being refocussed. Under the best conditions the refocussed beam was several times the magnitude of the residual beam, the residual beam being defined as that arriving at the detector with the stop-wire in position and the B field on but the A field off, the refocussed beam being defined as the increase in detected beam on switching on the A field.

The time constant of the detection system introduced a delay between a transition and its recording. This resulted in a difference between apparent transition frequencies measured in opposite directions of scan. As the rate of scan was sometimes as high as 1 kc/sec per sec, this difference could amount to 10 kc/sec or more. Consequently each quoted transition frequency is the result of averaging several scans in each direction and then taking the mean of the two averages.

Errors attached to quoted frequencies cover the range of measured values and are such as to give self-consistency for quantities such as eqQ calculated from several frequency differences.

RESULTS AND DISCUSSION

A. Observed Lines, Quadrupole Interactions

Rotational transitions belonging to the three vibrational states $v = 0, 1, 2$ were observed. These are listed in Table I. Typical recordings of several of these are shown in Fig. 2. These are all for the line $(J = 1, F_1 = 3/2) \leftarrow (J = 0)$

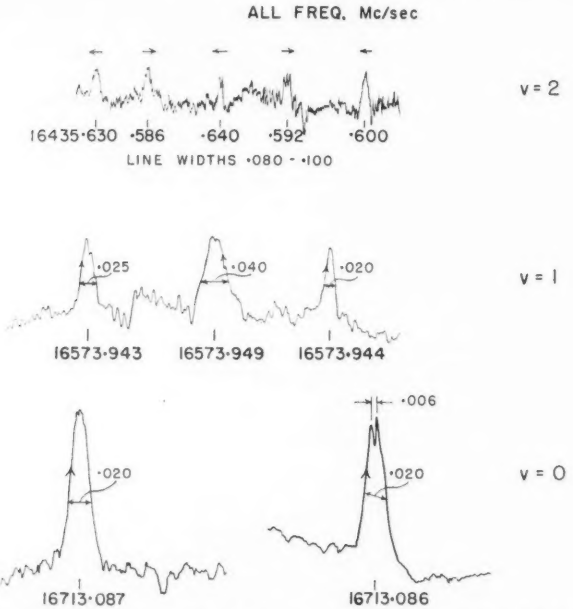

FIG. 2. Some typical transitions in $K^{39}F$: the line $(J = 1, F_1 = 3/2) \leftarrow (J = 0)$ for $v = 0$, 1, 2. For a given vibrational state the successive peaks shown are repeated observations of the same line, the arrows indicating the direction of increasing frequency scan. The frequencies shown are not corrected for a departure of about 5 parts in 10^7 of the 1 Mc/sec standard from its nominal value. The correction is made in the values tabulated in Table I.

for the three observed vibrational states. It can be seen how the signal-to-noise ratio decreases rapidly in the measurements of the higher vibrational states. The line width increases at the same time, probably because greater microwave power was required for the weaker lines. The .006-Mc/sec splitting shown in one of the $v = 0$ lines was initially ascribed to the $I_F.J$ interaction but attempts to reproduce it consistently were not successful. A similar but larger splitting was observed in line Y (Fig. 1). Since the splittings were not reproducible, they would not appear to be due to $I_F.J$ interaction. Their origin is not known. No correction is made for the effect of a finite C field caused by

contact potential as it is shown below that this amounts at most to 0.4 kc/sec and is therefore within the accuracy of our measurements.

TABLE I

Observed frequencies $J = 1 \leftarrow 0$ (Mc/sec)

Line	F_1 of $J = 1$ level	$v = 0$	$v = 1$	$v = 2$
Z	1/2	16,716.653±0.0015	16,577.462±0.005	
Y	5/2	16,715.067±0.001	16,575.897±0.005	16,437.542±0.010
X	3/2	16,713.083±0.001	16,573.936±0.005	16,435.599±0.010

The quadrupole interaction constants as measured in the $J = 1$ rotational state are given in Table II. The values obtained by Schlier and by Grabner and Hughes are shown for comparison. It is seen that good agreement exists in the cases of $v = 0$ and $v = 1$, where our results are obtained from all three

TABLE II

Values of eqQ (Mc/sec) as measured in the state $J = 1$

v	Schlier	Grabner and Hughes	This work
0	−7.9347±0.0011	−7.938±0.040	−7.932±0.003
1	−7.8391±0.0012	−7.828±0.040	−7.835±0.010
2	−7.7435±0.0013	−7.744±0.040	−7.772±0.055
3		−7.658±0.040	

lines, X, Y, and Z (Fig. 1). In the case of $v = 2$ where our result is obtained from the lines X and Y only, agreement is not so good but our result still overlaps that of Schlier within the large uncertainty quoted.

B. Rotational Constants

The positions of the rotational levels are determined in the absence of h.f.s. by the use of Fig. 1. In the case of $v = 2$ where there is considerable uncertainty in our value of eqQ, Schlier's value was used in conjunction with our measurement of the stronger line Y. The difference between the value so obtained and that obtained using our value of eqQ is only 1 kc/sec. The rotational transition frequencies unperturbed by h.f.s. are then as shown in Table III.

TABLE III

Calculated rotational transition frequencies in the absence of h.f.s. (Mc/sec) ($J = 1 \leftarrow 0$)

$v = 0$	16,714.670±0.002
$v = 1$	16,575.504±0.005
$v = 2$	16,437.155±0.010

The rotational constants calculated from these frequencies are shown in Table IV. For these calculations, use was made of the values of $Y_{10} \approx \omega_e = 400\ \text{cm}^{-1}$ and $Y_{20} \approx \omega_e x_e = 1.45\ \text{cm}^{-1}$ obtained by Barrow and Caunt

(1953) from ultraviolet absorption spectra. By assuming probable errors of 5% and 20% in these values of ω_e and $\omega_e x_e$, respectively, we obtain $B_e = Y_{01} + (0.170 \pm 0.068)$ Mc/sec. Thus the quoted error in B_e arises almost entirely from the errors in the vibrational constants.

TABLE IV

Rotational constants of $K^{39}F$ (Mc/sec)

$Y_{01} \approx B_e$	8392.312 ± 0.006
$-Y_{11} \approx \alpha_e$	69.991 ± 0.010
$Y_{21} \approx \gamma_e$	0.204 ± 0.004
B_e	8392.482 ± 0.070

C. Internuclear Distance

By using the relation $B_e = \hbar^2/2I$ we may obtain the value of the moment of inertia

$$I = (99.9809 \pm 0.0036) \times 10^{-40} \text{ g cm}^2.$$

In order to obtain the equilibrium internuclear distance r_e, it is usual to assume that the reduced mass μ, obtained from the atomic weights of the atoms concerned, may be substituted in the equation $I = \mu r_e^2$. The value we obtain in this way is

$$r_e = (2.17144 \pm 0.00005) \times 10^{-8} \text{ cm}$$

where the error arises almost entirely from those in Planck's constant and the atomic mass unit (Cohen *et al.* 1955). Although this calculation neglects several electronic effects in the molecule the above value of r_e is probably the best one obtainable in the absence of an exact knowledge of the molecular wave functions. The electronic effects neglected are:

(*i*) *The Ionic Nature of the Molecule*

The reduced mass of an ionic molecule cannot be obtained from the neutral atomic masses in the usual way because of the displacement of the valency electron. If we calculate the extreme case of this effect, where the valency electron is considered to be at the fluorine nucleus, we find that the change in r_e only amounts to -0.00002×10^{-8} cm which is negligible when compared with the experimental error in r_e.

(*ii*) *Electron Slip during Molecular Rotation*

This may occur both in valency electrons and in electrons bound to specific nuclei. Valency electrons having a spherical distribution about the molecular center of mass will be undisturbed by molecular rotation. Closed shells of electrons having a spherical distribution about a nucleus will follow the nucleus during molecular rotation but their orientation will remain fixed in space. However, in an ionic molecule, polarization will distort such spherical shells and the slip will be reduced.

We have calculated the contribution to the moment of inertia of the slip of bound electrons by use of eq. 8-34 of Townes and Schawlow. By assuming that no polarization exists and that all electrons are distributed in spherical

shells about their respective nuclei we are able to find the maximum contribution of this type of slip. The equilibrium internuclear distance then becomes

$$r_e^* = 2.17113 \times 10^{-8} \text{ cm}$$

which differs from the previous value by 1 part in 10^4. Because of the approximations used in the above treatment, no great reliance can be attached to this value and the previous value of r_e obtained directly from B_e will be used in the remaining discussion.

It is of interest to note that our observed value of r_e is approximately 2% higher than that calculated by Honig *et al.* on the basis of an empirical relation which they had found to be accurate to 1% in all other cases of alkali halides. This unexpectedly large discrepancy led to a considerable waste of time in the search for KF transitions, as it did for Barrett and Mandel (1954) with the high-temperature microwave spectrometer.

Pauling (1956) has published a treatment of interatomic distances in alkali halide gas molecules which is simpler than that of Honig *et al.* By using the Born expression for the repulsive potential between two ions and neglecting any polarization effects, Pauling has derived a simple formula for r_e in terms of ionic radii r^+ and r^- which had been previously obtained for crystals (Pauling 1948):

$$r_e = (r^+ + r^-)(0.291)^{1/(n-1)}$$

where n is the Born exponent of repulsive potential and $(0.291)^{1/(n-1)}$ is the factor representing the ratio of distances in the vapor and crystalline phases (see Honig *et al.* 1954, p. 638). He then assumes that n, which varies from molecule to molecule, may be written as $n = n^+ + n^-$, where n^+ is to be associated with the positive ion and n^- with the negative. Apparently by using 8 out of the 15 experimental values of r_e which were known at the time of his writing, he was able to assign values to the n^+'s for all the alkalis and to the n^-'s for all the halides. With these he was then able to calculate values of r_e for the other seven molecules which turned out to be in better agreement with experiment than Honig's; this is not surprising considering the number of standards used. Pauling's calculated values are shown in Table V along with the experimentally observed values. For comparison, values calculated by Honig *et al.* and by Krasnov (1959) are also included. As his standards, Pauling had presumably chosen the five bromides and CsF, KCl, and KI, for we were able to reproduce his calculated values most closely using these standards. The n^+ and n^- we used are not identical with Pauling's but it is believed that the latter had rounded his numbers off to the first place after the decimal. The values we used are $n^+ = 4.004$, 4.690, 4.656, 4.520, 4.189 for Li^+, Na^+, K^+, Rb^+, and Cs^+ respectively and $n^- = 2.073$, 3.949, 4.500, 5.299 for F^-, Cl^-, Br^-, and I^- respectively. It should be pointed out that the n^+ and n^- are not uniquely determined by the experimental data; other sets are permissible.

From Table V it can be seen that Pauling's calculated internuclear distances for the fluorides are not in very good agreement with the experimental values.

TABLE V

Comparison between experimental and calculated equilibrium internuclear distances in alkali halide gas molecules (in units of 10^{-8} cm)

	Experimental	Honig *et al.*	Pauling	Present authors using Pauling's method	Krasnov
LiF	1.51±0.08	1.527	1.518	1.527	1.584
NaF	—	1.840	1.833	1.856	1.917
KF	2.171	2.129	2.130	2.154	2.166
RbF	2.265	2.246	2.239	2.265(s)	2.259
CsF	2.345	2.346	2.345(s)	2.370	2.345(s)
LiCl	—	2.022	2.027		2.037
NaCl	2.361	2.356	2.353		2.361(s)
KCl	2.667	2.667(s)	2.667(s)		2.667(s)
RbCl	2.787	2.793	2.790		2.787(s)
CsCl	2.906	2.911	2.916		2.906(s)
LiBr	2.170	2.166	2.170(s)		2.170(s)
NaBr	2.502	2.500	2.502(s)		2.503
KBr	2.821	2.815	2.821(s)		2.821(s)
RbBr	2.945	2.944	2.945(s)		2.948
CsBr	3.072	3.065	3.072(s)		3.075
LiI	2.392	2.392	2.392		2.385
NaI	2.712	2.727	2.722		2.719
KI	3.048	3.051	3.048(s)		3.048(s)
RbI	3.177	3.182	3.174		3.180
CsI	3.315	3.307	3.306		3.315

NOTE: The quantities with (s) after them are those used as standards.

If instead of CsF we use RbF as the standard for the fluorides we get the values given in the fifth column in Table V. The average agreement with experiment for the fluorides is improved while for all the other alkali halides the agreement is unchanged. More recently, Krasnov (1959) has adapted the empirical relation of Honig *et al.* and obtained the best agreement so far between calculated and experimental values of the interatomic distances in alkali halide gas molecules.

He uses the equation

$$r_e = r_1 + r_2 - \frac{4(\alpha_1+\alpha_2)}{(n-1)(r_1+r_2)}$$

where α_1 and α_2 are the polarizabilities of the two ions, n is the Born exponent, and r_1 and r_2 are no longer the crystal ionic radii but are the ionic radii of free ions. A set of values of r_1 and r_2 are obtained by using certain experimental values of r_e as standards in much the same way as Pauling obtained his sets of n^+ and n^-. Once the r_1's and r_2's are known then the r_e's for the remaining molecules may be calculated. These values are shown in Table V. The improved agreement, particularly for the fluorides is immediately noticeable, the values predicted for RbF and KF agreeing to within 0.006×10^{-8} cm. It is therefore believed that Krasnov's results would be the most reliable for predicting transition frequencies of the remaining alkali halides (LiF, NaF, and LiCl).

D. Dipole Moment

As was mentioned earlier, the line Z was chosen for the measurement of the electric dipole moment in the $v = 0$ state. Static voltages of up to 12 volts

were applied to the C field in which the gap was 0.69065 cm. The shift Δf in the frequency of the line was measured with the static voltage first in one direction and then in the other. For $V_c = +12$ volts, $\Delta f = 0.122 \pm 0.002$ Mc/sec, for $V_c = -12$ volts, $\Delta f = 0.103 \pm 0.002$ Mc/sec. The difference between the two frequency shifts is caused by the contact potential of the C field. For this particular measurement the contact potential was 0.51 ± 0.09 volt. The electric dipole moment in the $v = 0$ state is then found by eq. 1 to be

$$\mu_E = (8.60 \pm 0.09) \times 10^{-18} \text{ e.s.u.}$$

This value may be compared with that of $(7.33 \pm 0.24) \times 10^{-18}$ e.s.u. obtained by Grabner and Hughes and of 8.07×10^{-18} e.s.u. calculated from Rittner's (1951) expression.

The contact potential of the C field is a variable quantity dependent upon the immediate history of the vacuum. Its highest measured value was 0.7 volt. This will affect the energy levels at nominally zero field. The $J = 0$ level shows the strongest dependence on the field and it is seen that for a field of 1.013 volts/cm corresponding to a contact potential of 0.7 volt, the shift in this level is 0.00038 Mc/sec. This is considerably smaller than frequency measurement errors in this experiment.

Although the values of the individual quantities μ_E and r_e (or B_e) as given by Grabner and Hughes have been shown to be in considerable error, it is of interest to note that the value they get for the composite quantity $\hbar^2\mu_E^2/2B_e$ is in excellent agreement with ours. They quote $\mu_E = (7.33 \pm 0.24) 10^{-18}$ e.s.u., $\hbar^2/2B_e = (138.4 \pm 6.9) 10^{-40}$ g-cm^2. Hence, ignoring the stated uncertainties for reasons given below the Grabner and Hughes' value is

$$\hbar^2\mu_E^2/2B_e = 7436 \times 10^{-76} \text{ g.cm}^2\text{.e.s.u.}^2$$

while we find (this work)

$$\hbar^2\mu_E^2/2B_e = 7394 \times 10^{-76} \text{ g.cm}^2\text{.e.s.u.}^2.$$

This agreement is not surprising. The frequency of the ΔM_J transition they observed is expresssible in the form (Hughes 1949)

$$\Delta f(1,0 \rightarrow 1, \pm 1) = \alpha E^2 - \beta E^4 + \gamma E^6$$

where E is the strength of the electric field in which the transition takes place:

$$\alpha = \frac{0.15}{h}\left(\frac{\mu_E^2}{B_e}\right), \qquad \beta = \frac{0.01076}{h}\left(\frac{\mu_E^4}{B_e^3}\right), \qquad \gamma = \frac{0.00125}{h}\left(\frac{\mu_E^6}{B_e^5}\right).$$

Thus it is seen that if the departure of the observed frequency from a quadratic dependence on E is small, i.e. if $\alpha \gg \beta$, then α may be determined with much greater accuracy than β. Since α immediately yields a value for μ_E^2/B_e while a knowledge of β is required for the extraction of the individual quantities μ_E and B_e, it is seen why the above agreements and discrepancies have occurred. For this reason too, the uncertainties quoted by Grabner and Hughes for the individual quantities cannot be carried over to the quantity $\hbar^2\mu_E^2/2B_e$.

If we substitute the accurate value of B_e found in the present work into the quantity $\hbar^2\mu_E^2/2B_e$ as found by Grabner and Hughes, we find

$$\mu_E = 8.63\times10^{-18} \text{ e.s.u.}$$

which agrees with our value very well.

The dipole moments of most of the alkali fluorides and of the alkali chlorides are now known. These are shown in Table VI (following Kusch and Hughes (1959), but with some later entries). It should be noted that for the fluorides the dipole moment reaches a peak at RbF as one goes down the column from Li to Cs. The dipole moment of CsF is distinctly smaller than that of RbF or KF. This does not seem to be the case in CsCl as compared with KCl.

TABLE VI

Permanent electric dipole moments of alkali fluorides and chlorides in Debyes (for vibrational state $v = 0$)

	F		Cl	
Li	6.6±0.3	Braunstein and Trischka (1955)	5.9±1.3	Marple and Trischka (1956)
Na	—		8.5±0.2	Tate and Strandburg (1954)
K	8.60±0.09	Present work	10.48±0.05	Lee *et al.* (1953)
Rb	8.80±0.10	Lew *et al.* (1958)	—	
Cs	7.875±0.006	Trischka (1956)	10.42±0.02	Trischka (1956)

E. Relationships between the Rotational and Rotational–Vibrational Constants in the Alkali Halides

(i) B_e and α_e

By assuming that the potential energy of a diatomic molecule may be described by a Morse function, Pekeris (1934) obtained the relationship

$$\alpha_e = \frac{6\sqrt{\omega_e x_e B_e^3}}{\omega_e} - \frac{6B_e^2}{\omega_e}. \tag{2}$$

If in this relation we substitute values of ω_e and $\omega_e x_e$ as tabulated in Honig *et al.* (1954) we find for α_e the values indicated by crosses in Fig. 3. For comparison the experimental values are also plotted and are indicated by dots. It is seen that the experimental points fall very nearly on a straight line which satisfies the relation (with the variables in megacycles per second)

$$\alpha_e = 2.15\times10^{-4}B_e^{1.4}. \tag{3}$$

In the case of the calculated points, however, at least part of the scatter must be ascribed to uncertainties in ω_e and $\omega_e x_e$.

Equation 3 proved of considerable help in finding transitions in neighboring vibrational states once the first transition had been found, since from the simple theory of rotational transitions

$$f_{\substack{J-1\leftarrow 0\\ v \quad v}} = 2B_v = 2\,[B_e - \alpha_e(v+\tfrac{1}{2})].$$

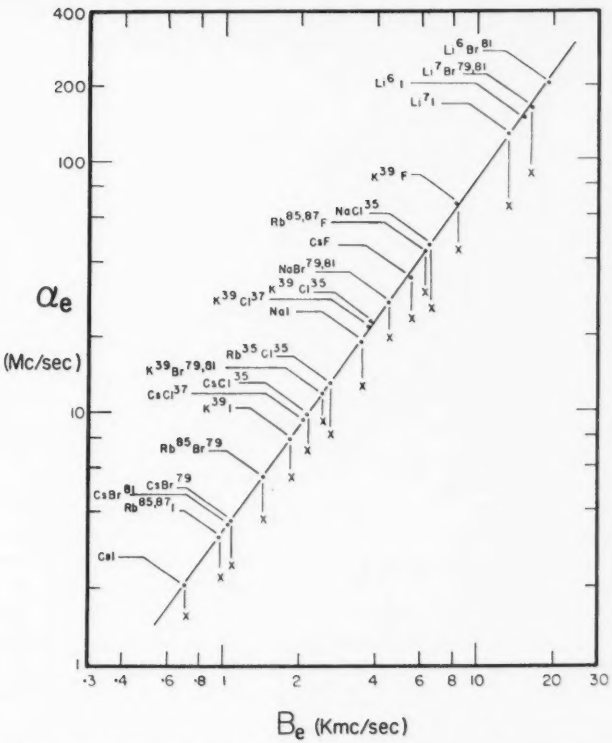

FIG. 3. A plot of α_e vs. B_e for the alkali halides. Except for RbF and KF, values are taken from Honig *et al.* The values of ω_e and $\omega_e x_e$ used in the calculated values of α_e are also from Honig *et al.* ● Experiment, × calculated.

(*ii*) B_e *and* γ_e

It is seen from Fig. 4 that the graph of log γ_e versus log B_e is also roughly linear in form but with considerable scatter. Expressing the variables in megacycles per second, the plot may be represented by the relation

$$\gamma_e = 1.16\times10^{-8}B_e^{1.85}. \tag{4}$$

From the figure again it can be seen that the CsF point deviates from the mean line by a much larger amount than any of the other points. The possibility of an error is suggested. An examination of the experimental data of Honig *et al.* shows that, with their errors of from 0.2 to 1.0 Mc/sec in the measured transition frequencies, the error in the value of γ_e can be much larger than as stated by the authors. Whether the accurately linear dependence of log α_e on log B_e and the similar though less accurate one between log γ_e and log B_e has any fundamental significance or not is not known.

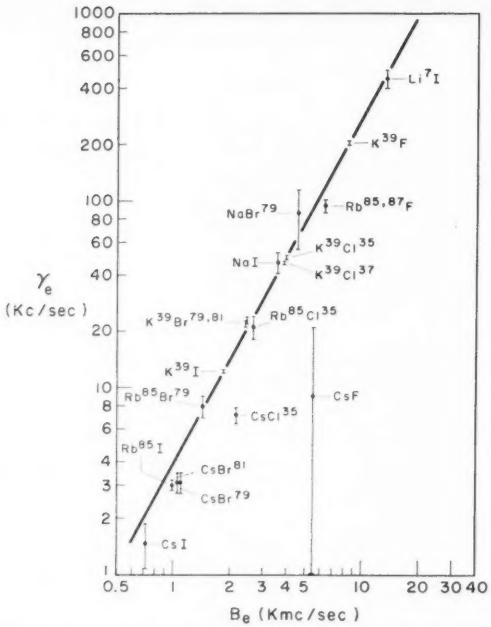

FIG. 4. A plot of γ_e vs. B_e for the alkali halides. Except for RbF and KF, values are taken from Honig *et al.*

REFERENCES

BARRETT, A. H. and MANDEL, M. 1954. Columbia Radiation Laboratory Quarterly Report, Jan. 30, p. 18.

BARROW, R. F. and CAUNT, A. D. 1953. Proc. Roy. Soc. (London), A, **219**, 120.

BRAUNSTEIN, R. and TRISCHKA, J. W. 1955. Phys. Rev. **98**, 1092.

CARLSON, R. O., LEE, C. A., and FABRICAND, B. P. 1952. Phys. Rev. **85**, 784.

COHEN, E. R., DRUMMOND, J. M. W., LAYTON, T. W., and ROLLETT, J. S. 1955. Revs. Modern Phys. **27**, 363.

DATZ, S. and TAYLOR, E. H. 1956. J. Chem. Phys. **25**, 395.

DUNHAM, J. L. 1932. Phys. Rev. **41**, 721.

GRABNER, L. and HUGHES, V. 1950. Phys. Rev. **79**, 819.

HONIG, A., MANDEL, M., STITCH, M. L., and TOWNES, C. H. 1954. Phys. Rev. **96**, 629.

HUGHES, H. K. 1947. Phys. Rev. **72**, 614.

——— 1949. Phys. Rev. **76**, 1675.

KRASNOV, K. C. 1959. Zhur. Neorg. Khim. **4**, 530.

KUSCH, P. and HUGHES, V. W. 1959. Handbuch der Physik, Vol. 37 (Springer-Verlag, Berlin), p. 1.

LEE, C. A., FABRICAND, B. P., CARLSON, R. O., and RABI, I. I. 1953. Phys. Rev. **91**, 1395.

LEW, H., MORRIS, D., GEIGER, F. E., Jr., and EISINGER, J. T. 1958. Can. J. Phys. **36**, 171.

MARPLE, D. T. F. and TRISCHKA, J. W. 1956. Phys. Rev. **103**, 597.

NIERENBERG, W. A., RABI, I. I., and SLOTNICK, M. 1948. Phys. Rev. **73**, 1430.

PAULING, L. 1948. Nature of the chemical bond, 2nd ed. (Cornell University Press, Ithaca, N.Y.).

——— 1956. Proc. Natl. Acad. Sci. India, A, **XXV**, 1.

PEKERIS, C. L. 1934. Phys. Rev. **45**, 98.

RITTNER, E. S. 1951. J. Chem. Phys. **19**, 1030.

SCHLIER, C. 1957. Z. Physik, **147**, 600.

TATE, P. A. and STRANDBURG, M. P. 1954. J. Chem. Phys. **22**, 1380.

TOWNES, C. H. and SCHAWLOW, A. L. 1955. Microwave spectroscopy (McGraw-Hill Book Co., Inc.).

TRISCHKA, J. W. 1956. J. Chem. Phys. **25**, 784.

SPIN–LATTICE RELAXATION EFFECTS OBSERVED IN THE CONTINUOUS POWER SATURATION OF PARAMAGNETIC LINES[1]

G. V. Marr and Prem Swarup[2]

ABSTRACT

The dependence of the conventional saturation parameter on the incident microwave power is considered for Lorentzian-shaped paramagnetic lines and applied to a study of the $(-\frac{1}{2} \rightarrow +\frac{1}{2})$ transitions of Cr^{+++} in $K_3Co(CN)_6$ and Gd^{+++} in $La(C_2H_5SO_4)_3 \cdot 9H_2O$ at 9 kMc/sec and 4.2° K. It is shown that the experimental observations may be explained on the basis of a spin–lattice transition probability which depends on spin–photon interactions. Values of the effective spin–lattice relaxation times are compared with pulse technique determinations and estimates of the corresponding phonon relaxation times are also given.

I. INTRODUCTION

With the advent of the solid-state maser suggested by Bloembergen (1956) and successfully demonstrated by Scovil, Feher, and Seidel (1957) and others using magnetically dilute paramagnetic crystals, the need for a clearer understanding of the processes involved in the transfer of energy from the paramagnetic ion to the lattice is required for the development of other suitable maser materials. In particular, the processes involved which determine the spin–lattice relaxation times are important. The experiments of Bloembergen, Purcell, and Pound (1948) show that the relaxation of nuclear magnetic states can be adequately explained by the Bloch equations (1946) with the aid of spin–spin and spin–lattice relaxation times. The success of these experiments, in which the onset of non-linearity or saturation between the incident power and the absorbed power is measured, led to the application of similar techniques to electron paramagnetic resonance (Eschenfelder and Weidner 1953; Feher and Scovil 1957; Giordmaine, Alsop, Nash, and Townes 1958).

An alternative approach to the problem has also been successfully employed (Davis, Strandberg, and Kyhl 1958), in which the paramagnetic sample is subjected to a high-power pulse of radiation, sufficient to saturate the sample, and the regrowth of the absorption is followed by means of a small monitoring signal. The exponential rise of the peak of the absorption line allows a value of the spin–lattice relaxation time T_1 to be determined. Davis *et al.* have pointed out that the value of T_1 obtained by their experiment decreases with increase in monitoring power and that their low power values are much larger than continuous power saturation experiments performed under similar conditions. In an earlier paper, Strandberg (1958) indicated that T_1 may depend upon the degree of saturation present if phonons play a significant part in the relaxation process.

[1]Manuscript received December 10, 1959.
Contribution from the Eaton Electronics Research Laboratory, Department of Physics, McGill University, Montreal, Que.
[2]N.R.C. Postdoctorate Fellow, on leave of absence from the Institute of Applied Physics, University of Allahabad, India.

The purpose of the present paper is to report the results of measurements performed on some paramagnetic resonance lines over a range of continuous power levels and to show how the results may be interpreted on the basis of a spin–lattice transition probability which changes with the incident power on the paramagnetic crystal.

II. THEORY

The magnetic properties of a paramagnetic substance can be described in terms of the complex magnetic susceptibility, where the imaginary part, χ'', is responsible for the absorption of the microwave energy in the medium. χ'' at a frequency ν is given by

$$\chi''(\nu) = \tfrac{1}{2}\pi\chi_0\nu_0 Z g(\nu) \tag{1}$$

where χ_0 is the static susceptibility, $g(\nu)$ the shape factor of the line concerned, Z the saturation term, and ν_0 the frequency at peak absorption. Studies of the paramagnetic spectra of

$$Cr^{+++} \text{ in } K_3Co(CN)_6 \text{ and on } Gd^{+++} \text{ in } La(C_2H_5SO_4)_3 . 9H_2O$$

(Swarup 1959) have shown that for small paramagnetic ion concentrations the line shape is Lorentzian. The shape factor may thus be written as

$$g(\nu) = \frac{2T_2}{1+4\pi^2(\nu_0-\nu)^2T_2^2} \tag{2}$$

where T_2 is the spin–spin relaxation time and is related to the width $\Delta\nu$ of the unsaturated line at half-maximum absorption by

$$T_2 = (\pi\Delta\nu)^{-1}. \tag{3}$$

The saturation term Z is defined by

$$Z = \frac{N_1-N_2}{N_{10}-N_{20}} \tag{4}$$

where N_1 and N_2 refer to the ion populations of the lower and upper energy states respectively and N_{10} and N_{20} are the equilibrium values in the absence of microwave radiation.

In the nuclear magnetic resonance experiments, the assumption is made (Bloembergen, Purcell, and Pound 1948) that the lattice may at all times be considered in thermal equilibrium with the bath surrounding the sample. Under these conditions, the peak value of the differential of χ'' is given by

$$\left(\frac{d\chi''}{d\nu}\right)_{max} \alpha[1+\tfrac{1}{2}\gamma^2H_1^2T_1T_2]^{-3/2} \tag{5}$$

where H_1 is the magnetic component of the linearly polarized radio-frequency field and γ is the gyromagnetic ratio. Equation 5, or some similar expression, is normally employed for the determination of T_1 by determining $(d\chi''/d\nu)_{max}$ at very low microwave power and when it has decreased by some fraction of its low power value.

While the above assumption is applicable for nuclear magnetic resonance, it is not necessarily valid in electron paramagnetic resonance. For this reason, the saturation term Z should be derived in terms which do not invoke the concept of spin and lattice temperatures as an initial assumption.

The rate of change in the population difference under the influence of microwave power is given by

$$\frac{d(N_1-N_2)}{dt} = 2N_2W_{21}-2N_1W_{12}-2Y(N_1-N_2) \tag{6}$$

where W_{21} is the transition probability from the upper ionic state to the lattice and W_{12} the transition probability for the reverse process. Y is the transition probability for the stimulated emission and absorption of microwave radiation. The spontaneous transition probability can be neglected in that it is several orders of magnitude less than Y in this region of the spectrum. Under steady-state conditions, the rate of change of population is zero, thus enabling Z to be determined. By standard radiation theory, the value for Y for the $(-\frac{1}{2} \rightarrow +\frac{1}{2})$ transition is given by

$$Y = \tfrac{1}{4}\gamma^2H_1^2g(\nu). \tag{7}$$

Substituting for $Zg(\nu)$ in equation (1) and differentiating w.r.t. ν we obtain

$$\frac{d\chi''}{d\nu} = \frac{1}{2}\pi\nu_0\chi_0\frac{N_2}{N_{20}}\frac{(W_{21}/W_{12})-1}{(W_{21}^0/W_{12}^0)-1}\frac{16\pi^2T_2^3(\nu_0-\nu)}{[1+4\pi^2(\nu_0-\nu)^2T_2^2+(\frac{1}{2}\gamma^2H_1^2T_2/W_{12})]^2} \tag{8}$$

where W_{21}^0 and W_{12}^0 are the thermal equilibrium values of the spin–lattice transition probabilities when Y is zero. By differentiation of equation 8, the peak value of $(d\chi''/d\nu)$ may be obtained as

$$\left(\frac{d\chi''}{d\nu}\right)_{\max} = \frac{1}{2}\pi\nu_0\chi_0\frac{N_2}{N_{20}}\frac{(W_{21}/W_{12})-1}{(W_{21}^0/W_{12}^0)-1}\frac{3\pi T_2^2}{[1+(\frac{1}{2}\gamma^2H_1^2T_2/W_{12})]^{3/2}}. \tag{9}$$

An examination of equation 9 shows that at least in the early stages of saturation, any significant change in $(d\chi''/d\nu)_{\max}$ must come from within the square bracket and any suspected change of the spin–lattice relaxation time T_1 with saturating power will be indicated by a change in W_{12} itself since T_1 may be written as W_{12}^{-1}.

Van Vleck (1940) considered the spin of the paramagnetic ion to be coupled to the lattice through the mixing of second- and higher-order perturbations of the spin–orbit and orbit–lattice coupling. Such mixing gives rise to spin–lattice matrix elements which depend on the parameters of the spin and electronic state of the ion, and in addition, upon the phonon excitation expressed in terms of a phonon quantum number n. Under these conditions, W_{12} can be written in the form

$$W_{12} = \rho(\nu).A\langle n\rangle \tag{10}$$

where A is the spin transition probability per unit of phonon excitation, $\langle n\rangle$ is the mean phonon quantum number for phonons having a characteristic frequency ν, and $\rho(\nu)$ is the density of phonon modes.

The microwave frequency of 9 kMc/sec used in the experiments is well away from the upper limit for phonon frequencies imposed by the interatomic distances in the lattice and consequently $\rho(\nu)$ can be represented by the Debye approximation as

$$\rho(\nu) = \left[\frac{1}{v_l}+\frac{2}{v_t}\right]4\pi\nu^2 \tag{11}$$

where v_l and v_t are the longitudinal and transverse phonon velocities respectively. In the absence of microwave radiation, energy is exchanged between phonons due to crystal imperfections, the coupling via the paramagnetic ion spins, etc., and the n values tend to fluctuate about their respective equilibrium values $\langle n_0\rangle$. The probability of a phonon mode having an energy E is governed by a Bose–Einstein distribution, and consequently the thermal equilibrium value of $\langle n\rangle$ is given by

$$\langle n_0\rangle = \left[\exp\frac{h\nu}{kT}-1\right]^{-1}. \tag{12}$$

Under the influx of the microwave radiation, energy is transferred from the spins to the lattice and the rate of change of $\langle n\rangle$ can be written (Strandberg 1958)

$$\frac{d\langle n\rangle}{dt} = \frac{Y(N_1-N_2)}{V\rho(\nu)\Delta\nu}-\frac{\langle n\rangle-\langle n_0\rangle}{\tau} \tag{13}$$

where $\Delta\nu$ is the excitation width for phonons in direct contact with the spins and is probably of the same order or less than the width of the resonance line itself. In this paper it is assumed that the two widths are equal; consequently the same symbol ($\Delta\nu$) is used for both widths. τ represents an over-all relaxation time for phonons by way of phonon–phonon and phonon–bath interactions.

For the steady state saturation conditions required here, $d\langle n\rangle/dt$ is zero and the departure of $\langle n\rangle$ from its thermal equilibrium value $\langle n_0\rangle$ is

$$\Delta n = \frac{Y(N_1-N_2)}{V\rho(\nu)\Delta\nu}\tau \tag{14}$$

and W_{12} becomes

$$W_{12} = A\rho(\nu)\langle n_0\rangle\left(1+\frac{\Delta n}{\langle n_0\rangle}\right). \tag{15}$$

In the initial stages of saturation, a value for Δn may be obtained by assuming the spin populations do not differ appreciably from their thermal equilibrium values, then substituting for Y, W_{12} may be written

$$W_{12} = A\rho(\nu)\langle n_0\rangle\left[1+\frac{\frac{1}{2}\gamma^2T_2\tau(N_{10}-N_{20})H_1^2}{V\rho(\nu)\Delta\nu\langle n_0\rangle}\right]. \tag{16}$$

The expected dependence of $(d\chi''/d\nu)_{\max}$ on H_1^2, at least in the initial stages of saturation may therefore be written as

$$\left(\frac{d\chi''}{d\nu}\right)_{\max} \alpha\left[1+\frac{KH_1^2}{1+CH_1^2}\right]^{-3/2} \tag{17}$$

where

$$K = \frac{\frac{1}{2}\gamma^2 T_2}{A\rho(\nu)\langle n_0\rangle} = \frac{1}{2}\gamma^2 T_2 T_1^0 \tag{18}$$

and

$$C = \frac{\frac{1}{2}\gamma^2 T_2 \tau (N_{10} - N_{20})}{V\rho(\nu)\Delta\nu\langle n_0\rangle}. \tag{19}$$

The difference between equations 17 and 5 is that C may not be zero for paramagnetic resonance.

III. EXPERIMENTAL

A conventional X-band paramagnetic resonance spectrometer utilizing a magic-T impedance bridge was employed. Phase-sensitive detection and amplification of the signal allowed the resonance line to be displayed as a derivative on a Rectiriter chart recorder. The cavity operated in the TE_{102} mode situated between the pole pieces of a 6-in. Varian magnet in suitable low-temperature Dewars. The cavity and crystal were immersed in liquid helium at 4.2° K in order to obtain as good a coupling between the crystal and the low-temperature bath as possible. A 1000 c/s modulation on the magnetic field was kept below a peak-to-peak value of 0.5 oersted. The steady magnetic field was swept at the rate of 2 oersteds/minute and was controlled by the driving motor of the recorder. A Pound stabilized X-13 klystron was used for the low-power measurements and a Sperry 2K39 for high-power saturation measurements. The power entering the cavity was monitored by measuring the reflected power (P_r) by a Polytechnic 650-A universal power bridge. The power incident on the cavity (P_i) was variable over the range 1×10^{-6} to 5×10^{-2} watts.

In conjunction with the observations of other workers (Meyer 1955), an initial experiment showed that the width at half-maximum absorption of a powdered sample of the free radical diphenyl picryl hydrazyl did not change with P_i and that the peak value of the derivative, I_p, increased linearly with increase of P_i over the range of power available. The crystals under study were all of 0.1 cc or less in volume and were placed in the cavity along with a small sample of the powdered D.P.P.H. Values of I_p could then be obtained for both the paramagnetic crystal and D.P.P.H. under identical power conditions. Ratios of I_p for the paramagnetic crystal to I_p for D.P.P.H., made over the range of P_i available, enabled the saturation of the paramagnetic crystal to be measured. These ratios, normalized to unity at low power levels are representative of equation 17. Measurements of the width of the paramagnetic line at low power enabled T_2 to be determined. The relation between H_1^2 and P_i was obtained from

$$H_1^2 = \frac{32}{\Gamma^2\nu}\left(\frac{\lambda}{\lambda_g}\right)^2 Q_L P_i(1-\Gamma) \tag{20}$$

taken from Meyer (1955) for the field in a rectangular cavity. Q_L is the loaded

Q of the cavity of volume V' and Γ is the reflection coefficient. For the experiments reported here, $Q_L \sim 3000$ and $\Gamma = 0.66$ giving $H_1^2 = 1.6\ P_i$ where P_i is measured in watts.

The crystals studied were $K_3CoCr(CN)_6$ and $LaGd(C_2H_5SO_4)_3.9H_2O$ and were prepared by mixing known proportions by weight of the diamagnetic salt with its isomorphous paramagnetic salt, dissolving the mixture in distilled water, and growing the combined crystals by slow evaporation. By this means, crystals were obtained where the nominal percentage of the diamagnetic ions replaced by paramagnetic ions were 0.1%, 0.5%, and 1% for the Cr^{+++} ion and 1% for the Gd^{+++} ion. A determination of the actual percentage made in the case of the 1% crystals by Atomic Energy of Canada Ltd. by X-ray fluorescence showed that the actual concentrations were somewhat less than the nominal concentrations which are used to designate the crystals.

IV. RESULTS

The normalized peak absorption derivative ratios obtained for different values of the microwave power incident on the cavity are shown in Fig. 1 for

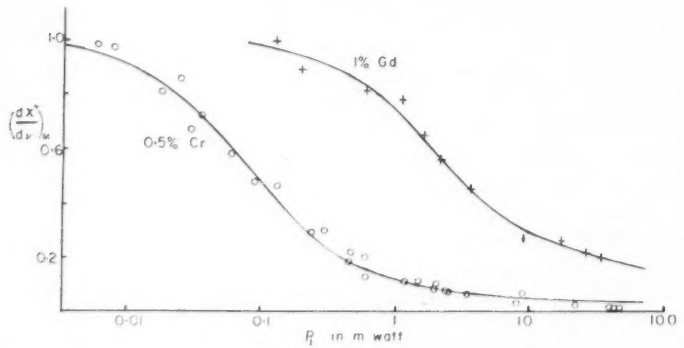

FIG. 1. The saturation of paramagnetic resonance lines at 4.2° K.
○ Experimental points for 0.5% Cr^{+++} in $K_3Co(CN)_6$.
+ Experimental points for 1.0% Gd^{+++} in $La(C_2H_5SO_4)_3.9H_2O$.
— Fitted theoretical curves of $\{1+[KH_1^2/(1+CH_1^2)]\}^{-3/2}$.

the $(-\frac{1}{2} \rightarrow +\frac{1}{2})$ transitions for the 0.5% Cr^{+++} ion and the 1% Gd^{+++} ion at 4.2° K. The full curves are plots of equation 17 with suitable values of K and C. A constant value for C was indicated from the experimental measurements with a slight departure for the 0.5% Cr^{+++} ion in the region of 10^{-2} to 10^{-1} watt range. This departure can be accounted for by the change in W_{21}/W_{12} and $N_1 - N_2$. The best fits to the experimental data were obtained with $K = 5600 \pm 100$ and $C = 525 \pm 50$ for the 0.5% Cr^{+++} ion and values of $K = 140 \pm 20$ and $C = 47 \pm 5$ for the 1% Gd^{+++} ion.

Attempts were made to extend the measurements on the Cr^{+++} ion to crystals which contained 0.1% and 1% nominal paramagnetic ion concentrations. In the former case, the very low powers needed for saturation and the decrease

in signal-to-noise ratio reduced the accuracy obtainable. In the case of the 1% crystal, an extension of the measurements to higher values of P_1 is required to determine C accurately.

Table I shows the experimental quantities obtained at 4.2° K. The values of T_1^0 are the inverse of the spin–lattice transition probabilities under thermal equilibrium conditions (W_{12}^0). Estimates of τ, the phonon–bath relaxation times, are obtained from the values of C assuming that the populations of the states concerned had not changed appreciably from thermal equilibrium values. Estimates of these populations were made with the aid of the actual concentrations available.

TABLE I

Experimental results at 4.2° K

Crystal*	ΔH, oersteds	T_2, sec	K	C	T_1^0, sec	τ, sec	A/sec
Cr 0.1%	6	2×10^{-5}	~12,500	~2,000	$\sim5\times10^{-3}$	10^{-6}	$\sim2\times10^{-4}$
Cr 0.5%	9	1.3×10^{-5}	5,600	525	2.2×10^{-3}	10^{-7}	4.5×10^{-4}
Cr 1.0% (.13)	14	0.8×10^{-5}	44	1–10	3.5×10^{-3}	10^{-8}–10^{-9}	3×10^{-2}
Gd 1% (.4)	20.8	0.6×10^{-5}	140	47	1.6×10^{-4}	10^{-7}	6×10^{-3}

*Actual concentrations shown in parentheses.

The change in effective T_1 with saturation is shown more clearly over a limited power range in Fig. 2. For C equal to zero, and consequently a constant

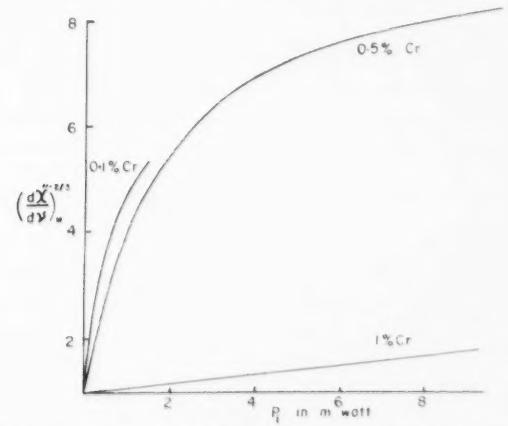

FIG. 2. Saturation curves of 0.1%, 0.5%, and 1.0% Cr^{+++} in $K_3Co(CN)_6$ at 4.2° K.

value of T_1, a straight line would be obtained. While this may be justified for the 1% Cr^{+++} ion at 4.2° K, it is by no means the case for the 0.1% and the 1% Cr^{+++} ion curves.

The absolute values of the relaxation times depend upon a large number of variables; however, they are probably correct to within an order of magnitude.

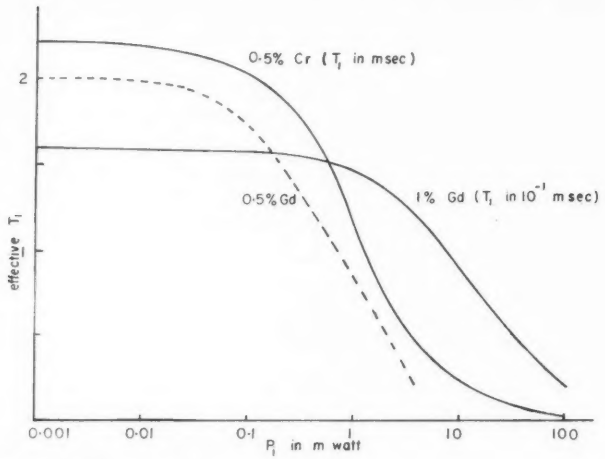

FIG. 3. Plots of effective T_1 with microwave power.
Full curves, 0.5% Cr^{+++} in $K_3Co(CN)_6$ and 1% Gd^{+++} in $La(C_2H_5SO_4)_3.9H_2O$ from continuous power saturation experiments.
Dotted curve: values obtained by Davis *et al.* (1958) for 0.5% Gd^{+++} in $La(C_2H_5SO_4)_3.9H_2O$.

The change in T_1 observed by Davis *et al.* for a crystal containing a nominal concentration of 0.5% Gd^{+++} in $La(C_2H_5SO_4)_3.9H_2O$, using their pulse technique and varying the monitoring power, is shown in Fig. 3 with the power level arbitrarily placed on the logarithmic scale (since the absolute power levels were not available). Also shown are the variations in the effective T_1 values for the 0.5% Cr^{+++} and the 1% Gd^{+++} obtained from the data in Table I. It appears likely that the same change is being observed in the two experiments. The absolute values of T_1 depend rather critically upon the concentration of the paramagnetic ion in the crystal. Table I indicates that T_1^0 decreases as concentration increases.

Since $\rho(\nu)$ and $\langle n_0 \rangle$ are computable it is possible to obtain an estimate of the spin–lattice transition probability per unit of phonon excitation which should depend only on the parameters of the spin and electronic state of the ion. These estimates are shown in Table I and it appears that the concentration of ions also affects the value of A. The phonon–bath relaxation times at 4.2° K also appear to change with concentration as shown in the table; whether they are in fact independent of the paramagnetic ion concerned, remains to be seen as more crystals are examined. The results obtained are in agreement with those suggested by Strandberg (1958) of less than 10^{-5} or 10^{-6} seconds.

Attempts were made to observe saturation of the crystals at liquid air temperatures but insufficient power was available to obtain very reliable results. They did, however, indicate that T_1^0 decreases as about T^{-1}. The phonon–bath relaxation times were not determinable at these temperatures.

ACKNOWLEDGMENTS

The authors are indebted to Professor G. A. Woonton, Director of the Laboratory, for his interest and advice, and to Professor L. Yaffe of the Chemistry Department for getting the crystals analyzed. The research was made possible by support from the Defence Research Board via Consolidated Grant No. 9512-20. One of us (P. S.) would also like to acknowledge the financial assistance received from the National Research Council of Canada while an N. R. C. Postdoctorate Fellow.

REFERENCES

BLOCH, F. 1946. Phys. Rev. **70**, 460.
BLOEMBERGEN, N. 1956. Phys. Rev. **104**, 324.
BLOEMBERGEN, N., PURCELL, E. M., and POUND, R. V. 1948. Phys. Rev. **73**, 679.
DAVIS, C. F., STRANDBERG, M. W. P., and KYHL, R. L. 1958. Phys. Rev. **111**, 1268.
ESCHENFELDER, A. H. and WEIDNER, R. T. 1953. Phys. Rev. **92**, 869.
FEHER, G. and SCOVIL, H. E. D. 1957. Phys. Rev. **105**, 760.
GIORDMAINE, J. A., ALSOP, L. E., NASH, F. R., and TOWNES, C. H. 1958. Phys. Rev. **109**, 302.
MEYER, J. W. 1955. M.I.T. Lincoln Lab. Report M35-46.
SCOVIL, H. E. D., FEHER, G., and SEIDEL, H. 1957. Phys. Rev. **105**, 762.
STRANDBERG, M. W. P. 1958. Phys. Rev. **110**, 65.
SWARUP, P. 1959. Can. J. Phys. **37**, 848.
VAN VLECK, J. H. 1940. Phys. Rev. **57**, 426.

γ-RADIATION AT AIR–GROUND INTERFACES WITH DISTRIBUTED Cs^{137} SOURCES*

C. E. CLIFFORD, J. A. CARRUTHERS,† AND J. R. CUNNINGHAM‡

For problems involving the γ-ray dose due to distributed sources it is important to take account of the scattering and absorption at the air–ground interface. In recent work at the Defence Research Chemical Laboratories (Clifford *et al.* 1959) measurements have been made that show the effects of different "ground" materials on the dose at varying heights and radial distances from a γ-source on the ground. Cs^{137} was used as the source since the γ-ray energy (0.66 Mev) is close to the average energy of γ-rays from fission "fall-out".

Some of the more important results of these measurements are given and it is also of interest to compare these results with calculations by Berger (1957) for somewhat similar conditions but for a higher photon energy of 1.28 Mev, corresponding to Co^{60} γ-rays.

Figure 1 shows the results of measurements made over smooth clay earth and compares the results to Berger's Monte Carlo calculations for 1.28 Mev in

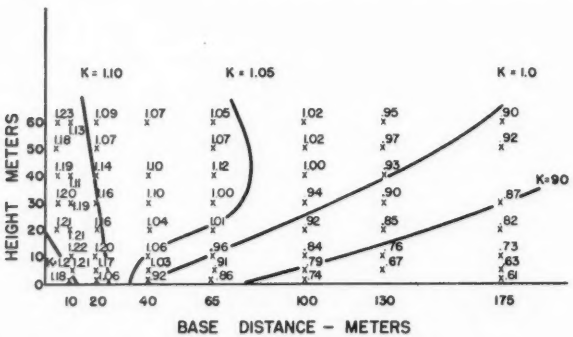

FIG. 1. Boundary correction factor K in air above smooth clay earth. ×, measured values with Cs^{137} at an air–ground interface; ——from Berger's calculations for Co^{60}.

which ground and air were assumed to have the same scattering properties per unit mass as water. The parameter K which appears is the factor by which the dose is altered by the presence of the denser medium. Since both Co^{60} and Cs^{137} γ-rays are in the energy region of Compton scatter for low and medium

*Issued as D.R.C.L. No. 296A.
†Present address: Department of Physics, McGill University, Montreal, Que.
‡Present address: Ontario Cancer Institute, Toronto, Ontario.

Z materials, it might be anticipated that K values calculated for 1.28 Mev would be little changed at 0.66 Mev when distances are expressed in mean free paths. At energies below the region of predominant Compton scatter, experimental K values would be expected to vary from those calculated at higher energies. Good experimental agreement with the calculations was reported by Titus (1958) at 1.28 Mev for a Co^{60} source at the plane boundary between media of steel wool and steel. The agreement shown in Fig. 1 for the lower energy γ-rays from Cs^{137} indicates the accuracy with which Berger's values could be used in fall-out analysis.

Similar K values, obtained from measurements made in a region of polyfoam (i.e. expanded polystyrene) of density 0.072 g/cc with a Cs^{137} source located at a polyfoam–concrete boundary, are shown in Fig. 2. Here the experimental K values shown were obtained by taking the ratio of the dose measured at the indicated base distance and height to the dose observed at an equivalent distance when the source and detector were embedded in polyfoam $3\frac{1}{2}$ feet above the polyfoam–concrete boundary.

Because Monte Carlo calculations were available (Berger 1957) giving K values for the limiting case of a source lying on the surface of a completely

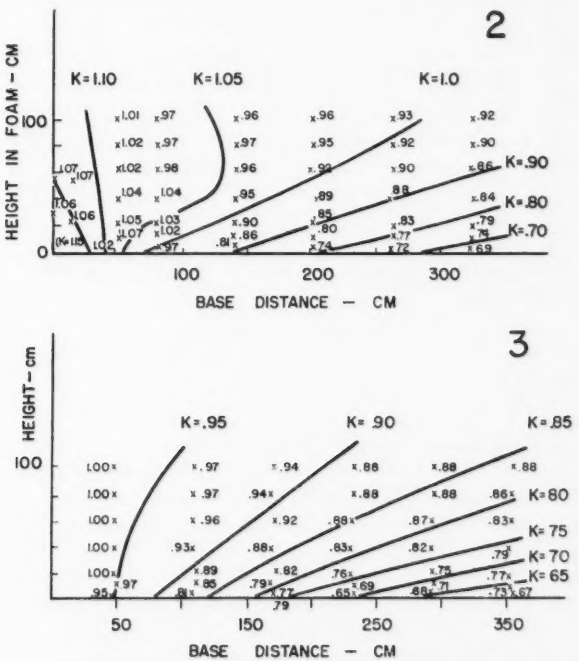

FIG. 2. Boundary correction factor K in polyfoam above concrete. ×, measured values with Cs^{137} at a concrete–polyfoam interface; ——from Berger's calculations for Co^{60}.

FIG. 3. Boundary correction factor K above a strongly absorbing medium. ×, measured values with Cs^{137} at a lead–foam interface; ——from Berger's calculations for Co^{60}.

absorbing medium, the polyfoam was used to obtain experimental values. This was done by stacking the polyfoam above a floor of lead bricks and measuring the dose at different distances and heights in the foam when a Cs^{137} source was placed on the surface between the lead and polyfoam. Since the ground is now an absorbing medium, the dose should be something less than the dose in an infinite polyfoam medium. The results are shown in Fig. 3 where the lines represent the Monte Carlo calculations for a Co^{60} source on an infinitely absorbing medium. The somewhat higher experimental K values are probably due to the use of a source of lower energy γ's than Co^{60} and to the extent to which the lead floor is not a perfect absorber. The trend of the K values is quite similar and further illustrates the reliability of Monte Carlo calculations.

The spectra of the collimated radiation received at various angles were measured and analyzed to give the dose received through a solid angle of 0.1 steradian as a function of the direction angle of a collimated detector located 1 meter above an air–ground interface uniformly contaminated with Cs^{137}. The resulting polar distribution of radiation is shown in Fig. 4 where the doses

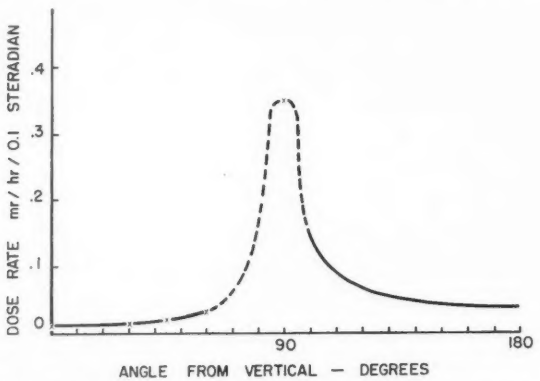

FIG. 4. Polar distribution of radiation. Dose rate per 0.1 steradian at a height of 1 meter above a plane uniformly contaminated with 1 mc Cs^{137}/(meter)^2.

calculated from the spectra are shown as crosses. The solid line between angles of 100° and 180° measured from the vertical was calculated for primary radiation only since a detector at a height of 1 meter will see only small amounts of scattered radiation arriving in these angular limits. When integrated over the 4π steradians this polar distribution should lead to the total dose actually observed at a height of 1 meter in a uniformly contaminated field. The dotted line was chosen to satisfy this requirement. It is interesting to note that the resulting curve indicates that 73% of the total dose is due to radiation received within $\pm 20°$ of the horizon. These measurements were made with contamination on a smooth plane. In the practical case of fall-out it is appreciated that the polar distribution of radiation would be modified somewhat depending on the extent of ground roughness.

BERGER, M. J. 1957. J. Appl. Phys. **28**, 1502.
CLIFFORD, C. E., CARRUTHERS, J. A., and CUNNINGHAM, J. R. 1959. Defence Research Chemical Laboratories, DRCL Report 296.
TITUS, F. 1958. Nuclear Sci. and Eng. **3**, 609.

RECEIVED NOVEMBER 6, 1959.
DEFENCE RESEARCH CHEMICAL LABORATORIES,
DEFENCE RESEARCH BOARD,
SHIRLEY BAY, ONTARIO.

A NOTE ON DIFFRACTION BY A HALF PLANE

W. E. WILLIAMS

INTRODUCTION

The problem of the diffraction of the field of a line source by a perfectly conducting half plane was first solved by Carslaw (1899) using a method similar to that employed by Sommerfeld (1896) in considering diffraction by a plane wave. The problem was also considered by Macdonald (1915) using a completely different approach and, in particular, he succeeded in expressing the solution in an extremely simple manner. This latter form of the solution was recently rederived by Clemmow (1950) using yet another method. Though the form of Macdonald's solution is extremely simple the methods used in obtaining it involve a considerable amount of analysis and the object of the present note is to give a simple method of solving this problem involving very little analysis. For plane-wave excitation a comparable type of simple solution has been obtained by Lamb (1906).

FORMULATION OF THE PROBLEM

A Cartesian co-ordinate system $0xyz$ is chosen so that the half plane occupies the region $y = 0$, $x \geqslant 0$, all z; it is also convenient to define polar co-ordinates (r,θ) by $x = r\cos\theta$, $y = r\sin\theta$. We shall consider an electric line source parallel to the z axis and its intersection with the plane $z = 0$ will be taken to be at the point (x_0,y_0) or, in polar co-ordinates, (r_0,θ_0). Two other geometrical quantities which will be required are the distances R_1 and R_2 of (x,y) from (x_0,y_0) and $(x_0,-y_0)$ respectively. In terms of polar co-ordinates they are defined by

$$R_1^2 = r^2+r_0^2-2rr_0\cos(\theta-\theta_0), \qquad R_2^2 = r^2+r_0^2-2rr_0\cos(\theta+\theta_0).$$

The only component of the electric field will be parallel to the z axis and it will be denoted by $\phi(x,y,x_0,y_0)\exp i\omega t$. Maxwell's equations show that

$$(\nabla_1^2+k^2)\phi = \delta(x-x_0)\delta(y-y_0), \tag{1}$$

where ∇_1^2 is the two-dimensional Laplacian operator, $\delta(x)$ is Dirac's function, and $k^2 = \omega^2\epsilon_0\mu_0$ where ϵ_0, μ_0 denote the electric susceptibility and magnetic permeability (in m.k.s. units) of free space.

ϕ is finite except at (x_0,y_0), it vanishes on the half plane, and it satisfies Sommerfeld's radiation condition at infinity. We also have that ϕ satisfies the reciprocity condition, i.e. $\phi(x,y,x_0,y_0) = \phi(x_0,y_0,x,y)$. In solving a diffraction problem it is necessary to make some assumption concerning the behavior of the solution near sharp edges of diffracting obstacles. In the present case we shall make the assumption, following Bouwkamp (1954), that ϕ behaves as $r^{\frac{1}{2}}$ near $r = 0$. All known solutions of diffraction problems involving thin sheets do, in fact, exhibit this behavior near the edge of the diffracting sheet. In fact, if it is assumed that ϕ behaves as r^{λ} near $r = 0$ then it may be shown that the smallest permissible value of λ is $\frac{1}{2}$. We shall make the assumption that, near $r = 0$, ϕ has the form $r^{\frac{1}{2}}f(\theta)$ where f is a function of θ. In order that ϕ satisfies equation 1 it is easily verified that $f = A \sin \frac{1}{2}\theta + B \cos \frac{1}{2}\theta$ where A, B are independent of r and θ. Furthermore, since $\phi = 0$ on the half plane, we have $B = 0$.

From ϕ we can construct a new function χ which also vanishes on the half plane and satisfies the radiation condition. This function is defined by $\chi = (\partial\phi/\partial x)+(\partial\phi/\partial x_0)$. From equation 1 it is seen that χ is non-singular at (x_0,y_0) and is, in fact, a solution of the homogeneous Helmholtz equation. Our assumption about the edge behavior of ϕ shows that, near $r = 0$, χ has the form $-\frac{1}{2}Ar^{-\frac{1}{2}} \sin \frac{1}{2}\theta$. Thus a possible solution for χ is $-\frac{1}{2}Ar^{-\frac{1}{2}} \sin \frac{1}{2}\theta \exp -ikr$. This solution satisfies the homogeneous Helmholtz equation, the radiation condition, the boundary condition on the half plane and possesses the appropriate edge singularity. The most general solution for χ consistent with our assumption about the edge behavior is thus obtained by adding to the above particular solution a second solution of Helmholtz' equation which is non-singular at the edge. This second solution is also to be finite everywhere and to satisfy Sommerfeld's radiation condition. The uniqueness theorem of Peters and Stoker (1954) shows that such a function is everywhere zero and hence $\chi = -\frac{1}{2}Ar^{-\frac{1}{2}} \sin \frac{1}{2}\theta \exp -ikr$. The form of χ shows that it satisfies the reciprocity condition and thus A must have the form $B \sin \frac{1}{2}\theta_0 r_0^{-\frac{1}{2}} \exp -ikr_0$ where B is a numerical constant.

The boundary value problem thus reduces to integrating the partial differential equation

$$\frac{\partial\phi}{\partial x}+\frac{\partial\phi}{\partial x_0} = -\frac{B \sin \frac{1}{2}\theta \sin \frac{1}{2}\theta_0}{2\sqrt{(rr_0)}} \exp -ik(r+r_0). \tag{2}$$

It is not immediately obvious how this equation may be integrated and the correct line of attack is obtained by considering the particular case of $k = 0$. This corresponds to determining a solution of Laplace's equation with a line charge at (r_0,θ_0); the solution to this problem may be obtained by conformal mapping (Jeans 1951). The solution is given as a linear combination of variables η_1 and η_2 defined by

$$\eta_1 = \sinh^{-1}\frac{2\sqrt{(rr_0)}}{R_1} \cos \tfrac{1}{2}(\theta-\theta_0), \qquad \eta_2 = \sinh^{-1}\frac{2\sqrt{(rr_0)}}{R_2} \cos \tfrac{1}{2}(\theta+\theta_0).$$

The form of η_1 and η_2 suggests writing the product of sines in equation 2 as a difference of cosines and writing ϕ as $\phi_1-\phi_2$ where

$$\frac{\partial \phi_1}{\partial x}+\frac{\partial \phi_1}{\partial x_0} = -\frac{B\cos\frac{1}{2}(\theta-\theta_0)}{4\sqrt{(rr_0)}}\exp -ik(r+r_0), \tag{3}$$

$$\frac{\partial \phi_2}{\partial x}+\frac{\partial \phi_2}{\partial x_0} = -\frac{B\cos\frac{1}{2}(\theta+\theta_0)}{4\sqrt{(rr_0)}}\exp -ik(r+r_0). \tag{4}$$

The form of the solution for $k = 0$ suggests that we choose η_1 and η_2 as new variables and it is easily verified that

$$\frac{\partial \eta_1}{\partial x}+\frac{\partial \eta_1}{\partial x_0} = \frac{\cos\frac{1}{2}(\theta+\theta_0)}{\sqrt{(rr_0)}}, \qquad \frac{\partial \eta_2}{\partial x}+\frac{\partial \eta_2}{\partial x_0} = \frac{\cos\frac{1}{2}(\theta-\theta_0)}{\sqrt{(rr_0)}},$$

$$r+r_0 = R_1\cosh\eta_1 = R_2\cosh\eta_2.$$

The above relations indicate that ϕ_1 is a function of R_2 and η_2 and ϕ_2 a function of R_1 and η_1. Thus, since $(\partial R_1/\partial x)+(\partial R_1/\partial x_0) = (\partial R_2/\partial x)+(\partial R_2/\partial x_0) = 0$, equations 3 and 4 may be integrated immediately to give the following particular integrals

$$\phi_1 = -\tfrac{1}{4}B\int_a^{\eta_2}\exp(-ikR_2\cosh\eta)d\eta, \qquad \phi_2 = -\tfrac{1}{4}B\int_b^{\eta_1}\exp(-ikR_1\cosh\eta)\,d\eta.$$

a and b are constants to be determined. In the neighborhood of $(x_0, -y_0)$, $\eta_2 \approx -\infty$ and $R_2 \approx 0$; thus ϕ will be infinite near $(x_0, -y_0)$ unless $a = -\infty$. $R_1 = R_2$ and $\eta_1 = \eta_2$ on the half plane and thus, since $\phi = 0$ on the half plane, $b = -\infty$. Thus choosing $a = b = -\infty$ produces a solution satisfying all the conditions imposed except that at (x_0,y_0). The behavior at the source is determined by an appropriate choice of B. If we let R_1 tend to zero in ϕ_2 then the integral representation of the Hankel function (Watson 1944) shows that, near (x_0,y_0), $\phi_2 \approx -\tfrac{1}{4}B\pi_i H_0^{(2)}(kR_1)$ and hence $B = 1$.

Thus the solution to the boundary value problem has been obtained by assuming the edge behavior of the solution and employing the reciprocity condition.

The above method may also be employed to determine time-dependent solutions of the wave equation. It is easily verified that the two-dimensional time-dependent Green's function is obtained when the exponential in equations 3 and 4 is replaced by

$$\delta\left\{t-\frac{1}{c}(r+r_0)\right\}$$

where c is the wave velocity. The integration of the equations is elementary and the solution obtained agrees with that given by Friedlander (1951). If the exponential is replaced by

$$u\left\{t-\frac{1}{c}(r+r_0)\right\},$$

where u is the unit function, then the solution for a cylindrical pulse is obtained. The problem for the spherical pulse, solved by Wait (1957), may also be treated in this manner. In this case the exponential is replaced by

$$\frac{4\pi^2 t(r+r_0)}{\{z^2+(r+r_0)^2\}^{\frac{1}{2}}\left\{t^2-\frac{1}{c^2}[z^2+(r+r_0)^2]\right\}^{\frac{1}{2}}}\, u\left\{t-\frac{1}{c}[z^2+(r+r_0)^2]^{\frac{1}{2}}\right\}.$$

The solution for a time harmonic point source is also easily obtained by the present approach.

BOUWKAMP, C. J. 1954. Repts. Progr. in Phys. **17**, 38.
CARSLAW, H. S. 1899. Proc. London Math. Soc. **30**, 121.
CLEMMOW, P. C. 1950. Quart. Jour. Mech. Appl. Math. **3**, 377.
FRIEDLANDER, F. G. 1951. Quart. Jour. Mech. Appl. Math. **4**, 344.
JEANS, J. H. 1951. Electricity and magnetism (Cambridge University Press), p. 283.
LAMB, H. 1906. Proc. London Math. Soc. **4**, 190.
MACDONALD, H. M. 1915. Proc. London Math. Soc. **14**, 410.
PETERS, A. S. and STOKER, J. 1954. J. Commun. Pure Appl. Math. **7**, 565.
SOMMERFELD, A. 1896. Math. Ann. **47**, 317.
WAIT, J. R. 1957. Can. J. Phys. **35**, 693.
WATSON, G. N. 1944. Theory of Bessel functions (Cambridge University Press), p. 170.

RECEIVED AUGUST 25, 1959.
DEPARTMENT OF APPLIED MATHEMATICS,
UNIVERSITY OF LIVERPOOL,
LIVERPOOL, ENGLAND.

FRANCK–CONDON FACTORS AND r-CENTROIDS FOR SOME BANDS OF THE CO FOURTH POSITIVE ($A^1\Pi$–$X^1\Sigma$) BAND SYSTEM

W. R. JARMAIN, RUBY EBISUZAKI,* AND R. W. NICHOLLS†

The Franck–Condon factor $q_{v'v''}$ arrays of a number of band systems of combustion interest discussed by Gaydon (1957) were recently published (Nicholls, Fraser, and Jarmain 1959). The extent of each of the arrays was limited to include only bands which were in the readily accessible wavelength region (2000 Å to 10,000 Å) of standard photographic spectroscopy, and whose $q_{v'v''}$ values were amenable to computation, by desk calculator or electronic computer, using the methods of Fraser and Jarmain (Fraser and Jarmain 1953; Jarmain and Fraser 1953; Fraser 1954) for Morse molecules. The fact that the bands of the CO fourth positive system (which as a whole extends in wavelength between about 1000 Å and 2800 Å), at longer wavelengths than 2000 Å, arise from transitions between high vibrational levels, precluded the use of the Fraser–Jarmain method for these bands although they are of combustion interest.

A partial Franck–Condon factor array ($v'+v'' \leqslant 7$) was, however, computed some years ago for this system as part of a routine program of such

*Now at Yerkes Observatory, Williams Bay, Wisconsin.
†Temporarily on leave of absence at the National Bureau of Standards, Washington, D.C.

calculations. It gives data for bands whose wavelengths are less than 1988 Å. The recent growth in interest in intensity aspects of vacuum ultraviolet spectra together with private requests for the array prompts us to present it in Table I together with band head wavelengths and r-centroids. The wave-

TABLE I

Franck–Condon factors $q_{v'v''}$, r-centroids $\bar{r}_{v'v''}$, and wavelengths $\lambda_{v'v''}$ for the CO fourth band system

v' \ v''	0	1	2	3	4	5	6	7
	0.11_4	0.26_1	0.28_5	0.19_6	0.09_6	0.03_8	0.01_0	(0.00_3)‡
0	1.181	1.211	1.241	1.271	1.302	1.334	1.366	1.398
	1545.3	1597.14	1653.05	1712.19	1774.90	1841.47	1912.8	1988.08†
	0.21_6	0.15_5	0.00_3	0.05_9	0.19_4	0.18_8	(0.09_4)	
1	1.160	1.190	1.220	1.248	1.280	1.311	1.342	
	1509.66	1560.14*	1613.99†	1669.68	1729.25	1792.38	1859.3	
	0.23_0	0.01_2	0.09_1	0.11_6	0.00_5	(0.07_8)		
2	1.141	1.170	1.200	1.223	1.259	1.289		
	1477.48	1525.75	1576.67	1630.40	1687.44†	1747.20		
	0.18_1	0.02_0	0.11_6	0.00_0	(0.10_8)			
3	1.123	1.151	1.179	1.209	1.238			
	1447.27	1493.60	1542.34	1593.97†	1647.90			
	0.11_9	0.08_8	0.03_4	(0.07_5)				
4	1.105	1.133	1.161	1.189				
	1418.91	1463.47*	1510.47†	1559.47				
	0.069	0.12_8	(0.00_5)					
5	1.088	1.115	1.143					
	1391.97	1435.28	1480.43†					
	0.03_7	(0.11_8)						
6	1.072	1.099						
	1367.70†	1408.8						
	(0.01_6)							
7	1.057							
	1344.27†							

LEGEND:

$q_{v'v''}$

$\bar{r}_{v'v''}$ (A)

$\lambda_{v'v''}$ (A)

*Bands observed overlapped, wavelengths thus calculated, not measured, by Read (1934).

†Bands not reported, wavelengths calculated.

‡Franck–Condon factors in parentheses not perturbation corrected.

lengths were taken from the work of Headrick and Fox (1930) and of Read (1934). The r-centroids were evaluated graphically by methods described by Nicholls and Jarmain (1956), and the Franck–Condon factors were evaluated by the method of Fraser and Jarmain (including perturbation correction) using the basic data for the transition tabulated by Herzberg (1950).

As expected for a band system which involves a moderately large change in internuclear separation ($\Delta r_e = 0.107$ Å), the primary Condon "Parabola" of the $q_{v'v''}$ values is fairly wide and does not quite include the (0,0) band. There is also evidence of a secondary parabola whose vertex is in the region

of the (2,2), (2,3), and (3,2) bands. Some recent studies by one of us on the analytical form of the Condon "Parabolae" in cases where the potentials involved are not parabolic will be published shortly. A much more extensive r-centroid array for the CO fourth positive system than that presented in Table I is available as part of a comprehensive compilation of such data for a wide variety of band systems, and is in the process of publication elsewhere.

This work has been supported in part by Research Grants from the National Research Council and Defence Research Board of Canada, and in part by contracts with the Department of Defence Production of Canada, the Air Force Cambridge Research Center, the Air Force Office of Scientific Research, and the Office of Naval Research.

FRASER, P. A. 1954. Proc. Phys. Soc. A, **67**, 939.
FRASER, P. A. and JARMAIN, W. R. 1953. Proc. Phys. Soc. A, **66**, 1145.
GAYDON, A. G. 1957. The spectroscopy of flames (Chapman & Hall Ltd., London).
HEADRICK, L. B. and FOX, G. W. 1930. Phys. Rev. **35**, 1033.
HERZBERG, G. 1950. The spectra of diatomic molecules (D. Van Nostrand Company, Inc., New York).
JARMAIN, W. R. and FRASER, P. A. 1953. Proc. Phys. Soc. A, **66**, 1153.
NICHOLLS, R. W. and JARMAIN, W. R. 1956. Proc. Phys. Soc. **69**, 253.
NICHOLLS, R. W., FRASER, P. A., and JARMAIN, W. R. 1959. Combustion and Flame, **3**, 11.
PEARSE, R. W. B. and GAYDON, A. G. 1950. The identifications of molecular spectra, 2nd ed. (Chapman & Hall, Ltd., London).
READ, D. N. 1934. Phys. Rev. **46**, 571.

RECEIVED DECEMBER 17, 1959.
MOLECULAR EXCITATION GROUP,
DEPARTMENT OF PHYSICS,
UNIVERSITY OF WESTERN ONTARIO,
LONDON, ONTARIO.

LETTERS TO THE EDITOR

Under this heading brief reports of important discoveries in physics may be published. These reports should not exceed 600 words and, for any issue, should be submitted not later than six weeks previous to the first day of the month of issue. No proof will be sent to the authors.

Frequency Measurement of Standard Frequency Transmissions[1]

Measurements are made at Ottawa, Canada, using N.R.C. caesium-beam frequency resonator as reference standard (with an assumed frequency of 9 192 631 770 c.p.s.). Frequency deviations from nominal are quoted in parts per 10^{10}. A negative sign indicates that the frequency is below nominal.

Date, December 1959	MSF, 60 kc/s	GBR, 16 kc/s		KK2XEI, 60 kc/s
		8½-hour average*	24-hour average	
1	−159	−164	−161	−82
2	N.M.	−166	−166	−81
3	N.M.	−164	−167	−80
4	N.M.	−163	−166	−81
5	N.M.	−169	N.M.	N.M.
6	N.M.	N.M.	N.M.	N.M.
7	N.M.	N.M.	N.M.	N.M.
8	−163	N.M.	N.M.	−78
9	N.M.	−164	−162	N.M.
10	−166	−160	−162	−79
11	−165	−165	−164	−82
12	−163	−164	−162	N.M.
13	−173	−164	−164	N.M.
14	−170	−160	−161	−79
15	−172	−161	−163	−78
16	−158	−160	−161	−76
17	−162	−163	−161	−78
18	−163	−161	−161	−78
19	−165	−163	−162	N.M.
20	−165	−162	N.M.	N.M.
21	N.M.	−160	−161	−80
22	N.M.	−162	−162	−79
23	N.M.	−160	−161	−77
24	N.M.	−164	−163	−78
25	−171	−164	−164	N.M.
26	N.M.	−163	−164	N.M.
27	−166	−166	−163	N.M.
28	−155	−161	−162	−76
29	−163	−164	−161	−78
30	−156	−161	−157	−74
31	−162	−163	−162	−73
Midmonthly mean	−164	−163	−163	−78
Midmonthly mean of WWV	−106			

NOTE: N.M. no measurement.
*Time of observations: 00.00 to 07.00 and 22.30 to 24.00 U.T.

RECEIVED JANUARY 14, 1960.
S. N. KALRA
DIVISION OF APPLIED PHYSICS,
NATIONAL RESEARCH COUNCIL,
OTTAWA, CANADA.

[1]Issued as N.R.C. No. 5570.
[2]Cf. Kalra, S. N. 1959. Can. J. Phys. **37**, 1328.

NOTES TO CONTRIBUTORS

Canadian Journal of Physics

MANUSCRIPTS

General.—Manuscripts, in English or French, should be typewritten, double spaced, on paper 8½×11 in. **The original and one copy are to be submitted.** Tables and captions for the figures should be placed at the end of the manuscript. Every sheet of the manuscript should be numbered. Style, arrangement, spelling, and abbreviations should conform to the usage of recent numbers of this journal. Greek letters or unusual signs should be written plainly or explained by marginal notes. Characters to be set in boldface type should be indicated by a wavy line below each character. Superscripts and subscripts must be legible and carefully placed. Manuscripts and illustrations should be carefully checked before they are submitted. Authors will be charged for unnecessary deviations from the usual format and for changes made in the proof that are considered excessive or unnecessary.

Abstract.—An abstract of not more than about 200 words, indicating the scope of the work and the principal findings, is required, except in Notes.

References.—References should be listed **alphabetically by authors' names,** unnumbered, and typed after the text. The form of the citations should be that used in current issues of this journal; in references to papers in periodicals, titles should not be given and only initial page numbers are required. The names of periodicals should be abbreviated in the form given in the most recent *List of Periodicals Abstracted by Chemical Abstracts.* All citations should be checked with the original articles and each one referred to in the text by the authors' names and the year.

Tables.—Tables should be numbered in roman numerals and each table referred to in the text. Titles should always be given but should be brief; column headings should be brief and descriptive matter in the tables confined to a minimum. Vertical rules should not be used. Numerous small tables should be avoided.

ILLUSTRATIONS

General.—All figures (including each figure of the plates) should be numbered consecutively from 1 up, in arabic numerals, and each figure referred to in the text. The author's name, title of the paper, and figure number should be written in the lower left corner of the sheets on which the illustrations appear. Captions should not be written on the illustrations.

Line drawings.—Drawings should be carefully made with India ink on white drawing paper, blue tracing linen, or co-ordinate paper ruled in blue only; any co-ordinate lines that are to appear in the reproduction should be ruled in black ink. Paper ruled in green, yellow, or red should not be used. All lines must be of sufficient thickness to reproduce well. Decimal points, periods, and stippled dots must be solid black circles large enough to be reduced if necessary. Letters and numerals should be neatly made, preferably with a stencil (**do NOT use typewriting**) and be of such size that the smallest lettering will be not less than 1 mm high when the figure is reduced to a suitable size. Many drawings are made too large; originals should not be more than 2 or 3 times the size of the desired reproduction. Whenever possible two or more drawings should be grouped to reduce the number of cuts required. In such groups of drawings, or in large drawings, full use of the space available should be made; the ratio of height to width should conform to that of a journal page (4¼×7½ in.), but allowance must be made for the captions. **The original drawings and one set of clear copies (e.g. small photographs) are to be submitted.**

Photographs.—Prints should be made on glossy paper, with strong contrasts. They should be trimmed so that essential features only are shown and mounted carefully, with rubber cement, on white cardboard, with no space between those arranged in groups. In mounting, full use of the space available should be made. **Photographs are to be submitted in duplicate;** if they are to be reproduced in groups one set should be mounted, the duplicate set unmounted.

REPRINTS

A total of 100 reprints of each paper, without covers, are supplied free. Additional reprints, with or without covers, may be purchased at the time of publication.

Charges for reprints are based on the number of printed pages, which may be calculated approximately by multiplying by 0.6 the number of manuscript pages (double-spaced typewritten sheets, 8½×11 in.) and including the space occupied by illustrations. Prices and instructions for ordering reprints are sent out with the galley proof.

Contents

Printed in Canada *by* University of Toronto Press